

https://dspace.org/

The Bioinorganic Chemistry of the First Row dBlock Metal IonsAn Introduction

Helder Marques

https://hdl.handle.net/10539/45790
WOS

Downloaded from a DSpace repository. https://dspace.org/

inorganics

MDPI

Review

The Bioinorganic Chemistry of the First Row d-Block Metal Ions—An Introduction

Helder M. Marques

Molecular Sciences Institute, School of Chemistry, University of the Witwatersrand, Johannesburg 2050, South Africa; helder.marques@wits.ac.za

Abstract: The role played by the metal ions of the first row of the block in biology is discussed using illustrative examples, and covering current thinking in the field. This will be of interest to current researchers in bioinorganic chemistry, as well as to senior undergraduate and novice postgraduate students entering the field.

Keywords: bioinorganic chemistry; d-block metal ions; metals in biology; catalysis; electron transfer; metalloenzymes; oxygen transport and storage

1. Introduction

Living systems on Earth primarily rely on a limited number of elements, notably C, H, N, O, P, and S. Together with Ca, these elements comprise approximately 98% of the human body by mass. Adding Na, Mg, Cl, and K brings the total close to 100% [1–4]. Despite their trace presence, d-block metal ions play crucial roles in biological processes, a concept underscored by the term *metallome* [5,6]. It has even been hypothesised that metal ions such as Fe, Mn, and Zn were essential for the actual emergence of modern metabolism [5,7]. In humans, metals like Mn, Fe, Co, Cu, and Zn are essential, while Cr and V offer some benefits [8,9]. The essentiality of Ni for humans is unclear, though it is vital for other life forms [10,11].

Many of these metal ions are biologically significant because of their variable oxidation states, with notable examples being Mn, Fe, Co, Ni, and Cu from the first row of the d block. Others, like Zn, primarily serve structural roles but also contribute to catalysis. Maintaining metal ion homeostasis is essential: a deficiency can harm the organism, but an excess is equally detrimental [12–17]. Indeed, while some elements may be beneficial at pharmacological concentrations, most are toxic at higher levels [17–19].

Trace metal ions in cells generally do not exist as free ions but as complexes, which falls under the domain of inorganic chemistry, particularly coordination chemistry. Understanding the role of metal ion complexes is central to bioinorganic chemistry, the intersection of inorganic chemistry and biology [20–26]. Despite their trace concentrations, these metals are integral to evolution, performing a variety of vital biological tasks [27–29]. Roughly one-third of all enzymes depend on metal ions for either catalytic function or structure [30,31]. Nature is also adaptable. Many enzymes can use different metal ions in their active sites. The superoxide dismutases and the ribonucleotide reductases, both of which will be discussed in this article, are examples. This adaptability to fluctuating metal availability has been important in the development of life on Earth [32].

Ions with closed-shell electron configurations, such as Na^+, K^+, Ca^{2+}, and Zn^{2+}, play diverse roles, including maintaining protein structure, catalysing reactions as Lewis acids,

check for updates

Academic Editor: Jun-Long Zhang

Received: 27 January 2025
Revised: 21 April 2025
Accepted: 22 April 2025
Published: 27 April 2025

Citation: Marques, H.M. The Bioinorganic Chemistry of the First Row d-Block Metal Ions—An Introduction. *Inorganics* **2025**, *13*, 137. https://doi.org/10.3390/inorganics13050137

Copyright: © 2025 by the author. Licensee MDPI, Basel, Switzerland. This article is an open access article distributed under the terms and conditions of the Creative Commons Attribution (CC BY) license (https://creativecommons.org/licenses/by/4.0/).

and regulating electrolyte and fluid balance. Metals with variable oxidation states, including Mn, Fe, Co, and Cu, facilitate redox catalysis, electron transport, oxygen transport and storage, defence against reactive oxygen, nitrogen, and sulphur species, and enzyme-catalysed reactions requiring changes in oxidation states [33].

The d-block metal ions important in biology are trace elements. An early definition of trace elements by Arnon and Stout [34], originally focused on plants, can be extended to other life forms:

- Without these elements, a plant cannot complete its life cycle.
- These elements are part of the essential constituents or metabolites of the plant.
- Deficiency of these elements leads to diseases, which can be corrected by their reintroduction.

Other definitions exist, such as the following:

- *"An element is essential when a deficient intake consistently results in impaired function, and supplementation at physiological levels, but not others, restores optimal function"* [1].
- *"An element is considered essential if it has a defined biochemical function, and its absence results in death or reproductive failure, reversible by dietary supplementation"* [35].
- The European Food Safety Authority (EFSA) defines an essential nutrient as "any substance an organism must consume from the diet to support normal health, development, and growth" [36].

A more comprehensive definition is provided in the classic textbook *Trace Elements in Human and Animal Nutrition* by Eric Underwood [37]:

A trace element is essential if it fulfils the following criteria:

- is present in all healthy tissues of living organisms;
- exists in relatively constant concentrations across individuals;
- causes physiological and structural abnormalities in its absence, which are reversible upon reintroduction;
- leads to specific biochemical changes when deficient, correctable by reversing the deficiency.

It is important to note the concept of partially essential or beneficial elements [38–40] and that the essentiality of elements varies across life forms. For example, while boron is essential for higher plants [41], it appears to be non-essential for animals (although this has been contested [41,42]); conversely, selenium is essential for animals, while its role in plants is unclear [38,43,44].

This article provides an introduction to bioinorganic chemistry, focusing on the first-row d-block metals and their biological (and sometimes medicinal) roles, whether essential or not. Using illustrative examples, it endeavours to reflect current thinking in the field to encourage deeper exploration and appreciation of ongoing developments. Given the breadth of the topic, the discussion is necessarily selective and illustrative rather than exhaustive. Moreover, this article should be particularly useful for the senior undergraduate and novice postgraduate student entering the field. Heavier metals like Mo and W, also important in biology, will be discussed elsewhere.

2. Scandium

Scandium is a relatively rare element found in the Earth's crust, soil, and water bodies, typically dispersed in small quantities. It is often present in aluminosilicate minerals, including clays, micas, and pyroxenes [45].

Scandium is not known to be essential for biological systems, and due to its low bioavailability, it is generally considered non-toxic [46]. Its increasing industrial use has raised concerns about its potential environmental impact [47] and further research

on its exposure risks is warranted [48]. Its potential toxicity in humans has been extensively reviewed [49].

Scandium oxide (Sc_2O_3) is probably non-toxic, supporting cell viability, growth, and proliferation [48,50]. Although certain bacteria are sensitive to scandium at millimolar concentrations, eukaryotic cells are not [51]. Scandium does not bioaccumulate; its concentration in plants is typically lower than in the surrounding soil, with higher levels found in roots compared to leaves and seeds [52].

The ionic radius of Sc^{3+} (74.5 pm) is larger than that of high-spin, six-coordinate Fe^{3+} (64.5 pm) [53], yet Sc^{3+} can still bind to human serum transferrin (HSTf), the mammalian iron transport protein, albeit with weaker affinity (log K_1 = 14.6 (2) and log K_2 = 13.3 (3) for Sc^{3+} [54] compared to 22.7 and 22.1 [55] or 22.5 and 21.4 [56] for Fe^{3+}). Sc^{3+} also interacts with other proteins, such as α-globulins [57], and β-globulins [58], and it forms complexes with ATP, such as $Sc(ATP)_2$ [59].

Complexes of Sc^{3+} have been explored for their antiviral, antibiotic, and antineoplastic activities. A diphthalocyanine complex of Sc^{3+} exhibits antiviral activity [60]. Coupling of Sc^{3+} with epoxypolysaccharide (EPS) derivatives improves the anti-metastatic properties of EPS [61]. Some complexes of scandium with europium oxide nanorod metallocene complexes exhibit anti-proliferative activity against some breast cancer and prostate cancer cell lines [62].

Sc^{3+} chelated with EDDHA (ethylenediamine-*N*,*N*′-bis(2-hydroxyphenylacetic acid)) binds to human serum albumin (HSA), likely through a bridging interaction involving EDDHA's phenolic groups [57]. Other chelators, such as NTA, EDTA, DTPA, and CDTA (NTA, nitrilotriacetic acid; EDTA, ethylenediaminetetraacetic acid; DTPA, diethylenetriaminepentaacetic acid; CDTA, cyclohexanediaminetetraacetic acid) do not form such complexes [63]. In mice, scandium behaves differently depending on its compound: Sc-EDTA is rapidly excreted in urine via the kidneys, whereas $ScCl_3$ accumulates in the liver and spleen [64]. Urinary scandium excretion may serve as a biomarker for environmental or occupational exposure [46,65]. Elevated circulating Sc^{3+} levels have been associated with chronic renal failure [66], and hair analysis suggests correlations between increased Sc^{3+} levels and health conditions such as diabetes and obesity [67].

In cellular systems, Sc^{3+} interacts with actin, a cytoskeletal protein critical for cell motility and structural integrity, displacing native Mg^{2+} and forming amorphous aggregates [68]. $ScF_x^{(x-3)-}$ can inhibit the ATPase activity of myosin, another key cytoskeletal protein involved in cellular motility, by interacting with its subfragment 1 [69].

There is interest in the use of the positron emitters ^{44}Sc ($t_{1/2}$ = 3.97 h) and ^{47}Sc ($t_{1/2}$ = 3.4 d) for thernanostic applications [70–73]; with its short lifetime, ^{44}Sc (and ^{43}Sc) is useful for PET imaging while ^{47}Sc is useful for therapy. Suitable chelates are required, with DOTA (1,4,7,10-tetraaza-cyclododecane-1,4,7,10-tetraacetic acid) as the current gold standard [73–75].

There is probably merit in the further exploration of Sc^{3+} complexes for their antiviral, antibiotic, and antineoplastic activities which might lead to the development of novel treatment regimes.

3. Titanium

Titanium plays no known biological role [76]. Humans typically ingest approximately 0.8 mg of titanium daily, primarily through food [77], but most of it passes through the body unabsorbed. Blood titanium levels in humans average around 45 μg L^{-1} [78]. Titanium alloys are highly biocompatible and widely utilised in joint replacements and dental implants [79–81] with negligible effects on blood titanium levels [78], although there is recent evidence of elevated titanium levels in the blood of patients after spinal surgery

and implants [82]. It has been suggested that titanium implants can contribute to peri-implantitis through mechanisms such as foreign body reactions and DNA methylation [83] and the chemical treatment of the implants may be appropriate [84]. A re-evaluation of the design of titanium alloys for use in implants may be necessary [85].

In oxidising environments, titanium predominantly exists as Ti^{4+} [86], with an ionic radius of 0.605 Å (for six-coordinate Ti^{4+} [53]), which is an intermediate between six-coordinate Al^{3+} (0.535 Å) and high-spin Fe^{3+} (0.645 Å).

3.1. Biomedical Applications

While titanium plays no role in biology, many of its compounds have been used in biomedical applications. Some examples are discussed here—and the list is by no means comprehensive.

Titanium compounds such as titanocene dichloride, Cp_2TiCl_2 (Figure 1), exhibit anti-tumour properties [87–93]. The anti-tumour property is thought to be a consequence of the accumulation of these compounds in nucleic acid-rich regions, particularly the chromatin of tumour cells, where they bind irreversibly to DNA via phosphate oxygen and, to a lesser extent, nitrogen bases [94,95]. This inhibits cell growth.

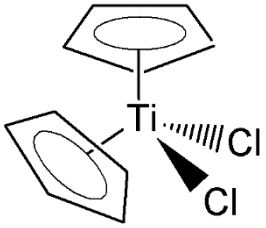

Figure 1. Titanocene dichloride, $(\eta^5\text{–}C_5H_5)_2TiCl_2$.

A recent review underscores the multifaceted nature of titanium's anticancer activity [96]. The mechanism of action for titanium-based anticancer drugs extends beyond DNA binding. Proposed mechanisms include inhibition of mitochondrial activity, induction of paraptosis via kinase activation, topoisomerase inactivation, apoptosis, and iron deprivation.

Ti^{4+} is transported to cancer cells by HSTf, forming complexes with the N and C lobes of HSTf [97]. Its strong Lewis acidity and higher charge density enable it to bind more strongly to HSTf than Fe^{3+} (log K_1 = 26.8 and log K_2 = 25.7 compared to 22.7 and 22.1 [55] or 22.5 and 21.4 [56] for Fe^{3+}). Cancer cells overexpress transferrin receptors [98], and their low intracellular pH facilitates Ti^{4+} release and DNA complexation.

The exploration of titanium complexes in oncology is the subject of ongoing research [90,91,95,96,99,100] and future interesting findings can be expected.

Titanium oxide nanoparticles have significant photocatalytic potential which generates high levels of reactive oxygen species (ROS). They are therefore potential antibacterial and anticancer agents [101,102]. In fungi, TiO_2 nanoparticles cause damage to the cells by impairing their ROS-scavenging system [103]. In *E. coli*, TiO_2 photocatalysis leads to damage of cell walls due to lipid and protein peroxidation, increasing their fluidity, and ultimately leading to cell lysis [104,105]. TiO_2 nanoparticles in the size range 10–100 nm penetrate tumour cells with minimal uptake by healthy cells. They induce oxidative stress and can be used in cancer therapy [106,107].

An interesting biomedical application of titanium is $Ti_3C_2T_X$-MXene, a two-dimensional material of the MXene family (a layered material of general formula $M_{n+1}AX_n$, M = a transition metal such as Ti or Nb, A = Al, Si, or Ga, X = C and/or N). These can serve as carriers

of poorly hydrophilic drugs to cancer cells and are also useful in photoacoustic imaging and photothermal therapy [108].

$BaTiO_3$ is a nano-acoustic sensitiser that can be used in sonodynamic therapy, a process that utilises sound waves to activate a sonosensitiser to generate localised effects that target cancer cells. The effects include tumour cell senescence, ferroptosis, and glutathione depletion [109].

3.2. Enzyme Inhibition

The five-coordinate Ti^{4+} complex $TiO(SO_4)(H_2O)$ potently inhibits trypsin-like serine proteases (enzymes that cleave peptide bonds in proteins [110,111]) by binding directly to Asp189 at the substrate binding pocket's base [112]. The specificity of this interaction is noteworthy as it excludes the chymotrypsin subclass, where the amino acid serine replaces aspartate. This distinction underscores the nuanced selectivity of $TiO(SO_4)(H_2O)$ in targeting specific protease families, which could have significant implications for therapeutic applications, especially in conditions where trypsin-like proteases are dysregulated.

Titanium complexes inhibit lipoprotein lipase (LPL) [113], which is important given LPL's critical role in lipid metabolism and its implications in conditions such as obesity and cardiovascular diseases [114].

Some hydrazide complexes of Ti(III) and Ti(IV) inhibit tyrosinases (which control the production of melanin) and lipoxygenases (which oxygenate polyunsaturated fatty acids and regulate inflammatory responses). They therefore are potentially useful in cosmetic and therapeutic applications for skin disorders (tyrosinase inhibition) [114] and anti-inflammatory therapies (lipoxygenase inhibition) [115].

The immobilisation of the bacterial metalloprotease serratiopeptidase onto TiO_2 nanoparticles is a significant advancement in enzyme engineering [116]. This process not only enhances the enzymatic stability of serratiopeptidase, which is known for its ability to degrade a variety of proteins, but also amplifies its antibacterial properties. The incorporation of TiO_2 nanoparticles provides a robust support matrix that can protect the enzyme from denaturation and degradation, thereby prolonging its functional lifespan. Exploiting such synergies between materials science and biological chemistry could lead to innovative applications in biomedicine, particularly in developing targeted therapies against bacterial infections, where serratiopeptidase's proteolytic activity can be harnessed to disrupt bacterial cell walls or biofilms.

3.3. Antibiotic Properties

Titanium complexes show promise as antibiotics [117]. For example, the Ti^{4+} complex $Ti(deferasirox)_2$ (Figure 2) demonstrates activity against methicillin-resistant *Staphylococcus aureus* with minimal human cell toxicity. Its antibiotic effect may stem from transmetalation with labile Fe^{3+}, inhibiting iron bioavailability and hence ribonucleotide reductase [117]. It has also been suggested that titanium is a natural antibiotic, mobilised by acid-producing bacteria [118]. Metal oxide nanoparticles, including TiO_2 nanoparticles, also show promising antibiotic properties [119–122].

3.4. Role in Agriculture

Titanium stimulates plant growth, as observed with Tytanit®, a Ti^{4+} complex of ethylene glycol and terephthalic acid used in agriculture [123]. Low concentrations of titanium enhance chlorophyll content, photosynthesis, nutrient uptake, stress tolerance, and crop yield [124–127]. These effects may involve an antagonistic interaction with iron, whereby titanium induces iron acquisition gene expression, so enhancing plant growth [124]. However, caution is necessary; excessive titanium can disrupt iron homeostasis, leading to

phytotoxicity [128]. TiO_2 nanoparticles can be used to extend the shelf life of fruit by removing bacteria [129].

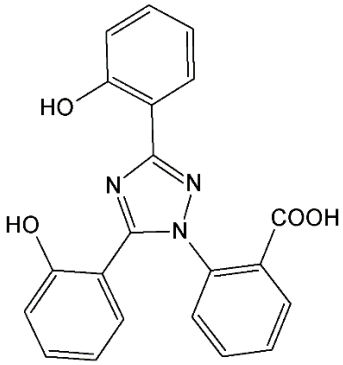

Figure 2. The structure of desferasirox.

3.5. Potential Biological Roles

Although titanium's biological role remains unconfirmed, it is known that some marine organisms sequester titanium [86]; there is a distinct possibility that this is merely an artefact of increasing levels of TiO_2 nanoparticles in aquatic ecosystems [130,131]. Suggestions have been advanced on how such a role—if it indeed exists—might be uncovered [76,132,133]. Hypothetical roles include leveraging its Lewis acidity for enzyme catalysis by deprotonating substrates in the active site of an enzyme; participation in redox electron transfer chains with suitable ligands to tune the Ti^{4+} | Ti^{3+} couple; as the active site of a redox metalloenzyme; or serving as an antimicrobial agent via singlet oxygen ($^1O_2$) and superoxide ($O_2^{\bullet-}$) generation under UV irradiation, as mentioned above. Titanium alloys could serve as temporary organs in organ transplant patients until a suitable donor is found [134]. Future studies may uncover new functions for titanium in biology.

4. Vanadium

Vanadium, with an abundance of 136 ppm in the Earth's crust [135], is relatively widespread and plays a small but significant role in biological systems [136–142]. While vanadium exhibits oxidation states ranging from −3 to +5 [135], only the +3, +4, and +5 states are known to participate in biological processes.

The role of vanadium in higher life forms is still unclear, but there is speculation that vanadium, in the form of oxidovanadium (IV) complexes may have played a significant role in the prebiotic world [143]. Some bacteria use V^{5+}–$H_2VO_4^-$ as an electron acceptor during respiration [140,144]. Intestinal bacteria of the sea squirt *Ciona robusta* accumulate V^{5+}, reducing it to V^{4+}, which is of considerable interest for possible bioremediation and biomineralization [145–148] and indeed might be extended in the future for mining in extra-terrestrial ore bodies [149].

Another notable role of vanadium is in the haloperoxidases of algae (*Ascophyllum nodosum*), fungi (*Curvularia inaequalis*), and certain cyanobacteria [142,150]. These enzymes catalyse the oxidation of halides to hypohalous acids, which may provide a defence mechanism against predators or parasites.

Vanadium is involved in nitrogenase enzymes, enabling bacteria like *Azotobacter* to fix nitrogen, converting it to NH_3. In some cases, vanadium substitutes for molybdenum, as observed in the nitrate reductase of *Pseudomonas isachenkovii* [151]. Ascidians and fan worms accumulate vanadium from seawater, possibly as a defence mechanism against predators [152].

Vanadium has potential therapeutical applications for treating diabetes, parasitic diseases, and cancer [153–158]. This will not be discussed in this article.

4.1. Vanadium in Respiration

As mentioned, some bacteria use V^{5+} ($H_2VO_4^-$) as an electron acceptor during respiration [140,144]. Understanding the processes is important for bioremediation efforts [146,159] since V^{5+} is toxic to humans. There are also potential bioengineering applications of these organisms as exoelectrogens in energy applications [160].

Geobacter metallireducens, a bacterium present in subsurface soil and which has served as a model for the physiology of microbes involved in biogeochemical recycling of metals [147], converts $H_2VO_4^-$ to $VO(OH)_2$ using lactate (or acetate) as a reductant (Figure 3, [140,144]). Other bacteria that occur in soils and groundwater, such as *Shewanella*, also oxidise V^{5+} (such as HVO_4^{2-}) to V^{4+} (as VO^{2+} or insoluble $VO(OH)_2$) using formate, lactate, or citrate as a reductant (Equation (1)).

$$2H_2VO_4^- + 2H^+ + HCOOH \rightarrow 2VO(OH)_2 + CO_2 \quad (1)$$

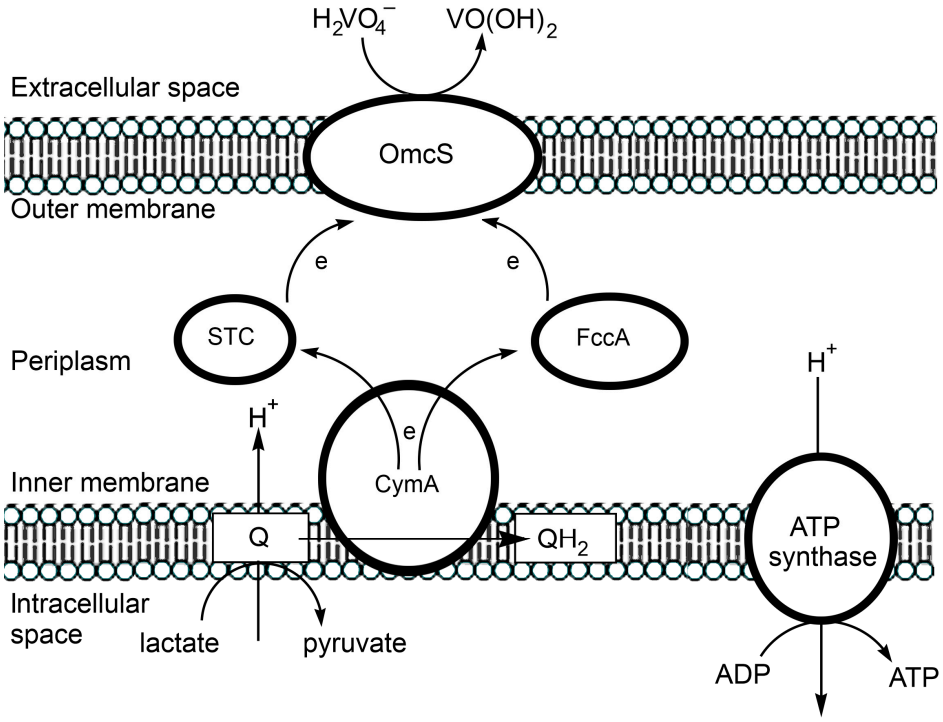

Figure 3. Electron transfer across a bacterial cellular membrane. The process begins with the oxidation of lactate or acetate at the cytosolic membrane and terminates with the reduction of vanadate at the outer membrane. Q/QH_2 is menaquinone/-hydroquinone. Refer to the text for other abbreviations. The electron transport from the cytosolic to the outer membrane is accomplished by a cascade of cytochrome *c*-type haemoproteins. The H^+ transport into the intracellular space is coupled to the formation of ATP.

Lactate, present in the cytosol, is oxidised to pyruvate by lactate dehydrogenase, a reaction that generates a limited amount of ATP, the primary energy currency of the cell. The electrons released are transferred to the quinol dehydrogenase CymA, a *c*-type tetrahaem protein [161], which oxidises reduced quinones such as menaquinone-7. CymA subsequently transfers these electrons to periplasmic cytochromes, including a small tetrahaem cytochrome (STC), which facilitates electron transfer between the inner and outer membranes [162]. Electrons are also directed to fumarate reductase (FccA) [163,164].

Both STC and FccA contribute to electron delivery to an outer membrane-associated complex. In *Geobacter* species, this complex includes OmcS, a six-haem cytochrome implicated in transmembrane electron transfer (see [165] and the references therein). OmcS

facilitates the export of electrons across the outer membrane to the extracellular environment, where the reduction of $H_2VO_4^-$ to $VO(OH)_2$ occurs.

This electron transport process is coupled to proton translocation from the cytosol to the periplasm, generating a proton-motive force across the inner membrane [166]. This electrochemical gradient is subsequently utilised by ATP synthase to drive ATP synthesis. For a detailed mechanistic overview of proton pumping in *Geobacter*, see [167].

Other bacteria that occur in soils and groundwater, such as *Shewanella*, also oxidise V^{5+} (such as HVO_4^{2-}) to V^{4+} (as VO^{2+} or insoluble $VO(OH)_2$) using formate, lactate, or citrate as a reductant (Equation (1)).

4.2. Haloperoxidases

Haloperoxidases have been known for over 25 years [168] and new haloperoxidases are still being discovered [169], or may yet be discovered [170]. They are widely distributed in seaweeds, cyanobacteria, fungi, and phytoplankton [171]. These enzymes catalyse the two-electron oxidation of halides (and thiocyanate) to hypohalous acids by a peroxide (Equation (2), using Br^- and H_2O_2 as an example) [172]. (Sometimes, perhaps arbitrarily [150], haloperoxidases that oxidise Cl^-, Br^-, and I^- are termed chloroperoxidases; the bromoperoxidases oxidise Br^- and I^-; while the iodoperoxidases act on I^- exclusively.)

$$H^+ + H_2O_2 + Br^- \rightarrow HOBr + H_2O \quad (2)$$

The hypohalide can subsequently halogenate an organic substrate, such as an aromatic compound, in the process converting a strong aromatic C-H bond into a C-halogen bond, a process facilitated by the structure of the protein which enables the binding of the substrate [173].

There is interest in these enzymes as they are useful synthesis tools that complement more traditional methods in organic synthesis and biosynthesis [174–180], and there are also potential bioengineering and biocatalysis applications [181]. There is medical interest as an increased level of haloperoxidases and halogenative stress is associated with Parkinson's disease [182].

One of the active sites of the hexameric vanadate-dependent bromoperoxidase from the algae *Ascophyllum nodosum* (Protein Data Base, PDB, reference code 5AA6 [183]) is shown in Figure 4. A His residue serves as the axial ligand of the metal, while the oxides of VO_4^{3-} (or $H_2VO_4^-$) interact with several amino acids of the protein.

An outline of the proposed reaction mechanism of a bromoperoxidase is shown in Figure 5 [183]. (See [150] for a more complete description.)

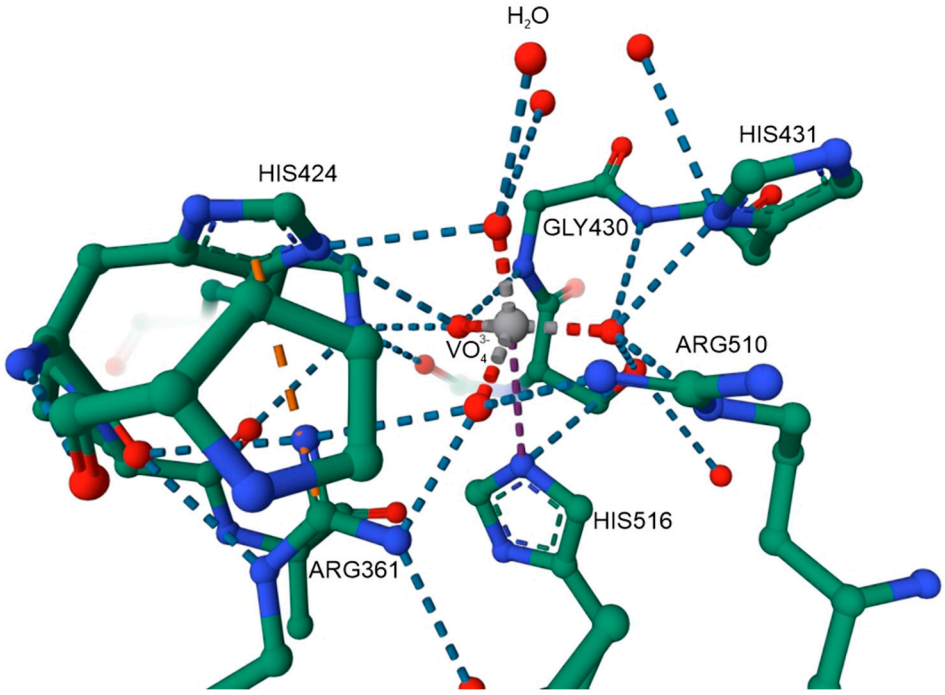

Figure 4. One of the active sites of the bromoperoxidase from *Ascophyllum nodosum* (PDB reference code 5AA6 [183]).

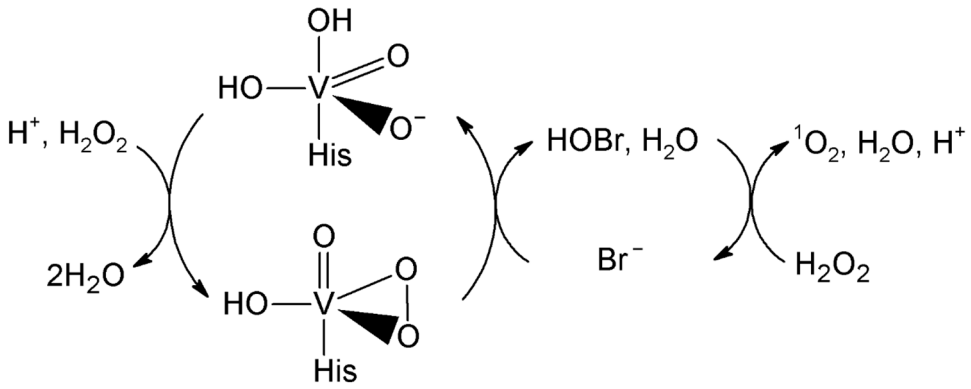

Figure 5. A proposed reaction scheme for the oxidation of Br^- to HOBr catalysed by a vanadium-dependent bromoperoxidase.

The nitrogenase enzymes catalyse the fixation of atmospheric nitrogen, reducing N_2 to NH_3. There is considerable interest in them as potentially they offer an alternative to the environmentally problematic Haber–Bosch industrial process. There are molybdenum-dependent nitrogenases, iron-only nitrogenases, and vanadium-dependent nitrogenases (V-Nase) [184]. The active site is an [MFe_7S_xC] cluster, with M = Mo, x = 9 in the molybdenum-dependent enzymes; M = Fe, x = 9 in the iron-only enzymes (the existence of a Fe_6C unit in the iron-only nitrogenases has been assumed and only recently demonstrated experimentally [185]); and M = V, x = 8 in the vanadium-dependent nitrogenases, with CO_3^{2-} bridging two of the iron centres. All these enzymes have a single evolutionary origin [186,187]. The V-Nases are only expressed under molybdenum-deficient conditions [188]. The iron-only nitrogenases are less active than the Mo-Nases and V-Nases and are only expressed under V- and Mo-deficient conditions [189].

The reaction catalysed by V-Nase, unlike Mo-Nase, uses a significant fraction of the reducing equivalents to produce H_2 (Equation (3)) and can indeed act purely as a hydrogenase in the absence of N_2.

$$N_2 + 12e + 14H^+ + 40MgATP \rightarrow 2NH_4^+ + 3H_2 + 40MgADP + 40\ P_i \quad (3)$$

By comparison, Mo-Nase consumes sixteen equivalents of MgATP and generates only one equivalent of H_2 per equivalent of N_2 reduced; it is a much more specific enzyme [190]. The reducing equivalents come from central metabolism and ATP hydrolysis [191] and are delivered to the substrate-reducing site via a [Fe_8S_7] relay (called the P-cluster) from an iron protein containing a [4Fe–4S] cluster [192]. The P-cluster of V-Nase is more readily reduced than that of Mo-Nase [193] and perhaps consists of fragmented iron–sulphur clusters rather than being a fully formed cluster [194]. In the resting state of V-Nase the [$VFe_7S_8C(CO_3)$] cluster includes a bridging CO_3^{2-}, which is linked to the protein through cysteine, histidine, and a homocitrate coordinated to V (Figure 6).

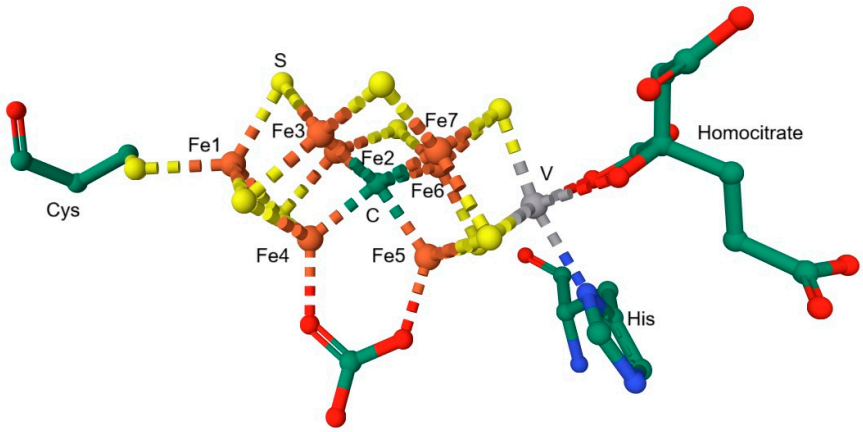

Figure 6. The active site [VFe_7S_8C] cluster of a vanadium nitrogenase (PDB 5N6Y [190]).

Nitrogenases are sensitive to and inhibited by O_2. Recent cryo-EM reports [195,196] show that when O_2 levels increase, a small protein, FeSII, is oxidised and forms a protective complex with two MoFe nitrogenases, and that this can grow into extended filaments. The nitrogenase is inactive under these conditions. Once O_2 levels drop, the complex dissociates as FeSII is reduced, and nitrogenase activity is restored. This protective strategy may well apply to V-Nase as well.

The substrate-reducing site of Mo-Nase contains (formally) three Fe^{2+} and four Fe^{3+} ions, and a d^3 Mo^{3+}, making up a [$MoFe_7S_9C$]$^-$ cluster [197] with a quartet ground state [198], although delocalisation of electron density makes the allocation of charges a moot point. In the substrate-reducing cluster of V-Nase, a carbonate rather than a sulphide bridges two of the iron centres. Vanadium is present as d^2 V^{3+} with $3Fe^{2+}$ and $4Fe^{3+}$ and a triplet ground state [199].

All three nitrogenase enzyme types can perform the reductive elimination of H_2. Details will differ depending on the enzyme type and there is by no means certainty about the mechanistic details.

It is known that N_2 activation occurs after a four-electron reduction of the cofactor (with—formally—all Fe^{3+} reduced to Fe^{2+}) [200]. Two hydrides leave as H_2 just prior to binding of N_2 [201]. There is evidence (for Mo-Nase) of both terminal and bridging S-H stretching frequencies, observed using surface-enhanced infrared absorption spectroscopy on Mo-Nase attached to gold electrodes, which served as the source of electrons for enzyme turnover [202]. A minimal scheme is shown in Figure 7 [203].

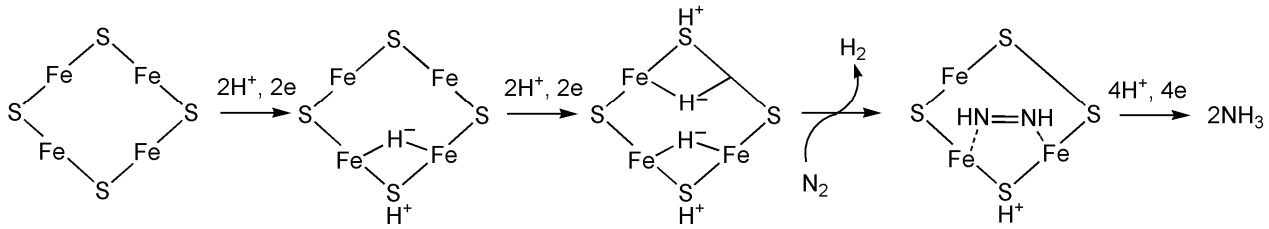

Figure 7. The reductive elimination of H_2 leads to conversion of N_2 to NH_3 by the nitrogenases.

Recent DFT modelling of the mechanism of V-Nase indicates that there is one additional step in V-Nase between the ground state and the state that binds N_2 (referred to as the E_4 state) since V^{3+} can be reduced to V^{2+} whilst the equivalent reduction of Mo^{3+} does not occur. The oxidation state of the cofactor prior to N_2 binding is (V^{2+}, $5Fe^{2+}$, $2Fe^{+}$) in V-Nase but (Mo^{3+}, $5Fe^{2+}$, $2Fe^{+}$) in Mo-Nase; see [198] for details. Another difference is the initial binding site of N_2 in the two enzymes—to Fe6 in V-Nase, but to Fe4 in Mo-Nase; see Figure 6 for the numbering of the Fe atoms. (It should be borne in mind that predictions using DFT methods can depend on the functional and basis set used, as demonstrated when modelling the formation of H_2 during enzyme turnover of Mo-Nase [204].)

The rate-determining step in Mo-Nase, and probably in V-Nase as well, is the protonation of bound N_2. An intermediate in the catalytic cycle of V-Nase featuring a μ^2-bridging ligand, purportedly nitrogen, has been reported [205] and sheds some light on the mechanism of the nitrogenases, although QM/MM calculations [206,207] suggest that it is likely to be OH^- rather than NH^{2-} or NH_2^- that occupies the active site.

Why one equivalent of H_2 is produced by Mo-Nase per enzyme turnover, but three equivalents during V-Nase turnover, is not clear. Clearly, this unproductive step is the penalty paid for having to use vanadium instead of molybdenum under molybdenum-starved conditions.

In addition to the reduction of N_2 to NH_4^+ (Equation (3)), V-Nase, unlike the Mo-dependent enzymes, is also capable of reducing CO and CO_2 to hydrocarbons with chain lengths of 2–7 [189,208–211] (for example, Equations (4) and (5) [212]), and the reduction of alkenes (Equation (6)).

$$2CO + 10H^+ + 10e \rightarrow C_2H_6 + 2H_2O \quad (4)$$

$$CO_2 + H^+ + e \rightarrow \rightarrow C_nH_{2n+2} (+ H_2O) \quad (5)$$

$$C_2H_4 + 2H^+ + 2e \rightarrow C_2H_6 \quad (6)$$

The difference in the chemistry of V-Nase and Mo-Nase is probably a consequence of differences in the overall structure of the protein [190]. The crystal structure of V-Nase with CO bridging two Fe ions of the active site, and replacing one of the sulphides, has been reported [213]. But the formation of a C–C bond implies that two CO molecules must be coordinated to the active site—and the crystal structure of such a complex has indeed appeared (PDB 7AIZ) [209]. The active site is shown in Figure 8.

4.3. Vanadium in Marine and Fungal Systems

Ascidians and fan worms accumulate vanadium from seawater, likely as a defence mechanism against predators [152]. In fan worms, VO^{2+} binds to and suppresses a nucleoside diphosphate kinase, an enzyme which helps maintain the balance of nucleotide pools in the cell [214]. Ascidians take up vanadium in the form of $H_2VO_4^-$; this is reduced to VO^{2+} in two successive steps, and finally by CysMet to V^{3+} after binding to the lysine residues of vanabin (a cysteine-rich vanadium-binding metalloprotein),

Equation (7) [215]. (Cys is the reductant while Met is thought to ensure the structural integrity of the reaction environment).

$$HVO_4^{2-} \xrightarrow{NADPH_2} VO^{2+} \xrightarrow{CysMet} V^{3+} \quad (7)$$

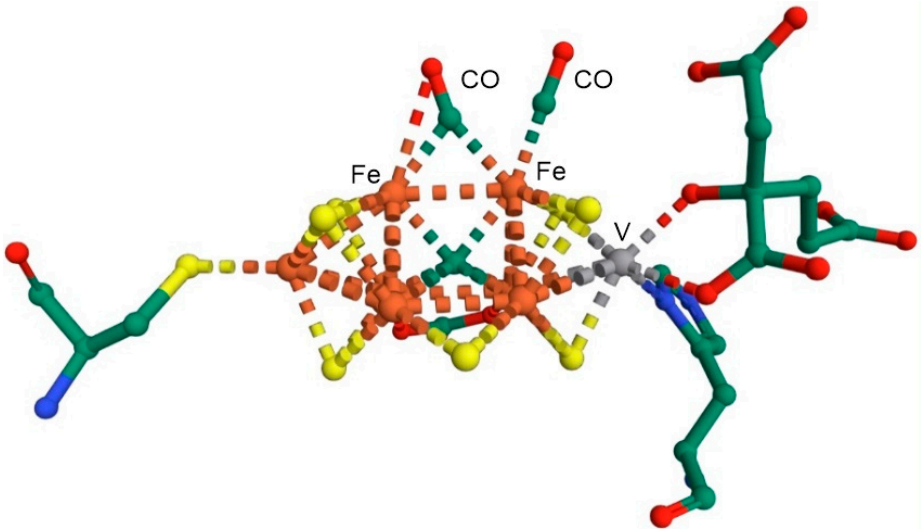

Figure 8. The active site of a V-Nase with two bound CO ligands (PDB 7AIZ [209]).

Accumulated vanadium activates glucose-6-phosphate dehydrogenase, which catalyses the conversion of D-glucose-6-phosphate to 6-phospho-D-glucono-1,5-lactone.

Poisonous *Amanita* mushrooms contain the eight-coordinate V^{4+} complex amavanadin, $[V[NO[CH(CH_3)CO_2]_2]_2]^{2-}$ (Figure 9). The function of amavanadin is unclear [140]; it can act as both a catalase and a peroxidase [140,216,217] (Equations (8) and (9), where the oxidation state of vanadium in amavanadin is shown in each case).

$$4[V]^{5+} + 4H_2O_2 \rightarrow 4[V]^{4+} + 3O_2 + 2H_2O + 4H^+ \quad (8)$$

$$2[V]^{5+} + 2RSH \rightarrow 2[V]^{4+} + RSSH + 2H^+ \quad (9)$$

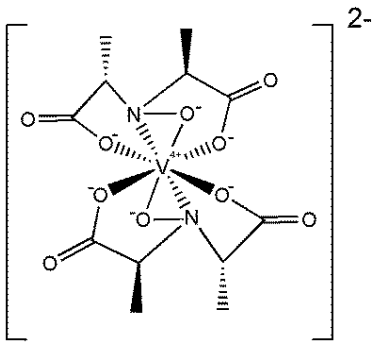

Figure 9. Amavanadin, found in *Amanita* mushrooms.

4.4. Vanadium and Human Biology

As far as is known at present, vanadium plays no essential role in human biology [218]. Vanadium uptake in humans occurs primarily from dietary sources, and it is absorbed from the gastrointestinal tract [219], although other routes are possible [154]. Once absorbed, vanadium is transported in the bloodstream bound to, for example, HSTf [220] or HSA [221].

It can accumulate in inert alia, the liver, kidney, bones, and spleen, although the majority of vanadium is excreted from the body through urine [219].

Vanadium in excess can induce reproductive toxicity in humans [222,223] and in rats [223]. Lipid peroxidation is a metabolic disease caused by the oxidative deterioration of lipids catalysed by reactive oxygen species (ROS) [224,225]. Some vanadium compounds enhance ROS formation (Figure 10, showing formation of hydroxyl radicals as an example), and hence have a deleterious effect on cell structure and function. Superoxide, $O_2^{\bullet -}$, is the result of the one electron reduction of O_2 and is produced by many processes [226].

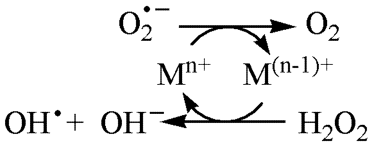

Figure 10. The production of hydroxyl from the reaction of superoxide and hydrogen peroxide, catalysed by a metal ion.

Certain vanadium complexes may exert beneficial physiological effects [227], although their therapeutic potential is often constrained by associated toxicity concerns [228]. For instance, V^{5+}, ($H_2VO_4^-/HVO_4^{2-}$, pK_a = 8.95 [229]) along with a variety of VO^{2+} salts, have been shown to enhance insulin activity in patients with type II diabetes. These effects are primarily mediated through the inhibition of intracellular protein tyrosine phosphatase (PTP-1B) or the activation of cytosolic protein tyrosine kinase (cyt-PTK), thereby promoting the signal transduction pathways involved in glucose uptake [230–232].

Because of the chemical similarity of vanadate and phosphate [218], there is potential for the use of vanadate and vanadium coordination compounds in the treatment of diabetes, cancer, and cardiovascular conditions, probably a consequence of vanadate/phosphate antagonism [154,233]. It is uncertain whether vanadium, in low concentrations, is essential for higher organisms as an antagonist and hence as a regulator of the phosphatases [152].

5. Chromium

Chromium is present in the body in trace amounts (<1.4 μg L^{-1} in human serum; RDA ≈ 30 μg day^{-1} for adults [234]). The biological role of Cr^{3+} remains largely unknown [18,235], though it is widely marketed as a food supplement [236,237], often in forms such as a picolinate, histidinate, or dinicocysteinate complex [238], aimed at weight loss and muscle development. The efficacy of these supplements is contested [35,239,240].

Chromium supplementation is sometimes thought to benefit individuals with insulin resistance [18,241,242], but this too is contentious [243–245]. As Vincent has pointed out, drawing conclusions about human health based upon the results of rat model studies is problematic [246]. Cr^{3+} is believed to enhance insulin activity, aiding glucose uptake into cells and regulating carbohydrate metabolism. Despite this, it is not known to be part of any enzyme's active site. Only about 0.2% of ingested Cr^{3+} is absorbed in the intestine [18], with the rest excreted. In blood, Cr^{3+} binds to HSTf [247,248], with lower affinity than Fe^{3+} (log K_1 = 10.2 M^{-1} and log K_2 = 5.3 [249]) cf. Fe^{3+} (22.7 and 22.1 [55] or 22.5 and 21.4 [56]). While transferrin receptor-mediated endocytosis might mediate cellular uptake, transferrin binding could serve a detoxification role [250].

Cr^{3+} has been associated with the glucose tolerance factor (GTF) derived from brewer's yeast and may facilitate its delivery to cells deficient in this ion [251]. It is also believed to modulate insulin signalling, as well as lipid and carbohydrate metabolism, and to stimulate the synthesis of fatty acids and cholesterol [252]. Chromium deficiency has

been linked to diabetes-like symptoms, impaired growth, reduced fertility, and increased cardiovascular risk [253–255].

Within animal cells, Cr^{3+} binds to a low molecular weight peptide known as the chromium-binding substance (LMWCr), or chromodulin, which comprises Asp, Cys, Glu, and Gly residues [256,257]. This peptide cooperatively binds four Cr^{3+} ions ($K_f = 10^{21}$ M^{-1}, Hill coefficient = 3.47) [258–260], and exhibits a high degree of specificity for Cr^{3+} [261]. Variable-temperature magnetic susceptibility measurements, along with X-ray absorption spectroscopy and EPR studies [262], indicate the presence of a binding site for a single Cr^{3+} ion, as well as an asymmetric trinuclear Cr^{3+} cluster bridged by oxo ligands. The precise physiological role of chromodulin, however, remains speculative.

Cr^{3+}-loaded chromodulin (homochromodulin) binds to the insulin receptor on insulin-sensitive cells, thereby promoting insulin binding [263]. It is proposed that this interaction enhances insulin receptor activity by prolonging tyrosine kinase signalling, ultimately leading to improved glucose uptake [264]. Homochromodulin may thus function as a secondary messenger, amplifying insulin signalling [258]. It is well established that Cr^{3+} is translocated from the bloodstream to peripheral tissues in response to elevated insulin levels [247,258]. The enhancement of insulin receptor β-subunit kinase activity may involve the phosphorylation of three tyrosine residues, along with the activation of downstream effectors such as PI3-kinase and Akt [265,266]. When insulin concentration decreases, homochromodulin is released from the cell to relieve its effect.

Recent evidence [267] indicates that the activity of Cr^{3+} is predominantly in the mitochondria where eight Cr^{3+}-binding proteins have been identified. The proteins are associated with the activity of ATP synthase. The binding of Cr^{3+} supresses its activity and this leads to the activation of adenosine monophosphate-activated protein kinase (AMPK) [268,269], which has been termed the "guardian of metabolism and mitochondrial homeostasis" [270,271]. This activation improves the metabolism of glucose, protecting mitochondria from fragmentation due to hyperglycaemia [272]. It has been argued, though, that how the inhibition of ATP synthase arises is still an open question [273].

Conversely, Cr^{6+} is toxic to virtually all life forms [274–282] and the effect of Cr^{6+} and its biological effects have been extensively reviewed [238,250,283]. Several bacteria (e.g., *Pseudomonas*, *Bacillus*, *Escherichia*) can enzymatically reduce Cr^{6+} to Cr^{3+} using NADH or other electron donors, undoubtedly as a protective mechanism, although this process does generate reactive oxygen species [284–289].

6. Manganese

Manganese is a geochemically abundant transition metal, with an average crustal concentration of approximately 1000 ppm [290]. It is distinguished by its capacity to adopt a wide spectrum of oxidation states, ranging from +2 (as in d^{10} $[Mn(NO)_3CO]$) through to +7 (d^0 as in $[MnO_4]^-$) [135]. Nonetheless, the oxidation states most frequently encountered in nature span from +2 to +7 (see Figure 11). Given both its prevalence and the versatility of its redox chemistry, the centrality of manganese to a range of biological processes is to be expected [291].

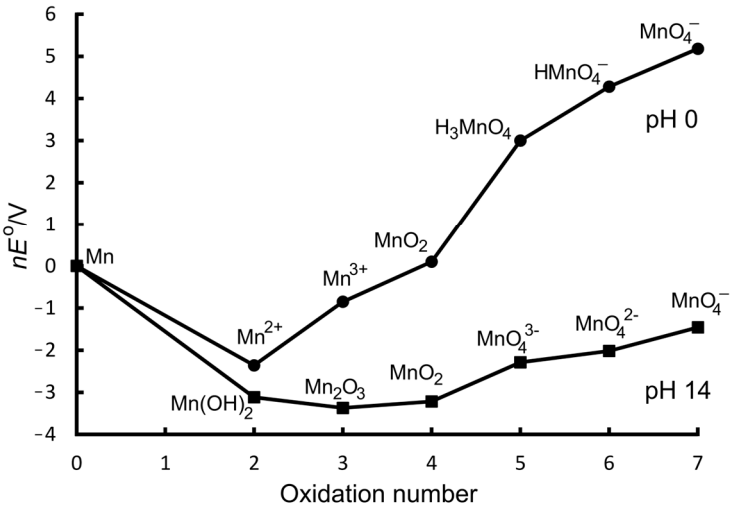

Figure 11. Frost diagram of manganese.

As an essential trace element, manganese is indispensable across diverse biological taxa. In mammals, it plays a critical role in the metabolism of amino acids, lipids, proteins, and carbohydrates, and is also requisite for normal reproductive function [292–294]. A wide array of Mn-dependent enzymes has been characterised, encompassing oxidoreductases, transferases, hydrolases, lyases, isomerases, and ligases [295]. In photosynthetic organisms, manganese assumes a pivotal role within the oxygen-evolving complex (OEC) of the thylakoid membrane in chloroplasts, where it facilitates the terminal photooxidation of water during the light-dependent phase of photosynthesis [296,297].

The most common Mn oxidation states in biological systems are +2, +3, and +4. These states exhibit diverse coordination geometries, predominantly with N and O donor ligands. Ligand identity significantly influences the redox potential of the metal. Mn^{2+} is the most prevalent oxidation state, and it is almost always high-spin ($S = {}^5/_2$); low-spin ($S = {}^1/_2$) Mn^{2+} complexes are known but uncommon due to the high pairing energy required [298–301].

In humans, dietary intake serves as the primary source of Mn, and maintaining Mn homeostasis is crucial to prevent overloading and toxicity [302–306]; overloading affects mostly the brain, altering cognitive functions and locomotion [307–309].

Several transporters are known (or suspected) to facilitate Mn transport within the body [3,292,310–312]. These include the divalent metal ion transporter (DMT-1), which mediates the transport of Fe^{2+} and other divalent metal ions across plasma membranes and out of endosomes [313]; the zinc transporter families ZNT and ZIP [310,311,314]; and HSTf, which transports Mn in its +3 oxidation state [315]. In plasma, most Mn^{2+} binds to globulin and albumin [292].

What follows is a brief discussion of several Mn-dependent enzymes, highlighting the diverse biological functions of this essential metal ion.

6.1. Superoxide Dismutase

Superoxide dismutase (SOD) is a crucial enzyme in a living system's defence against oxidative stress [316]. It is responsible for the conversion of $O_2^{\bullet -}$ to H_2O_2 and O_2 with proton-coupled electron transfer (PCET, Equation (10)).

$$2O_2^{\bullet -} + 2H^+ \rightarrow H_2O_2 + O_2 \quad (10)$$

The formation of reactive oxygen species (ROS), including singlet oxygen $^1O_2$, superoxide $O_2^{\bullet -}$, hydrogen peroxide H_2O_2, and (especially) hydroxyl radical $OH^{\bullet}$, is inevitable

in an oxidising atmosphere and was a challenge that life on Earth had to overcome to survive [317]. The main challenge is $OH^{\bullet}$ which reacts virtually indiscriminately with many biomolecules, including DNA, membranes, and proteins [318].

ROS production is sometimes (mistakenly) attributed to the Haber–Weiss cycle, catalysed by a metal ion complex [M^{n+}] (Equations (11)–(13)).

$$[M^{n+}] + O_2^{\bullet -} \rightarrow [M^{(n-1)+}] + O_2 \quad (11)$$

$$[M^{(n-1)+}] + H_2O_2 \rightarrow [M^{n+}] + OH^{\bullet} + OH^{-} \text{ (Fenton reaction)} \quad (12)$$

$$O_2^{\bullet -} + H_2O_2 \rightleftarrows O_2 + OH^{\bullet} + OH^{-} \text{ (net Haber–Weiss reaction)} \quad (13)$$

However, $O_2^{\bullet -}$ reacts faster with itself than with H_2O_2 [319,320]. The Fenton reaction is important because it initiates a chain reaction (Equations (14) and (15)), which is then terminated (Equation (16)).

$$OH^{\bullet} + H_2O_2 \rightarrow O_2^{\bullet -} + H_2O + H^{+} \quad (14)$$

$$O_2^{\bullet -} + H_2O_2 + H^{+} \rightarrow O_2 + H_2O + OH^{\bullet} \quad (15)$$

$$[M^{(n-1)+}] + OH^{\bullet} + H^{+} \rightarrow [M^{n+}] + H_2O \quad (16)$$

Given this crucial role, SODs are widespread in living systems. Some bacteria have an MN-SOD [321,322]. Mn-SOD is found in the mitochondrial matrix of eukaryotes; it role is vital for maintaining the viability of mitochondria [323], having to deal with the $O_2^{\bullet -}$ produced by electrons leaking from the mitochondrial electron transport chain [324]. A SOD with a Cu-Zn active site is found in the extracellular matrix and cytosol of eukaryotes [325,326]. Superoxide dismutases are key to preserving health [327–329]. Fe-SODs are found in bacteria and the chloroplasts of plants [330–332]. A Ni-SOD is found in prokaryotes [333].

SOD is an example of an oxidoreductase enzyme that couples the concerted transfer of protons and electrons (PCET). The overall reaction catalysed by Mn-SOD is given in Equations (17) and (18) [334].

$$Mn^{3+} + O_2^{\bullet -} \rightarrow Mn^{2+} + O_2 \quad (17)$$

$$Mn^{2+} + O_2^{\bullet -} + 2H^{+} \rightarrow Mn^{3+} + H_2O_2 \quad (18)$$

In a typical Mn-SOD, the metal ion has a distorted trigonal bipyramidal structure with three His, one Asp, and an H_2O (or OH^{-}) as ligands (Figure 12). The outer coordination sphere of human Mn-SOD contains five amino acid residues (two Tyr, His, Gln, and Glu, which is itself hydrogen-bonded to a Trp) which may be important in proton shunting to the active site.

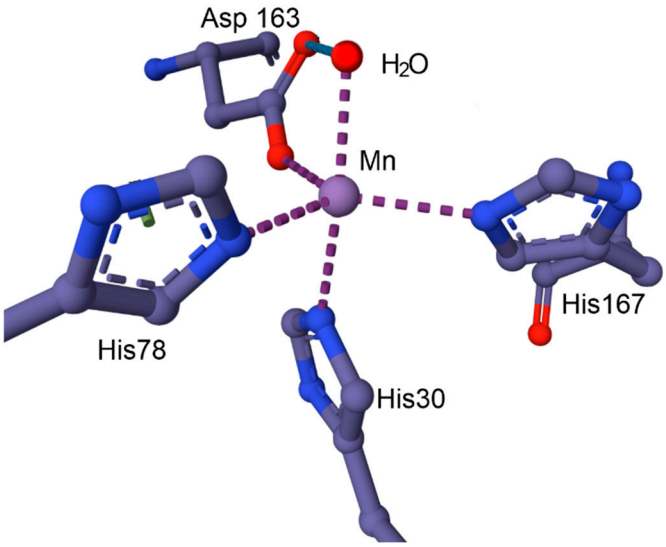

Figure 12. The active site of Mn-SOD from *Trichoderma reesei* [335].

It has been suggested that the substrate binds opposite the Asp ligand to form a six-coordinate intermediate [336–338]. An alternative suggestion [339,340] is that the substrate displaces Asp from the metal's coordination site and that the six-coordinate complex, observed with ligands such as N_3^- [341], is actually an inactive form of the enzyme. Lys and Arg residues form a positive surface near the active site and are thought to contribute electrostatically to guiding the substrate to the metal ion [342].

Using the results from neutron diffraction studies, a possible mechanism for the coupling of proton transfer to electron transfer in human Mn-SOD has been proposed recently from the direct visualisation of active site protons in the Mn^{2+} and Mn^{3+} redox states of the enzyme [343]. Proton transfer occurs among the coordinated H_2O, a solvent H_2O, and amino acids (two Tyr, a His, and Glu) that constitute the secondary coordination sphere of the metal ion and is driven by changes in the metal's oxidation state as it cycles between Mn^{3+} and Mn^{2+} (Figure 13). It is still unclear whether the reactions proceed through an inner sphere mechanism where there is direct bonding between the metal and $O_2^{\bullet-}$ and O_2 in the second step (as shown in Figure 13), or whether the reactions proceed through an outer sphere mechanism [325,342,344]. Indeed, QM/MM calculations, complemented with CASSCF/CASPT2/MM single-point energy calculations, suggest that the first step proceeds through an inner sphere mechanism, and the second step through an outer sphere mechanism with His or Tyr serving as proton donors for the formation of H_2O_2 [345].

There is a potential problem having an enzyme that generates H_2O_2: whilst it is important as a signalling molecule [346], over-production will lead to deleterious effects. For example, H_2O_2 is a potent apoptotic agent and there is a causal link between cellular H_2O_2 and enhanced apoptosis, the driving force behind auto-antigenic exposure and chronic immune activation in systemic lupus erythematosus [347]. Fortunately, MnSOD is itself inhibited by H_2O_2, ensuring a steady-state H_2O_2 concentration. In the inhibited state, HO_2^- replaces the OH^- ligand of the resting state of the enzyme [348]. A disturbance of this steady-state concentration is characteristic of several diseases [349].

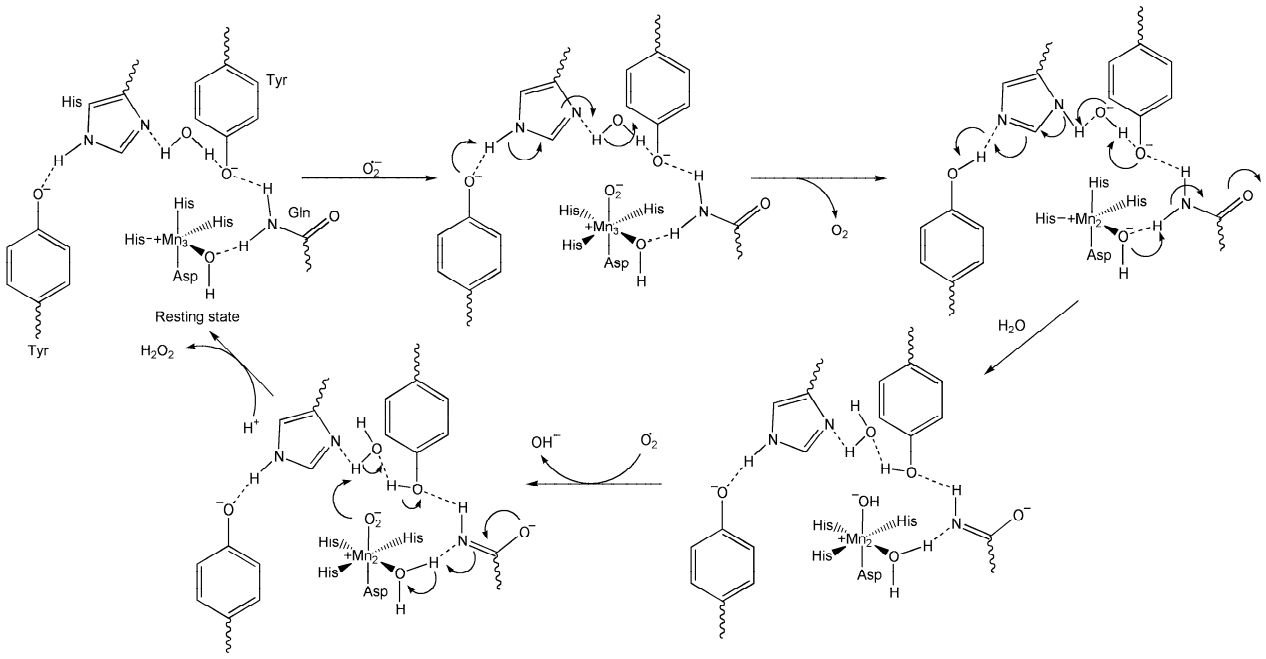

Figure 13. A possible mechanism, based on neutron diffraction observations, for the action of Mn-SOD, converting two equivalents of superoxide to hydrogen peroxide and oxygen during each enzyme turnover [343]. The movement of protons is a response to the change in the oxidation state of the metal.

6.2. Photosystem II

Possibly one of the earliest uses of manganese by living systems was in Photosystem II (PSII, water-plastoquinone oxidoreductase) [291,350], a system responsible for using light to oxidise water to O_2 and four reducing equivalents (Equation (19)) and located in the thylakoid membrane of cyanobacteria, plants, and algae. Manganese deficiency is detrimental to the growth of crops [351].

$$2H_2O \xrightarrow{h\nu} O_2 + 4e + 4H^+ \quad (19)$$

In the process, protons are pumped into the lumen, and the proton gradient thus created is used to drive the synthesis of ATP by ATP synthase. A schematic of the redox-active cofactors and the electron transfer chain in PSII of cyanobacteria is given in Figure 14 (adapted from [352]).

Light energy is captured by antenna complexes, known as light-harvesting complexes (LHC) in plants, typically composed of (bacterio)chlorophylls and (bacterio)pheophytins [353]. This energy is then transferred to the two branches, D1 and D2, of the reaction centre (RC). The D1 branch contains the oxygen-evolving complex (OEC), which features a cubic Mn_3CaO_5 structure with an additional Mn ion connected through a μ-oxo bridge (Figure 15). How the manganese cluster is assembled has been reviewed and summarised [354]. The LHC can respond to a variation in energy flux. Under conditions of high light intensity, quenching mechanisms are activated to prevent photodamage [355–358]. Replacement of Mn by one or more Fe ions leads to a decrease in activity (with 3 Mn and 1 Fe) or activity but only as far as producing H_2O_2 rather than O_2 [359]. Mn is clearly essential for optimum functioning of the LHC.

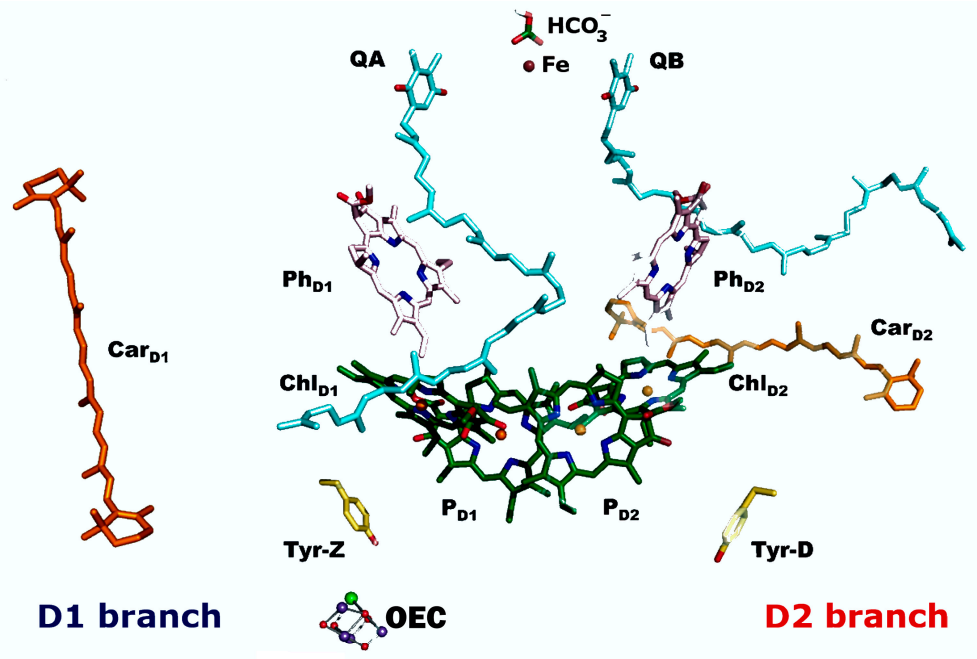

Figure 14. The D1 and D2 branches of PSII (adapted from [352]).

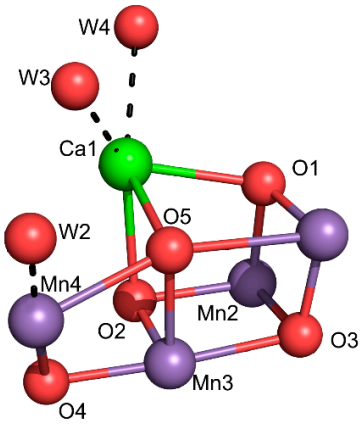

Figure 15. The OEC of PSII from the cyanobacterium *T. vulcans*, PDB code 3WU2 [360]. W = H_2O. Adapted from https://commons.wikimedia.org/w/index.php?curid=47294160, accessed on 16 February 2025.

The OEC structure is nearly identical across plants, algae, and cyanobacteria, suggesting it dates to the early evolution of photosynthetic organisms that triggered the Great Oxidation Event approximately 2.7 billion years ago. This event transformed Earth's atmosphere from mildly reducing to oxidising [361–363]. The OEC is surrounded by amino acid residues, including tyrosine Y_Z, two Cl^- ions (which are essential for electron transfer from H_2O to the manganese cluster, probably by blocking a proton exit channel [364–366]), and several water molecules [360,367–370]. Additionally, the RC houses a "special pair" of chlorophyll-*a* molecules (P_{D1} and P_{D2}), two chlorophyll-*a* molecules (Chl_{D1} and Chl_{D2}), two pheophytin-*a* molecules (Ph_{D1} and Ph_{D2}), two quinones (Q_A and Q_B), and a bicarbonate ion coordinated to a non-haem iron. The D_1 branch also contains a carotenoid, Car_{D1}.

Charge separation occurs at Chl_{D1} (commonly referred to as P680) upon the absorption of light. Photoexcited P680* reduces pheophytin Phe_{D1}, initiating a series of electron transfers via Q_A and Q_B that ultimately reduce a plastoquinone. $P680^+$ is a potent oxidant ($E \approx -1.3$ V) and oxidises tyrosine Y_Z. The oxidised tyrosine drives the cyclic mechanism responsible for oxidising H_2O to O_2 within the OEC. Changes in protein conformation are

important for controlling the entire process and in effect control the rate of electron transfer of the system [371,372].

Water oxidation in the OEC proceeds through five distinct S states: the Kok–Joliot cycle (Figure 16) [373]. With each step, the Mn_4CaO_5 cluster in the OEC is incrementally oxidised, and after the fourth step, O_2 is released. Electrons from the cluster are transferred via Tyr_Z to $P680^+$, reducing it back to P680, thereby completing the cycle. The role of Ca^{2+} appears to be to stabilise a hydrogen bonding network connecting two water molecules with tyrosine Y_Z [374,375], and substitution with other metal ions leads to decrease in activity (when Ca^{2+} is substituted by Sr^{2+}) or no activity at all (when substituted by other cations). The oxidation of Tyr_Z lowers the energy barrier for proton transfer from the OEC along a pathway of conserved carboxylate groups and water molecules [366]. There is evidence that some singlet oxygen, $^1O_2$, may be produced as an unwanted product of the process of O_2 evolution [376].

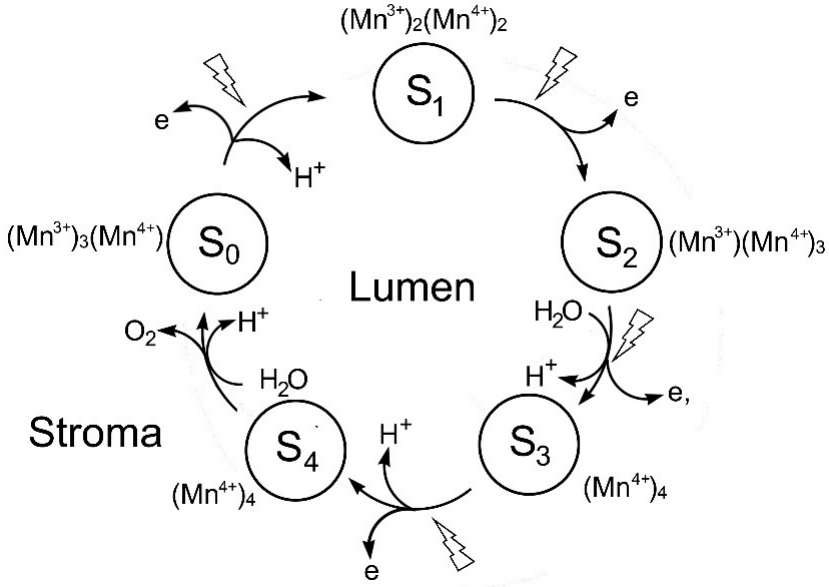

Figure 16. The Kok–Joliot cycle of the OEC of PSII with *possible* oxidation states of the four Mn ions [377,378]. While there is general agreement on the structures of S_0, S_1, and S_2, the structures of S_3 and S_4 are uncertain.

The oxidation states of Mn in each of the five states is still a matter for conjecture and the subject of ongoing research, undoubtedly prompted not only by the desire to understand one of the fundamental reactions of nature, but also by the promise (hope?) that such knowledge may be invaluable in the development of artificial photosynthesis systems as we move (and we must!) from a carbon-based energy economy [354,379]. The "low oxidation (LO)" model features an $(Mn^{3+})_3(Mn^{4+})$ cluster, whilst the "high oxidation (HO)" model features an $(Mn^{3+})(Mn^{4+})_3$ cluster [380–382]. Evidence from photoactivation of PSII microcrystals suggests that the S_0 state corresponds to $(Mn^{3+})_3(Mn^{4+})$, the S_2 state to $(Mn^{3+})(Mn^{4+})_3$, and the S_3 state to $(Mn^{4+})_4$ [383]. This is supported by computational modelling [384]. For a detailed analysis of the S_2 state, see [385]. The S_4 state is a transient intermediate, and its structure is uncertain [377,378]. Details of the S_1–S_2–S_3 transitions obtained using serial femtosecond crystallography (SFX) have recently become available [379,386]. SFX captures snapshots of proteins in action at near-atomic resolution whilst avoiding the inevitable damage from X-rays in traditional XRD methods [379]. For a comprehensive review of the literature on structure determination of the Mn_4CaO_5 cluster from experimental and computational methods, see [379].

One possible mechanism is shown in Figure 17, using the HO model. The formation of the O-O bond occurs in S_4. For another possible mechanism, based on quantum chemical calculations, see [387]. An alternative proposal invokes the +3, +4, and +7 oxidation states of Mn [378]—all well-established stable oxidation states of the metal (Figure 11). Whatever the mechanism of the reaction, it is clear that what is being exploited to effect the oxidation of H_2O to O_2 are the variable oxidation states of manganese [388].

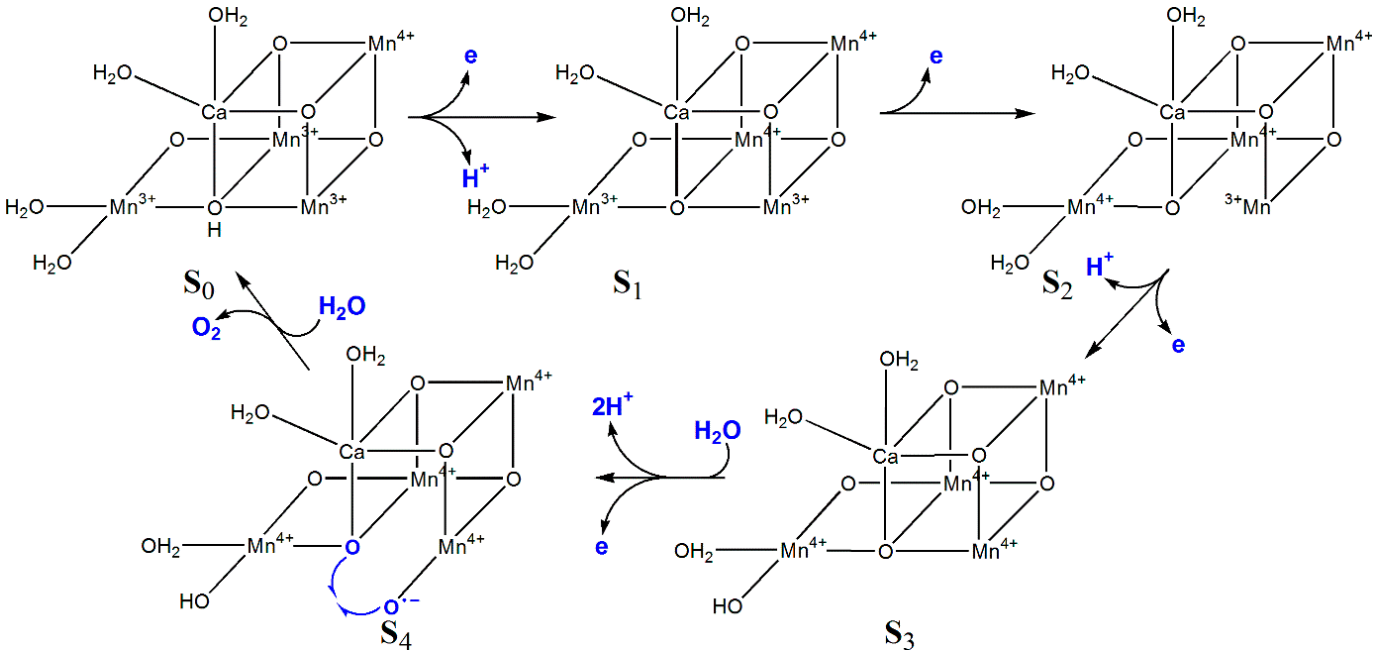

Figure 17. A possible mechanism for the evolution of oxygen at the OEC. (Adapted from [377]).

6.3. Examples of Other Mn-Containing Enzymes That Involve a Change in the Metal's Oxidation State

Iron is much more commonly used than manganese in metalloenzymes where there is a change in the oxidation state of the metal during enzyme turnover, perhaps because of its greater natural abundance during the early stages of the evolution of life and its lower redox potential [291]. Nevertheless, there are many enzymes that use the redox chemistry of manganese. Some illustrative examples follow.

6.3.1. Ribonucleotide Reductase (RNR)

There are three classes of these enzymes; they all catalyse the conversion of nucleotides to deoxynucleotides, the building blocks of DNA [389]. The reactions involve the generating of a Cys radical by some means, and all RNRs basically follow the same reaction mechanism (Figure 18) [390].

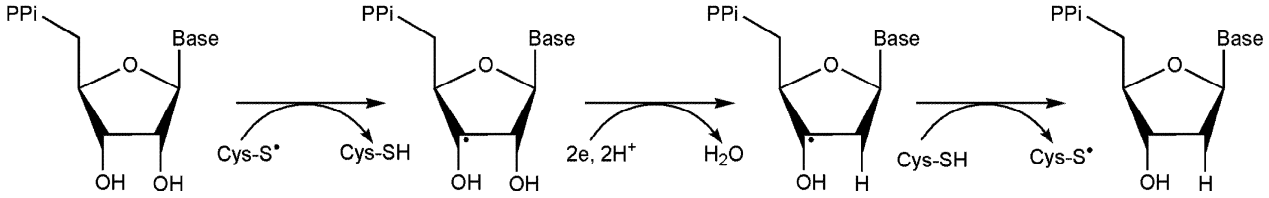

Figure 18. The reaction mechanism of a ribonucleotide reductase. A Cys• radical initiates the reaction by abstracting the 3′-H of the substrate; the reaction is initiated by a one-electron oxidation. Ribose 2′-OH is released as water on a two-electron reduction. The abstracted H, present on Cys, is returned to the 3′ position and the Cys• radical is regenerated.

The capacity to generate the reactive Cys• is stored remotely within the enzyme, spatially separated from the relatively accessible active site. The precise location of this radical-generating machinery varies among the three classes of RNRs [391,392].

Class I RNRs are heterodimeric enzymes composed of two distinct subunits. The larger subunit, variously designated R1, NrdA, or NrdI, is the site of ribonucleotide reduction, whereas the smaller subunit (R2, NrdB, or NrdF) is responsible for radical generation. In the latter, a stable tyrosyl radical is located in proximity to a binuclear metal centre. Class I RNRs are further categorised into five subclasses, based on the metal composition of the bimetallic site [393].

Class II RNRs generate the required radical through homolytic cleavage of the Co–C bond in adenosylcobalamin, [AdoCbl], whereby the resulting adenosyl radical (Ado•) directly initiates the formation of Cys• [394].

By contrast, Class III RNRs utilise a distinct mechanism involving the reductive cleavage of the 5′-C–S bond in S-adenosyl-*L*-methionine, catalysed by a dedicated activating enzyme. The resulting Ado• radical generates a glycyl radical (Gly•), which in turn oxidises a Cys residue in a reversible manner.

A schematic representation of tyrosyl radical generation near a dimanganese centre in the Class Ib RNR from the Gram-positive bacterium *Bacillus subtilis* is shown in Figure 19 [395]. Unlike the diiron variants of Class Ib RNRs, dimanganese enzymes are unreactive towards O_2. Instead, they require the reduced form of a flavodoxin-like protein, $NrdI_{hq}$ (hq = hydroquinone), which is oxidised to the semiquinone form, $NrdI_{sq}$ (sq = semiquinone), and in the process reduces O_2 to $O_2^{\bullet-}$ [396]. The superoxide radical subsequently interacts with the bimetallic centre to form an Mn^{3+}–(O)(OH)–Mn^{4+} intermediate, which serves to oxidise a nearby tyrosine residue to yield Tyr•.

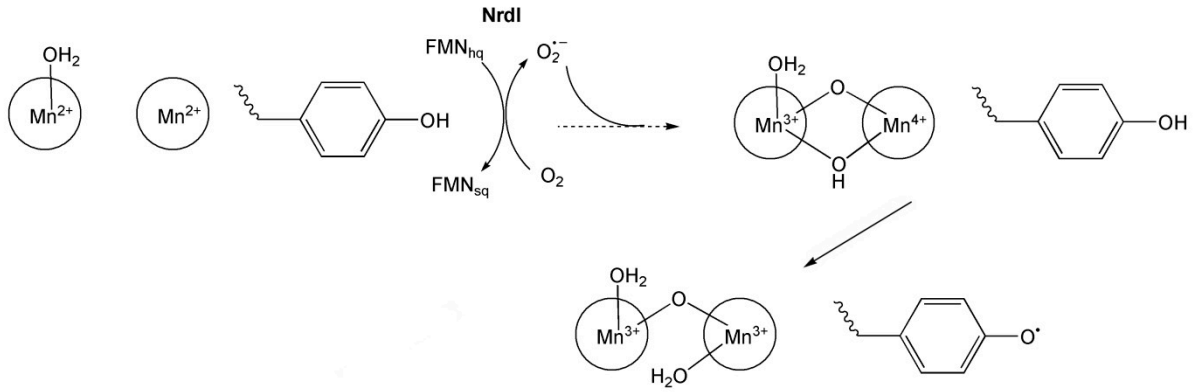

Figure 19. In the class Ib RNRs, a tyrosyl radical is generated near a di-Mn centre. This initiates the formation of Cys• (Figure 18). Adapted from [389].

The crystal structure of NrdI from *Mycobacterium tuberculosis* has been elucidated [396], revealing a channel extending from the protein surface to the buried flavin mononucleotide (FMN) cofactor. This structural feature likely facilitates O_2 access to FMN, where it undergoes reduction to form $O_2^{\bullet-}$.

The use of femtosecond crystallography with an X-ray-free electron laser (to avoid photoreduction) on the NrdI complex from *Bacillus cereus* showed that the FMN moiety is sterically strained, which probably tunes its redox potential to be able to reduce O_2 [397].

There is evidence for such a mechanism from model complexes. Using [$Mn^{2+}{}_2$(TPDP)(O_2CPh)$_2$](BPh4) (TPDP = 1,3-bis(bis(pyridin-2-ylmethyl)amino)propan-2-ol, Ph = phenyl), Doyle et al. observed the formation of a peroxido-$Mn^{2+}Mn^{3+}$ species on its reaction with $O_2^{\bullet-}$ [398]. It is very likely that such a complex precedes the cleavage of the O-O bond and formation of the $Mn^{3+}Mn^{4+}$ complex shown in Figure 19 which then generates the tyrosyl

radical. Indeed, formation of both a peroxido Mn^{2+}-O-O-Mn^{3+} species and the subsequent formation of an Mn^{3+}-(μ-O)(μ-OH)-Mn^{4+} species on addition of an H^+ donor was observed with a different model compound [399].

There are many variations. The class Ic RNR from the bacterium *Chlamydia trachomatis*, for example, contains a Phe rather than a Tyr near an Mn^{2+}/Fe^{2+} cluster [400,401]. Using Mn instead of Fe provides the enzyme with an oxidised Mn^{4+}/Fe^{3+} cluster that has sufficient oxidising power to generate $Cys^{\bullet}$ [401]. Pulsed multifrequency EPR spectroscopy of the enzyme from *Geobacillus kaustophilus* provided evidence of an MN^{3+}-(μ-O)(μ-OH)-Fe^{3+} species [402].

The class Id RNRs from the bacteria *Facklamia ignava* and *Leeuwenhoekiella blandensis* use a similar strategy, but with an MN^{4+}/Mn^{3+} cluster to directly generate $Cys^{\bullet}$ without intermediate formation of $Tyr^{\bullet}$ [403]. In this case, Tyr is directed away from the bimetallic site, with a Lys residue occupying its usual position. The class Id RNRs do not react directly with O_2, but instead with one equivalent of $O_2^{\bullet-}$ or two equivalents of H_2O_2 in addition to a one electron reduction. Clearly, manganese is a useful, but not essential, element to carry out the RNR reactions.

6.3.2. Manganese Peroxidase

The manganese peroxidases (MnPs) are oxidoreductase enzymes produced by white-rot fungi and some bacteria [404,405]. White-rot fungi play an important role in the degradation of solid organic matter in ecosystems [406]. The MnPs are primarily responsible for degrading lignin; their activity has been employed for treating organic pollutants and other contaminants in wastewater streams [405,407,408] and for the biological pre-treatment of biomass [409]. They may be useful for the control of mycotoxins, an important issue in global food safety [410].

A representative of the active site of a manganese peroxidase is shown in Figure 20. (There is some variability in the structure of the active site of these enzymes [404].) The active site comprises an iron porphyrin and an MN^{2+} ion bound in an octahedral environment by one of the porphyrin propionates, two Glu, one Asp, and two H_2O molecules.

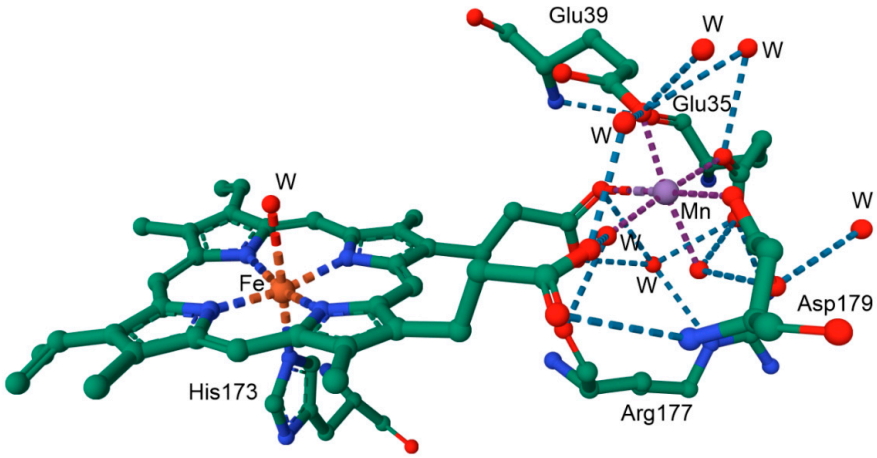

Figure 20. The active site of manganese peroxidase from *Phanerochaete chrysosporium*. W = H_2O. PDB code 3M5Q [411].

MnP features an MN^{3+} chelate as a mobile oxidising agent. The reaction begins with the two-electron oxidation of the iron porphyrin by H_2O_2 to form an iron hydroperoxide intermediate [412]. Loss of H_2O leads to the formation of an [Fe^{4+}=O]–$Porph^{\bullet+}$ species (referred to as Compound I in the catalytic cycle of the peroxidases). Compound I oxidises one equivalent of Mn^{2+}, complexed by a suitable chelating agent (oxalate, tartrate, lactate, mal-

onate, for example), producing [Fe^{4+}=O]–Porph, Compound II. The Mn^{3+} is then released from the enzyme and replaced by Mn^{2+}. Compound II in turn oxidises Mn^{2+} and a second Mn^{3+} chelate is released (Figure 21). The Mn^{3+} chelate acts as a one electron oxidant for a variety of substrates in the environment, including phenols, amines, aromatics, carboxylic acids, thiols, and unsaturated fatty acids. The enzyme, as well as other enzymes such as lignin peroxidase and laccase, may be useful to tackle the degradation of polyethylene and other plastics, which is a serious environmental problem [413–415]. Manganese peroxidase enzymes are known which have Mn^{2+}-independent activity, albeit at significant slower rates [416]. Mn^{2+} is therefore important, but not essential, for the activity of these enzymes.

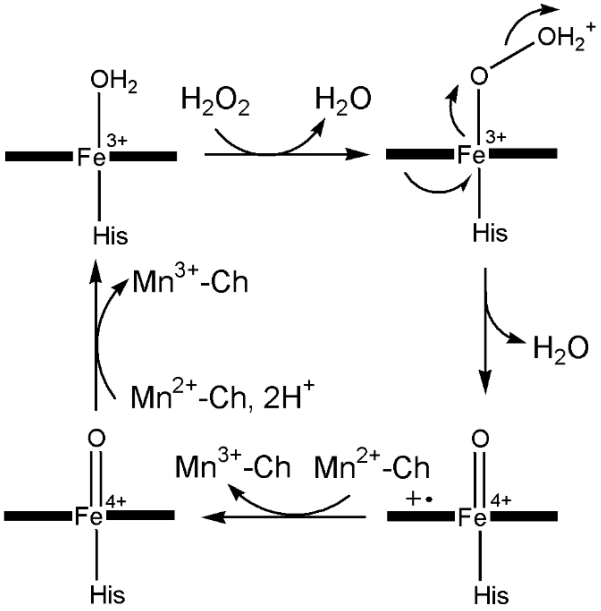

Figure 21. Oxidation of chelated Mn^{2+} to Mn^{3+} by H_2O_2, catalysed by an iron porphyrin.

6.3.3. Manganese Lipoxygenase

Lipoxygenases (LOXs) catalyse the oxidation of polyunsaturated fatty acids to hydroperoxides [417]. These non-haem enzymes are widespread in nature [418,419]. The active site metal in LOXs of animals, plants, and prokaryotes contain iron; in fungi, both iron-containing and manganese-containing LOXs are found. A simplified scheme of a typical LOX-catalysed reaction is shown in Figure 22 [420].

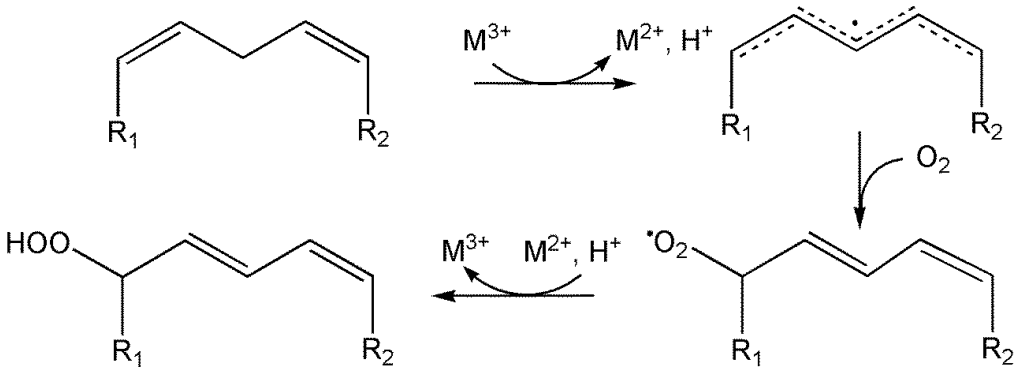

Figure 22. A LOX-catalysed oxidation of a polyunsaturated fatty acid. M = Fe or Mn.

The metal binding site of Mn-LOX from *Pyricularia oryzae* is shown in Figure 23. The metal ion (Fe^{3+} or Mn^{3+}) extracts an electron from a 1,4-diene, and a base abstracts the proton. O_2 reacts with the resultant organic radical, forming a peroxyl radical. This

abstracts an electron from the reduced metal ion, and picks up a proton from the base, regenerating M^{3+} (M = Fe or Mn) [421].

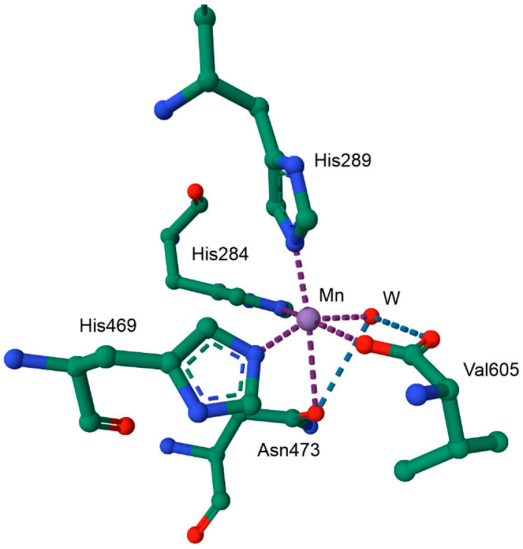

Figure 23. The binding of Mn in LOX (PDB code 5FNO) [422]. W = H_2O.

6.4. Examples of the Non-Redox Bioinorganic Chemistry of Manganese

In addition to exploiting manganese's rich redox chemistry, nature also uses it as a Lewis acid.

The glycosyltransferases and glycosidases catalyse the assembly, processing, and turnover of glycans such as cellulose [423,424]. One example of such an enzyme is *β*-1,4-galactosyltransferase-1. It catalyses the transfer of galactose from the donor, uridine 5′-(*α*-D-galactopyranosyl diphosphate) to the acceptor, *N*-acetylglucosamine, producing *N*-acetyl-lactosamine [425]. Mn^{2+} acts as a Lewis acid in the enzyme.

One possible mechanism envisages Mn^{2+}, bound to the diphosphate of the donor, helping to generate an oxocarbenium ion-like transition state in an S_N2 reaction (Figure 24) [426]. (Other mechanisms, including an S_N1 mechanism, are feasible [427].)

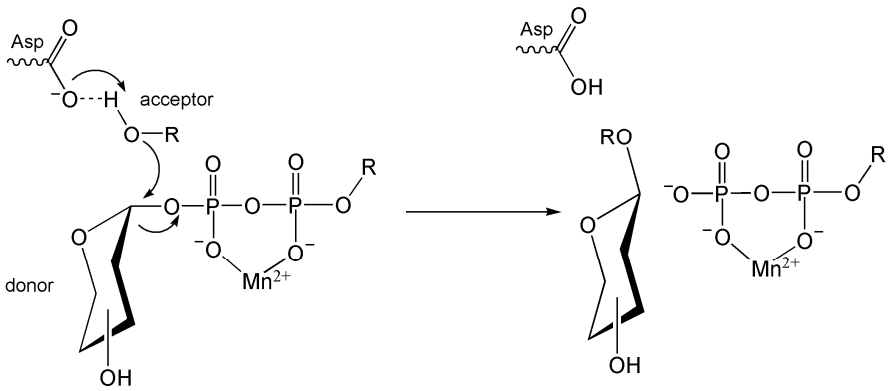

Figure 24. The Lewis base properties of Mn^{2+} exploited to enable attack of ROH to form a new β-1,4-glycosidic bond. An Asp residue in the active site is essential. Adapted from [427].

Arginase is an enzyme in the urea cycle responsible for the hydrolysis of arginine to urea and ornithine (Equation (20)) [428,429]. It performs important cellular functions in the cardiovascular system [430]. Arginase contains a binuclear Mn^{2+} site (Figure 25). The metal ions are important not only for catalysis, but also for maintenance of the proper geometry of the active site [431]. The two Mn^{2+} ions are bridged by H_2O (or OH^-). It is

this coordinated OH^- that initiates a nucleophilic attack on the substrate which is bound nearby (Figure 26); see also [428,432].

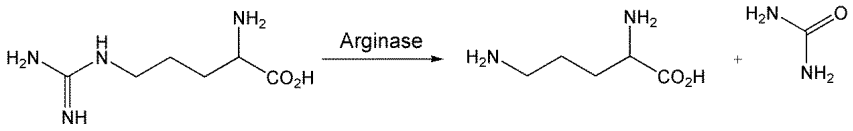

(20)

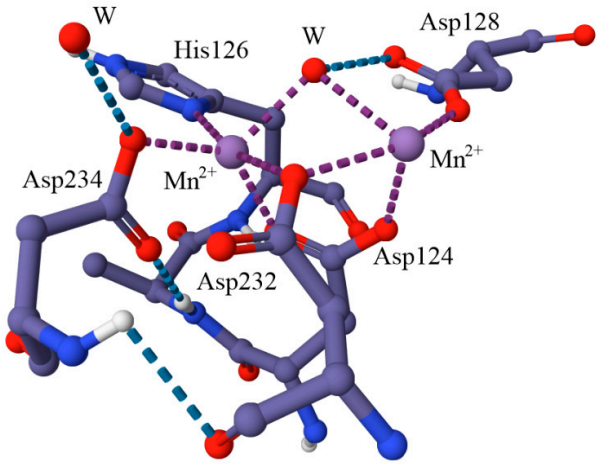

Figure 25. The bimetallic active site of arginase from rat liver (PDP code 1RLA [433]). W = H_2O (or OH^-).

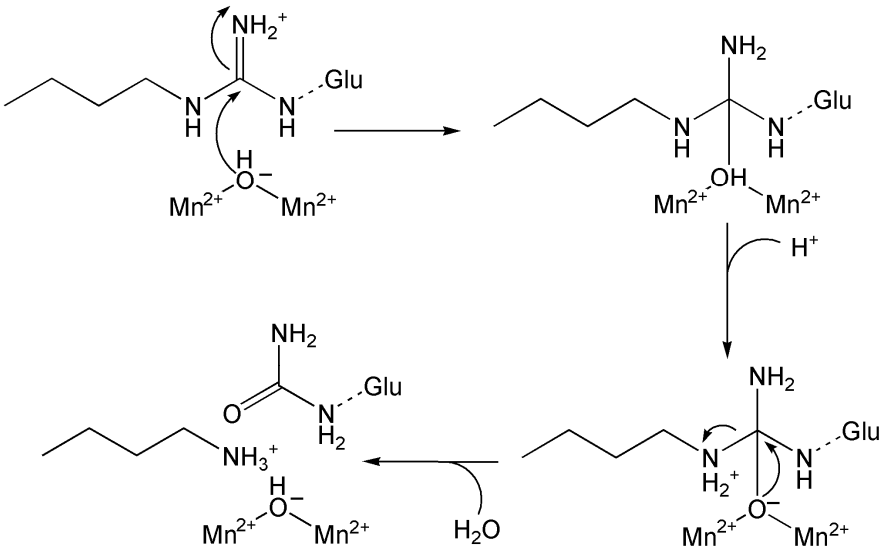

Figure 26. Proposed mechanism for the breakdown of arginine to ornithine and urea by arginase [428,432]. The attacking nucleophile is a metal-activated hydroxide.

7. Iron

Iron-containing systems fulfil many functions in biology [434–439]. Among these are the haem proteins responsible for the transport and storage of dioxygen [440–444]; electron transport [445–447]; redox partners to other enzymes [448–451]; and as catalysts in the oxidases [452–455], peroxidases [453,456–459], catalases [460–462], and the superfamily of the cytochromes P450 [453,463–466] (Figure 27); in photosynthesis [467–469]; and (using siroheme, a porphyrin with reduced A and B rings in the reduction of ni-

trite [470–472] and sulphite [472–474]). The uptake of iron, and its haemostasis, is crucial for human health [475–477].

The predominant oxidation states of iron in biological systems are Fe^{2+} and Fe^{3+}, though Fe^{4+} appears transiently during the reaction cycles of some haemoproteins. Iron-containing complexes are ubiquitous in electron transfer reactions within living organisms. Fe^{3+} is a hard metal ion, preferring hard donor ligands (e.g., hydroxyl, ether, and carboxylate groups), while Fe^{2+}, with intermediate hardness, favours nitrogen and sulphur donors. Both oxidation states exhibit diverse coordination geometries, typically four-, five-, or six-coordinate.

The redox potential of an iron centre can be manipulated by varying the ligands, the coordination geometry, and the environment of the complex, thus affording redox potentials virtually across (or at least near) the entire range of nature's ambient "electrochemical window" (in an aqueous environment, potentials between the oxidation of H_2O with evolution of O_2 and the reduction of H^+ to produce H_2; under standard conditions at pH 7 this is +817 mV and −413 mV, respectively.) Both Fe^{3+} and Fe^{2+} are relatively labile (rate constants for H_2O exchange typically 10^2 and 10^6 s^{-1} [478]), and this facilitates rapid ligand exchange when this is required.

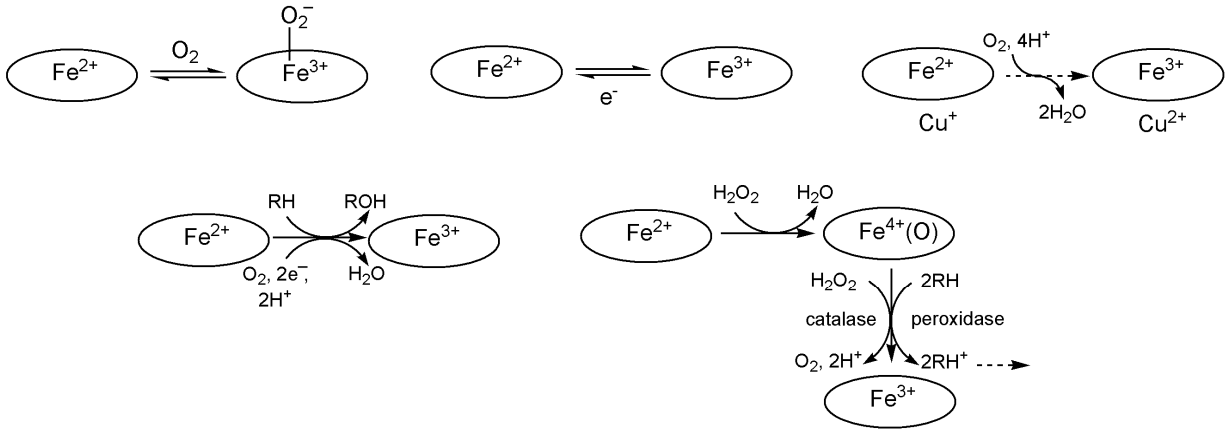

Figure 27. Examples of the roles played by haemoproteins (adapted from [479]).

Iron is abundant on Earth, constituting some 80% of its inner and outer cores [480] and ranks as the fourth most abundant element in the crust [481]. Before the Great Oxidation Event approximately 2.7 billion years ago, Fe^{2+} was abundant in Earth's oceans. However, the GOE, driven by oxygenic photosynthesis by cyanobacteria, transformed the atmosphere from reducing to oxidising [482–485]. (While the advent of the GOE is generally accepted, there is an intriguing recent report on the generating of "dark oxygen"—oxygen produced in the absence of sunlight—in the deep ocean due to a potential difference of up to 950 mV in polymetallic modules which can lead to the electrolysis of water [486].) Fe^{3+} is much less soluble than Fe^{2+} ($K_{sp} \approx 10^{-39}$, pH 7 [487]), so obtaining this essential metal from the environment was essential. Prokaryotes developed chelators such as ferrichromes and siderophores to bind Fe^{3+} and facilitate its uptake [488–490]. For example, ferrichromes are found among fungi, yeasts, and moulds; bacteria tend to use chelates based on catechols. These ligands feature hard donors to complex hard Fe^{3+} (Figure 28).

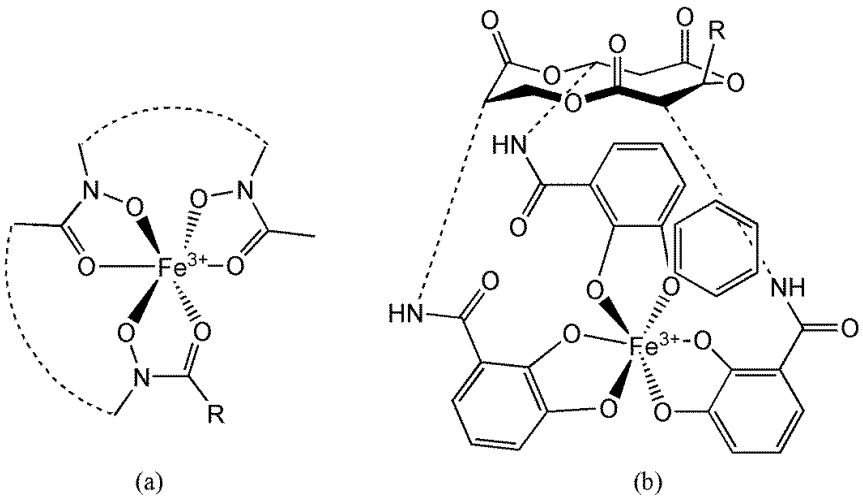

Figure 28. A schematic representation of (**a**) a ferrichrome chelate and (**b**) a catechol chelate for Fe^{3+}.

In humans, iron is absorbed in the duodenum and proximal jejunum and is transported by HSTf before being stored in ferritin within the liver, spleen, bone marrow, and other tissues [491]. This tightly regulated process is essential for maintaining iron homeostasis, a critical aspect of human health [492–494]. Iron plays an important role in ferroptosis, a regulated form of cell death [495,496].

HSTf contains two binding sites, one in the N- and the other in the C-lobe of the protein; the sites have a high affinity for Fe^{3+} (log K_1 = 22.7 and 22.1 [55] or 22.5 and 21.4 [56] and $E_{1/2} < -500$ mV [497]). The binding site consists of two Tyr, His, Asp, and a carbonate anion (Figure 29). Carbonate, through hydrogen bonding, modulates the structure of the protein to ensure a high affinity for Fe^{3+}. On binding to the Tf receptor on the cell surface membrane, the acidic environment leads to loss of CO_3^{2-}, and $E_{1/2}$ is then raised by >200 mV, facilitating release of iron as Fe^{2+}, since Tf has a relatively low affinity for this ion (log K = 7.6 [498,499]).

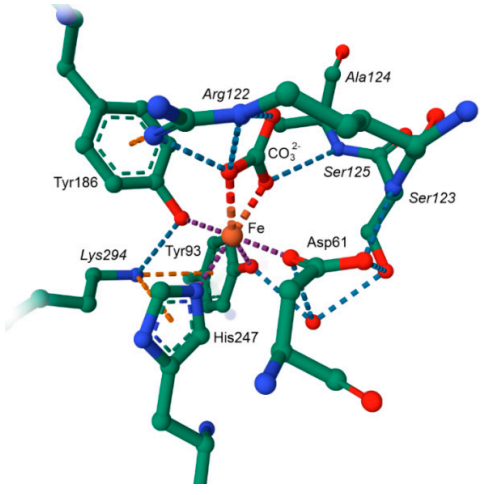

Figure 29. The iron binding site of Tf.

The haemoproteins containing iron coordinated to a porphyrin are used for the transport and storage of O_2, for its activation, and for electron transfer. Some examples of haems are shown in Figure 30.

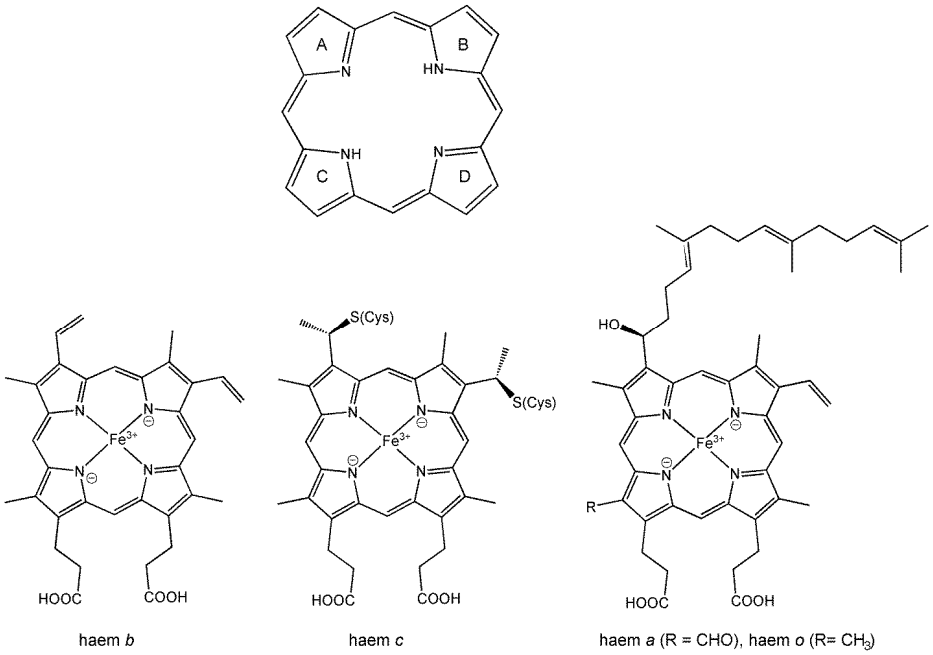

Figure 30. The basic structure of a porphyrin, a tetrapyrrole (**top**), and some common haems (iron porphyrins, (**bottom**), all shown in their ferric form). Different haems have different porphyrin side chains. Haem *c* is covalently linked to two Cys residues of the protein. The haem in haem *o* is anchored to the protein by a farnesyl group. The replacement of a methyl group in haem *o* by a formyl group in haem *a* causes an increase in the redox potential by some 180 mV [500,501]. This high potential haem is then exploited in the terminal oxidases. In haem *d*, one of the double bonds of a pyrrole ring has been reduced so the complex is a chlorin rather than a porphyrin.

There are many ways in which iron-containing proteins can be classified; this is often done to reflect the role played by the metal ion [438]: structural, metal storage and transport, oxygen storage and transport, electron transfer, or catalytic. The reader will appreciate that the bioinorganic chemistry of iron is a vast field, and only selected examples from each are discussed below.

7.1. The Transport and Storage of O_2

The mechanisms by which oxygen is carried by haemoglobin (Hb) and stored by myoglobin (Mb) in higher eukaryotes are well understood (see for example [29,502–505]). While haemoglobin has additional functions [506], its primary role in oxygen transport is complemented by myoglobin's role in oxygen storage.

Mb has a single haem binding site for O_2 and so binds O_2 in a hyperbolic manner, following a standard binding isotherm. Hb is tetramer (with subunits α_1 and α_2, and subunits β_1 and β_2) and binds O_2 in a sigmoidal manner (Figure 31)—which means that in Hb the affinity of one site depends on whether another site is occupied or not: the behaviour is cooperative. A passage from the Christian Bible, Matthew (13:12), is sometimes quoted as an analogy: "Whoever has will be given more, and they will have an abundance. Whoever does not have, even what they have will be taken from them." This "Matthew Effect" highlights the principle of increasing returns, which parallels the enhanced binding affinity of haemoglobin as O_2 occupancy increases.

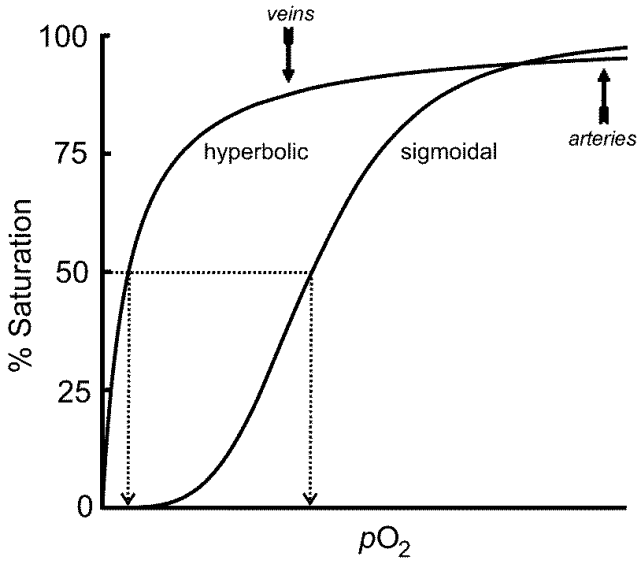

Figure 31. The binding of O_2 in a non-cooperative (hyperbolic) or cooperative (sigmoidal) manner. As an example, the dotted arrows show that half the load of O_2 can be released at a much higher pO_2 if the bonding is cooperative, which is essential for efficient delivery to bodily tissues.

The physiological advantage of cooperative binding is obvious: it would have required a much lower partial pressure of O_2 in the target tissue for the carrier system to release half its O_2 load if the binding were non-cooperative (so a non-cooperative O_2 binder would have too high an affinity for its load to be an effective transport agent). CO_2 binds to terminal amino groups of each of the four subunits of Hb, forming carbaminohaemoglobin; this lowers the affinity of Hb for O_2 and is one of the ways that CO_2 is transported from the tissues to the lungs [507].

The basis of the cooperative behaviour of Hb hinges on the differences in the coordination geometry of a deoxygenated and an oxygenated iron porphyrin. For Hb (and Mb) to bind O_2, iron must be in its ferrous form. In deoxyHb, Fe^{2+} is five-coordinate, paramagnetic, and displaced from the mean porphyrin plane towards the proximal His ligand [508,509]. OxyHb is diamagnetic with iron in the mean porphyrin plane (see for example [510], and Figure 32). The spin change accompanying the oxygenation of Fe^{2+} incurs a very small energy penalty thanks to the flexibility of the porphyrin [511]. A distal His forms a strong hydrogen bond with bound O_2, enhancing O_2 affinity, slowing autoxidation, and offering some protection against CO poisoning [512].



Figure 32. The crystal structures of the iron porphyrin in (**left**) deoxyHb (PDB: 2HBS) [509] and (**right**) oxyHb (PDB: 3A0G) [510].

The nature of the Fe–O_2 bond has long been the subject of considerable debate [513–517]. It has been variously described as a resonance hybrid of two structures involving O_2 coordinated to Fe^{2+} [508]; as an Fe^{3+}–O_2^- complex, in which the bond is predominantly ionic, with antiferromagnetic coupling between the unpaired electrons on low-spin Fe^{3+} and O_2^- [513,515]; or as an intermediate-spin Fe^{2+} species antiferromagnetically coupled to $^3O_2$ [516,517].

Although substantial direct and indirect evidence, by analogy with cobalt–oxygen porphyrin and corrin complexes, supports the formulation of an Fe^{3+}–O_2^- complex, including vibrational spectroscopy [518,519], fluorescence emission [520], UV-vis [520], EPR [521], Mössbauer [522], and ENDOR measurements [523], other techniques suggest a more nuanced picture. X-ray Kβ emission and K-edge absorption spectroscopy, along with theoretical approaches such as TD-DFT and CASSCF calculations [524], indicate that the iron centre is best described as essentially S = 1 Fe^{2+}, with limited charge transfer to O_2. This imparts a degree of superoxide character to the bound ligand. The Fe–O_2 bond exhibits notable double-bond character and is characterised by a three-centre, ozone-like electron delocalisation. Although the complex undergoes autoxidation to yield Fe^{3+} and $O_2^{\bullet-}$, the reaction proceeds relatively slowly, with a half-life of approximately 11 h at pH 7 for MbO_2 [525].

Extensive evidence from multiple disciplines has illuminated the mechanism of cooperative O_2 binding by haemoglobin (Hb) (see, for example, [526]). In essence, cooperative binding refers to the phenomenon whereby the binding of O_2 to one haem group increases the affinity of the remaining sites for O_2, as discussed above. The Hb tetramer exists in dynamic equilibrium between a low-affinity 'tense' (T) state and a high-affinity 'relaxed' (R) state (Figure 33).

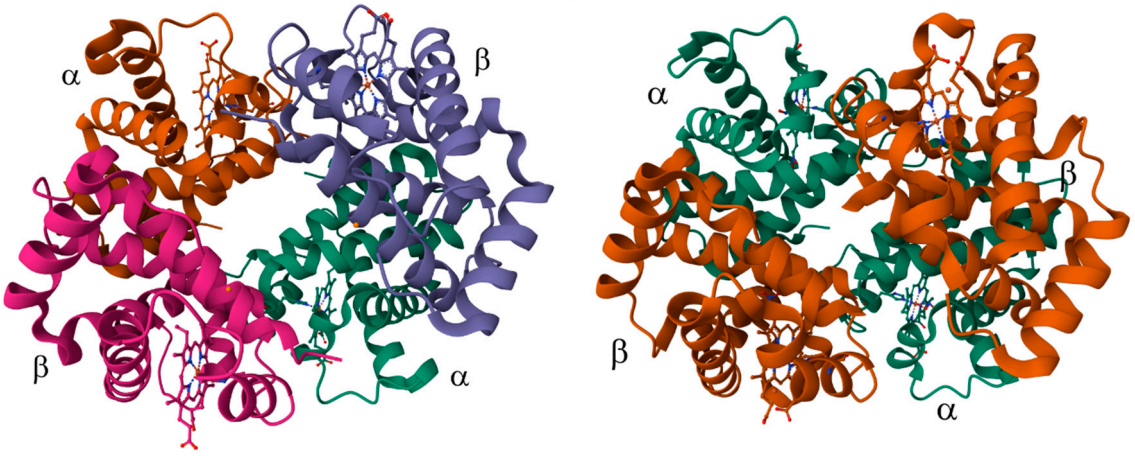

(**a**) (**b**)

Figure 33. (**a**) The structure of the low-O_2-affinity T state (human deoxyHb, PBD 2HHB) [527]. (**b**) The structure of the high-affinity R state (human Hb PDB 3OO5) [528].

As Perutz showed [529,530], there is a set of salt bridges at the interface of the subunits in the T state. The structural changes at haem that accompany O_2 binding (Figure 32) moves the helix of the subunit, breaks the salt bridges, releasing a proton, destabilises the structure of the subunit interface between the α and β subunits, and biases the overall structure towards the R state. When the switch to R occurs, after the binding of the second O_2 molecule, the affinity for O_2 increases. A quantitative description of the Perutz mechanism was later developed by Szabo and Karplus [531]. If Hb remains in the T state, then binding is virtually non-cooperative, as demonstrated by the binding of O_2 to crystals of Hb locked in the T state [532,533]. Flexibility is essentially for the switching between states.

There are many regulators of this conformation change; endogenous regulators include 2,3-diphosphoglycerate (2,3-BPG), CO_2, protons, and Cl^-, while exogenous regulators include inositol hexaphosphate, inositol tripyrophosphate, and vanillin [534,535].

The binding of O_2 to a ferrous porphyrin involves a change of spin state (oxyhaem is a singlet; O_2 is a triplet; and ferrous haem is a quintet). The process is therefore a spin-forbidden reaction and expected to be very slow; this would obviously be a problem for an oxygen carrier system. Fortunately, ferrous porphyrins have a number of different spin states that lie very close in energy to the ground state quintet [536]. DFT calculations [537] show that a ferrous porphyrin with a His proximal ligand is an excellent system for the binding of triplet O_2 because the seven lowest-lying spin states examined (two singlets, three triplets, a quintet, and a septet) are all within 15 kJ mol^{-1}; this makes the probability of spin inversion high, facilitating the rapid binding of O_2. It was estimated that the activation energy barrier for binding of O_2 is <15 kJ mol^{-1}, and the rate of binding is increased by some 11 orders of magnitude compared to binding to a non-haem Fe^{2+} centre [537,538]. The porphyrin clearly plays a crucial role.

7.2. Electron Transport

The transfer of electrons from a donor to an acceptor is a fundamental process in biological chemistry [324,539,540]. Several notable examples are discussed below.

7.2.1. Cellular Respiration in Mitochondria

A key example of an electron transport chain (ETC) is that involved in mitochondrial respiration in eukaryotic cells [541,542]. In this process, the thermodynamically favourable reduction of oxygen by electron donors such as NADH releases energy. This energy is used to pump protons across the mitochondrial membrane, generating a proton gradient and establishing a proton-motive force [166]. The resulting electrochemical potential drives ATP synthesis via the ATP synthase complex, producing ATP, the cell's primary energy currency (Figure 34). The ETC comprises several iron-containing proteins essential for electron transfer.

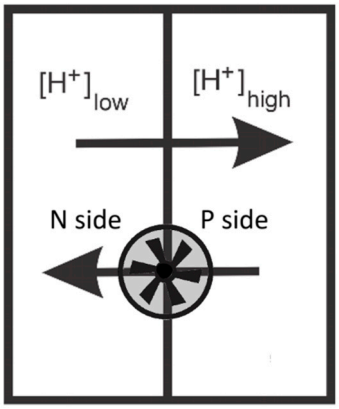

Figure 34. The energy released from the reduction of an electron acceptor by an electron donor is used to pump protons across a membrane against a proton gradient, from the side the membrane with a low $[H^+]$ (the negative or N side) to the side with a high $[H^+]$ (the positive or P side). This sets up a proton-motive force which is used by the molecular machine, ATP synthase, to drive the non-spontaneous synthesis of ATP.

7.2.2. Overview of Mitochondrial Respiration

The overall reaction for mitochondrial respiration is given in Equation (21), and a simplified overview is shown in Figure 35.

$$\text{NADH} \rightarrow \text{Complex I} \rightarrow \text{QH}_2 \rightarrow \text{Complex III} \rightarrow \text{cytochrome c} \rightarrow \text{Complex IV} \rightarrow \text{O}_2 \quad (21)$$

Complex I (NADH:ubiquinone oxireductase) catalyses the transfer of electrons from NADH, generated in the Krebs cycle, to ubiquinone (coenzyme Q) [543], Equation (22).

$$\text{NADH} + \text{H}^+ + \text{Q} + 4\text{H}^+_{in} \rightarrow \text{NAD}^+ + \text{QH}_2 + 4\text{H}^+_{out} \quad (22)$$

Here, *in* and *out* refer to the mitochondrial matrix and the intermembrane space, respectively. Proton pumping also occurs at Complex III (cytochrome bc_1) and Complex IV (cytochrome *c* oxidase). The chemiosmotic coupling across these complexes [544,545] establishes a transmembrane potential exploited by Complex V (ATP synthase) to synthesise ATP. Various models have been proposed to explain the coupling of electron transport with proton pumping [544,546–553].

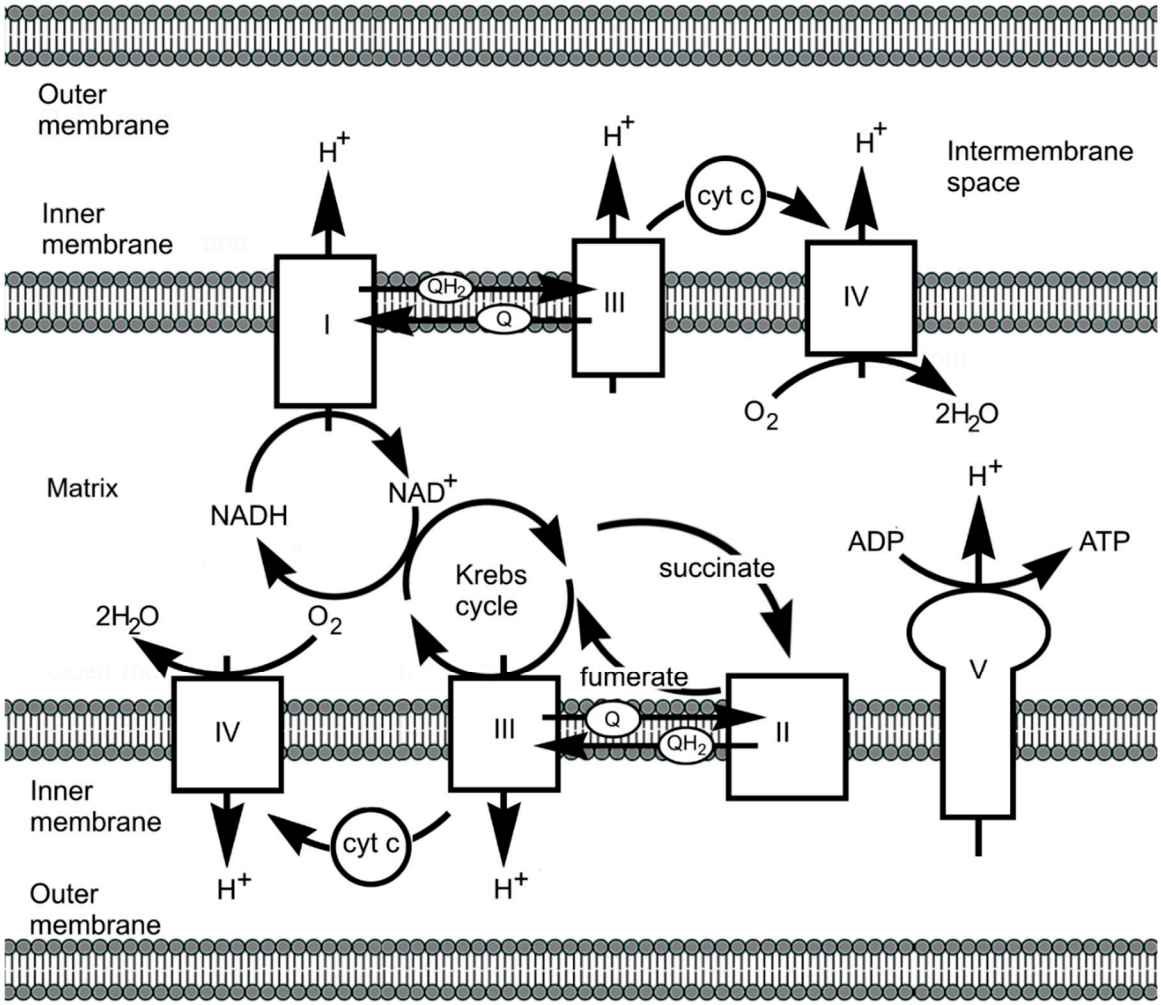

Figure 35. Schematic of the mitochondrial electron transport chain, showing Complexes I through V. Adapted from [554].

Electron donors and acceptors within the mitochondrial ETC have increasing midpoint redox potentials, $E_{1/2}$, providing the thermodynamic impetus for electron flow (Figure 36). Control over these $E_{1/2}$ values is critical to ETC function and is influenced by several factors, most notably the nature of the metal ion involved [555]. For instance, copper-containing proteins operate at the upper end of the biological redox spectrum (350–800 mV for blue copper proteins), while iron–sulphur proteins function at lower potentials (−700

to −100 mV). High-potential iron–sulphur proteins (HiPIPs) occupy an intermediate range (50–400 mV), and the iron porphyrin-containing cytochromes span a mid-range potential (−400 to 300 mV).

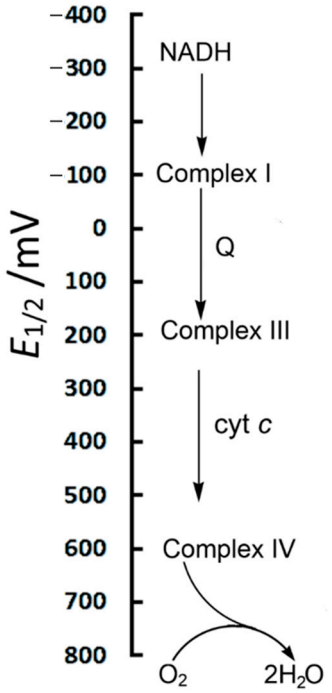

Figure 36. The cascade of electrons from NADH to O_2 in the mitochondrial ETC.

The redox potential of iron–sulphur proteins depends on their accessible oxidation states. HiPIPs, for instance, cycle between $[4Fe–4S]^{2+/3+}$, whereas ferredoxins use the $[4Fe–4S]^{1+/2+}$ couple. Determining the precise oxidation state of the individual ions within a cluster is a moot point, of course, and the clusters are best described as valence-delocalised systems [556,557].

7.2.3. Haems and Electron Transport

The ETC exemplifies the versatility of iron in biology. In Complex I, iron is coordinated within iron–sulphur clusters, coordinated in four positions thanks to the relatively large radius of sulphide ions. By contrast, in haems (iron porphyrins) of Complex III, iron is six-coordinate. The redox potentials of cytochrome *b* and cytochrome c_1 haems in Complex III are approximately 120 mV, −30 mV, and 240 mV, respectively [558].

Both high- and low-potential haems utilise His as axial ligands [559], yet the surrounding environments differ. High-potential haems are typically found in solvent-exposed cavities, whereas low-potential haems are shielded from solvents. This illustrates how the microenvironment modulates redox potential. Haems are also more oxygen-tolerant than iron–sulphur clusters and likely evolved later, in response to the rise of atmospheric oxygen driven by cyanobacterial photosynthesis [560]; iron–sulphur clusters, by contrast, are much more oxygen-sensitive and are thought to have emerged earlier in life's evolution [15,561].

In *b*-type haems, the porphyrin ring is embedded within a hydrophobic pocket, with axial ligands maintaining its orientation. In *c*-type haems, the porphyrin is covalently attached to the protein via thioether bonds to Cys residues [562].

7.2.4. Iron–Sulphur Clusters

Iron–sulphur clusters span a broad range of $E_{1/2}$ values, from <−600 mV (e.g., [7Fe–8S] in some ferredoxins) to > +460 mV (e.g., [4Fe–4S] in HiPIPs). These clusters are essential in

respiratory and photosynthetic electron transport [563–565] and their existence likely echoes prebiotic chemistry [566]. Typically coordinated by Cys (or occasionally His) residues, they are often buried within proteins to mitigate oxygen sensitivity. Examples of these clusters and their common oxidation and spin states are shown in Figure 37.

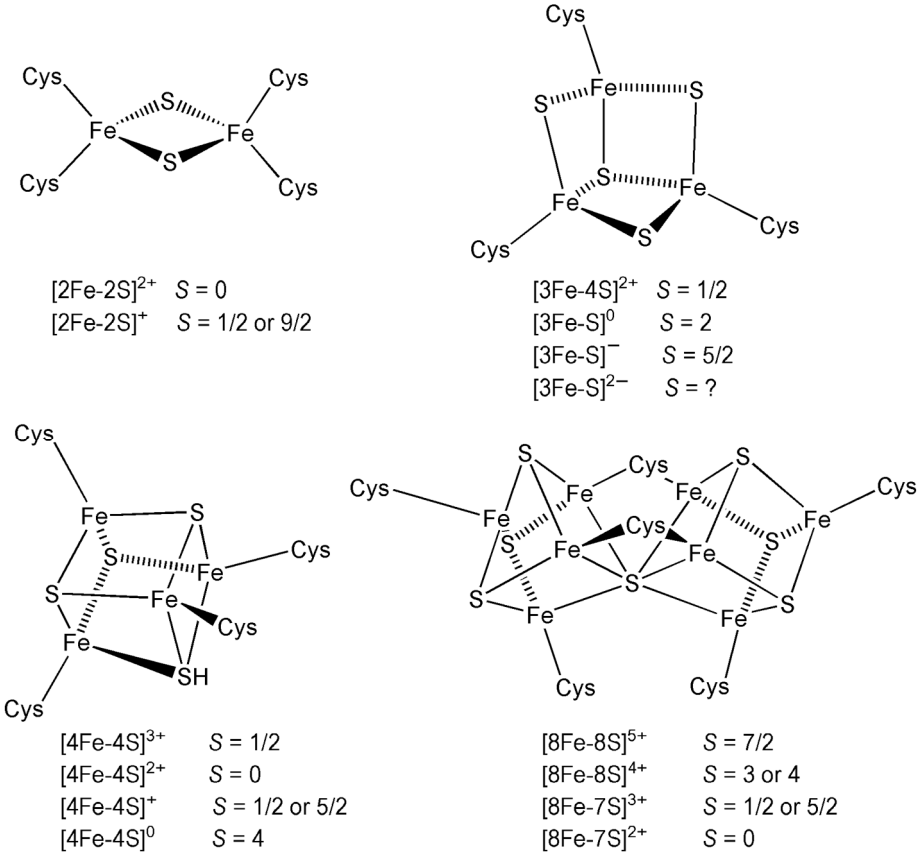

Figure 37. Some iron–sulphur clusters found in biological systems (adapted from [563]).

These clusters generally access two oxidation states and mediate one-electron transfer. In addition to electron transfer, they play catalytic roles (e.g., in aconitase), serve as signalling molecules, and contribute to magnetic sensing in birds [567,568].

Cysteine commonly acts as a terminal ligand, though in cases such as the Rieske centre of Complex III, two His and two Cys residues provide coordination [569]. The protonation state of His residues introduces pH-dependence to $E_{1/2}$, and hydrogen bonding between the cluster and its protein environment provides additional fine-tuning [570]. Rhomboidal [2Fe–2S] clusters coordinated solely by Cys residues tend to have pH-independent $E_{1/2}$ values, as the ligands retain their negative charge over the physiological pH range.

Replacing two Cys ligands with His in the Rieske centre increases the potential from −240 mV (Complex I) to approximately 150 mV [571]. Such ligand substitution, combined with structural adjustments by the protein matrix [572], provides a means for precise tuning of the redox potential [573].

Though typically one-electron carriers, some iron–sulphur centres, such as the [8Fe–(7/8)S] P-cluster of nitrogenase, can mediate two-electron transfer processes [574,575]. Some nitrogenase variants contain an [8Fe–9S] structure, formed by two [4Fe–4S] units bridged by a sulphide [576,577].

Nature demonstrates exquisite control over $E_{1/2}$ values through ligand identity, protein environment, and redox-linked protonation equilibria. Rieske centres exemplify this, with protonation of His residues significantly altering $E_{1/2}$ by as much as 450 mV [573]. By

contrast, iron–sulphur clusters coordinated by four Cys ligands exhibit lower potentials due to the influence of the four negatively charged ligands, resembling the potential of a fully deprotonated Rieske centre. The Rieske centres in Complex III, for instance, have high, pH-dependent $E_{1/2}$ values, typically around 350 mV at pH 7. On the other hand, ferredoxins in bacterial oxygenases, which participate in the catabolism of aromatic compounds, display lower $E_{1/2}$ values (around −150 mV) that appear to be independent of pH.

Electrostatic interactions between the metal centre and the surrounding protein influence both $E_{1/2}$ and the pK_a of ligands. Oxidation state and ligand protonation are often coupled, with the pK_a of the oxidised state up to five units lower than that of the reduced state [573,578]. These effects facilitate precise redox potential tuning within the ETC.

Minimising structural reorganisation during redox transitions reduces reorganisation energy (λ), a key determinant of electron transfer rates, as described by the Marcus theory of outer sphere electron transfer [579] (see Section 10.1). The value of λ is influenced by the local environment, with aqueous media increasing it [580]. Protein architecture also matters: β-sheets, being more rigid than α-helices, support a more efficient electron transfer process [580].

The importance of structure is well-illustrated by the [2Fe–2S] and [4Fe–4S] clusters of some ferredoxins, as well as the [Fe(Cys)$_4$] centre in rubredoxins, the iron–sulphur proteins involved in one-electron transfer in many biological reactions. In these clusters, the similar energies of Fe(3d) and S(3p) orbitals result in significant covalent character, which facilitates easy changes in oxidation state [557]. Importantly, the oxidation state changes in each iron centre do not substantially alter its essentially tetrahedral structure; changes in λ are therefore minimised [581].

It should be appreciated that the redox properties of metal centres in vivo often differ markedly from those in vitro [437,582,583], owing to influences such as the coordination geometry, protein matrix, solvent accessibility, and conformational dynamics [555,584–589].

To summarise, the key factors that control the $E_{1/2}$ of an iron–sulphur centre include the following:

- *Ligand identity and coordination*
  - The type of ligands (e.g., Cys or His) strongly influences $E_{1/2}$.
  - Cys ligands, being negatively charged, generally lower $E_{1/2}$, while harder His ligands, as in Rieske centres, raise $E_{1/2}$.
- *Protein environment and electrostatic effects*
  - The surrounding protein matrix, including electrostatic interactions and hydrogen bonding, fine-tunes the redox potential.
  - Burial within a hydrophobic environment, proximity to charged residues, and the extent of exposure to solvent significantly impacts $E_{1/2}$.
- *Protonation states and pH dependence*
  - Protonation states of coordinating ligands, especially His, introduce pH-dependent shifts in $E_{1/2}$.
  - In Rieske centres, deprotonation of His can lower $E_{1/2}$ by up to 450 mV.
- *Cluster type and delocalisation*
  - The specific iron–sulphur cluster (e.g., [2Fe–2S], [4Fe–4S]) and the accessibility of oxidation states (e.g., valence delocalisation) affect $E_{1/2}$.
  - HiPIPs exhibit higher potentials due to cycling between [4Fe–4S]$^{2+/3+}$, while ferredoxins operate between [4Fe–4S]$^{1+/2+}$.

7.2.5. From Complex I to Complex IV

The entry point to Complex I, a large assembly of polypeptides with a combined mass of approximately 1 MDa, involves the reduction of flavin FMN to $FMNH_2$ by NADH, resulting in the production of NAD^+. The $E_{1/2}$ of FMN within Complex I is ≈ -340 mV, significantly lower than that of free FMN (-207 mV) [590]. This illustrates once again how the redox potential of a given species can be modulated and finely tuned by its surrounding protein environment.

Electrons subsequently pass through a chain of eight iron–sulphur clusters [591,592] (perhaps the echo of prebiotic chemistry [542,593–595]), eventually reducing ubiquinone (coenzyme Q, $E_{1/2}$ = 100 mV) to ubiquinol (QH_2). The QH_2 generated is then utilised by Complex III to reduce cytochrome *c* ($E_{1/2}$ = 260 mV) in the intermembrane space. Finally, cytochrome *c* donates electrons to Complex IV, where O_2, $E_{1/2}$ = 820 mV, is reduced to water (see Figure 35).

The iron–sulphur clusters located at the beginning of the chain exhibit $E_{1/2}$ values of about -250 mV, whereas the terminal cluster possesses the highest potential in the chain, ≈ -100 mV, as would be expected.

The reaction catalysed by Complex III is given in Equation (23), and that catalysed by Complex IV in Equation (24).

$$QH_2 + 2\text{cyt } c^{3+} + 2H^+_{in} \rightarrow Q + 2\text{cyt } c^{2+} + 4H^+_{out} \quad (23)$$

$$O_2 + 4\text{cyt } c^{2+} + 8H^+_{in} \rightarrow 2H_2O + 4\text{cyt } c^{3+} + 4H^+_{out} \quad (24)$$

Complex II (succinate–quinone oxidoreductase) provides an alternative entry point for electrons into the electron transport chain.

One of the challenges faced by living organisms in an oxidising environment is the formation of reactive oxygen species (ROS), including singlet oxygen ($^1O_2$), superoxide ($O_2^{\bullet -}$), H_2O_2, and especially the hydroxyl radical ($OH^\bullet$) [317,596]. Complex III exemplifies this issue. Under normal physiological conditions, it operates in a low-ROS-producing steady state. However, in the absence of oxygen (anoxia), the complex adopts an alternative steady state characterised by elevated ROS production [597]. This high-ROS state may persist for some time even after re-exposure to oxygen-rich conditions. It is important to recognise, however, that low concentrations of $O_2^{\bullet -}$ and H_2O_2 play essential roles in mitochondrial signalling, which modulates mitochondrial function [598]; it is the accumulation of these species that poses a physiological threat. ROS are also generated at Complex I [599].

An outline of the mechanism of Complex III is shown in Figure 38 [600–602]. The reaction catalysed by Complex III begins with the [2Fe–2S] centre of the Rieske iron–sulphur protein accepting an electron from ubiquinol QH_2, resulting in the formation of $Q^{\bullet -}$ and the release of two protons into the intermembrane space. The Rieske protein then transfers the electron to cytochrome c_1, which subsequently reduces cytochrome *c*. Meanwhile, the semiquinone radical passes its remaining electron to the low-potential cytochrome b_L of cytochrome *b*, which in turn reduces the high-potential cytochrome b_H. Cytochrome b_H then donates an electron to a second ubiquinone molecule, forming another semiquinone intermediate. During a second turnover of the cycle, this semiquinone is further reduced by a second electron from cytochrome b_H, regenerating QH_2. The binding of QH_2 on the intermembrane-space-facing side of the complex initiates another catalytic cycle. The semiquinone radicals generated in this process can react with molecular oxygen, producing $O_2^{\bullet -}$ [603].

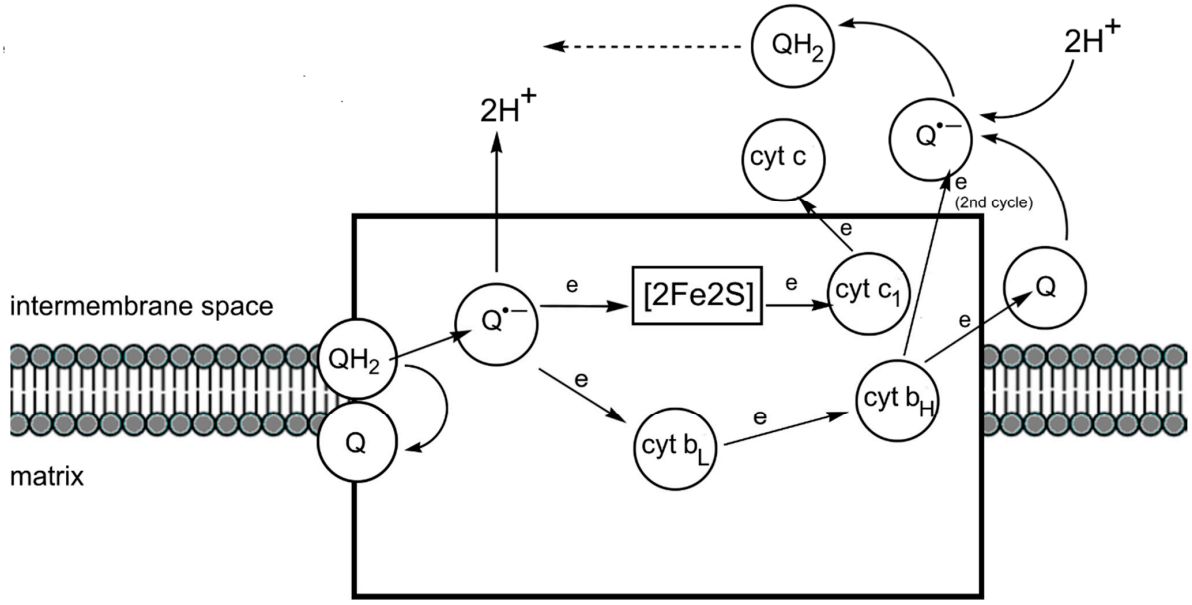

Figure 38. Schematic of the reactions of Complex III [600–602].

Mitochondrial cytochrome *c* oxidase (Complex IV) [604] contains a binuclear copper centre (Cu_A) coordinated by Cys, Met, His, and Glu residues. The complex receives electrons from cytochrome *c* ($E_{1/2} \approx 250$ mV), which are first transferred to haem *a*. The electrons then proceed to haem a_3 (homologous to haem *b* in some reductase families), which is positioned adjacent to a Cu_B centre coordinated by three His residues ($E_{1/2} \approx 800$ mV). Molecular oxygen binds in a bridging configuration between Cu_B and the iron centre of haem a_3, and is effectively reduced by two electrons to O_2^{2-}, with Fe^{2+} and Cu^+ each donating one electron (see Figure 39). This two-electron reduction strategy circumvents the otherwise spin-forbidden nature of the direct reduction of $^3O_2$ by singlet-state NADH—a reaction that would otherwise proceed very slowly. The cooperative action of the iron and copper centres allows for a rapid, spin-allowed two-electron reduction of molecular oxygen [605].

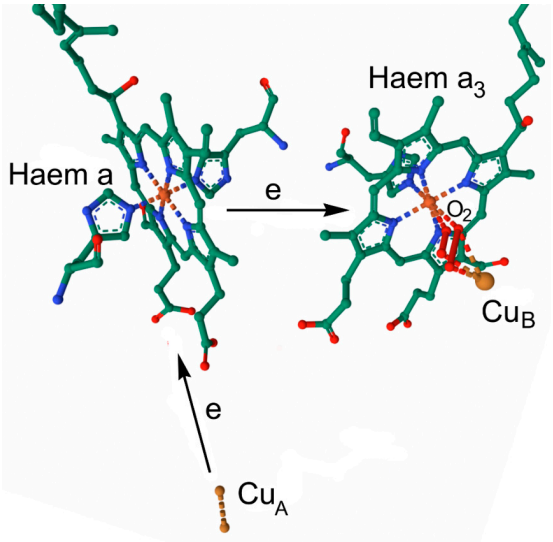

Figure 39. Electron transfer through Complex IV. Electrons flow from a dicopper centreto haem *a*, and from there to haem a_3 with nearby Cu_B. Illustrated is the structure from fully oxidised bovine heart cytochrome *c* oxidase (PDB 5XDQ) [606]. Bound O_2 (disordered over two positions) is coordinated by the iron of haem a_3 and Cu_B.

The entire catalytic cycle consists of six stages: R, A, P, F, O, and E [607] (Figure 40). Stage P can be further divided into two sub-stages, P_M and P_R. Each proton uptake by the catalytic cytochrome a_3–Cu_B centre is coupled with the transfer of a proton across the membrane from the high-pH (negative or N) side to the low-pH (positive or P) side (see Figure 34). Under physiological conditions, the reduction of O_2 to $2H_2O$ releases about 210 kJ of energy. The stoichiometric efficiency of this energy conversion into ATP synthesis ranges between 75% and 90% [607,608].

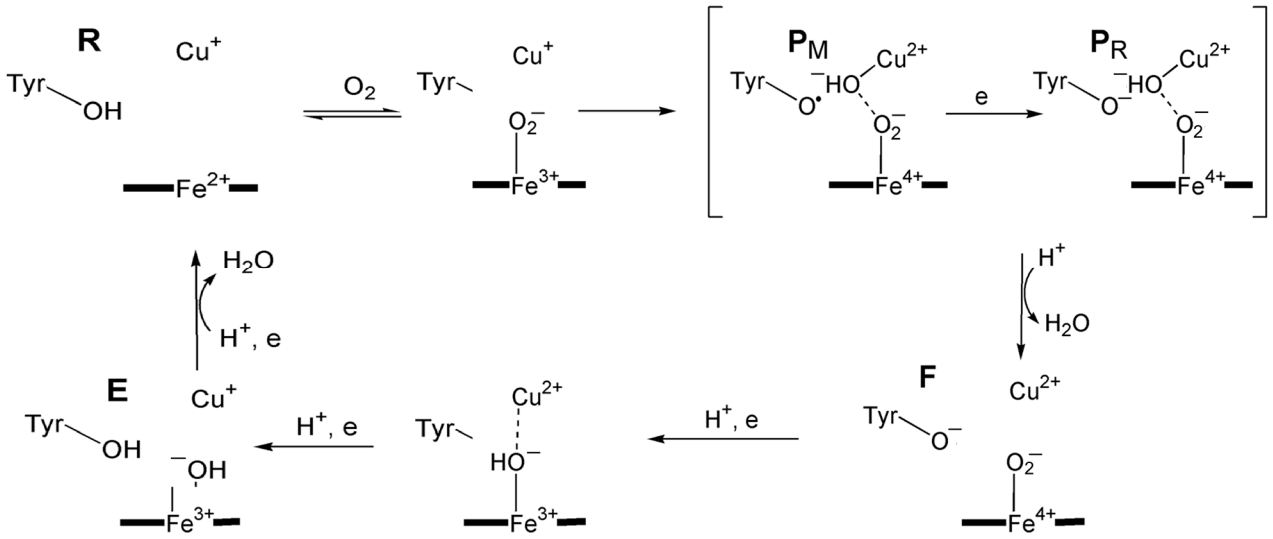

Figure 40. An outline of the catalytic cycle of cytochrome *c* oxidase (see [607] for greater detail).

7.3. An Example of an Iron Enzyme: The Cytochromes P450

The oxy compounds of iron porphyrins play a crucial role in various enzymes, providing protection against oxidative stress and enabling the spin-forbidden reaction between $^3O_2$ and singlet substrates by coordinating oxygen to iron. This mechanism is one way to overcome this spin-forbidden reaction, as seen in cytochrome *c* oxidase (see Section 7.2).

The cytochrome P450 superfamily is a prime example [609–613]. These enzymes function as monooxygenases or mixed-function oxidases, using pyridine nucleotides as electron donors to facilitate the oxidation of organic substrates (Equation (25)):

$$NAD(P)H + O_2 \rightarrow NAD(P)^+ + RO + H_2O \quad (25)$$

They are potentially useful for biotechnology applications, especially in the design of biosensors [614]. Their ability to catalyse the formation of C-N and C-S bonds holds promise for their use in biosynthetic applications [615]. P450 is capable of catalysing oxidative dehalogenation reactions, opening up the possibility of using them to oxidise organofluorine pollutants [616]. P450 is one way in which herbivorous insects cope with toxic alkaloids that plants deploy to try to ward them off [617].

Other examples of oxy compounds of iron porphyrins include haem-containing dioxygenases, which incorporate both oxygen atoms from O_2 into organic substrates [618]; catalases, which degrade H_2O_2 into H_2O and O_2, thus protecting cells from oxidative damage [619]; nitrite reductases which reduce nitrite to nitric oxide or ammonia [471]; and peroxidases, which catalyse the oxidation of substrates using H_2O_2 or other peroxides, playing a critical role in removing phenolic compounds, peroxides, and degrading mycotoxins (Equation (26)) [620,621].

$$ROOH + AH_2 \rightarrow ROH + A + H_2O \quad (26)$$

The P450 enzymes feature a thiolate group from a Cys residue as a proximal ligand to iron. This is essential for cleaving the O–O bond, facilitating substrate binding, electron transfer, and ensuring proper protein folding [622]. Electron transfer in the P450 catalytic cycle is mediated by a flavoprotein or an iron–sulphur protein [612,623].

The generalised mechanism of the P450s is shown in Figure 41; precise details vary depending on the enzyme in question and, in particular, the substrate RH [612]. Clearly, the efficient transfer of electrons from NAD(P)H to the haem centre is essential to ensure catalytic efficiency [624].

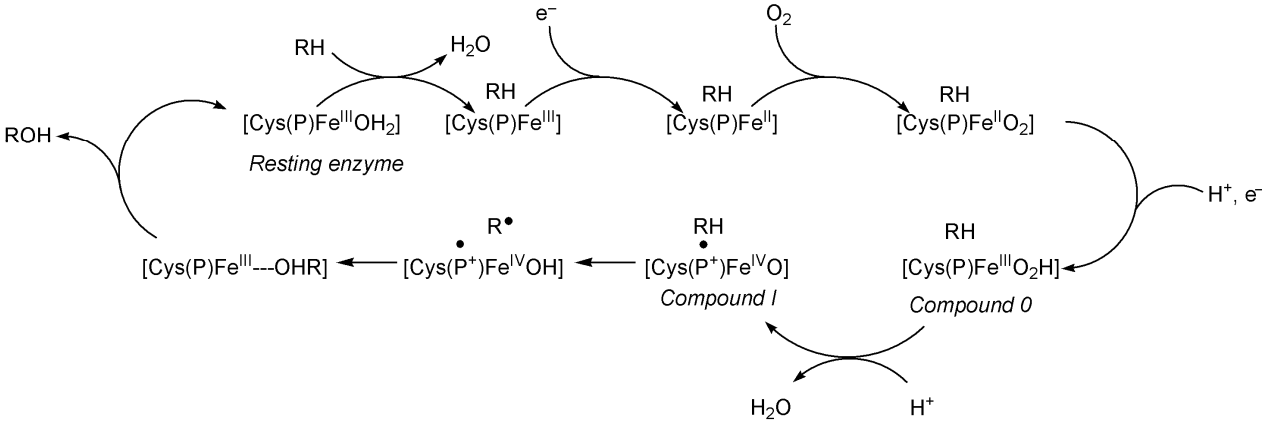

Figure 41. A generalised mechanism of the cytochromes P450. In the scheme, (P) represents the porphyrin equatorial ligand.

There is experimental evidence for some of the intermediates: a crystal structure of the oxy-ferrous intermediate, $[Cys(P)Fe^{II}O_2]$, is available [625]; the occurrence of Compound 0, $[Cys(P)Fe^{III}O_2H]$, in the cycle is well established [626–629]; and the occurrence of Compound I, $[Cys(P^{\bullet+})Fe^{IV}O]$, which features the porphyrin as a radical cation and iron in the +4 oxidation state, has been demonstrated kinetically and spectroscopically [630,631].

Another important iron-containing enzyme is nitrogenase. It contains a multi-iron and molybdenum active site [632]. Found in nitrogen-fixing bacteria and archaea, nitrogenase catalyses the conversion of N_2 to NH_3 and plays a crucial role in the global nitrogen cycle. Its structure and the mechanism of the reaction will be discussed elsewhere when the biological chemistry of the second and third row of the d block is addressed.

8. Cobalt

Cobalt is not a very common element in the Earth's crust (15 to 30 ppm) [633]. That Co^{3+} plays a small, albeit important, role in biology—and that it features as the active site of several enzymes—may be surprising. Virtually all six-coordinate complexes of Co^{3+} are low-spin, and low-spin Co^{3+} and Cr^{3+} are the outstanding examples of kinetically inert metal ions from the first row of the d block because of the large ligand field contribution to the activation energy [634,635]. The residence time of H_2O in $Co^{3+}{}_{aq}$ [636] and $Cr^{3+}{}_{aq}$ [637] is of the order of 10^5 s, compared to 10^{-5} s for $Fe^{3+}{}_{aq}$ and $Ti^{3+}{}_{aq}$ [638] and 10^{-8} s for $Co^{2+}{}_{aq}$ [639]. Clearly cobalt in biology is involved in some unusual chemistry that is perhaps not readily accessible by other enzymatic systems based on, for example, iron porphyrins.

The most prominent role played by Co^{3+} is in the enzymes containing a cobalt corrinoid (a derivative of cyanocobalamin, [CNCbl], vitamin B_{12}) as cofactor (Figure 42) [394,640–643]. These include methionine synthase, essential for the biosynthesis of methionine [644]; methylmalonyl-coenzyme A mutase, which is essential for the metabolism of amino acids (isoleucine, valine, methionine, and threonine), of odd-chain fatty acids, and of cholesterol [645]; ribonucleotide reductase, which converts ribonucleotides to deoxyribonucleotides in some bacteria [646];

and reductive dehalogenases, found in certain anaerobic bacteria, which break down halogenated hydrocarbons [647]. The structure and electronic properties of the cobalt corrinoids have been studied by a wide range of experimental and computational techniques (for recent examples, see [394,648–663]).

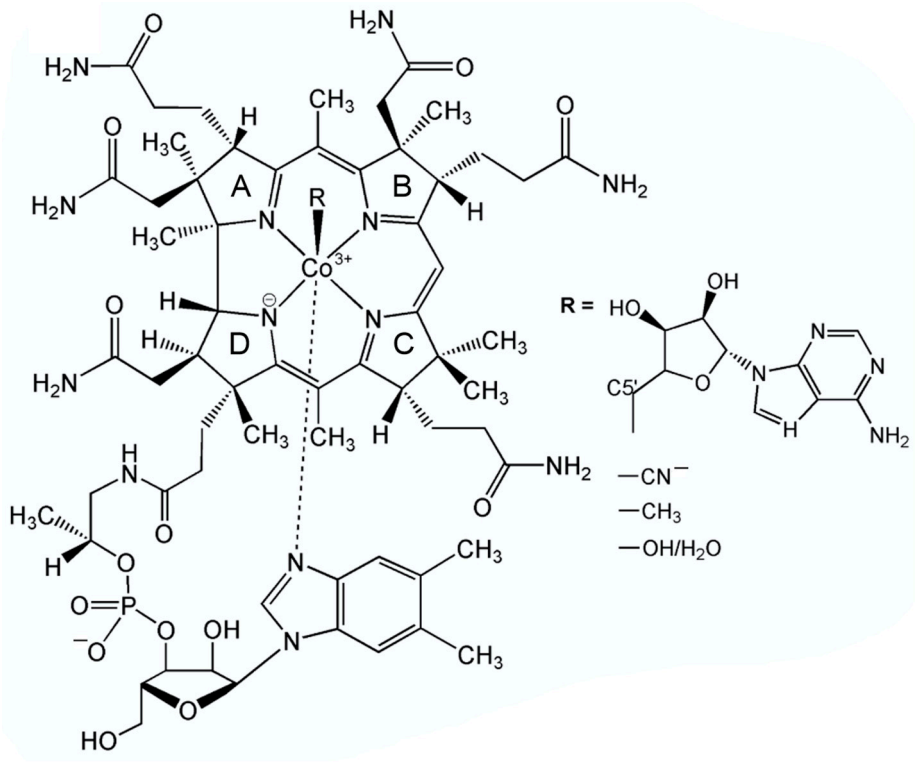

Figure 42. The structure of the cobalamins, the corrinoids that contain a nucleotide loop that ends in a base that coordinates the lower (α) face of the corrin. The usual base is 5,6-dimethylbenzimidazole, dmbzm. In adenosylcobalamin, [AdoCbl], or coenzyme B_{12}, the ligand occupying the upper (β) coordination site, R = 5′-deoxyadenosyl. Cyanocobalamin or vitamin B_{12} itself, [CNCbl], has R = CN^-. Methylcobalamin, [MeCbl], has R = CH_3^-; in aquacobalamin, or vitamin B_{12a}, $[H_2OCbl]^+$, R = H_2O and in hydroxocobalamin, [HOCbl], R = OH^-. There are derivatives of B_{12} with different β ligands [394].

[CNCbl] itself plays no role in biology and is an artefact of the isolation of B_{12} produced by bacterial fermentation [664]. It must be converted into its active forms before being used in its biological roles. Bacteria, archaea, and eukaryotes, but not plants, require B_{12} for growth [665–667]. That plants do not require B_{12} suggests that cobalt's role in biology is, in theory, not essential.

The biological chemistry of cobalt probably dates to the origins of life [668,669]. There is recent evidence from phylogenomic analyses of the proteins involved in B_{12} synthesis that B_{12} metabolism was retained in the last common land plant ancestor [670], but plants now have an alternative methionine synthase that does not require B_{12}. There is also evidence that corrin synthesis probably dates back to the last universal common ancestor of all life forms (LUCA) and that corrin synthesis played a role in the origin of free-living cells [671].

Higher organisms have to absorb B_{12} from their diet or procure it in symbiotic relationships [672] and there is a complex absorption and transportation system for B_{12} and its derivatives [673–676]. B_{12} is produced industrially by bacterial fermentation with an annual global market value of some $280 M [677,678] and is widely used in vitamin supplements and in pharmaceutical preparations.

Much has been written about cobalt corrinoid chemistry (see for example [394,679,680]), but there are several cobalt-containing enzymes not based on B_{12}. In these the metal ion typically activates H_2O to catalyse a hydrolytic reaction [640,681–684]. These enzymes include

methionine aminopeptidase [685], prolidase [686], nitrile hydratase [687], thiocyanate hydrolase [688], glucose isomerase [689], methylmalonyl-CoA carboxytransferase [690], aldehyde decarbonylase [691], lysine-2,3-aminomutase [692,693], and bromoperoxidase [694]. There are also relatively recent discoveries on the role of cobalt corrinoids as photo-receptors in light-dependent gene regulation [695–698] (prompting an investigation into the photolytic properties of organocobalamins [697,699–701]), as B_{12}-sensing riboswitches in, for example, *Mycobacterium tuberculosis* [702], and in modulating the structure of microbial communities and their response to toxic substances in the human gut [703–705] and in marine environments [706]. We will focus on the biological chemistry of the cobalt corrinoid-containing enzymes.

Cobalt in excess is toxic to humans [707–709], but B_{12} deficiency has severe health consequences including anaemia, neurological consequences, birth defects, and cell ageing [710–714]. B_{12} is also thought to protect DNA against genotoxicity by xenobiotic metabolites [715]. So-called "antivitamins-B_{12}" are of interest for their ability to induce B_{12} deficiency in organisms, from the resistant bacteria that plague some hospitals, to laboratory mice [716–720]. They contain for example a large organic ligand such as $PhCH_2CH_2$- or an alkynyl ligand (R-C≡C-); or a metal other than Co such as Rh; or a corrin ring with an interrupted conjugation (referred to as a stable yellow corrinoid). They resist the biological B_{12} tailoring that leads to the formation of the cobalamin active forms. They may even prove to be useful as growth inhibitors of tumour cells.

The inherent inertness of Co^{3+} is altered by coordination with the corrin macrocycle, which features a 13-atom, 14-electron π-electron delocalised system. In cobalt corrinoids, Co^{3+} undergoes ligand substitution reactions at relatively fast rates [394], suggesting that the corrin macrocycle significantly enhances the lability of the metal ion. This effect may arise from the corrin imparting a degree of labile Co^{2+}-like character to the cobalt centre. The challenge of assigning a formal oxidation state to a metal ion in a complex of ligands with a delocalised electronic system has long been recognised [721–723]. The corrin ligand, in effect, is nature's solution to overcoming the inertness of Co^{3+}.

The biosynthesis, uptake, metabolism, and biochemical reactions of the cobalamins in biological systems is well-documented ([666,674,679,724–739]). An overview of the biochemistry requiring a cobalt corrinoid is shown in Figure 43 [737].

As mentioned, vitamin B_{12} itself is biologically inactive and must be converted to the active form, methylcobalamin ([MeCbl]) or 5′-deoxyadenosylcobalamin ([AdoCbl]), which both feature a Co–C bond. This is the key to the chemistry of the B_{12}-dependent enzymes. The Co–C bond in Co^{3+}–R^- can undergo heterolytic (Equations (27) and (28)) or homolytic cleavage (Equation (29)):

$$Co^{3+}–R^- \rightleftarrows Co^{3+} + R^- \quad (27)$$

$$Co^{3+}–R^- \rightleftarrows Co^{+} + R^+ \quad (28)$$

$$Co^{3+}–R^- \rightleftarrows Co^{2+} + R^\bullet \quad (29)$$

The reactions are readily mimicked with many protein-free alkyl cobalt corrinoids and are an intrinsic property of these organometallic complexes [394,740]. Strategies that mimic B_{12} organometallic chemistry have been widely explored and applied in synthetic organic chemistry [741,742].

The biological chemistry of cobalt centres primarily on the $Co^{3+}|Co^{+}$ and $Co^{3+}|Co^{2+}$ couples, with Co^{4+} appearing to play no known role. Biological reactions involving homolytic cleavage of a Co–C bond must be tightly regulated, as Co^{2+} corrinoids are readily oxidised to Co^{3+}. Moreover, reactions with strong oxidants such as H_2O_2 can disrupt the conjugated π-system of the corrin macrocycle, resulting in the formation of stable yellow corrinoids [394,743,744].

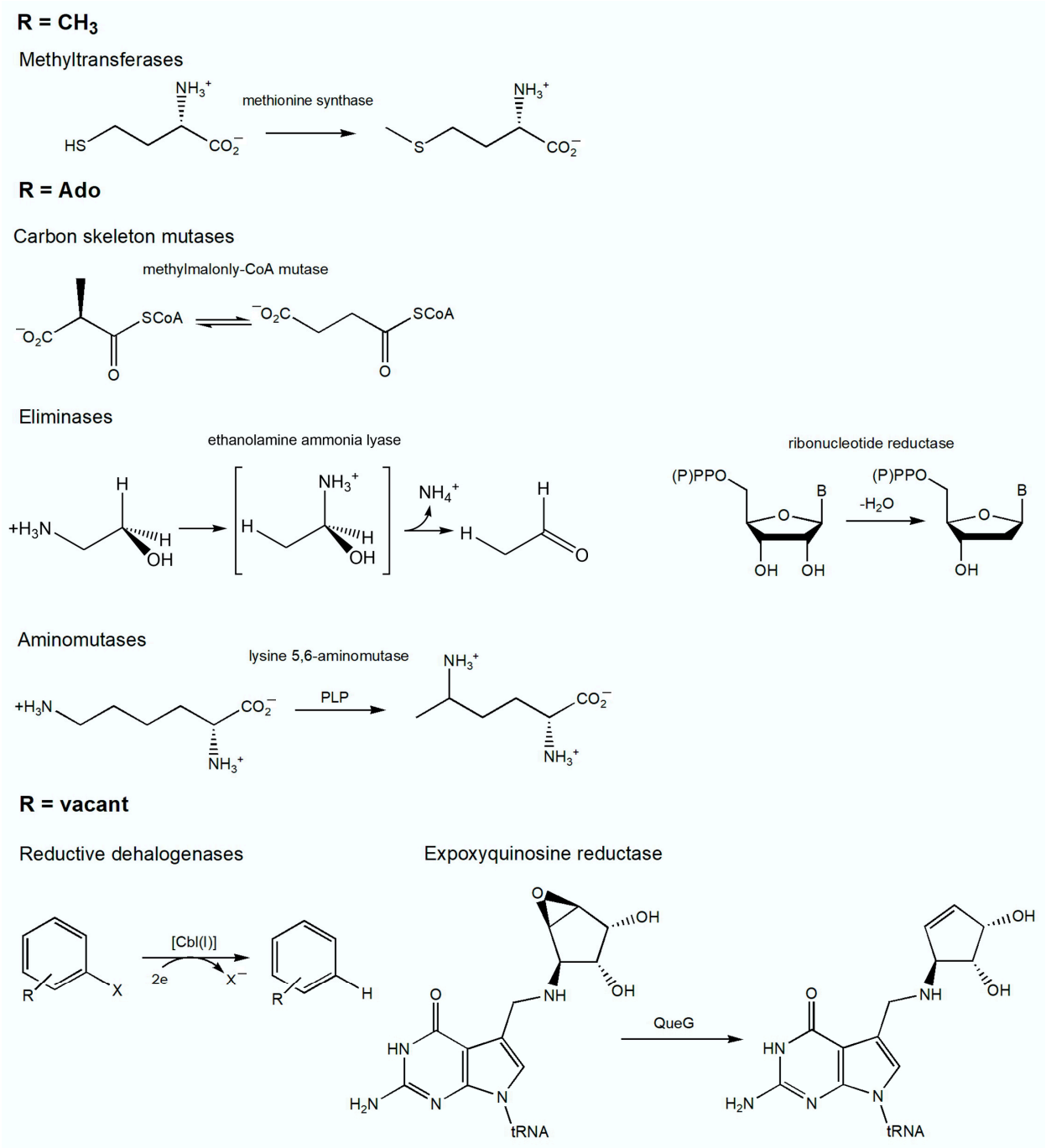

Figure 43. Examples of cobalamin-dependent proteins as defined by the nature of the upper ligand (adapted from [737]). [MeCbl]-dependent methyl transferases catalyse the transfer of a methyl cation to a substrate. [AdoCbl]-dependent enzymes include carbon skeleton mutases, eliminases, and aminomutases. [AdoCbl] is also involved in light-dependent gene regulation of the carotenoid (Car) biosynthetic operon via the transcriptional regulator CarH. A third type of Cbl-dependent enzymes, which includes the reductive dehalogenase PceA and the queuosine biosynthetic enzyme QueG, do not have an upper axial ligand and are denoted as "open"-Cbl-dependent enzymes.

Both [MeCbl] and [AdoCbl] are comparatively resistant to reduction due to the electron-donating properties of the axial alkyl ligand of the cobalt centre (−1.36 V for [MeCbl], pH 7 [745,746]; −1.07 V for [AdoCbl] [747], in contrast to 0.200 V for the Co^{3+} | Co^{+} and −0.647 V for the Co^{2+} | Co^{+} couple of $[H_2OCbl]^{+}$ [748]).

These redox potentials lie well outside the ambient thermodynamic stability window of water, which spans from −0.41 V (for the $2H^{+}$ | H_2 couple) to 0.82 V (O_2 | H_2O, 25 °C,

pH 7). This demonstrates how coupling redox processes to subsequent chemical transformations enables circumvention of the thermodynamic constraints imposed by an aerobic aqueous environment, an essential strategy for harnessing the strong reducing power of the Co^{+} state.

Given that the biological reactivity of cobalt corrinoids hinges upon homolytic or heterolytic cleavage of the Co–C bond, it follows that this bond must be relatively weak. The bond dissociation energy for heterolysis of the Co–CH_3 in [MeCbl] is 155 kJ mol^{-1} [749]. That for homolysis in [AdoCbl] is even more modest, about 125 kJ mol^{-1} [750,751].

Humans possess two enzymes that utilise cobalamin chemistry. Methionine synthase (MS), which employs [MeCbl], is involved in the regeneration of tetrahydrofolate via the synthesis of methionine from homocysteine. Methylmalonyl-CoA mutase, which requires [AdoCbl], catalyses the conversion of methylmalonyl-CoA to succinyl-CoA.

8.1. The [MeCbl]-Dependent Enzymes

These enzymes catalyse the heterolytic cleavage of the Co–CH_3 bond to form the "supernucleophile" cob(I)alamin, $[Cbl(I)]^{-}$ [752], and a methyl carbocation that is transferred to a nucleophilic acceptor. An example is methionine synthase, MS (called MetH in bacteria). It receives the cobalt corrinoid cofactor (as aquacobalamin or hydroxocobalamin) from the human cobalamin trafficking protein MMADHC (also called CblC) [753,754]. This is then reduced to [Cbl(II)] and methylated by methyltetrahydrofolate (CH_3-THF), forming methylcobalamin, [CH_3Cbl], the active cofactor of the enzyme.

During enzyme catalysis, MS catalyses the transfer of a methyl group from 5-methyltetrahydrofolate (CH_3-THF) to homocysteine (Hcy) for methionine synthesis [755–758] (Figure 44) and achieves a rate enhancement of between 10^6 to nearly 10^8 times compared to realistic protein-free methyl transfer reactions [759]. Impairment to MS activity has severe health consequences [760]. See [761] for a detailed discussion of the chemistry of MS.

The SAM-dependent methyltransferases are also capable of catalysing many other reactions [762] including, for example, the fluoromethylation of unactivated carbon centres through intermediate formation of [CH_2FCbl] [763], a challenging reaction in synthetic organic chemistry; the methylation of high-value small molecules; the transfer of other alkyl groups; the targeted labelling of oligonucleotides and proteins [764]; and Friedel–Crafts alkylations [765].

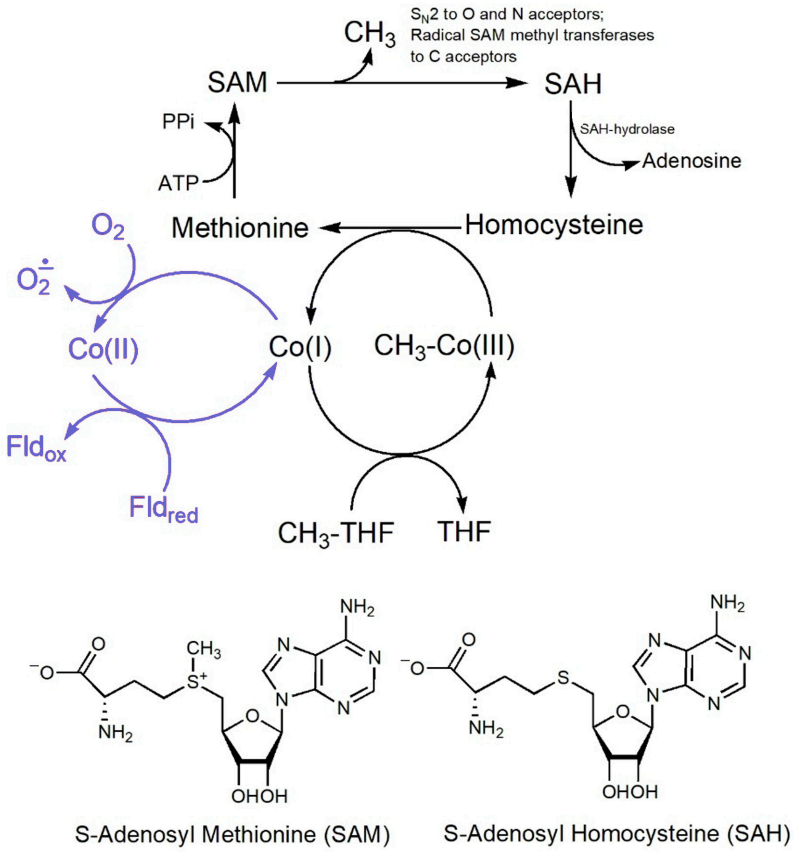

Figure 44. The transfer of a methyl group from 5-methyltetrahydrofolate to homocysteine, producing methionine, catalysed by methionine synthase. Occasionally, Co(I) is oxidised by O_2 or reactive oxygen species (ROS) to inactive cob(II)alamin, [Cbl(II)] [766] (in blue). Function is restored by reduction of Co(II) to Co(I) by methionine synthase reductase (MSR), a diflavin reductase. It uses both FAD and FMN as intramolecular electron carriers during catalysis [767].

8.2. The [AdoCbl]-Dependent Enzymes

The [AdoCbl]-dependent enzymes catalyse the exchange of a hydrogen atom on one carbon atom of the substrate with an electron-withdrawing group X on a neighbouring carbon atom (Equation (30)). The reactions hinge on the homolysis of the Co-C bond between the metal and the Ado ligand, and formation of an Ado• radical [768].

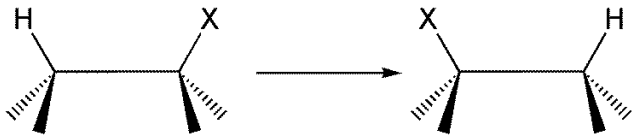

(30)

There are three classes of [AdoCbl]-dependent enzymes [732,769]. The Class I enzymes, the mutases, catalyse a carbon skeleton rearrangement in which the migrating group is a carbon fragment. An example is methylmalonyl-CoA mutase (MCM); see Figure 43. AdoCbl is synthesised from [Cbl(II)] in a reductive adenosylation reaction catalysed by adenosyltransferase, which also acts as an escort and delivers AdoCbl to MCM [770].

The Class II enzymes include the eliminases [771], which catalyse the migration and subsequent elimination of a hydroxyl or amino group (the reaction catalysed by ethanolamine ammonia-lyase is shown in Figure 43), and ribonucleoside-triphosphate reductase [772], which catalyses the reduction of ribonucleoside triphosphates (Figure 43). Ribonucleotide reductase catalyses a reduction reaction, rather than a rearrangement

reaction, although the removal of the 2′-OH group of the substrate is like the reactions catalysed by the eliminases. Finally, the Class III enzymes, the aminomutases, catalyse the migration of an amino group to an adjacent carbon (the reaction of lysine-5,6-aminomutase on DL-lysine is shown in Figure 43).

In the Class I and Class III enzymes, the dmbzm base of [AdoCbl] is displaced from the α coordination site by a His residue of the protein (referred to as the "base-off/His-on form"), and the nucleotide loop is buried in a hydrophobic pocket. [MeCbl] is bound in a similar manner in methionine synthase [773]. In the Class II enzymes, [AdoCbl] is bound with the axial dmbzm ligand coordinated to the metal (the "base-on/His-off form"). That the chemistry catalysed by the [AdoCbl]-dependent enzymes is carried out with either dmbzm or His as an axial ligand suggests that the identity of the axial ligand in cobalamin chemistry is of minor importance (but see below). There is both experimental evidence [394,774] and evidence from theoretical calculations [775] indicating that the bond between cobalt and its proximal ligand is quite flexible and has little influence on the Co–C bond dissociation energy [776,777].

The loss to the Ado moiety from the AdoCbl-dependent enzymes and formation of hydroxocobalamin leads to loss of enzyme activity, and organisms have strategies to reactivate the enzymes [778].

The reaction of MCM is used to illustrate a typical reaction catalysed by an [AdoCbl]-dependent enzyme (see Figure 43). A schematic of the reaction is shown in Figure 45.

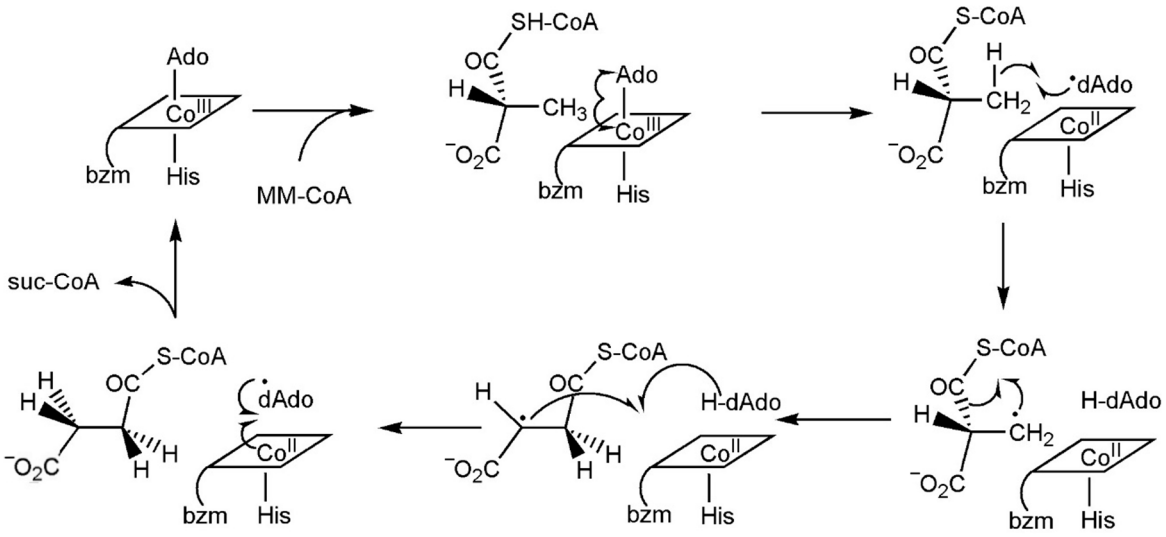

Figure 45. The reaction catalysed by methylmalonyl-coenzyme A mutase (MCM).

In the first step of the reaction, the Co–C bond between cobalt and the adenosyl moiety is cleaved, producing an Ado• radical [779,780]. This radical abstracts a hydrogen atom from the substrate, generating a substrate radical [781]. Remarkably, the enzyme accelerates this reaction by approximately 12 orders of magnitude [750,782,783]. The mechanism behind this extraordinary rate enhancement has been a subject of debate and speculation [784–791], and it appears to vary between enzymes. For instance, in ethanolamine ammonia-lyase, time-resolved, full-spectrum EPR analysis shows that $\Delta H^{\ddagger}$ is identical to that in aqueous solution, but $\Delta S^{\ddagger}$ is ten times larger; the catalysis is entropy-driven [792] and is probably the consequence of changes in the interactions between the active site residues and the Ado ligand when the enzyme binds the substrate [793]. Similarly, entropy drives the formation of the Co(II)-cysteine thiyl radical ion pair in ribonucleotide triphosphate reductase [794]. However, in methylmalonyl-CoA mutase, the driving force is primarily enthalpic [779].

Several factors contribute to this rate enhancement [795]. First, stabilisation of the post-homolysis products, Co^{2+} and the Ado• radical, through van der Waals and electrostatic interactions with the protein, plays a significant role ([796] and references therein). Additionally, the proximal histidine ligand is part of a hydrogen-bonded network known as the catalytic triad (DXHXGXK or DXHXGXN in 2-methyleneglutarate mutase) [797–799]. Proton uptake by the catalytic triad reduces charge donation by the proximal ligand, so stabilising the Co^{2+} state. Other contributing factors include [800] the following: (i) a reduction in the bond dissociation energy of the Co–C bond in the enzyme compared to free [AdoCbl]; (ii) moderate stabilisation of the protein when the cofactor is in its dissociated form; and (iii) steric interactions with protein residues which deform the coenzyme, decreasing its bond dissociation energy.

8.3. The Reductive Dehalogenases

Reductive dehalogenases (RDases) catalyse the removal of halogen atoms from organic substrates (Figure 46) [801,802]. These enzymes are capable of degrading both naturally occurring [647] and anthropogenic organohalogen compounds present in the environment [803]. To date, no homologous enzymes have been identified in humans.

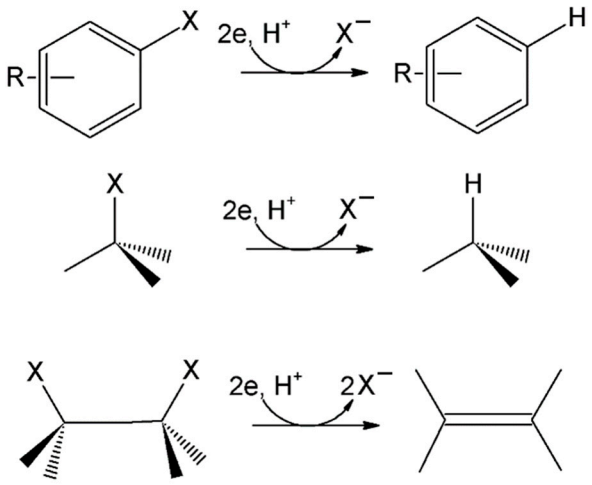

Figure 46. Some examples of reactions catalysed by the RDAses.

Several mechanistic pathways have been proposed for RDase-catalysed reactions, all of which feature Co^{+} as the nucleophile that initiates an attack on the substrate [801,804].

Typically, RDases contain two iron–sulphur clusters—either two [4Fe–4S] clusters or one [4Fe–4S] and one [3Fe–4S]—in addition to a cobalt corrinoid cofactor, in which a water molecule (or hydroxide ion) occupies the β axial coordination site of cobalt. The electron source for these reductive reactions can include reduced metal ions such as iron, tin, or zinc [805], or metal-containing porphyrinoid cofactors such as cobalamin, coenzyme F_{430}, or haemin [805]. However, for the majority of RDases, the identity of the physiological electron donor remains unresolved [647].

8.4. Why Corrin, and Why Cobalt?

Perhaps the first question that arises when contemplating the biological chemistry of B_{12} and its derivatives is why the corrin ring, an apparently much more complex structure than, for example, a porphyrin, has been retained in nature [806]. And why use a kinetically inert metal ion as the prosthetic group of an enzyme?

The biosynthesis of the corrinoids and the porphyrins initially follows a common pathway [807,808], which begins with the tetramerisation of the biological pyrrole porphobilinogen [809] and the formation of the tetrapyrrole uroporphyrinogen III. The paths

then deviate to the porphyrins and the corrinoids. Many bacteria are able to synthesise corrinoids while primitive anaerobes such as acetogens and methanogens are unable to synthesise porphyrins; this suggests that the biosynthesis of corrins has its origins in prebiotic chemistry and actually predates that of porphyrins ([810] and references therein). Many of the apparently complex structural elements that characterise a corrin, including the ring contraction that leads to the direct link between rings A and D, arise quite readily when a corrin precursor, a corphinoid, is coordinated to a smaller metal ion such as Co or Ni, but not Fe [811]. So, the occurrence in nature of the seemingly complex macrocyclic structure of a corrin in nature is probably not surprising.

As mentioned above, the corrin appears to confer on inert Co^{3+} some measure of labile Co^{2+} character—much more so than does a porphyrin, for example, since ligand substitution reactions at a Co^{3+} corrin are much faster than at a Co^{3+} porphyrin [394]. Co^{3+} corrinoid complexes are six-coordinate; Co^{2+} complexes are usually five-coordinate; and Co^{+} complexes are four-coordinate. However, in each case the metal is retained in a predominantly low-spin state (see [394] for a discussion of the ground state electronic configuration of these complexes). Crystallographic evidence shows that reduction of six-coordinate low-spin Co^{3+} to five-coordinate low-spin Co^{2+} has virtually no effect on the average bond length between the metal and the N donors of the corrin [394]. There is consequently little influence on the reorganisation energy, one of the major factors that controls the rate of an electron transfer reaction [579]. This clearly contributes to an efficient conversion between (formally) Co^{3+} and Co^{2+} in the [AdoCbl]-dependent enzymes and undoubtedly plays a role in the fast kinetics of their reactions.

In iron porphyrins, the spin state of the metal ion depends on its oxidation state and its coordination number. Six-coordinate Fe^{2+} and Fe^{3+} porphyrins are usually low-spin ($S = {}^{1}/_{2}$), whereas when five-coordinate, the metal ion is typically high-spin ($S = {}^{5}/_{2}$) [812,813]. In four-coordinate Fe^{2+} porphyrins, the delocalisation of electron density between the metal centre and the π system of the porphyrin stabilises the intermediate-spin state ($S = {}^{3}/_{2}$) over the high-spin state [814]. Moreover, porphyrins show a dependence of the metal–N_{porph} bond lengths on the spin state of the metal [815]. The Fe^{3+} analogue of B_{12} can be reduced to Fe^{+}, but cannot be methylated [816]. A ferric corrin therefore could not catalyse the reactions catalysed by [MeCbl]. A Fe^{+} porphyrin is highly reactive and can be generated only transiently [817]—for example, electrochemically [818,819].

The Fe^{3+}–CH_3 bond dissociation energy in a porphyrin is only 88 kJ mol^{-1} [820], significantly weaker than the Co–CH_3 bond in [MeCbl]. So, while a metal–carbon bond that is not too strong is important, it cannot be too weak. The Fe–C bond in complexes of the type [(porph)Fe^{3+}–R^{-}], R = ethyl, butyl) is readily homolysed in the presence of CO or CO_2 to form an intermediate Fe^{2+}–CO or Fe^{3+}–$CO_2{}^{-}$ complex which is then attacked by the caged alkyl radical [821]. One of the likely reasons for the use of a Co–C bond in biology is its resistance to hydrolysis, which is important in an aqueous environment [822]. Theoretical calculations show that a Co–C bond is between 33 and 48 kJ mol^{-1} more resistant to hydrolysis than an Fe–C bond [812].

Clearly, iron porphyrin compounds cannot perform cobalt corrinoid-type chemistry, rationalising the occurrence of cobalt in biology.

Organometallic chemistry in biology, while not common, is by no means confined to the chemistry of the cobalt corrinoids. Some examples are the M cluster of nitrogenase (Fe–C–Fe) [823–825]; Fe–CO in [Fe]-hydrogenase [826,827], Fe–Ado in the radical *S*-adenosyl methionine (SAM) intermediate omega [828,829]; and the C cluster of carbon monoxide dehydrogenase (CODH, Ni–C(O)O–Fe) [830–832]. Nor are methyl transfer reactions in biology confined to the cobalt corrinoids. For example, F_{430}, a Ni hydrocorphin, is

the active site in methyl-coenzyme M reductase (MCR) which catalyses the reaction shown in Equation (31). This is an important reaction in the global carbon cycle [833–835].

$$CH_3–S–CoM + CoB–SH \rightarrow CoM–S–S–CoB + CH_4 \quad (31)$$

In the reaction, Ni^+ acts as the attacking nucleophile on the S–CH_3 bond of $CoMSCH_3$ [834,836,837], in a manner analogous to the action of Co^+ in the [MeCbl]-dependent enzymes.

As discussed in Section 7, an important function of six-coordinate iron porphyrins in biology is to act as electron transfer agents in electron transport chains. The reorganisation energy for the Fe^{3+} | Fe^{2+} couple in such a case is a very modest 8 kJ mol^{-1}; for the Co^{3+} | Co^{2+} couple in a cobalt corrinoid with two axial His ligands this is an untenable 197 kJ mol^{-1} because of the location of the unpaired electron density in $3d_z^2$ [812]. Cobalt corrinoids would not be suitable for this function. DFT calculations also show that for the oxidation states +1 through +3, and for virtually all axial ligands investigated, cobalt corrin and iron porphyrin systems are thermodynamically more stable than iron corrin and cobalt porphyrin systems [812], offering an explanation for the matching of the metal to the macrocycle in nature [813].

An important function of iron porphyrin-containing proteins is the transport and storage of O_2 (Section 7). This is chemistry that cannot be performed by the cobalt corrinoids. At low temperatures, cob(II)alamin will indeed bind O_2, forming what is essentially a Co^{3+}–O_2^- complex; however, near-room temperature cob(II)alamin is rapidly oxidised to Co^{3+} [838,839]. Cob(I)alamin is very rapidly oxidised by O_2. Co^{2+} porphyrins, and cobalt-reconstituted Hb and Mb [840,841], can reversibly bind O_2 [840,842–849], but substituting Fe-protoporphyrin IX with a cobalt porphyrin in human adult Hb decreases its O_2 affinity by over a factor of 10 [848].

Living systems could probably have evolved in the total absence of cobalt; nevertheless, cobalt corrinoids fulfil an important, albeit niche, role in nature. A memorable—if somewhat simplistic—parallel has been drawn between iron porphyrins and cobalt corrinoids: the first act as reversible oxygen carriers, the latter as reversible free radical carriers [850,851].

9. Nickel

Nickel is not a particularly abundant element in the Earth's crust (≈75 ppm), but it is an essential trace element for various prokaryotes, algae, fungi, and plants [10,837,852–854]. Its role as a trace element in animals, including humans, however, remains to be fully established [10].

Whilst an essential trace element for some life forms, in high concentrations nickel is toxic and there is considerable concern about the effect of high levels of nickel from anthropogenic sources [10,855–860]. For instance, nickel can displace Mg^{2+} from the active site of GTPase, rendering the enzyme inactive [10,855].

In biological systems, nickel predominantly exhibits oxidation states of +1, +2, and +3 [861]. Nickel's primary biological function is as a redox-active metal or as a structural anchor for nucleophiles, such as OH^-, at the active site of specific enzymes. These have been found in archaea, bacteria, plants, and primitive eukaryotes, and include acireductone dioxygenase, CO-dehydrogenase, glyoxalase, lactate racemase, methyl-coenzyme M reductase, Ni-superoxide dismutase (Ni-SOD), [NiFe] hydrogenase, prolyl cis-trans isomerase, and urease [10,854].

To illustrate nickel's biological roles, we will examine specific Ni-containing enzymes: one where nickel serves a structural role, two where its redox properties are exploited, and

one where its function is not yet fully understood. The general mechanism of superoxide dismutases (SODs), discussed in Section 6, likely applies to Ni-SOD as well [333,862].

9.1. Urease

Urease plays an important role in the global nitrogen cycle, where it catalyses the decomposition of urea to ammonia and carbamate (Equation (32)), with a rate enhancement of some 10^{14} or higher [863], making it one of the most efficient enzymes known. It is also used by pathogens to infect host cells [864], and the increase in pH can have a negative effect on human health [865]. *Helicobacter pylori* [866,867], *Staphylococcus aureus* [868], and *Mycobacterium tuberculosis* [869] are examples of pathogens that contain urease. Urease-utilising species have evolved an elaborate delivery system to ensure that toxic Ni is delivered to the enzyme active site without diffusing into the cytoplasm [867,870–873].

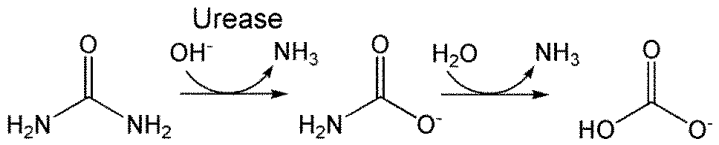

(32)

It has been known since the 1970s that urease requires two Ni atoms in each of its subunits for catalytic activity [874]. The number of subunits in urease varies across different organisms [875]. In the active site of urease, two Ni^{2+} ions are positioned approximately 3.5 Å apart, bridged by a hydroxide ion and a carbamylated Lys residue. The active site structure from *Klebsiella aerogenes* (KAU) (PDB 1FWJ [876]) is shown in Figure 47, along with a schematic representation.

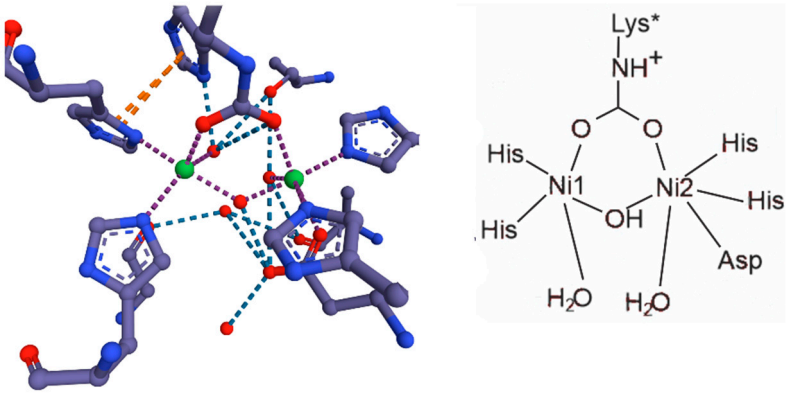

(**a**) (**b**)

Figure 47. (**a**) The active site of the urease from *Klebsiella aerogenes* (PDB 1FWJ [876]). (**b**) Schematic of the active site. Lys* is a carbamylated Lys residue.

In this structure, Ni1 is coordinated by two His residues and a water molecule, while Ni2 is coordinated by two His residues, a monodentate Asp, and H_2O. Additionally, a third water molecule is located near the active site. These water molecules are typically labelled W1, W2, and W3. When urea binds at the active site, it displaces W1 and W3, and its carbonyl group coordinates with Ni1. The specific coordination mode of urea—whether it binds monodentately through its carbonyl group or through one of its NH_2 groups to Ni2—has been a subject of debate [877–880].

Either the coordinated OH^- or deprotonated W2 acts as the nucleophile, attacking bound urea. The Ni^{2+} ions in urease do not perform a redox function. Instead, they serve as Lewis acids, playing key roles in (i) coordinating and anchoring the substrate; (ii) increasing the electrophilicity of the urea carbonyl group; and (iii) stabilising the attacking nucleophile.

Over the years there have been several proposals for the mechanism of the reaction, as well documented by Mazzei et al. [875]. Computational modelling (QM and QM/MM MD [881]) favours—but of course does not prove—the mechanism shown in Figure 48, involving bidentate coordination of urea. See [880] for alternative proposals based on the results from the urease activity of models of the active site.

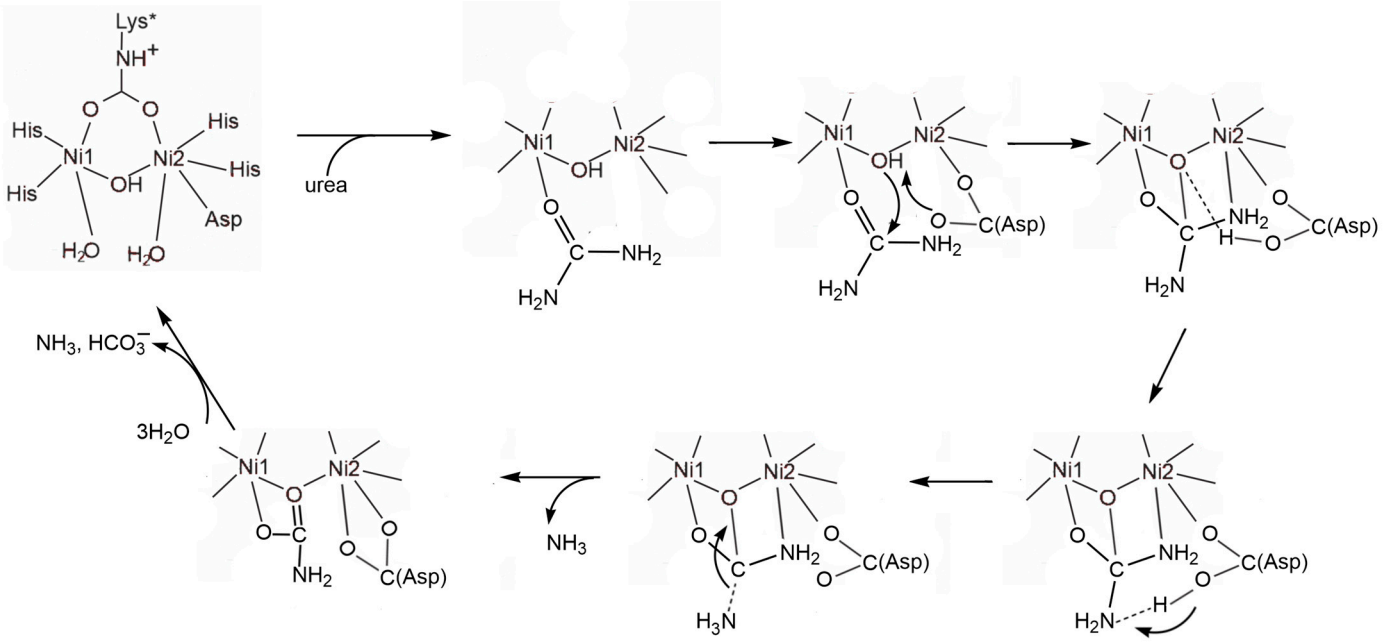

Figure 48. A possible mechanism for the conversion of urea to ammonia and carbamate by urease. Carbamate spontaneously decomposes to bicarbonate and ammonia.

However, as pointed out by Mazzei and co-workers [882], understanding the dynamics of an enzyme requires knowledge of its entire conformational space. Using cryo-EM methods, they demonstrated the importance of the mobility of a mobile flap in the urease from *Sporosarcina pasteurii* in flipping between the inactive open-flap state and the closed-flap, catalytically efficient, state of the enzyme. Both a Cys and His residue on the flexible flap are essential for catalytic function [883,884].

9.2. Methyl-Coenzyme M Reductase

Methyl-coenzyme M reductase (MCR) catalyses the terminal step of methane formation in the energy metabolism of all methanogenic archaea, and the terminal step in the anaerobic oxidation of methane; these are important reactions in the global carbon cycle [833–835,885,886]. In the reaction, methyl-coenzyme M (CH_3–S–CoM) and coenzyme B (CoB–SH) are converted into methane and a heterodisulphide (Equation (33)).

$$CH_3\text{–S–CoM} + \text{CoB–SH} \rightarrow \text{CoM–S–S–CoB} + CH_4 \quad (33)$$

The enzyme also catalyses the reverse reaction, the anaerobic activation, and oxidation of CH_4, which entails the cleaving of a C-H bond. The active site contains a Ni hydrocorphin, F_{430} (Figure 49).

In the reaction catalysed by MCR, Ni must be in its +1 oxidation state to function effectively [887,888]. Ni^+ acts as a nucleophile, and one of the key roles of the hydrocorphin macrocycle is to stabilise and make this oxidation state accessible. In F_{430}, the standard reduction potential of the $Ni^{2+}|Ni^+$ redox couple is −0.65 V [889]. Although this is more negative than the −0.41 V of the $2H^+|H_2$ couple at pH 7 (the lower limit of nature's "electrochemical window"), it is significantly higher than, for instance, the −1.3 V observed

in a Ni-isobacteriochlorin complex. This illustrates how the structure of a macrocycle can fine-tune the redox potential of a metal complex, bringing it into a useful biological range.

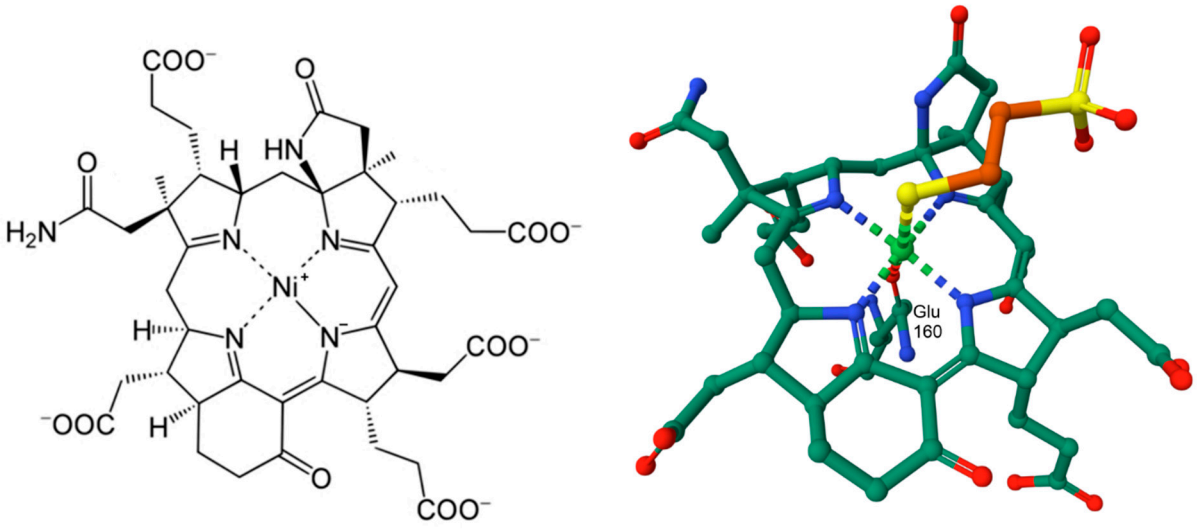

(**a**) (**b**)

Figure 49. (**a**) Structure of a nickel-containing hydrocorphin, F_{430}. (**b**) F_{430} from the crystal structure of methyl-coenzyme M reductase from *Methanosarcina barkeri* (PDB 1E6Y [890]) with Glu160 and the substrate mimic thioethane-sulphonic acid as axial ligands.

Several structural features of F_{430} facilitate the reduction of Ni^{2+} to Ni^{+}. First, the macrocycle is a monoanion, in contrast to porphyrins and isobacteriochlorins, which are dianions. Second, there is an electron-withdrawing carbonyl group attached to the C15 meso position (Figure 49), which further aids the reduction of Ni^{2+} [641]. When Ni^{2+} is reduced, the added electron density resides on the metal, forming an $S = {}^{1}/_{2}$ species. This differs from Ni porphyrin or Ni chlorin complexes, where the reducing equivalent is mainly located on the macrocycle, weakening the metal's ability to act as a nucleophile. In MCR the nucleophilic activity of Ni^{+} is crucial, allowing it to behave similarly to cob(I)alamin, which serves as a "supernucleophile" in methylcobalamin-dependent chemistry (see Section 8).

The requirement for the Ni^{+} state makes the enzyme highly sensitive to oxidation by O_2 or other oxidants. To address this, methanogens employ an ATP-dependent enzymatic system to reactivate the enzyme when it is oxidised [888].

Several mechanisms have been proposed for the MCR-catalysed reaction [836,891–893], with current evidence supporting the mechanism depicted schematically in Figure 50 [834,836,837,894]. In the oxidised form of the coenzyme, Ni^{2+} is axially coordinated by a Gln residue [890,895,896] (Figure 49), but it likely becomes four-coordinate in the reduced, Ni^{+}-active form. The conversion of the oxidised Ni^{2+} form to the active Ni^{+} form is facilitated by a multicomponent [4Fe–4S] protein [897]. An electric field aligned along the CH_3-S-CoM thioether bond facilitates its homolytic bond cleavage [898], emphasising that it is not only the structure of the active site, but of the protein as a whole, that is important for the activity of an enzyme.

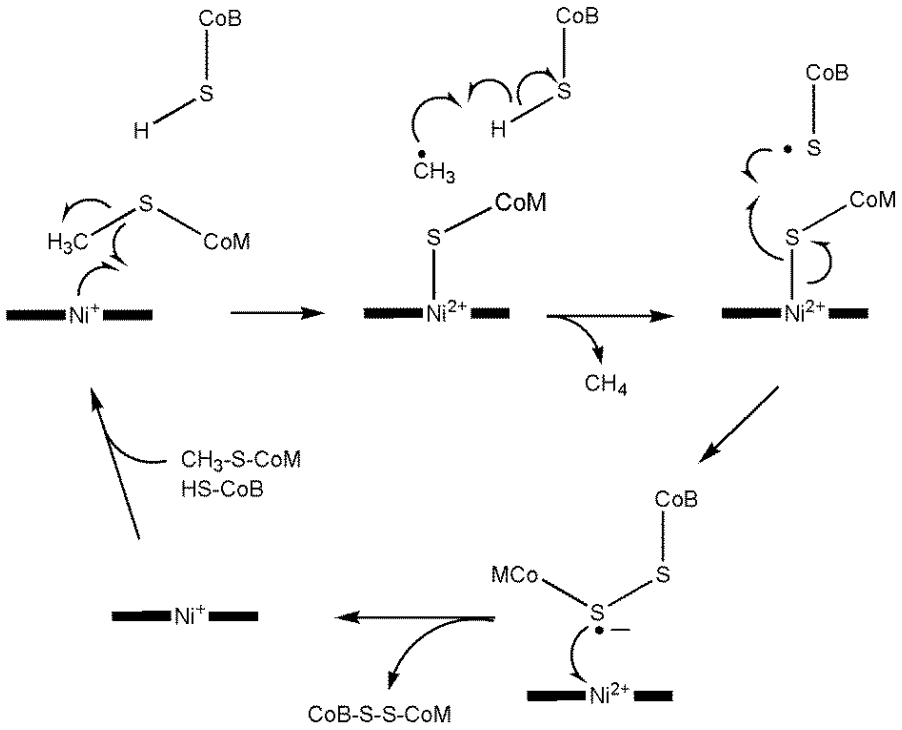

Figure 50. A possible mechanism of the reaction of CH_3–S–CoM and CoB–SH catalysed by methyl-coenzyme M reductase.

9.3. NiFe Hydrogenases

Hydrogenases are enzymes that catalyse the reversible oxidation of H_2 [899–903]. They typically contain a bimetallic active site ([NiFe] or [FeFe]) and catalyse the reaction shown in Equation (34).

$$H_2 \rightleftharpoons H^- + H^+ \rightleftharpoons 2H^+ + 2e \quad (34)$$

It is speculated that Complex I of the mitochondrial electron transport chain may have evolved from a primordial hydrogenase [542,595]. There is considerable interest in these enzymes as it may be feasible to exploit them—or model their chemistry—in biofuel cells to produce H_2 [902,904].

The NiFe active site features an Fe ion coordinated by a CO and two CN^- ligands. Two thiolates of Cys residues bridge the two metals ions, and Ni is terminally coordinated by two Cys residues [905]. The CN^- ligands are synthesised from carbamoylphosphate by maturases and the CO arises from N^{10}-formyl-tetrahydrofolate [906]. Details from the crystal structure of the NiFe hydrogenase from *Cupriavidus necator* are shown in Figure 51 [907].

The formal oxidation states of the metals of the active site in the reduced (active) form of the enzyme are Fe^{2+} and Ni^{2+}. During the catalytic cycle, Fe remains in the low-spin, +2 oxidation state (S = 0) [899] while Ni cycles between (formally) the oxidation states +3, +2, and +1 (Figure 52) [908]. In addition, an electron transport chain of iron–sulphur clusters leads from the active site to the surface of the protein where electrons are passed on to the electron acceptor, cytochrome c_3 [909] (Figure 51).

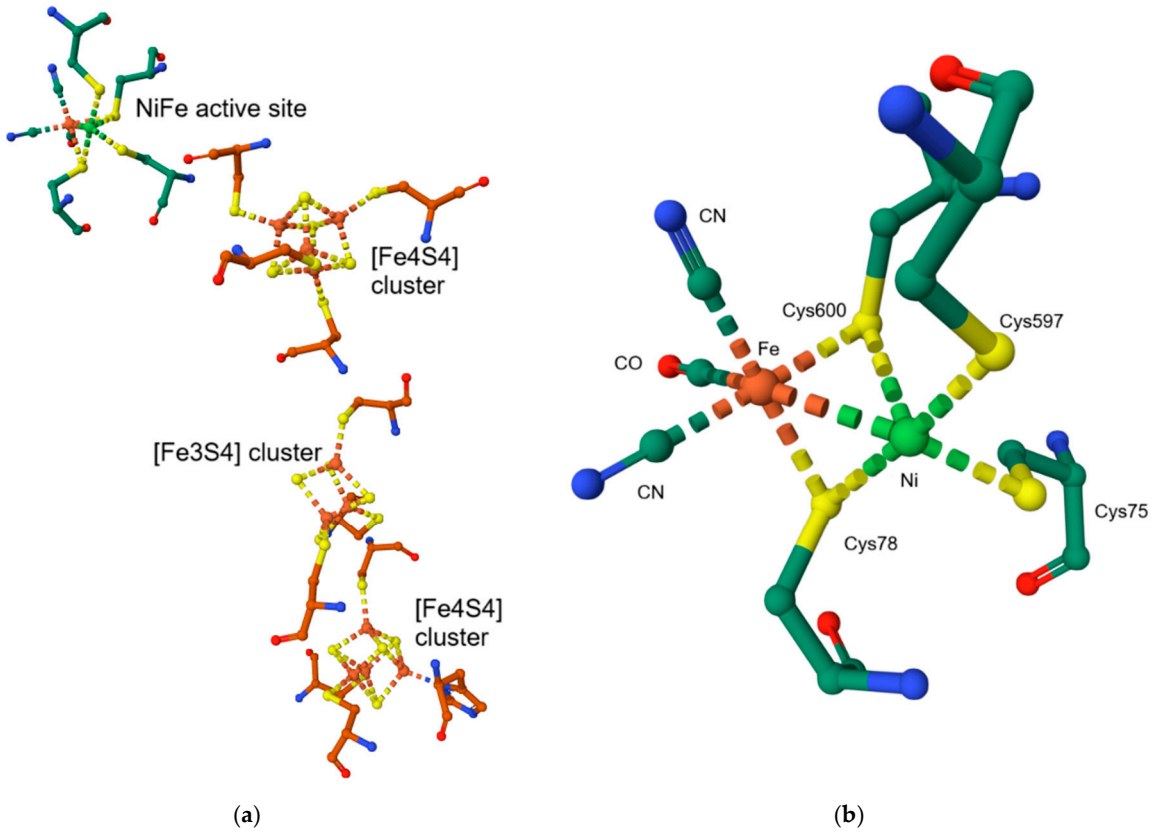

Figure 51. The [NiFe] hydrogenase from *C. necator* (PDB 8POV [907]). (**a**) The chain of iron–sulphur clusters and the NiFe active site. (**b**) The NiFe active site.

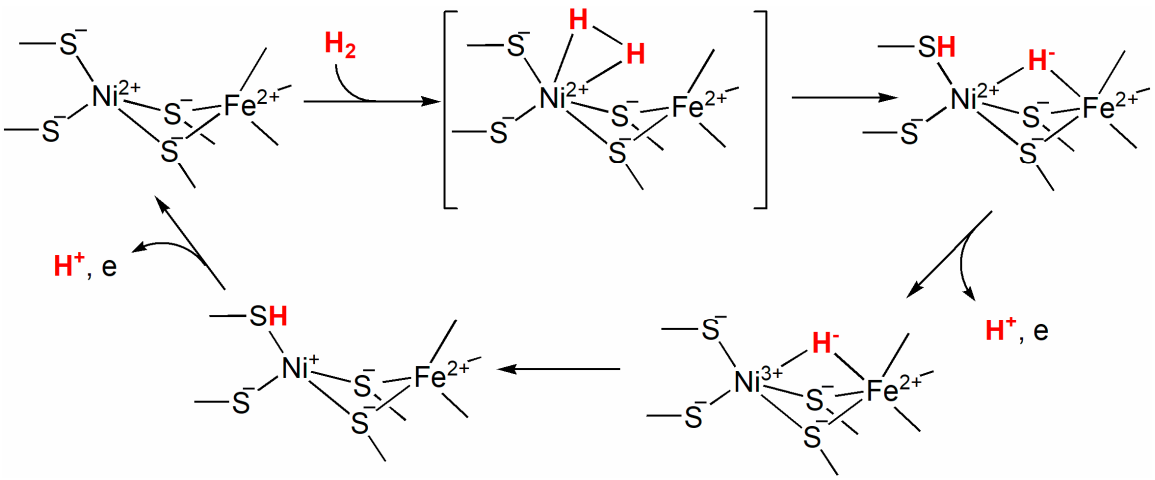

Figure 52. Possible mechanism of the oxidation of H_2 by NiFe hydrogenase [908].

The initial site of H_2 binding is probably Ni^{2+}, as suggested by QM/MM calculations [910]. Enzyme efficiency is ensured by coupling the proton and electron transfer processes (involving a Cys ligand of Ni and the carboxylate of a neighbouring Glu residue) [911,912]. There is also considerable knowledge, if not yet a complete understanding, of the gas-access tunnel in the enzyme (for details see [902]). A possible mechanism is shown in Figure 52.

9.4. Lactate Racemase

Lactate racemase is a Ni-containing enzyme that isomerises L-lactate to D-lactate (Equation (35)). The active site contains a nickel-pincer nucleotide (NPN) as a cofactor, with two S atoms and a C atom bonded to nickel, a cofactor that is used in a large family of α-hydroxyacid racemases and epimerases [913] (Figure 53). How NPN is biosynthesised has been described [914,915].

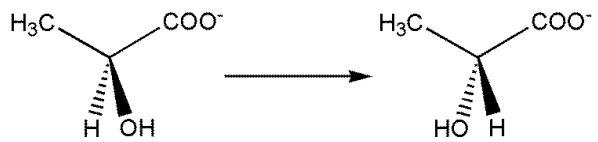

(35)

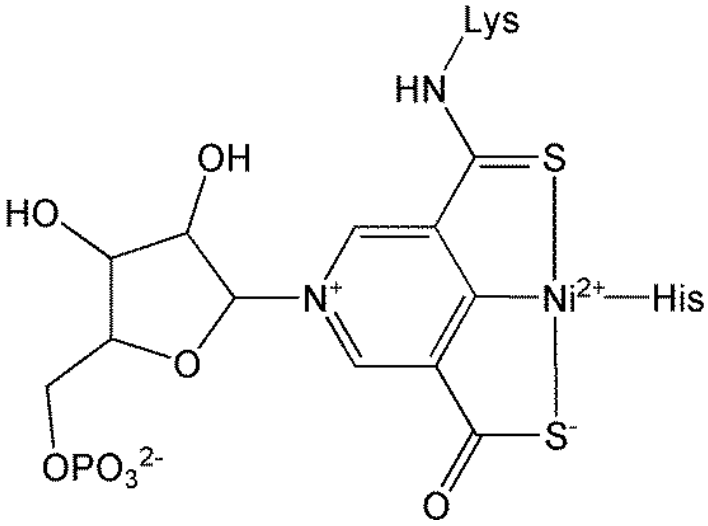

Figure 53. The nickel-pincer nucleotide (NPN) cofactor of lactate racemase.

There is still debate concerning the mechanism of the reaction, with proposals including a proton-coupled electron transfer mechanism in which nickel, originally in the +3 oxidation state, oxidises lactate to form a transient $CO_2^{\bullet -}$ radical anion and is reduced to Ni^{2+} (Figure 54a) [916], and a proton-coupled hydride transfer mechanism, with nickel in the +2 oxidation state, featuring the transient formation of pyruvate (Figure 54b) [917–920]. The experimental evidence (rather than computational results) appears to favour the latter proposal: there is no evidence of an EPR signal for Ni^{3+}, and pyruvate is detected in quenched solutions of lactate racemase [920]. The inactivation of the enzyme by $NaBH_4$ also favours this proposal [921].

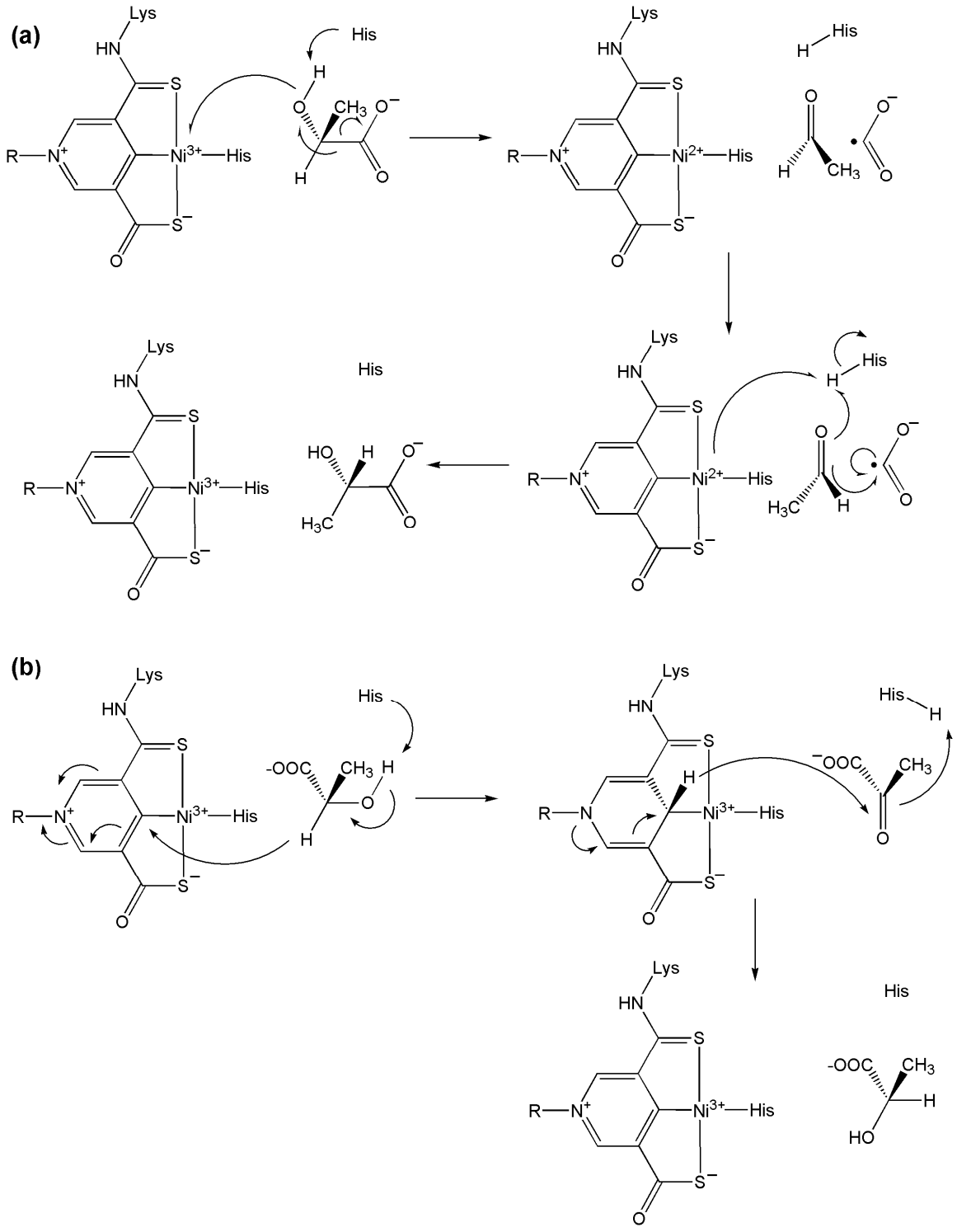

Figure 54. Possible mechanisms for the conversion of L-lactate to D-lactate by lactate racemase: (**a**) proton-coupled electron transfer; (**b**) proton-coupled hydride transfer. The location of the hydride could be on C, as shown, or on nickel [920].

10. Copper

Copper is relatively scarce in the Earth's crust, with a concentration of 27 ppm [922]. Nevertheless, with two readily accessible oxidation states, +2 and +1, copper has been integrated into a wide range of biological systems [923–926]. While Cu^{+} would have been sequestered as an insoluble sulphide in Earth's primordial reducing atmosphere, Cu^{2+} became more accessible in an oxidising environment following the Great Oxidation

Event, due to its moderate solubility in mildly acidic solutions (K_{sp} of $Cu(OH)_2$ = 2.2 × 10^{-20} [927]). Iron-based biochemistry likely predates copper-based biochemistry [926,928]. However, it has been proposed that copper, along with other metals, played a critical role in prebiotic chemistry [929–934]. For instance, the copper-catalysed condensation of amino acids may have contributed to the formation of prebiotic peptides [929], and Cu^{2+} may have been involved in the activation of nucleotides [930].

Many enzymes utilise Cu^{2+} | Cu^{+} chemistry [935–938]. The ability to exploit these two oxidation states, which lie within or near nature's electrochemical window, is a key feature in electron transfer proteins and in catalytic enzymes such as oxidases and oxygenases (Figure 55). As with all metal ions, maintaining copper homeostasis is essential for the health of the organism [939–941].

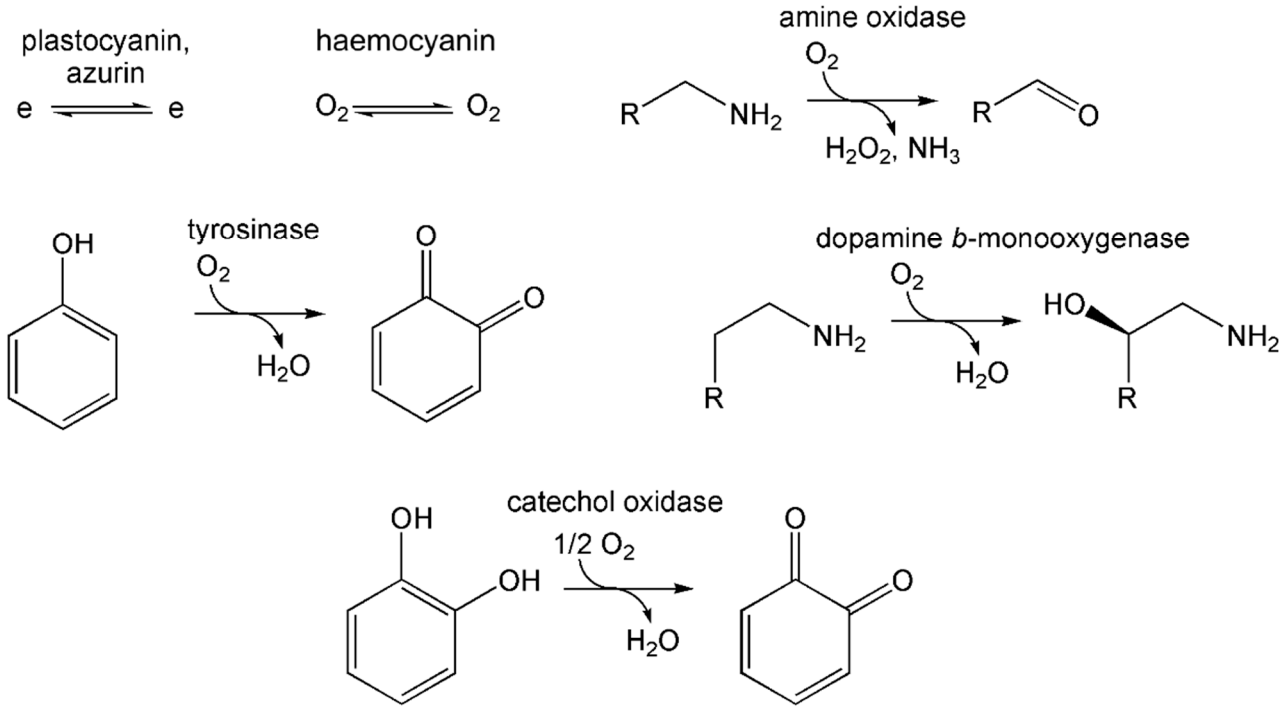

Figure 55. Examples of reactions catalysed by copper metalloproteins and enzymes.

10.1. The Coordination Environment of Copper: The Blue Copper Proteins

Copper is found in a variety of coordination environments within copper-containing enzymes [942–944], several of which are illustrated in Figure 56. One of the most prominent structural motifs employed in copper coordination is the cupredoxin domain, a three-dimensional protein fold utilised in type I (blue copper) proteins [945]. This fold is typically rigid and exhibits minimal conformational change upon metal binding. Notably, however, the apo form of cupredoxin is considerably more flexible, becoming rigid only upon coordination with the metal ion [946]. The primary role of blue copper proteins is to function as outer-sphere, one-electron transfer agents [82,947,948]; an example of such a function in photosynthesis was discussed in Section 7.2.

Copper centres in enzymes may be either mononuclear or multinuclear. Mononuclear type I (class I) centres are typically four-coordinate, featuring a distorted tetrahedral geometry with Cys, two His, and Met as ligands [949] as exemplified by plastocyanin ($E_{1/2}$ = 370–400 mV vs. SHE [950]) (Figure 57).

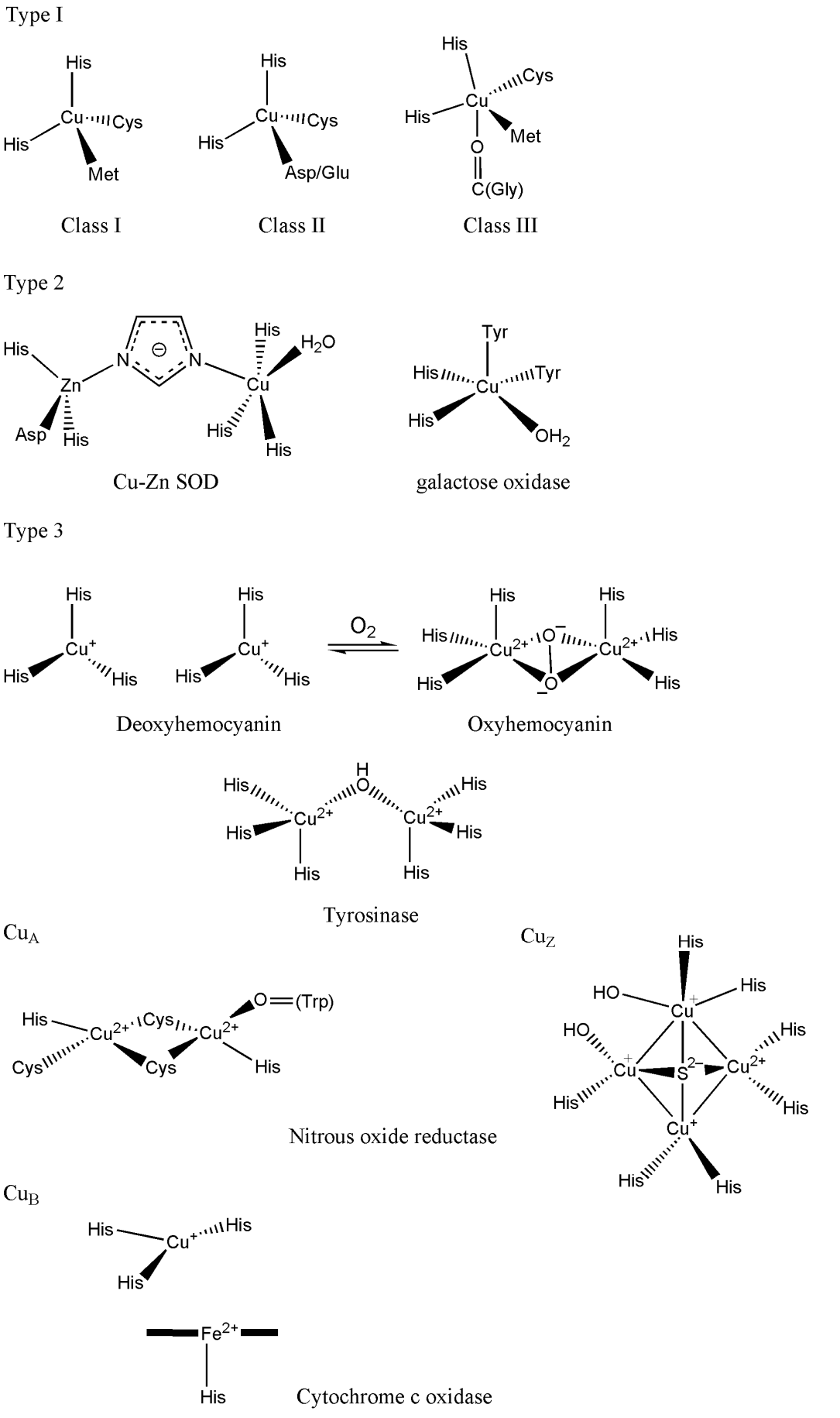

Figure 56. Examples of the coordination environment of copper in copper-containing enzymes.

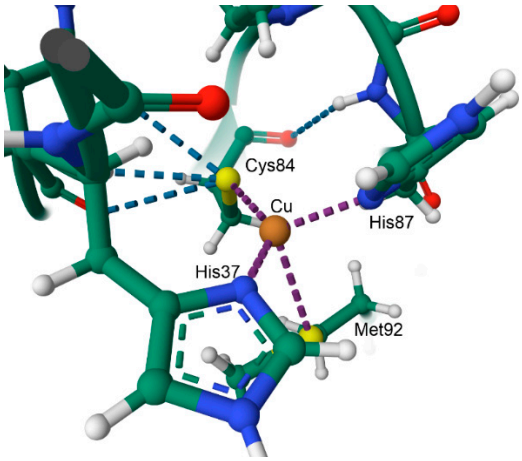

Figure 57. The copper-binding site of plastocyanin.

In these proteins, the copper ion forms strong bonds with the two His and a Cys, while the interaction with Met is comparatively weaker. Typical Cu–Cys and Cu–Met bond lengths are approximately 2.1 Å and 2.9 Å, respectively. The intense blue colour characteristic of these proteins ($\varepsilon \approx 5$ mM^{-1} cm^{-1}) arises from a ligand-to-metal charge transfer (LMCT) transition at 600 nm, specifically from the S(Cys) to $Cu^{2=}$ orbitals, due to a strong π-interaction between $Cu^{2+}(d_x{}^2{}_{-y}{}^2)$ and a sulphur pπ orbital [951], hence the name "blue copper proteins".

The covalent character of the Cu^{2+}–S^{2-} bond results in partial delocalisation of the unpaired electron onto the sulphur, yielding a significantly reduced $A_{||}$ hyperfine coupling constant in the EPR spectrum (ca. 60×10^{-4} cm^{-1}) compared to the values typically observed for Cu^{2+} complexes (ca. 150×10^{-4} cm^{-1}) [952]. Extensive spectroscopic characterisation, backed up by theoretical studies, has yielded profound insight into the structure and function of these proteins [953].

The coordination geometry of the copper centre in blue copper proteins is intermediate between the tetrahedral preference of d^{10} Cu^{+} and the square planar preference of d^{9} Cu^{2+}, placing the metal in what is referred to as an "entatic state" [954–958]. This concept describes a distortion of the ground state coordination geometry to resemble that of the reaction transition state, thereby minimising the reorganisation energy (λ) associated with redox transition, one of the principal barriers to electron transfer, as described by Marcus' theory [579,959] (see below). Indeed, only minimal structural reorganisation is observed upon redox cycling of the copper centre in blue copper proteins [952]. For comparative analyses of plastocyanin structures from various sources, and for investigations of their solution-phase geometries using NMR spectroscopy, see [960].

The rate of electron transfer, k_{ET}, between an electron donor D and an electron acceptor A is given in Equation (36).

$$k_{ET} = \frac{2\left\langle H_{DA}^{o}\right\rangle^{2} e^{-\beta r}}{h}\left(\frac{\pi^{3}}{4\lambda RT}\right)^{\frac{1}{2}} e^{-\frac{\Delta G^{\ddagger}}{RT}} \quad (36)$$

In this equation, $\left\langle H_{DA}^{o}\right\rangle$ is the Hamiltonian that describes the coupling between the wavefunctions of D and A; β is a parameter reflecting the sensitivity of the coupling to the edge-to-edge distance, r, between D and A; λ is the reorganisation energy; and $\Delta G^{\ddagger}$ is the Gibbs energy of activation, as defined in Equation (37), where ΔG^{o} is the change in Gibbs

energy for an electron transfer from the ground state of D to the ground state of A and is therefore related to the standard reduction potentials of D and A by $\Delta G^{o} = -nFE^{o}$.

$$\Delta G^{\ddagger} = \frac{1}{4}\lambda\left(1 + \frac{\Delta G^{o}}{\lambda}\right)^{2} \quad (37)$$

The magnitude of λ is influenced by the surrounding medium: aqueous environments generally result in larger reorganisation energies [580]. Protein structure also plays a significant role: β-sheets, being relatively rigid, facilitate stronger electronic coupling than the more flexible α-helices [580]. In multicopper oxidases, efficient electron transfer is enabled by strong donor–acceptor coupling [953], consistent with the quadratic dependence $k_{ET} \propto \langle H^{o}_{DA} \rangle^{2}$. A small λ is typically associated with blue copper proteins [961], though this remains a topic of debate [962].

Blue copper proteins exemplify the profound influence of protein structure on the redox potential of the $Cu^{2+}|Cu^{+}$ couple, which is 159 mV in aqueous solution [963]. These potentials vary widely. For instance, laccase (a class I blue copper protein coordinated by two His, Cys, and Met) exhibits redox potentials in the range 400–800 mV, whereas stellacyanin (class II, with 2 His, Cys, and either Asp or Glu) has a lower potential range of 200–350 mV. The S(Cys) $\rightarrow$ Cu^{2+} LMCT transition at 600 nm reflects the contribution of a redox-active molecular orbital (RAMO) in the ground state wavefunction, which is key to long-range, outer-sphere electron transfer [952,953].

Class III blue copper proteins such as azurin possess a five-coordinate copper ion (2 His, Cys, Met, and a backbone carbonyl oxygen, e.g., from Gly), adopting a distorted trigonal bipyramidal geometry. Both the inner and outer coordination spheres contribute to the modulation of the copper centre's redox potential, enabling effective electron transfer between physiological donors and acceptors [952,964–966]. Importantly, redox potential is influenced not only by ligand identity but also by the protein scaffold. For example, in plastocyanin, the redox potential is tuned via the interaction between the Met ligand and Cu^{+} in the reduced state [967]. Site-directed mutagenesis has demonstrated that strengthening this interaction leads to an increase in the midpoint redox potential. Furthermore, interactions between the metal ion's primary coordination sphere and its secondary environment influence the spin density on the metal centre, so contributing to the tuning of its redox potential [968,969].

10.2. The Coordination Environment of Copper: Type II and Type III Centres, and the Multicopper Oxidases (MCOs)

Type II copper centres are also mononuclear and have the metal ion in a tetragonal five- or six-coordinate geometry with N and O ligands (Figure 57). Their EPR spectra are consistent with an $S = {}^{1}/_{2}$ Cu^{2+}-oxidised ground state, and the absence of an intense LMCT band confirms the absence of Cys in the coordination sphere. Among the copper enzymes with a Type II centre are superoxide dismutase (see below), amine oxidase [970], lysyl oxidase [971], and galactose oxidase [972].

Type III centres are binuclear, with each copper ion coordinated by three His residues. The ions are antiferromagnetically coupled and exhibit no EPR signal. These copper proteins are involved in oxygen transport and activation (for example, haemocyanin [973] and tyrosinase [974], respectively). The copper A centre (Cu_A), found for example in cytochrome *c* oxidase (Section 7) and nitrous oxide reductase [975,976], features two copper ions bridged by Cys residues, with His, Met, Glu, and Trp typically providing the remaining ligands to each four-coordinate metal ion.

A trinuclear centre (TNC), an association of a type I and a type II centre, occurs in enzymes such as ascorbate oxidase [977] and thiocyanate dehydrogenase [978]. The three

metal ions are coordinated by seven His residues. Nitrous oxide reductase has a four-copper ion centre (see below), with His again featuring as the prominent ligand. Copper plays an important role in cytochrome *c* oxidase and in photosynthesis (Section 7). Lytic polysaccharide monooxygenases (LPMOs) use a copper-based oxidative mechanism to cleave glycosidic bonds [979].

Multicopper oxidases (MCOs) oxidise a wide variety of substrates while (usually) reducing O_2 to H_2O [935,980,981]. Examples include laccase (found in fungi and plants and which oxidises diamines and phenols), ascorbate oxidase (found in higher plants; it catalyses the oxidation of ascorbic acid to L-dehydroascorbic acid) and nitrite reductase (a bacterial and fungal enzyme that reduces NO_2^- to NO and H_2O). Other MCOs, termed metallo-oxidases, use Fe^{2+}, Cu^+, or Mn^{2+} as their source of electrons. They all have multiple copper sites.

Typically, electrons are accepted at a mononuclear copper site, usually a type I site, [Cu(His_2CysMet)], and pass through a His-Cys-His pathway [982] to a multi-copper site some distance from it (≈13 Å) where reduction of O_2 (or N_2O) occurs. The evolutionary relationship between MCOs, an ancestry dating back to small mononuclear copper proteins, has been delineated [981,983,984]. The trinuclear cluster of the multicopper oxidase CueO from *E. coli* is shown in Figure 58 [985]. The enzyme is involved in copper tolerance under aerobic conditions [986]. It contains two Cu ions coordinated to three His ligands and solvent H_2O (or OH^-), termed Cu_{T3}, and a Cu ion coordinated to two His residues and a solvent H_2O (or OH^-), termed Cu_{T2}.

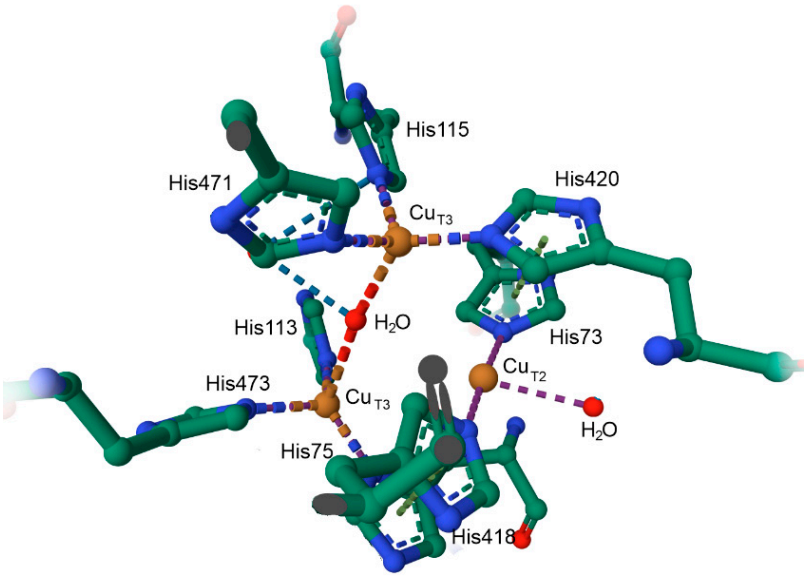

Figure 58. The trinuclear copper site of the multicopper oxidase CueO from *E. coli* (PDB 1KV7 [985]). In the resting state of the enzymes, all copper ions are in the +2 oxidation state.

A proposed mechanism for the reduction of O_2 to H_2O by the multicopper oxidases is shown in Figure 59 [987,988]. The proposal is based on experimental evidence backed by theoretical calculations. The three Cu ions interact with O_2. This provides the protein with the means of, initially, reducing O_2 to O_2^{2-}, so overcoming the spin-forbidden reduction of $^3O_2$ by, for example, an organic substrate (S = 0), and then to perform four one-electron transfers to the substrate with a minimal release of ROS.

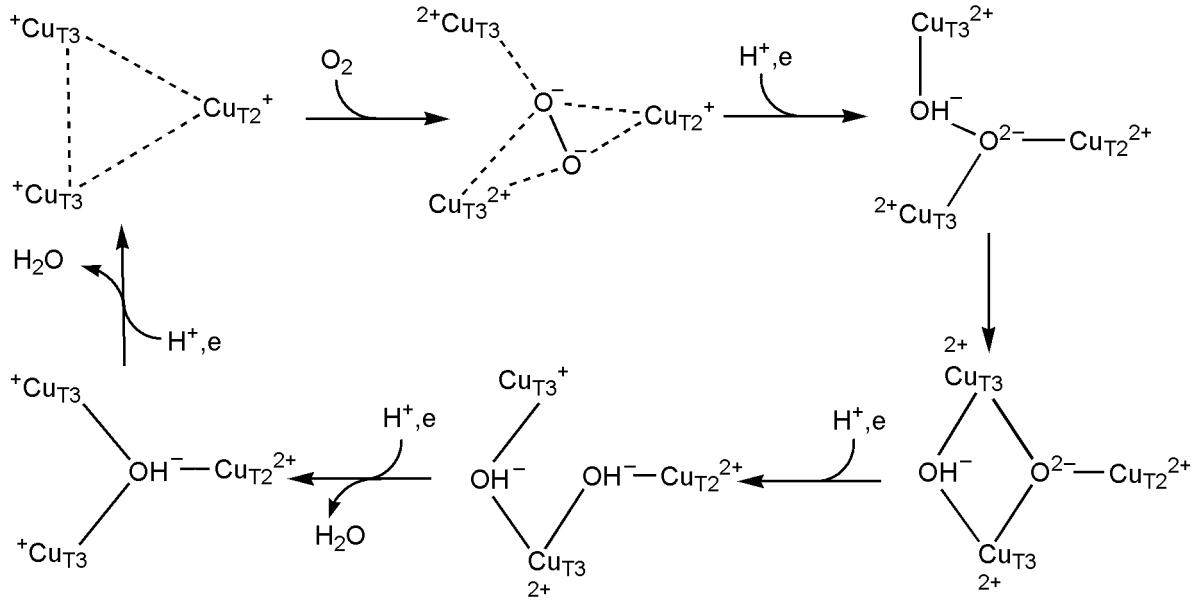

Figure 59. A proposed catalytic cycle for the MCOs. All copper ions are present as Cu^+ in the reduced state of the enzyme. Binding of O_2 ($k \approx 10^6$ M^{-1} s^{-1}) leads to formation of bound O_2^{2-} with the oxidation of the two Cu_{T3} ions to the +2 oxidation state [989], and O_2^{2-} interacts with all copper ions [990]. On the uptake of the first electron the O–O bond of peroxide is cleaved (with a small barrier of some 65 kJ mol^{-1} [980,988,991]. This is the rate-determining step of the entire cycle [988]. On uptake of three more electrons and four protons, and release of $2H_2O$, the reduced form of the enzyme is formed, completing the catalytic cycle.

10.3. Some Illustrative Examples of Copper-Based Enzymes

10.3.1. Superoxide Dismutase

The importance of superoxide dismutases was discussed in Section 6. We shall merely consider here the mechanism of the Cu-Zn SODs, widespread among eukaryotes and in some prokaryotes. There are also copper-only superoxide dismutases found for example in bacteria such as *Vibrio cholerae* and *Helicobacter pylori* [992].

The dismutation of superoxides to O_2 and H_2O_2 is clearly the principal function of SOD, but it performs other functions as well; for example, it is a very efficient oxidase of H_2S, which, in excess, is cytotoxic as it inhibits cytochrome *c* oxidase [993]; it boosts the degradation of biomass by glycoside hydrolases, demonstrating its competency to act as an oxidase [994]; and it indirectly leads to the promotion of NADH as a consequence of its antioxidant function [995].

The enzymatic dismutation of $O_2^{\bullet -}$ by Cu-Zn SOD is very rapid ($k \approx 10^9$ M^{-1} s^{-1}) [996], and under normal physiological conditions the rate of enzyme turnover is far from saturation. The reaction is generally thought to take place in two steps (Equations (38) and (39)). The active site of bovine SOD (PDB 1Q0E [997]) is shown in Figure 60 and a possible mechanism is shown in Figure 61. The importance of an Arg residue near the active site is clear. Zinc plays a structural, but not a catalytic role (Zn-depleted SOD is active [998]), and it also plays an important role in ensuring the proper membrane attachment of the enzyme [999]).

$$Cu^{2+} + O_2^{\bullet -} \rightarrow Cu^+ + O_2 \quad (38)$$

$$Cu^+ + O_2^{\bullet -} + 2H^+ \rightarrow Cu^{2+} + H_2O_2 \quad (39)$$

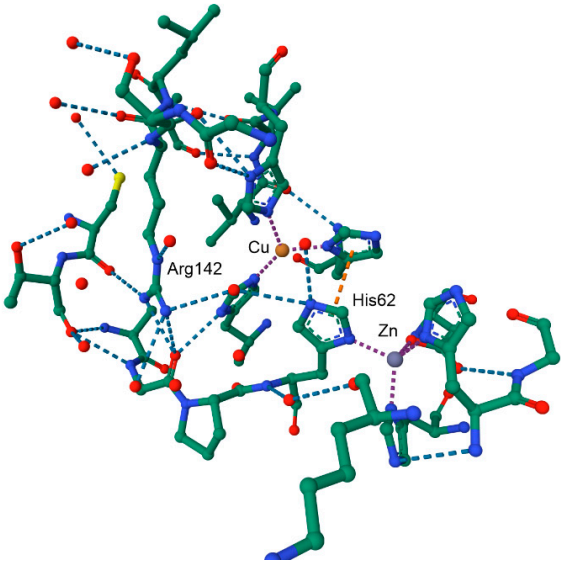

Figure 60. The active site and immediate surroundings of bovine SOD, showing an Arg residue near the copper ion.

Under various physiological conditions Cu-Zn SOD can catalyse a variety of side reactions, using, for example, thiols such as GSH, to generate reactive oxygen species which, in excess, can have deleterious effects [1000].

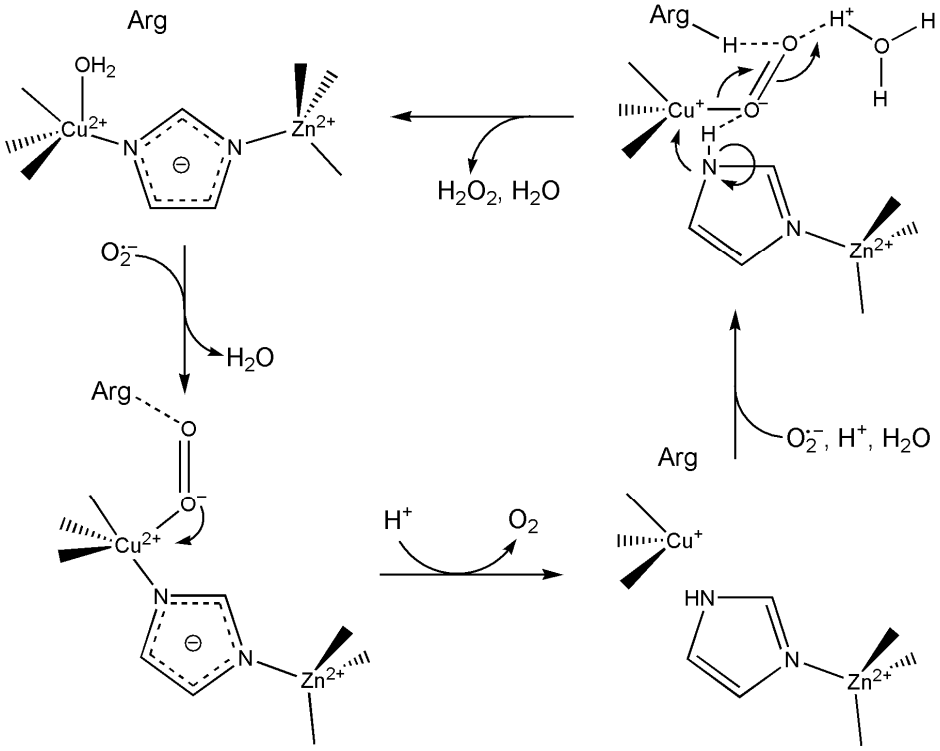

Figure 61. A possible mechanism for the dismutation of superoxide catalysed by SOD [1001]. A conserved Arg residue is important for the reaction [1002]. The H_2O ligand coordinated to Cu^{2+} in the resting enzymes exchanges rapidly with solvent H_2O.

10.3.2. Nitrous Oxide Reductase

The emission of N_2O into the atmosphere, arising in part from the use of fertilisers, is of environmental concern as it is a powerful greenhouse gas [1003]. Bacterial denitrification of soils occurs in four steps (Equation (40)) and is stimulated by high nitrogen input and

low oxygen pressure [1004]; hence, agricultural land is tilled to keep it aerobic. The oxides of nitrogen are used as the terminal electron acceptors in anaerobic respiration by these organisms. Archaea and some fungi also use these enzymes.

$$NO_3^- \xrightarrow[Mo]{\text{Nitrate reductase}} NO_2^- \xrightarrow[\text{Type II Cu}]{\text{Nitrite reductase}} NO \xrightarrow[\text{Haem Fe}]{\text{NO reductase}} N_2O \xrightarrow[Cu_A, Cu_Z]{N_2O\ \text{reductase}} N_2 \quad (40)$$

Nitrous oxide reductase is the final enzyme in this chain, and catalyses the reaction shown in Equation (41) [1005]. It is not a true MCO as it lacks the TNC of those enzymes but uses a similar proton-coupled electron transfer mechanism to reduce N_2O to N_2. This is a thermodynamically favourable reaction ($\Delta G^o = -340$ kJ mol^{-1}) but has a large activation energy ($\Delta G^{\ddagger} = +250$ kJ mol^{-1}) and therefore requires a catalyst.

$$N_2O + 2H^+ + 2e \rightarrow N_2 + H_2O \quad (41)$$

The enzyme contains two copper sites. The first, termed Cu_A because of its similarity with the Cu_A site of cytochrome *c* oxidase, contains two Cu ions (Figure 62a) and is the entry point for the electrons that are used to reduce N_2O. The second copper centre, Cu_Z, contains four copper ions coordinated by seven His residues and a μ^4-sulphido ligand which caps the tetranuclear copper core [1006]; this is the catalytic centre of the enzyme [1007,1008] (Figure 62b).

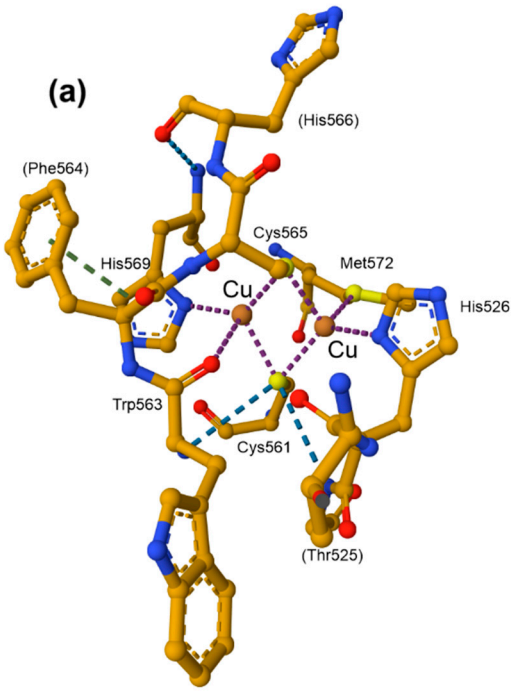

Figure 62. *Cont.*

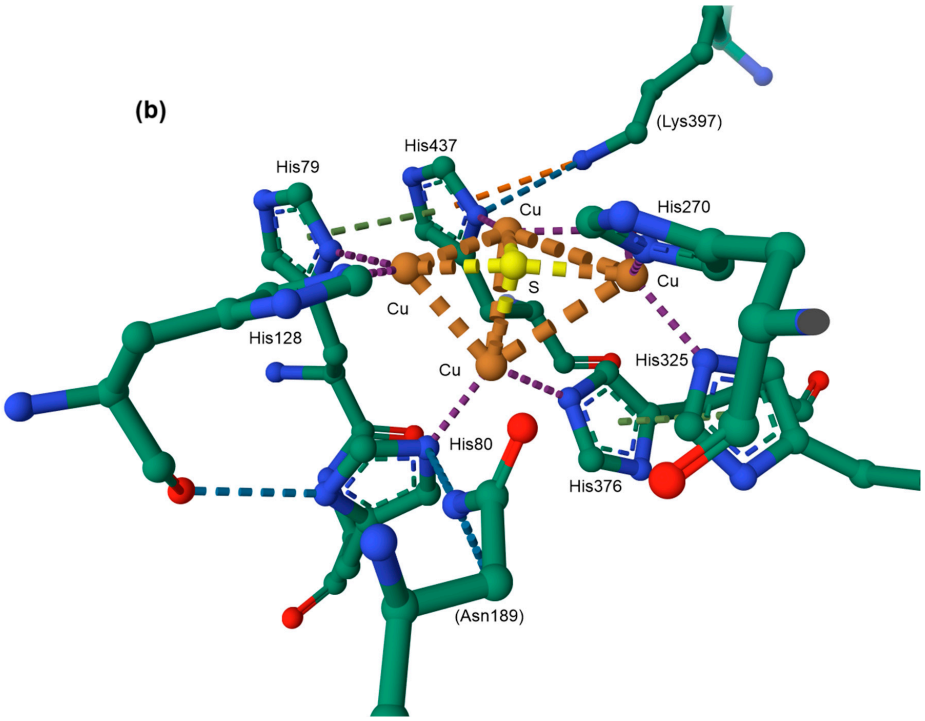

Figure 62. (**a**) The Cu_A site of nitrous oxide reductase from *Pseudomonas nautica* (PDB 1QNI [1006]). (**b**) The Cu_Z site, (Cu_4S), often referred to as Cu_Z*, from the same enzyme. Some nitrous oxide reductases contain two sulphur ions in the active site (Cu_4S_2); the site is then usually referred to as Cu_Z. Cu_Z* is associated with aerobic conditions in which one of the sulphides of anaerobic Cu_Z is replaced by H_2O. The two sites (from two different monomers in the homodimeric protein) are some 10 Å apart, facilitating electron transfer.

The Cu_A site is a mixed-valent [$Cu^{1.5}Cu^{1.5}$] site [1009,1010] with the unpaired electron in the oxidised form delocalised over the two metal ions, which are 2.43 Å apart. LMCT bands (S(Cys) → Cu) occur at 480 and 525–540 nm. The principal function of the site is to provide electrons to the catalytic site, Cu_Z in some enzymes, Cu_Z* in others. This is a proton-coupled transfer, gated by one of the His ligands of the Cu_A site [1011,1012].

The oxidised form of Cu_Z features (formally, anyway) two Cu^{2+} and two Cu^{+} ions and is often termed the "2-hole Cu_Z" site, referring to the two d^9 Cu^{2+} ions. A single electron reduction produces the one-hole site with the unpaired electron delocalised over the copper ions, as determined by EPR, and with protonation of the bridging sulphide [1013]. The oxidised form of the Cu_Z* site contains three Cu^{+} ions and one Cu^{2+} ion and is therefore termed the "1-hole Cu_Z*" site.

The catalytically active form of the Cu_Z* site is the zero-hole [$4Cu^{+}$] form, which cycles between this and the one-hole [$3Cu^{+}$:Cu^{2+}] form; the Cu_Z site cycles between the one-hole [$3Cu^{+}$:Cu^{2+}] and the two-hole [$2Cu^{+}$:$2Cu^{2+}$] forms [1014]. Both types of Z site therefore act as sequential one-electron reductants of the N_2O substrate. A possible mechanism for reduction of Cu_Z* by Cu_A and the reduction of N_2O to N_2 has been proposed, Figure 63 [1015] (also [1008] and references therein) and features (like the MCOs) a sequence of proton-coupled electron transfer reactions.

10.3.3. Tyrosinase

Tyrosinase is an enzyme with a type 3 copper centre, responsible for regulating melanin production. It is found in plant and animal tissues, including in melanosomes which are synthesised by melanocytes in the skin. The enzyme catalyses the hydroxylation of monophenols, followed by subsequent oxidation reactions. This includes the conversion

of o-diphenols into o-quinones (Equation (42)) [1016], which are precursors to melanin. These reactions are coupled with the reduction of O_2 to H_2O. The enzymes also are active on aromatic amines [1017].

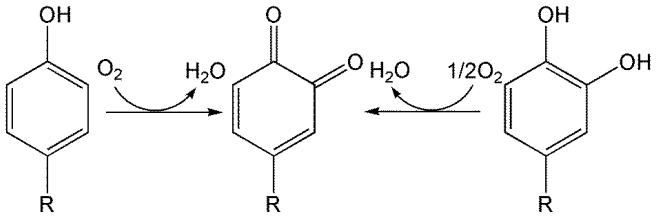

(42)

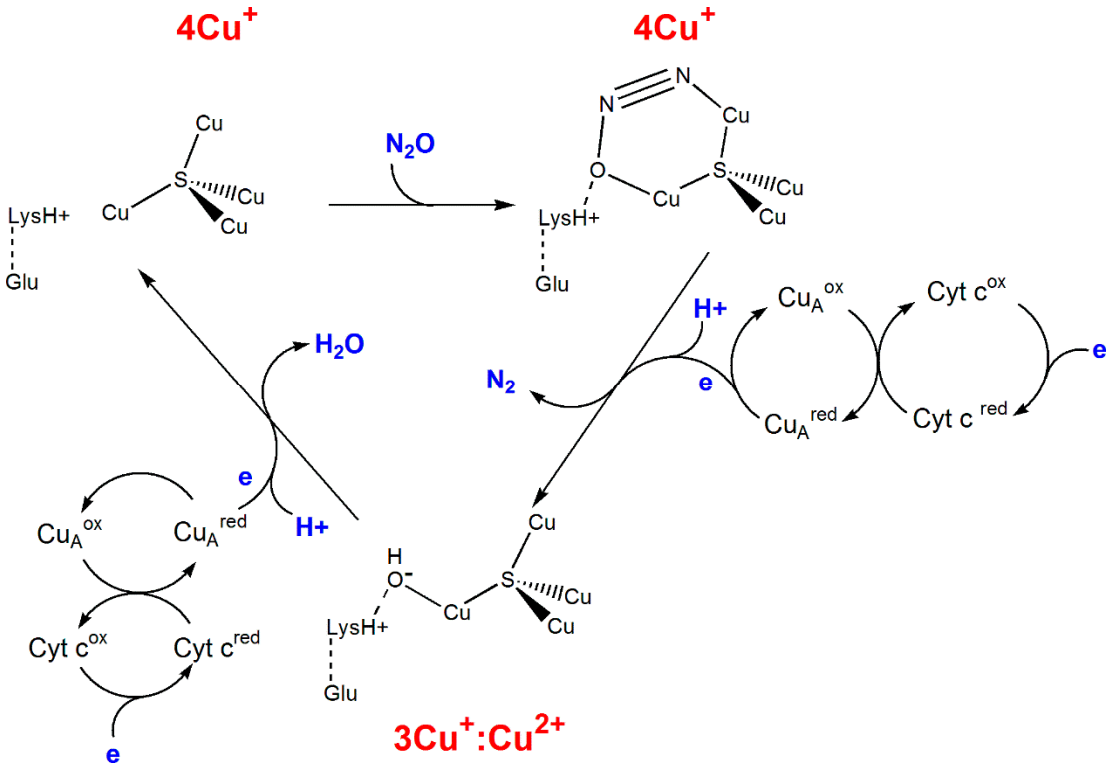

Figure 63. Possible mechanism for the reduction of N_2O at the Cu_Z* site [1008,1015].

Tyrosinase inhibition is a target for the cosmetics industry to produce products that counter changes in pigmentation, one of the effects of skin ageing [1018]. Flavonoids, compounds that are commonly found in the human diet, are reported to inhibit tyrosinase by binding to the active site of the enzyme [1019], and many other inhibitors—both natural products and synthetic compounds—are known [1020–1024]. Tyrosinase activity can be inhibited by mercury, a common component of skin-whitening creams, but this has very significant health risks [1025].

The action of tyrosinase within the substantia nigra, a part of the brain that controls movement and is involved in chemical signalling, leads to the breakdown of dopaminergic neurons, the main source of dopamine [1026]. Decline in dopamine contributes to the development of Parkinson's disease.

The active form of the enzyme contains two Cu^+ ions which bind O_2 in a μ-η^2:η^2 side-on manner producing Cu^{2+}–O_2^{2-}–Cu^{2+} [1027]. This species oxidises the substrate. A possible mechanism is shown in Figure 64 [1028,1029].

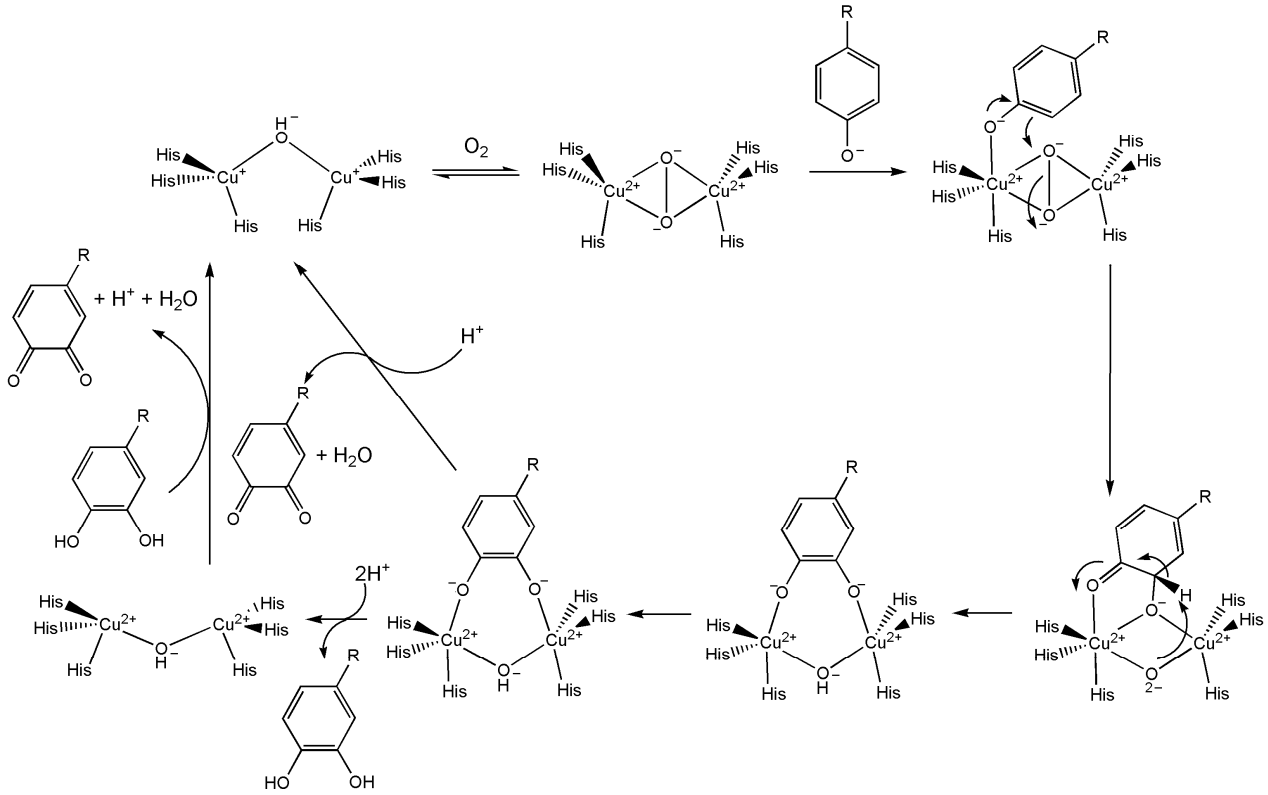

Figure 64. Catalytic cycle of tyrosinase.

11. Zinc

Zinc is important for many life forms including animals, plants, and microorganisms [1030,1031], and important for human health [1032–1035]. Zinc has only one physiologically readily accessible oxidation state, Zn^{2+}, and it functions as a Lewis acid in biological systems [1036,1037].

Zn^{2+}, a d^{10} metal ion with no ligand field stabilisation, has a variable coordination number, from 2 to 8, with 4 and 6 being most common [135]. It is also kinetically labile; the water exchange rate of $[Zn(H_2O)_6]^{2+}$ in aqueous solution is 4×10^8 s^{-1} [1038]. In terms of Pearson's classification of Lewis acids [1039], Zn^{2+} is borderline between a hard and a soft acid and is therefore receptive to a variety of donor ligands. In proteins it is usually coordinated by O, N, and S donors, usually in a distorted tetrahedral or trigonal bipyramidal geometry [1040]. A bioinformatics search of the human genome predicted there are some 2800 human proteins (or some 10% of the human proteome) that are potential Zn^{2+}-binders, with the most abundant being the so-called zinc finger proteins [1041,1042] with Zn^{2+} coordinated by four Cys, or two Cys and two His ligands [1043].

The cellular concentration of Zn^{2+} is high, around 200 μM [1044], so the buffering of Zn^{2+} in cells is essential for it not to compete with other metal ions in the metal binding sites of proteins. Free Zn^{2+} (i.e., complexes of Zn^{2+} such as $Zn(GSH)_2$, $Zn(citrate)_2$, and Zn-ATP [1044], capable of releasing the metal to the metal binding sites of proteins) is limited to a few hundred pM [1045], with excess zinc stored in vesicular compartments [1046]. There are sophisticated mechanisms that control zinc homeostasis [1047,1048], and an excess of Zn^{2+} (and Cu^{2+}), i.e., metal ion intoxication, is one way in which a host reduces the intracellular survival of pathogens [1049].

Zinc performs many functions in biology [1050]. Zinc-dependent enzymes include DNA and RNA polymerases [1051–1053], proteinases [1054], carbonic anhydrase [1055–1057], and alkaline phosphatase [1058–1060]. Zinc finger proteins, discovered in 1985 [1061], use Zn^{2+} to

stabilise their structure and play an important role in health and in disease [1041,1042,1062]; they are involved in processes such as regulating gene expression by binding to DNA [1041], cellular development [1063], differentiation [1064], and apoptosis [1062]. Shown in Figure 65 is an example of how Zn^{2+} ensures the integrity of the three-dimensional structure of a protein.

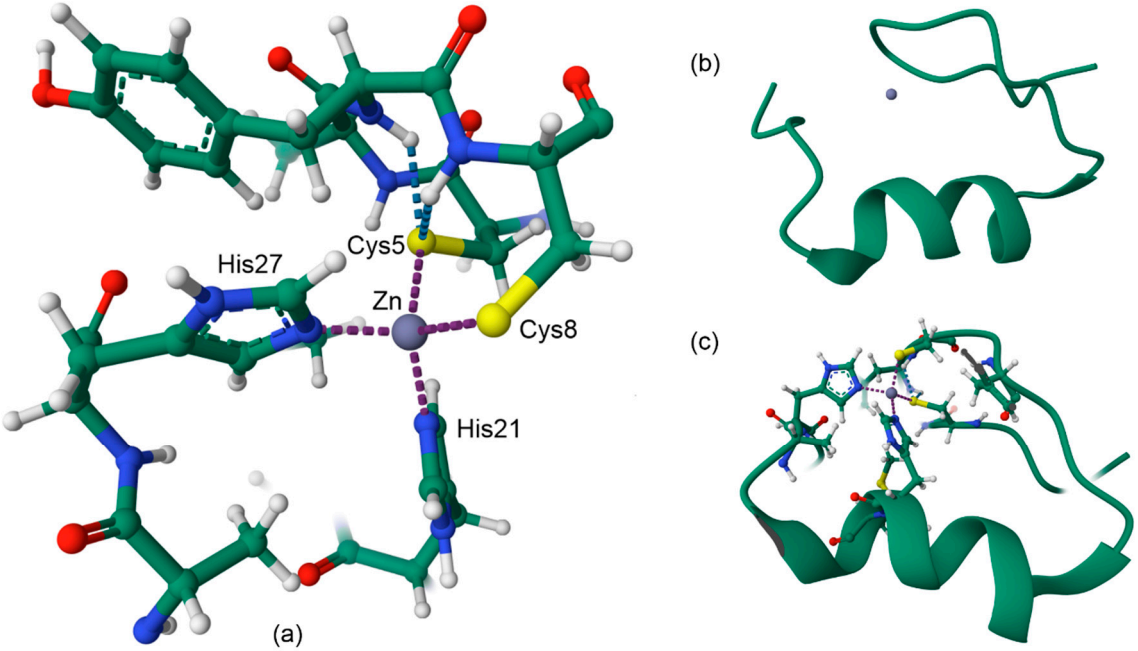

Figure 65. (**a**) The coordination sphere of Zn^{2+} from a human enhancer-binding protein (PDB 4ZNF [1065]); (**b**) the overall structure of the protein; (**c**) illustration of how Zn^{2+} is responsible for maintaining the 3D structure.

Zinc is important for maintaining a healthy immune system [1066] and zinc deficiency can lead to impaired immune response and an increased susceptibility to infections [1067]. As we have seen (Section 10.3.1), Zn^{2+} is a component of the active site of superoxide dismutase and hence plays a role in controlling the concentration of ROS. Zinc is vital for cognitive development and high levels are found in the human brain where it is involved in functions such as neurotransmission and sensory processing, activating both pro-survival and pro-death neuronal signalling pathways [1068]. Zinc is important for tissue repair [1069], hormonal regulation [1070–1072], and reproductive health [1073]. A diet heavy in processed foods may lead to zinc deficiency [1074].

We shall limit our discussion to the role of zinc in a few enzymes other than CuZn-SOD, which was discussed in Section 10.3.1.

In catalytic zinc sites, Zn^{2+} has at least one H_2O ligand, the key component of the site [1040]. This can be deprotonated to hydroxide (as in carbonic anhydrase [1075]), polarised to generate a nucleophile (as in carboxypeptidase A [1076]), or displaced by the substrate (as in alkaline phosphatase [1060]).

11.1. Carbonic Anhydrase

The principal function of Zn^{2+} in enzymes that catalyse hydration or hydrolysis reactions is to stabilise a coordinated OH^- ion as well as to stabilise the developing negative charges in the transition state of the reaction. The enzymes that catalyse the reversible hydration of carbon dioxide to bicarbonate and protons, playing pivotal roles in a variety of biological processes including respiration, calcification, acid-base balance, and CO_2 fixation, are found in many life forms [1077–1079].

An example is human carbonic anhydrase II (CAII) which catalyses the hydration of CO_2 to HCO_3^- and H^+ [1080]. Coordination of H_2O by Zn^{2+} decreases the pK_a of H_2O from 15.7 to around 9, an effect which is augmented by hydrogen bonding between bound OH^- with (in CAII) Thr199. The hydrogen bond also fixes the orientation of OH^- about the Zn^{2+}–OH^- bond, optimising it for nucleophilic attack on the substrate, CO_2, contributing to a near diffusion-controlled limit of enzyme turnover. The active site of CAII, with acetate replacing the active site OH^-, is shown in Figure 66, while an outline of the probable mechanism is given in Figure 67.

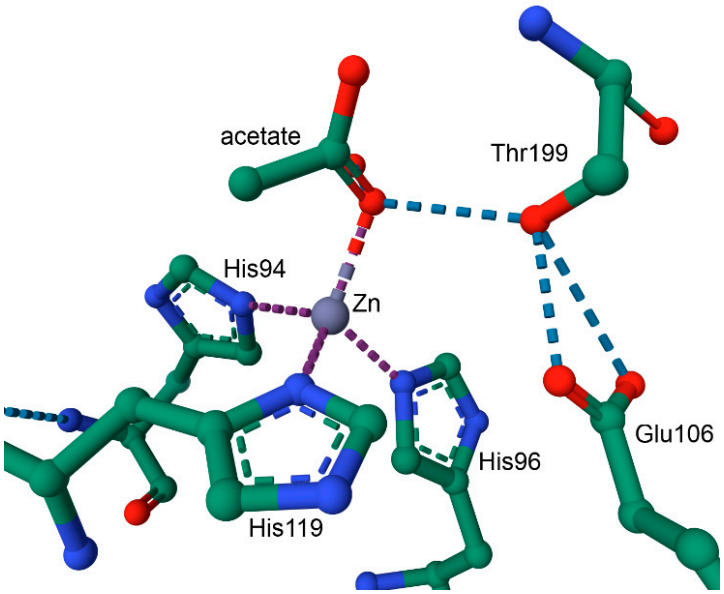

Figure 66. The active site of human CAII (with acetate in the substrate's position), PDB 1XEG [1081].

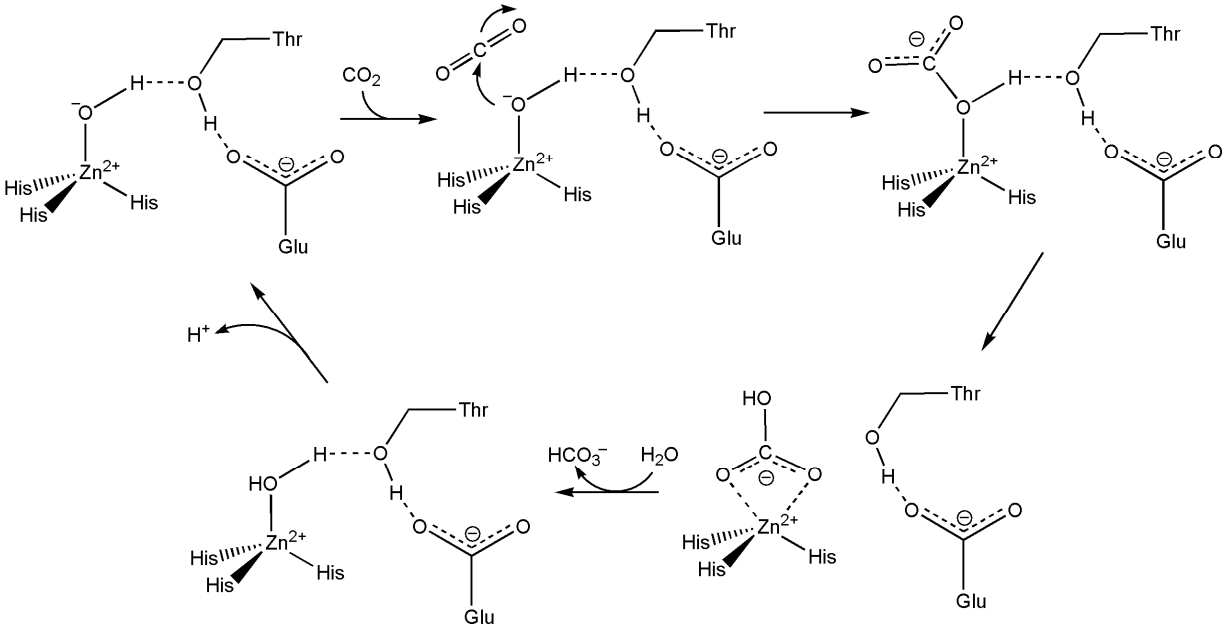

Figure 67. The hydration of CO_2 by CAII. The released H^+ is carried to the enzyme's surface by a His shuttle [1080].

11.2. Zinc-Dependent Phosphoesterases

These enzymes, members of the S1-P1 nuclease family, are found in bacteria, kinetoplastids, fungi and plants; Ca^{2+}-, Mg^{2+}-, and Mn^{2+}-dependent enzymes are also widely

distributed [1082]. They participate in a wide range of biological process where they hydrolyse the P–O3′ bond of nucleic acids and mononucleotides (Equation (43)) [1083–1085].

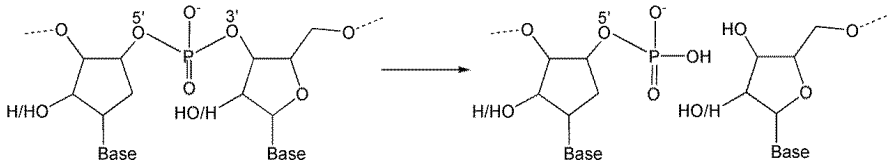

(43)

The catalytic site consists of a trinuclear zinc cluster with a Lys or Arg residue, and a nearby site, called Nucleoside Binding Site 1 (NBS1), responsible for binding the substrate. The trinuclear zinc site of the S1 nuclease from *Aspergillus oryzae* (PDB 5FB9) is shown in Figure 68 [1086]. The mechanism of the reaction (Figure 68) entails deprotonation of the bridging water W1, and the resultant hydroxide then acts as the attacking nucleophile on the P–O3′ bond [1086–1088].

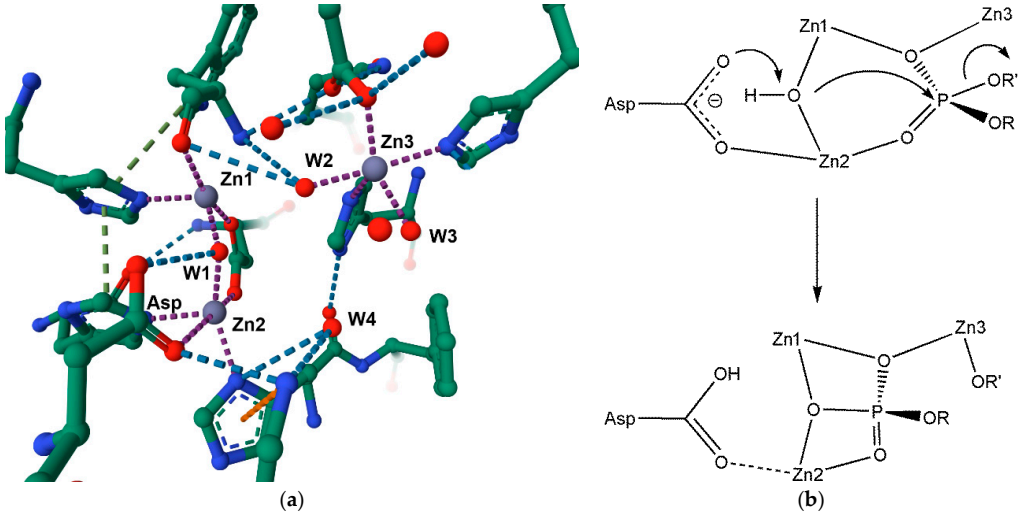

Figure 68. (**a**) The trinuclear zinc site of S1 nuclease from *Aspergillus oryzae* (PDB 5FB9). (**b**) The probable mechanism that leads to the cleavage of the P–O3′ bond.

11.3. A Zinc Proteinase: Carboxypeptidase A

The most widespread zinc enzymes are hydrolases, referred to as matrix metalloproteinases (MMPs) or zinc proteinases [1047]. Capable of cleaving extracellular matrix proteins, they play a major role in in-cell differentiation, apoptosis, angiogenesis and wound healing [1089]. It is now known that MMPs also have an intracellular function, contributing to the pathogenesis of diseases such as inflammation and cardiovascular renal disorders, and exerting bactericidal and antiviral effects [1054]. One of the most widely studied of these enzymes is carboxypeptidase A [1076,1090,1091]. The enzyme hydrolyses the C-terminal peptide bond of a peptide, releasing the C-terminal amino acid (Equation (44)). It is also capable of hydrolysing esters.

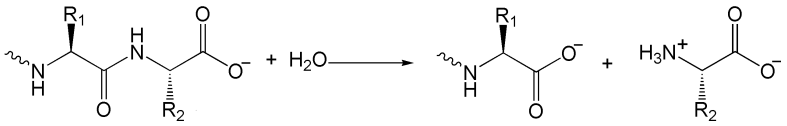

(44)

The active site contains Zn^{2+} coordinated by 2 His and a Glu, together with a water molecule. An important Glu residue is in the second coordination shell. Two mechanisms can be envisaged [1092–1096]: one involves attack by Zn-coordinated OH^- (deprotonated

by the second sphere Glu), the other envisages Glu playing the role of the attacking nucleophile. The first is the mechanism used by the enzyme in its proteolysis reactions [1096].

11.4. Alkaline Phosphatase

Co-catalytic zinc enzymes have more than one Zn^{2+} ion (or Zn^{2+} and another metal ion) in proximity that effect the catalytic event. Although only one Zn^{2+} ion plays a role in the catalysis, the other ions are essential (see Section 11.2). Some examples are leucine aminopeptidase (two Zn^{2+} ions) [1097], alkaline phosphatase (two Zn^{2+} and an Mg^{2+}) [1060], and phospholipase C [1098] and nuclease P1 [1085], with three Zn^{2+} ions. In CuZn-SOD, the catalytic site is Cu (see Section 10.3.1), but Zn^{2+} plays an important if indirect role in the catalysis.

Alkaline phosphatase contains two Zn^{2+} ions and one Mg^{2+} ion (Figure 69 shows the active site of the enzyme from *E. coli* with bound phosphate [1099]). The enzyme catalyses the hydrolysis of phosphate esters under alkaline conditions [1100]. One Zn^{2+} (often referred to as Zn_1) is coordinated by two His residues and an Asp residue (and H_2O occupies the remaining two coordination sites in the absence of phosphate); the other (Zn_2) is coordinated by His, Ser102, and two Asp residues (as well as phosphate in the structure shown in Figure 69). The coordination sphere of Mg^{2+} consists of three H_2O, Glu, Thr, and Asp. The PO_4^{3-} is also coordinated by an Arg residue, Arg166.

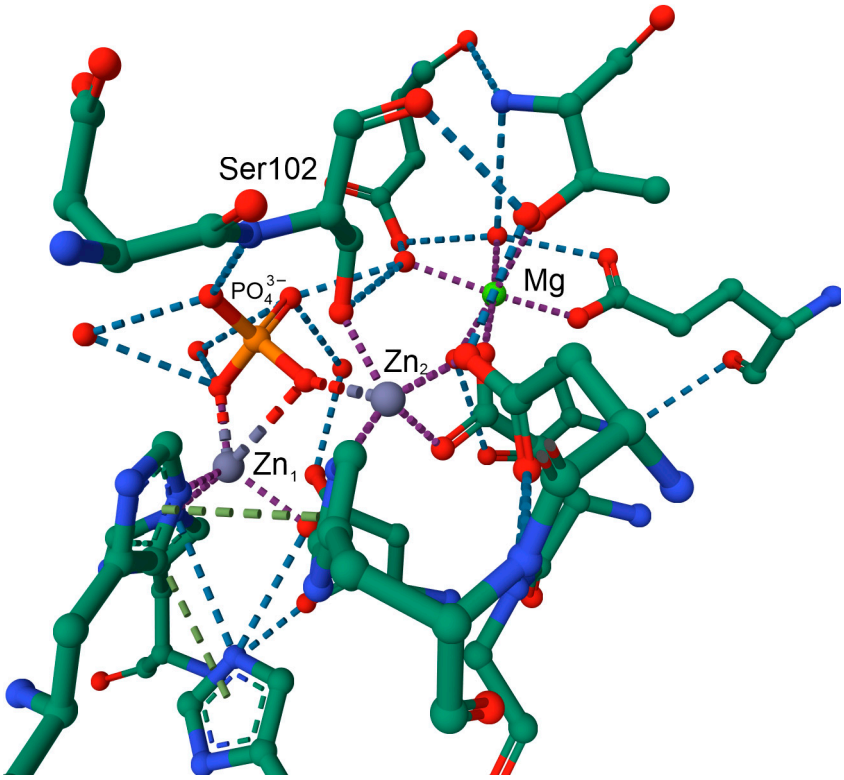

Figure 69. The active site of alkaline phosphatase from *E. coli* (PDB 3TG0 [1099]).

An outline of the mechanism (somewhat simplified) of the hydrolysis of a phosphate monoester, RPO_3^{2-}, is shown in Figure 70 [1060,1101,1102]. The attacking nucleophile is zinc-coordinated Ser-102, leading to the formation of a phosphoseryl intermediate. This is then hydrolysed to produce an enzyme–phosphate complex. If a phosphate acceptor, AOH, is present, the reaction leads to transphosphorylation, $ROPO_3^{2-}$ + AOH → ROH + $AOPO_3^{2-}$. [1060]. The role of the second Zn^{2+} is to coordinate the leaving phosphate as well as activate a solvent water (perhaps as OH^-) for attack on coordinated phosphate in the second step of the reaction. The role of Mg^{2+} is to stabilise the structure of the

enzyme [1103] and to correctly hold the carboxylate of one of the Asp ligands of Zn^{2+} to alternatively donate, and then withdraw, electron density during the reaction [1103,1104].

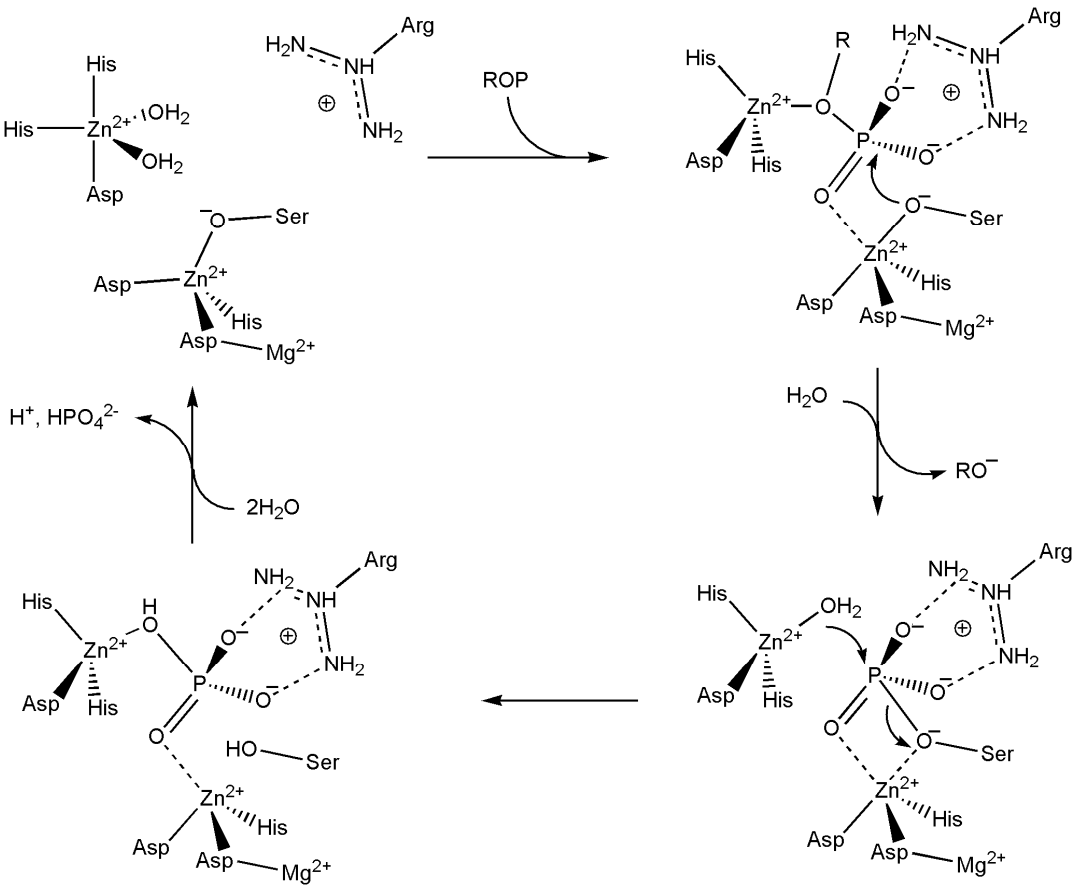

Figure 70. The hydrolysis of a phosphate monoester by alkaline phosphatase.

12. Concluding Remarks

Metal ions constitute by mass a very small percentage of living systems, but they play a crucial role: they are essential trace elements. We have not looked at the role played by the main group metal ions; Na^+, K^+, Ca^{2+}, and Mg^{2+} are important in biology. Na^+ and K^+ are involved in many processes including nerve function and nerve impulse transmission [1105,1106], the contraction of muscles [1107,1108], regulating cell volumes [1109,1110], and the regulation of cardiac repolarisation [1111,1112]. Ca^{2+} plays a critical role in, for example, the maintenance of membrane potential [1113,1114], the regulation of the life cycle of a cell [1115,1116], and the activation of many enzymes [1117,1118]. We have seen a number of cases where Mg^{2+} plays a supporting role in catalysts; in addition, the role of Mg^{2+} in the cardiovascular system is critical and there are a number of diseases linked to its deficiency [1119].

The attention here was focused on the elements of the first row of the d block. As far as is known at present, scandium and titanium play no role in biological system. All other elements are essential to one form of life or another or, in some cases, to virtually all life forms. Cobalt, for example, is not required by plants, many fungi and some bacteria, but is vital for animals and many microorganisms. Iron, copper and manganese are widely used by many life forms but there are organisms such as bacteria and archaea that have developed strategies for thriving in, for example, iron-deficient environments using copper or manganese to perform the chemistry usually performed by iron.

There are many metal-containing enzymes, or metalloenzymes, that require metal ions as cofactors. Among the examples discussed was manganese at the heart of Photosystem II, iron in the cytochromes, cobalt in the adenosylcobalamin-dependent enzymes, nickel in urease, copper in superoxide dismutase and zinc in alkaline phosphatase. The metal ions either participate directly in the catalytic process or bind the substrate or activate an entity such as coordinated OH^- to initiate a reaction.

We have seen the key role that iron and copper in particular play in electron transport chains, which are critical for cellular respiration and photosynthesis. The iron–sulphur clusters and cytochromes, and the blue copper proteins, play key roles in the transfer of electrons, facilitating energy production in cells. Iron porphyrins in haemoglobin and myoglobin are vital for the transport and storage of oxygen in animals.

Metal ions may be necessary to stabilise the structure of biomolecules. Zinc fingers, for example are important for protein folding, and they perform many other functions that we have not looked at, including the binding of zinc finger proteins to specific DNA sequences, regulating gene expression [1120,1121] and the regulation of apoptosis [1122,1123].

Bioinorganic chemistry is a very large and interdisciplinary field that explores the role played by metal ions in biological systems, spanning biology and inorganic chemistry. This short overview will hopefully have provided you with a glimpse into some aspects of the discipline: the biological inorganic chemistry of the metals of the first row of the d block—and it will hopefully provide a stimulus for further exploration.

Much has been learned since the pioneering work in the 1960s and 1970s of researchers such as R. J. P. Williams, Harry B. Gray, Richard H. Holm, and Robert H. Crabtree. Insights have been provided into important biological processes involving metal ions, and the discipline has provided the knowledge that has contributed to the development of metal-based drugs and imaging techniques. The development of techniques such as X-ray diffraction crystallography, cryo-electron microscopy, NMR, EPR, and Mössbauer spectroscopy, and, more recently, computational chemistry methods such as density functional theory, have contributed greatly to advances in the field.

But undoubtedly much has still to be learned. The mechanism of many enzymes, such as nitrogenase (involved in nitrogen fixation) and hydrogenase (involved in hydrogen metabolism), remain elusive. Moreover, the rapidly growing area of bioinspired catalysis holds promise for transformative industrial applications.

The future of bioinorganic chemistry lies in the hands of the next generation of researchers and their students who will undoubtedly lead the discipline to new heights in the years ahead.

Funding: This research received no external funding.

Institutional Review Board Statement: Not applicable.

Informed Consent Statement: Not applicable.

Data Availability Statement: No new data were created or analyzed in this study.

Conflicts of Interest: The author declares no conflict of interest.

References

1. Mertz, W. The Essential Trace Elements. *Science* **1981**, *213*, 1332–1338. [CrossRef] [PubMed]
2. Sigel, A.; Sigel, H.; Sigel, R.K.O. *Interrelations Between Essential Metal Ions and Human Diseases*; Springer: Dordrecht, The Netherlands, 2013; Volume 13.
3. Jomova, K.; Makova, M.; Alomar, S.Y.; Alwasel, S.H.; Nepovimova, E.; Kuca, K.; Rhodes, C.J.; Valko, M. Essential metals in health and disease. *Chemico-Biol. Interact.* **2022**, *367*, 110173. [CrossRef] [PubMed]
4. Zoroddu, M.A.; Aaseth, J.; Crisponi, G.; Medici, S.; Peana, M.; Nurchi, V.M. The essential metals for humans: A brief overview. *J. Inorg. Biochem.* **2019**, *195*, 120–129. [CrossRef]

5. Williams, R.J.P. Chemical selection of elements by cells. *Coord. Chem. Rev.* **2001**, *216–217*, 583–595. [CrossRef]
6. Sanchez, T.R.; Hu, X.; Zhao, J.; Tran, V.; Loiacono, N.; Go, Y.-M.; Goessler, W.; Cole, S.; Umans, J.; Jones, D.P.; et al. An atlas of metallome and metabolome interactions and associations with incident diabetes in the Strong Heart Family Study. *Environ. Intern.* **2021**, *157*, 106810. [CrossRef]
7. Dupont, C.L.; Butcher, A.; Valas, R.E.; Bourne, P.E.; Caetano-Anollés, G. History of biological metal utilization inferred through phylogenomic analysis of protein structures. *Proc. Natl. Acad. Sci. USA* **2010**, *107*, 10567–10572. [CrossRef]
8. Van Cleave, C.; Crans, D.C. The First-Row Transition Metals in the Periodic Table of Medicine. *Inorganics* **2019**, *7*, 111. [CrossRef]
9. Liang, Y.; Pan, Z.; Zhu, M.; Gao, R.; Wang, Y.; Cheng, Y.; Zhang, N. Exposure to essential and non-essential trace elements and risks of congenital heart defects: A narrative review. *Front. Nutr.* **2023**, *10*, 1121826. [CrossRef] [PubMed]
10. Genchi, G.; Carocci, A.; Lauria, G.; Sinicropi, M.S.; Catalano, A. Nickel: Human Health and Environmental Toxicology. *Int. J. Environ. Res. Public Health* **2020**, *17*, 679. [CrossRef]
11. Begum, W.; Rai, S.; Banerjee, S.; Bhattacharjee, S.; Mondal, M.H.; Bhattarai, A.; Saha, B. A comprehensive review on the sources, essentiality and toxicological profile of nickel. *RSC Adv.* **2022**, *12*, 9139–9153. [CrossRef]
12. Nelson, N. Metal ion transporters and homeostasis. *EMBO J.* **1999**, *18*, 4361–4371. [CrossRef] [PubMed]
13. Ba, L.A.; Doering, M.; Burkholz, T.; Jacob, C. Metal trafficking: From maintaining the metal homeostasis to future drug design. *Metallomics* **2009**, *1*, 292–311. [CrossRef]
14. Palmer, A.E.; Franz, K.J. Introduction to "Cellular Metal Homeostasis and Trafficking". *Chem. Rev.* **2009**, *109*, 4533–4535. [CrossRef] [PubMed]
15. Aulakh, S.K.; Varma, S.J.; Ralser, M. Metal ion availability and homeostasis as drivers of metabolic evolution and enzyme function. *Curr. Opin. Genet. Dev.* **2022**, *77*, 101987. [CrossRef]
16. Sullivan, M.J.; Terán, I.; Goh, K.G.K.; Ulett, G.C. Resisting death by metal: Metabolism and Cu/Zn homeostasis in bacteria. *Emerg. Top. Life Sci.* **2024**, *8*, 45–56. [CrossRef] [PubMed]
17. Zhang, Y.; Ma, K.; Fang, X.; Zhang, Y.; Miao, R.; Guan, H.; Tian, J. Targeting ion homeostasis in metabolic diseases: Molecular mechanisms and targeted therapies. *Pharmacol. Res.* **2025**, *212*, 107579. [CrossRef]
18. Maret, W. Chromium in Human Health, Metabolic Syndrome, and Diabetes. In *Metal Ions in Life Sciences*; Carver, P.L., Ed.; W. de Gruyter: Berlin, Germany, 2019; Volume 19, pp. 231–251.
19. Bansal, S.L.; Asthana, S. Biologically Essential and Non-Essential Elements Causing Toxicity in Environment. *J. Environ. Anal. Toxicol.* **2018**, *8*, 1000557. [CrossRef]
20. Brown, D.H.; Smith, W.E. Metal ions in biological systems. In *Enzyme Chemistry: Impact and Applications*; Suckling, C.J., Ed.; Springer: Dordrecht, The Netherlands, 1984; pp. 162–195.
21. Lippard, S.J.; Berg, J.M. *Principles of Bioinorganic Chemistry*; University Science Books: Mill Valley, CA, USA, 1994.
22. Farrer, B.T.; Pecoraro, V.L. Bioinorganic Chemistry. In *Encyclopedia of Physical Science and Technology*, 3rd ed.; Meyers, R.A., Ed.; Academic Press: New York, NY, USA, 2003; pp. 117–139.
23. Bertini, I.; Gray, H.B.; Stiefel, E.I.; Valentine, J.S. (Eds.) *Biological Inorganic Chemistry: Structure and Reactivity*; University Science Books: Sausalito, CA, USA, 2007.
24. Hosmane, N.S. Bioinorganic Chemistry and Applications. In *Advanced Inorganic Chemistry*; Hosmane, N.S., Ed.; Academic Press: Boston, MA, USA, 2017; pp. 225–249.
25. Crichton, R. (Ed.) *Biological Inorganic Chemistry*, 3rd ed.; Academic Press: Amsterdam, The Netherlands, 2019.
26. Jordan, R.B. Bioinorganic Chemistry. In *Principles of Inorganic Chemistry: Basics and Applications*; Jordan, R.B., Ed.; Springer International Publishing: Cham, Switzerland, 2024; pp. 823–852.
27. Williams, R.J.P. The natural selection of the elements. *Chem. Br.* **1997**, *53*, 816–829.
28. Williams, R.J.P.; Frausto da Silva, J.J.R. *The Chemistry of Evolution: The Development of our Ecosystem*; Elsevier: Amsterdam, The Netherlands, 2006.
29. Frausto da Silva, J.J.R.; WIlliams, R.J.P. *The Biological Chemistry of the Elements: The Inorganic Chemistry of Life*, 2nd ed.; Oxford University Press: Oxford, UK, 2001.
30. Ghosh, D.; Pecoraro, V.L. Probing metal–protein interactions using a de novo design approach. *Curr. Opin. Chem. Biol.* **2005**, *9*, 97–103. [CrossRef]
31. Belmonte, L.; Mansy, S.S. Metal Catalysts and the Origin of Life. *Elements* **2016**, *12*, 413–418. [CrossRef]
32. Smethurst, D.G.J.; Shcherbik, N. Interchangeable utilization of metals: New perspectives on the impacts of metal ions employed in ancient and extant biomolecules. *J. Biol. Chem.* **2021**, *297*, 101374. [CrossRef] [PubMed]
33. Crans, D.C.; Kostenkova, K. Open questions on the biological roles of first-row transition metals. *Commun. Chem.* **2020**, *3*, 104. [CrossRef]
34. Arnon, D.I.; Stout, P.R. The essentiality of certain elements in minute quantity for plants with special reference to copper. *Plant Physiol.* **1939**, *14*, 371–375. [CrossRef] [PubMed]
35. Vincent, J.B. New evidence against chromium as an essential trace element. *J. Nutr.* **2017**, *147*, 2212–2219. [CrossRef]

36. EFSA: Nutrient. Available online: https://www.efsa.europa.eu/en/glossary/nutrient (accessed on 15 May 2023).
37. Underwood, E. *Trace Elements in Human and Animal Nutrition*, 4th ed.; Academic Press: New York, NY, USA, 1977.
38. Pais, I. The biological importance of titanium. *J. Plant Nutr.* **1983**, *6*, 3–131. [CrossRef]
39. Epstein, E. *Mineral Nutrition of Plants: Principles and Perspectives*; John Wiley & Sons, Inc.: New York, NY, USA, 1972.
40. Hewitt, E.L. Essential and functional aspects of trace elements. In *Chemistry and Agriculture*; Royal Chemical Society: London, UK, 1979; pp. 91–127.
41. Wimmer, M.A.; Abreu, I.; Bell, R.W.; Bienert, M.D.; Brown, P.H.; Dell, B.; Fujiwara, T.; Goldbach, H.E.; Lehto, T.; Mock, H.-P.; et al. Boron: An essential element for vascular plants. *New Phytol.* **2020**, *226*, 1232–1237. [CrossRef]
42. Goldbach, H.E.; Wimmer, M.A. Boron in plants and animals: Is there a role beyond cell-wall structure? *J. Plant Nutr. Soil Sci.* **2007**, *170*, 39–48. [CrossRef]
43. Gupta, M.; Gupta, S. An Overview of Selenium Uptake, Metabolism, and Toxicity in Plants. *Front. Plant Sci.* **2017**, *7*, 2074. [CrossRef]
44. Pecoraro, B.M.; Leal, D.F.; Frias-De-Diego, A.; Browning, M.; Odle, J.; Crisci, E. The health benefits of selenium in food animals: A review. *J. Anim. Sci. Biotech.* **2022**, *13*, 58. [CrossRef]
45. Emsley, J. Unsporting scandium. *Nat. Chem.* **2014**, *6*, 1025. [CrossRef]
46. He, X. Scadium, Biological Effects. In *Encyclopedia to Metalloproteins*; Kretsinger, R.H., Uversky, V.N., Permyakov, E.A., Eds.; Springer: New York, NY, USA, 2013; pp. 1882–1884.
47. Falandysz, J.; Fernandes, A.R. A critical review of the occurrence of scandium and yttrium in mushrooms. In *Advances in Applied Microbiology*; Gadd, G.M., Sariaslani, S., Eds.; Academic Press: New York, NY, USA, 2023; Volume 125, pp. 107–141.
48. Nnomo Assene, A.; Dieme, D.; Jomaa, M.; Côté, J.; Bouchard, M. Toxicokinetic study of scandium oxide in rats. *Toxicol. Lett.* **2024**, *392*, 56–63. [CrossRef] [PubMed]
49. Horovitz, C. (Ed.) *Biochemistry of Scandium and Yttrium*; Kluwer/Plenum: New York, NY, USA, 2000.
50. Herath, H.M.T.U.; Silvio, L.D.; Evans, J.R.G. Scandia—A potential biomaterial? *J. Mater. Sci. Mater. Med.* **2005**, *16*, 1061–1065. [CrossRef] [PubMed]
51. Kawai, K.; Wang, G.; Okamoto, S.; Ochi, K. The rare earth, scandium, causes antibiotic overproduction in *Streptomyces* spp. *FEMS Microbiol. Lett.* **2007**, *274*, 311–315. [CrossRef] [PubMed]
52. Shtangeeva, I. Scandium. In *Advances in Ecological Sciences: Trace and Ultratrace Elements in Plants and Soil*; Shtangeeva, I., Ed.; WIT Press: Southampton, UK, 2005; Volume 20.
53. Shannon, R.D. Revised Effective Ionic Radii and Systematic Studies of Interatomic Distances in Halides and Chalcogenides. *Acta Cryst.* **1976**, *32*, 751–767. [CrossRef]
54. Li, H.; Sadler, P.J.; Sun, H. Rationalization of the Strength of Metal Binding to Human Serum Transferrin. *Eur. J. Biochem.* **1996**, *242*, 387–393. [CrossRef]
55. Martin, R.B.; Savory, J.; Brown, S.; Bertholf, R.L.; Wills, M.R. Transferrin binding of Al^{3+} and Fe^{3+}. *Clin. Chem.* **1987**, *33*, 405–407. [CrossRef]
56. Tinoco, A.D.; Valentine, A.M. Ti(IV) Binds to Human Serum Transferrin More Tightly Than Does Fe(III). *J. Am. Chem. Soc.* **2005**, *127*, 11218–11219. [CrossRef]
57. Rosoff, B.; Spencer, H. Binding of rare earths to serum proteins and DNA. *Clin. Chim. Acta* **1979**, *93*, 311–319. [CrossRef]
58. Perkins, D. The interaction of trivalent metal ions with human transferrin. In *Protides of the Biological Fluids—14th Colloquium 1966, Bruges*; Peeters, H., Ed.; Proteins and Related Subjects; Elsevier: Amsterdam, The Netherlands, 1966; Volume 14.
59. Shyy, Y.J.; Tsai, T.C.; Tsai, M.D. Metal-nucleotide interactions. 3. Oxygen-17, phosphorus-31, and proton NMR studies on the interaction of scandium(III), lanthanum(III), and lutetium(III) with adenosine 5′-triphosphate. *J. Am. Chem. Soc.* **1985**, *107*, 3478–3484. [CrossRef]
60. Kulvelis, Y.V.; Lebedev, V.T.; Torok, D.; Melnikov, A.B. Structure of the water salt solutions of DNA with sulfonated scandium diphthalocyanine. *J. Struct. Chem.* **2007**, *48*, 740–746. [CrossRef]
61. Muñoz-Garcia, J.; Mazza, M.; Alliot, C.; Sinquin, C.; Colliec-Jouault, S.; Heymann, D.; Huclier-Markai, S. Antiproliferative Properties of Scandium Exopolysaccharide Complexes on Several Cancer Cell Lines. *Mar. Drugs* **2021**, *19*, 174. [CrossRef] [PubMed]
62. Caporale, A.; Palma, G.; Mariconda, A.; Del Vecchio, V.; Iacopetta, D.; Parisi, O.I.; Sinicropi, M.S.; Puoci, F.; Arra, C.; Longo, P.; et al. Synthesis and Antitumor Activity of New Group 3 Metallocene Complexes. *Molecules* **2017**, *22*, 526. [CrossRef]
63. He, X. Scandium and albumin. In *Encyclopedia to Metalloproteins*; Kretsinger, R.H., Uversky, V.N., Permyakov, E.A., Eds.; Springer: New York, NY, USA, 2013; pp. 1881–1882.
64. Lachine, E.E.; Noujaim, A.A.; Ediss, C.; Wieber, L.I. Toxicity, tissue distribution and excretion of $^{46}ScCl_3$ and ^{46}Sc-EDTA in mice. *Int. J. Appl. Rad. Isot.* **1976**, *27*, 373–377. [CrossRef] [PubMed]

65. Tanida, E.; Usuda, K.; Kono, K.; Kawano, A.; Tsuji, H.; Imanishi, M.; Suzuki, S.; Ohnishi, K.; Yamamoto, K. Urinary scandium as predictor of exposure: Effects of scandium chloride hexahydrate on renal function in rats. *Biol. Trace Elem. Res.* **2009**, *130*, 273–282. [CrossRef] [PubMed]
66. Sánchez-González, C.; López-Chaves, C.; Rivas-García, L.; Galindo, P.; Gómez-Aracena, J.; Aranda, P.; Llopis, J. Accumulation of Scandium in Plasma in Patients with Chronic Renal Failure. *Sci. World J.* **2013**, *2013*, 782745. [CrossRef]
67. Kist, A.A.; Zhuk, L.I.; Danilova, E.A.; Makhmudov, E.A. On question of biological role of scandium. In Proceedings of the Abstracts of International Conference on Nuclear Science and Its Application, Samarkand, Uzbekistan, 25–28 September 2012; p. 476.
68. Barden, J.A.; Curmi, P.M.G.; Dos Remedios, C.G. Crystalline actin tubes: III. The interaction of scandium and yttrium with skeletal muscle actin. *Biochim. Biophys Acta* **1981**, *671*, 25–32. [CrossRef]
69. Gopal, D.; Burke, M. Formation of stable inhibitory complexes of myosin subfragment 1 using fluoroscandium anions. *J. Biol. Chem.* **1995**, *270*, 19282–19286. [CrossRef]
70. Müller, C.; Domnanich, K.A.; Umbricht, C.A.; van der Meulen, N.P. Scandium and terbium radionuclides for radiotheranostics: Current state of development towards clinical application. *Brit. J. Radiol.* **2018**, *91*, 20180074. [CrossRef]
71. Vaughn, B.A.; Koller, A.J.; Boros, E. Aqueous chemistry of the smallest rare earth: Comprehensive characterization of radioactive and non-radioactive scandium complexes for biological applications. In *Methods in Enzymology*; Cotruvo, J.A., Ed.; Academic Press: New York, NY, USA, 2021; Volume 651, pp. 343–371.
72. Kilian, K.; Pyrzyńska, K. Scandium Radioisotopes—Toward New Targets and Imaging Modalities. *Molecules* **2023**, *28*, 7668. [CrossRef]
73. Ioannidis, I.; Lefkaritis, G.; Georgiades, S.N.; Pashalidis, I.; Kontoghiorghes, G.J. Towards Clinical Development of Scandium Radioisotope Complexes for Use in Nuclear Medicine: Encouraging Prospects with the Chelator 1,4,7,10-Tetraazacyclododecane-1,4,7,10-tetraacetic Acid (DOTA) and Its Analogues. *Int. J. Molec. Sci.* **2024**, *25*, 5954. [CrossRef]
74. Vaughn, B.A.; Ahn, S.H.; Aluicio-Sarduy, E.; Devaraj, J.; Olson, A.P.; Engle, J.; Boros, E. Chelation with a twist: A bifunctional chelator to enable room temperature radiolabeling and targeted PET imaging with scandium-44. *Chem. Sci.* **2020**, *11*, 333–342. [CrossRef] [PubMed]
75. Orteca, G.; Sinnes, J.-P.; Rubagotti, S.; Iori, M.; Capponi, P.C.; Piel, M.; Rösch, F.; Ferrari, E.; Asti, M. Gallium-68 and scandium-44 labelled radiotracers based on curcumin structure linked to bifunctional chelators: Synthesis and characterization of potential PET radiotracers. *J. Inorg. Biochem.* **2020**, *204*, 110954. [CrossRef] [PubMed]
76. Zierden, M.R.; Valentine, A.M. Contemplating a role for titanium in organisms. *Metallomics* **2015**, *8*, 9–16. [CrossRef] [PubMed]
77. Gad, S.C. Titanium. In *Encyclopedia of Toxicology*, 3rd ed.; Wexler, P., Ed.; Academic Press: Oxford, UK, 2014; pp. 584–585.
78. Ipach, I.; Schäfer, R.; Mittag, F.; Leichtle, C.; Wolf, P.; Kluba, T. The development of whole blood titanium levels after instrumented spinal fusion—Is there a correlation between the number of fused segments and titanium levels? *BMC Musculoskel. Disord.* **2012**, *13*, 159. [CrossRef]
79. Williams, D.F. The biological applications of titanium and titanium alloys. In *Materials Sciences and Implant Orthopedic Surgery*; Kossowsky, R., Kossovsky, N., Eds.; Martinus Nijhoff Publishers: Dordrecht, The Netherlands, 1986; Volume NATO ASI Series; Volume 116, pp. 107–116.
80. Wilson, W.; Chye Khoon, P. Titanium Alloys in Orthopaedics. In *Titanium Alloys*; Jan, S., Waldemar, Z., Eds.; IntechOpen: Rijeka, Croatia, 2013; Chapter 1.
81. Kun, M.; Cuie, W.; Elena, P.I.; Christopher, C.B.; James, W. Sputtered Hydroxyapatite Nanocoatings on Novel Titanium Alloys for Biomedical Applications. In *Titanium Alloys*; Jan, S., Waldemar, Z., Eds.; IntechOpen: Rijeka, Croatia, 2013; Chapter 1.
82. Burgos, J.; Hevia, E.; Sanpera, I.; García, V.; de Santos Moreno, M.T.; Mariscal, G.; Barrios, C. Elevated blood metal ion levels in patients undergoing instrumented spinal surgery: A systematic review and meta-analysis. *Spine J.* **2024**, *24*, 947–960. [CrossRef]
83. Asa'ad, F.; Thomsen, P.; Kunrath, M.F. The Role of Titanium Particles and Ions in the Pathogenesis of Peri-Implantitis. *J. Bone Metab.* **2022**, *29*, 145–154. [CrossRef]
84. Abreu, H.; Lallukka, M.; Raineri, D.; Leigheb, M.; Ronga, M.; Cappellano, G.; Spriano, S.; Chiocchetti, A. Evaluation of the immune response of peripheral blood mononuclear cells cultured on Ti6Al4V-ELI polished or etched surfaces. *Front. Bioeng. Biotechnol.* **2024**, *12*, 1458091. [CrossRef]
85. Rabbitt, D.; Villapún, V.M.; Carter, L.N.; Man, K.; Lowther, M.; O'Kelly, P.; Knowles, A.J.; Mottura, A.; Tang, Y.T.; Luerti, L.; et al. Rethinking Biomedical Titanium Alloy Design: A Review of Challenges from Biological and Manufacturing Perspectives. *Adv. Healthc. Mater.* **2025**, *14*, 2403129. [CrossRef]
86. Buettner, K.M.; Valentine, A.M. Bioinorganic Chemistry of Titanium. *Chem. Rev.* **2012**, *112*, 1863–1881. [CrossRef]
87. Köpf-Maier, P.; Martin, R. Subcellular distribution of titanium in the liver after treatment with the antitumor agent titanocene dichloride. *Virchows Arch. B* **1989**, *57*, 213–222. [CrossRef]
88. Meléndez, E. Titanium complexes in cancer treatment. *Crit. Rev. Onco./Hemat.* **2002**, *42*, 309–315. [CrossRef] [PubMed]
89. Caruso, F.; Rossi, M. Antitumor titanium compounds. *Mini Rev. Med. Chem.* **2004**, *4*, 49–60. [PubMed]

90. Tshuva, E.Y.; Miller, M. Coordination Complexes of Titanium(IV) for Anticancer Therapy. In *Metal Ions in Life Sciences*; Sigel, A., Sigel, H., Freisinger, E., Sigel, R.K.O., Eds.; Walter de Gruyter GmbH: Berlin, Germany, 2018; Volume 18.
91. Zhao, T.; Wang, P.; Zhang, X.; Liu, N.; Zhao, W.; Zhang, Y.; Yuan, P.; Li, S.; Yang, M.; Yang, Z.; et al. Anti-tumoral Titanium(IV) Complexes Stabilized with Phenolato Ligands and Structure-Activity Relationship. *Curr. Top. Med. Chem.* **2023**, *23*, 1835–1849. [CrossRef] [PubMed]
92. Gomez-Lopez, S.; Serrano, R.; Cohen, B.; Martinez-Argudo, I.; Lopez-Sanz, L.; Guadamillas, M.C.; Calero, R.; Ruiz, M.J. Novel Titanocene Y derivative with albumin affinity exhibits improved anticancer activity against platinum resistant cells. *J. Inorg. Biochem.* **2024**, *254*, 112520. [CrossRef]
93. Pedko, A.; Rubanovich, E.; Tshuva, E.Y.; Shurki, A. Hydrolytically Stable and Cytotoxic [ONON]$_2$Ti(IV)-Type Octahedral Complexes. *Inorg. Chem.* **2022**, *61*, 17653–17661. [CrossRef]
94. Vera, J.L.; Román, F.R.; Meléndez, E. Study of titanocene-DNA and molybdenocene-DNA interactions by inductively coupled plasma-atomic emission spectroscopy. *Anal. Bioanal. Chem.* **2004**, *379*, 399–403. [CrossRef]
95. Kumar, N.; Kaushal, R.; Awasthi, P. A Comprehensive Review on the Development of Titanium Complexes as Cytotoxic Agents. *Curr. Top. Med. Chem.* **2024**, *24*, 2117–2128. [CrossRef]
96. Cini, M.; Bradshaw, T.D.; Woodward, S. Using titanium complexes to defeat cancer: The view from the shoulders of titans. *Chem. Soc. Rev.* **2017**, *46*, 1040–1051. [CrossRef]
97. Gao, L.M.; Hernández, R.; Matta, J.; Meléndez, E. Synthesis, Ti(IV) intake by apotransferrin and cytotoxic properties of functionalized titanocene dichlorides. *J. Biol. Inorg. Chem.* **2007**, *12*, 959–967. [CrossRef]
98. Prajapati, A.; Rangra, S.; Patil, R.; Desai, N.; Jyothi, V.G.S.S.; Salave, S.; Amate, P.; Benival, D.; Kommineni, N. Receptor-Targeted Nanomedicine for Cancer Therapy. *Receptors* **2024**, *3*, 323–361. [CrossRef]
99. Hernández, R.; Méndez, J.; Lamboy, J.; Torres, M.; Román, F.R.; Meléndez, E. Titanium(IV) complexes: Cytotoxicity and cellular uptake of titanium(IV) complexes on caco-2 cell line. *Toxicol. Vitr.* **2010**, *24*, 178–183. [CrossRef] [PubMed]
100. Immel, T.A.; Groth, U.; Huhn, T.; Öhlschläger, P. Titanium Salan Complexes Displays Strong Antitumor Properties In Vitro and In Vivo in Mice. *PLoS ONE* **2011**, *6*, e17869. [CrossRef]
101. Chatterjee, S.; Sil, P.C. Mechanistic Insights into Toxicity of Titanium Dioxide Nanoparticles at the Micro- and Macro-levels. *Chem. Res. Toxicol.* **2024**, *37*, 1612–1633. [CrossRef] [PubMed]
102. Wolf, S.; Sriram, K.; Camassa, L.M.A.; Pathak, D.; Bing, H.L.; Mohr, B.; Zienolddiny-Narui, S.; Samulin Erdem, J. Systematic review of mechanistic evidence for TiO_2 nanoparticle-induced lung carcinogenicity. *Nanotoxicology* **2024**, *18*, 437–463. [CrossRef] [PubMed]
103. Liu, Z.; Zhang, M.; Han, X.; Xu, H.; Zhang, B.; Yu, Q.; Li, M. TiO_2 nanoparticles cause cell damage independent of apoptosis and autophagy by impairing the ROS-scavenging system in Pichia pastoris. *Chem.-Biol. Interact.* **2016**, *252*, 9–18. [CrossRef]
104. Pulgarin, C.; Kiwi, J.; Nadtochenko, V. Mechanism of photocatalytic bacterial inactivation on TiO_2 films involving cell-wall damage and lysis. *Appl. Cat. B Environ.* **2012**, *128*, 179–183. [CrossRef]
105. Carré, G.; Hamon, E.; Ennahar, S.; Estner, M.; Lett, M.-C.; Horvatovich, P.; Gies, J.-P.; Keller, V.; Keller, N.; Andre, P. TiO_2 Photocatalysis Damages Lipids and Proteins in *Escherichia coli*. *Appl. Environ. Microbiol.* **2014**, *80*, 2573–2581. [CrossRef]
106. Bogdan, J.; Pławińska-Czarnak, J.; Zarzyńska, J. Nanoparticles of Titanium and Zinc Oxides as Novel Agents in Tumor Treatment: A Review. *Nanoscale Res. Lett.* **2017**, *12*, 225. [CrossRef]
107. Srivastava, R.; Rahman, Q.; Kashyap, M.; Singh, A.; Jain, G.; Jahan, S.; Lohani, M.; Lantow, M.; Pant, A. Nano-titanium dioxide induces genotoxicity and apoptosis in human lung cancer cell line, A549. *Hum. Exp. Toxicol.* **2013**, *32*, 153–166. [CrossRef]
108. Deb, V.K.; Jain, U. Ti(3)C(2) (MXene), an advanced carrier system: Role in photothermal, photoacoustic, enhanced drugs delivery and biological activity in cancer therapy. *Drug Deliv. Transl. Res.* **2024**, *14*, 3009–3031. [CrossRef]
109. Li, S.; He, N.; Wu, X.; Chen, F.; Xue, Q.; Li, S.; Zhao, C. Characteristics of Ultrasound-Driven Barium Titanate Nanoparticles and the Mechanism of Action on Solid Tumors. *Int. J. Nanomed.* **2024**, *19*, 12769–12791. [CrossRef] [PubMed]
110. Wei, Y.; Huang, M.; Jiang, L. Advancements in Serine Protease Inhibitors: From Mechanistic Insights to Clinical Applications. *Catalysts* **2024**, *14*, 787. [CrossRef]
111. Paschkowsky, S.; Hsiao, J.M.; Young, J.C.; Munter, L.M. The discovery of proteases and intramembrane proteolysis. *Biochem. Cell Biol.* **2019**, *97*, 265–269. [CrossRef]
112. Duffy, B.; Schwietert, C.; France, A.; Mann, N.; Culbertson, K.; Harmon, B.; McCue, J.P. Transition metals as protease inhibitors. *Biol. Trace Elem. Res.* **1998**, *64*, 197–213. [CrossRef]
113. Ani, A.; Ani, M.; Moshtaghie, A.-A.; Ahmadvand, H. Effect of titanium on lipoprotein lipase activity in vivo and in vitro. *J. Trace Elem. Med. Biol.* **2010**, *24*, 95–98. [CrossRef]
114. Geldenhuys, W.J.; Lin, L.; Darvesh, A.S.; Sadana, P. Emerging strategies of targeting lipoprotein lipase for metabolic and cardiovascular diseases. *Drug Discov. Today* **2017**, *22*, 352–365. [CrossRef]

115. Shaikh, Z.; Ashiq, U.; Jamal, R.A.; Gul, S.; Mahroof-Tahir, M.; Sultan, S.; Salar, U.; Khan, K.M. Synthesis, characterization, lipoxygease and tyrosinase inhibitor activities of non-cytotoxic titanium(III) and (IV) hydrazide complexes. *Bull. Chem. Soc. Ethiop.* **2023**, *37*, 315–333. [CrossRef]
116. Melchor-Moncada, J.J.; Vasquez-Giraldo, S.; Zuluaga-Vélez, A.; Orozco, L.M.; Veloza, L.A.; Sepúlveda-Arias, J.C. Bioconjugation of Serratiopeptidase with Titanium Oxide Nanoparticles: Improving Stability and Antibacterial Properties. *J. Funct. Biomater.* **2024**, *15*, 300. [CrossRef]
117. Rodríguez, I.; Fernández-Vega, L.; Maser-Figueroa, A.N.; Sang, B.; González-Pagán, P.; Tinoco, A.D. Exploring Titanium(IV) Complexes as Potential Antimicrobial Compounds. *Antibiotics* **2022**, *11*, 158. [CrossRef]
118. Yaghoubi, S.; Schwietert, C.; McCue, J.P. Biological roles of titanium. *Biol. Trace Elem. Res.* **2000**, *78*, 205–217.
119. Stankic, S.; Suman, S.; Haque, F.; Vidic, J. Pure and multi metal oxide nanoparticles: Synthesis, antibacterial and cytotoxic properties. *J. Nanobiotech.* **2016**, *14*, 73. [CrossRef]
120. de Dicastillo, C.L.; Correa, M.G.; Martínez, F.B.; Streitt, C.; Galotto, M.J. Antimicrobial Effect of Titanium Dioxide Nanoparticles. In *Antimicrobial Resistance*; Mareș, M., Lim, S.H.E., Lai, K.-S., Cristina, R.-T., Eds.; IntechOpen: Rijeka, Croatia, 2020; Chapter 5.
121. Tamilselvi, R.; Kalaiarasi, M.; Elumalai, M.; Malarkodi, T.; Venkatesh, A.; Prakash, V. Antimicrobial Activity of Metal Oxide Nanoparticles. *Biomed. Pharmacol. J.* **2024**, *17*, 1757–1767. [CrossRef]
122. Serov, D.A.; Gritsaeva, A.V.; Yanbaev, F.M.; Simakin, A.V.; Gudkov, S.V. Review of Antimicrobial Properties of Titanium Dioxide Nanoparticles. *Int. J. Mol. Sci.* **2024**, *25*, 10519. [CrossRef]
123. Li, W.; Tang, H.; Xiao, A.; Xie, T.; Sun, Y.; Liao, Y. Effects of applying titanium contained trace-element fertilizer to several grain crops in Hunan. *Hunan Agric. Sci.* **2011**, *21*, 55–58.
124. Lyu, S.; Wei, X.; Chen, J.; Wang, C.; Wang, X.; Pan, D. Titanium as a Beneficial Element for Crop Production. *Front. Plant Sci.* **2017**, *8*, 597. [CrossRef] [PubMed]
125. Faraz, A.; Faizan, M.; Fariduddin, Q.; Hayat, S. Response of Titanium Nanoparticles to Plant Growth: Agricultural Perspectives. In *Sustainable Agriculture Reviews 41: Nanotechnology for Plant Growth and Development*; Hayat, S., Pichtel, J., Faizan, M., Fariduddin, Q., Eds.; Springer International Publishing: Cham, Switzerland, 2020; pp. 101–110.
126. Chaudhary, I.; Singh, V. Titanium Dioxide Nanoparticles and its Impact on Growth, Biomass and Yield of Agricultural Crops under Environmental Stress: A Review. *Res. J. Nanosci. Nanotech.* **2020**, *10*, 1–8.
127. Silva, S.; Dias, M.C.; Silva, A.M.S. Titanium and Zinc Based Nanomaterials in Agriculture: A Promising Approach to Deal with (A)biotic Stresses? *Toxics* **2022**, *10*, 172. [CrossRef] [PubMed]
128. Feizi, H.; Kamali, M.; Jafari, L.; Rezvani Moghaddam, P. Phytotoxicity and stimulatory impacts of nanosized and bulk titanium dioxide on fennel (*Foeniculum vulgare* Mill). *Chemosphere* **2013**, *91*, 506–511. [CrossRef]
129. Yiblet, Y.; Abdu, I.; Belew, B. Comprehensive Literature Review on Metal Nanoparticle for Enhanced Shelf Life of Mango Fruit. *Sci. World J.* **2024**, *2024*, 4782328. [CrossRef]
130. Asztemborska, M.; Jakubiak, M.; Stęborowski, R.; Chajduk, E.; Bystrzejewska-Piotrowska, G. Titanium Dioxide Nanoparticle Circulation in an Aquatic Ecosystem. *Water Air Soil Pollut.* **2018**, *229*, 208. [CrossRef]
131. Shi, W.; Han, Y.; Guo, C.; Su, W.; Zhao, X.; Zha, S.; Wang, Y.; Liu, G. Ocean acidification increases the accumulation of titanium dioxide nanoparticles ($nTiO_2$) in edible bivalve mollusks and poses a potential threat to seafood safety. *Sci. Rep.* **2019**, *9*, 3516. [CrossRef]
132. Valentine, A.M. Exploring a Role for Titanium in Bioinorganic Chemistry. *The Chemist* **2015**, *88*, 7–10.
133. Davis-Gilbert, Z.W.; Tonks, I.A. Titanium redox catalysis: Insights and applications of an earth-abundant base metal. *Dalton Trans.* **2017**, *46*, 11522–11528. [CrossRef] [PubMed]
134. Mallapaty, S. Report: Man survives with titanium heart for 100 days—A world first. *Nature* **2025**, *639*, 848–849. [CrossRef] [PubMed]
135. Greenwood, N.N.; Earnshaw, A. *Chemistry of the Elements*, 2nd ed.; Elsevier: Oxford, UK, 1997.
136. Crans, D.C.; Smee, J.J.; Gaidamauskas, E.; Yang, L. The Chemistry and Biochemistry of Vanadium and the Biological Activities Exerted by Vanadium Compounds. *Chem. Rev.* **2004**, *104*, 849–902. [CrossRef]
137. Wever, R.; Renirie, R.; Hasan, Z. Vanadium in Biology. In *Encyclopedia of Inorganic and Bioinorganic Chemistry*; Scott, R.A., Ed.; Wiley: London, UK, 2011.
138. Rehder, D. Vanadate-dependent peroxidases in macroalgae: Function, applications, and environmental impact. *Oceanography* **2014**, *2*, 121–127.
139. Costa Pessoa, J.; Garribba, E.; Santos, M.F.A.; Santos-Silva, T. Vanadium and proteins: Uptake, transport, structure, activity and function. *Coord. Chem. Rev.* **2015**, *301–302*, 49–86. [CrossRef]
140. Rehder, D. The role of vanadium in biology. *Metallomics* **2015**, *7*, 730–742. [CrossRef]
141. Leblanc, C.; Vilter, H.; Fournier, J.-B.; Delage, L.; Potin, P.; Rebuffet, E.; Michel, G.; Solari, P.-L.; Feiters, M.; Czjzek, M. Vanadium haloperoxidases: From the discovery 30 years ago to X-Ray crystallographic and V K-edge absorption spectroscopic studies. *Coord. Chem. Rev.* **2015**, *301–302*, 134–146. [CrossRef]

142. Wever, R.; Krenn, B.E.; Renirie, R. Chapter Six—Marine Vanadium-Dependent Haloperoxidases, Their Isolation, Characterization, and Application. In *Methods in Enzymology*; Moore, B.S., Ed.; Academic Press: New York, NY, USA, 2018; Volume 605, pp. 141–201.
143. Campitelli, P.; Crucianelli, M. On the Capability of Oxidovanadium(IV) Derivatives to Act as All-Around Catalytic Promoters Since the Prebiotic World. *Molecules* **2020**, *25*, 3073. [CrossRef]
144. Rehder, D. Is vanadium a more versatile target in the activity of primordial life forms than hitherto anticipated? *Org. Biomol. Chem.* **2008**, *6*, 957–964. [CrossRef]
145. Zhang, B.; Wang, S.; Diao, M.; Fu, J.; Xie, M.; Shi, J.; Liu, Z.; Jiang, Y.; Cao, X.; Borthwick, A.G.L. Microbial Community Responses to Vanadium Distributions in Mining Geological Environments and Bioremediation Assessment. *J. Geophys. Res. Biogeosci.* **2019**, *124*, 601–615. [CrossRef]
146. Yan, G.; Sun, X.; Dong, Y.; Gao, W.; Gao, P.; Li, B.; Yan, W.; Zhang, H.; Soleimani, M.; Yan, B.; et al. Vanadate reducing bacteria and archaea may use different mechanisms to reduce vanadate in vanadium contaminated riverine ecosystems as revealed by the combination of DNA-SIP and metagenomic-binning. *Water Res.* **2022**, *226*, 119247. [CrossRef]
147. Lovley, D.R. Microbe Profile: Geobacter metallireducens: A model for novel physiologies of biogeochemical and technological significance. *Microbiol.* **2022**, *168*, 001138. [CrossRef] [PubMed]
148. Yuliani, D.; Morishita, F.; Imamura, T.; Ueki, T. Vanadium Accumulation and Reduction by Vanadium-Accumulating Bacteria Isolated from the Intestinal Contents of Ciona robusta. *Mar. Biotech.* **2024**, *26*, 338–350. [CrossRef]
149. Cockell, C.S.; Santomartino, R.; Finster, K.; Waajen, A.C.; Nicholson, N.; Loudon, C.-M.; Eades, L.J.; Moeller, R.; Rettberg, P.; Fuchs, F.M.; et al. Microbially-Enhanced Vanadium Mining and Bioremediation Under Micro- and Mars Gravity on the International Space Station. *Front. Microbiol.* **2021**, *12*, 641387. [CrossRef]
150. Wever, R.; Hemrika, W. Vanadium Haloperoxidases. In *Handbook of Metalloproteins*; Messerschmidt, A., Huber, R., Poulas, T., Wieghardt, K., Cygler, M., Bod, W., Eds.; John Wiley & Sons, Ltd.: London, UK, 2006; pp. 1–12.
151. Antipov, A.N.; Lyalikova, N.N.; Khijniak, T.V.; L'vov, N.P. Molybdenum-free nitrate reductases from vanadate-reducing bacteria. *FEBS Lett.* **1998**, *441*, 257–260. [CrossRef]
152. Rehder, D. Vanadium: Biological, Environmental, and Engineering Aspects. *Adv. Chem. Res.* **2020**, *2*, 2001002. [CrossRef]
153. Pessoa, J.C.; Etcheverry, S.; Gambino, D. Vanadium compounds in medicine. *Coord. Chem. Rev.* **2015**, *301–302*, 24–48. [CrossRef]
154. Treviño, S.; Díaz, A.; Sánchez-Lara, E.; Sanchez-Gaytan, B.L.; Perez-Aguilar, J.M.; González-Vergara, E. Vanadium in Biological Action: Chemical, Pharmacological Aspects, and Metabolic Implications in Diabetes Mellitus. *Biol. Trace Elem. Res.* **2019**, *188*, 68–98. [CrossRef]
155. Santos, M.F.A.; Sciortino, G.; Correia, I.; Fernandes, A.C.P.; Santos-Silva, T.; Pisanu, F.; Garribba, E.; Costa Pessoa, J. Binding of $V^{IV}O^{2+}$, $V^{IV}OL$, $V^{IV}OL_2$ and $V^{IV}O_2L$ Moieties to Proteins: X-ray/Theoretical Characterization and Biological Implications. *Chemistry* **2022**, *28*, e202200105. [CrossRef]
156. Paolillo, M.; Ferraro, G.; Sahu, G.; Pattanayak, P.D.; Garribba, E.; Halder, S.; Ghosh, R.; Mondal, B.; Chatterjee, P.B.; Dinda, R.; et al. Interaction of $V^{V}O_2$-hydrazonates with lysozyme. *J. Inorg. Biochem.* **2024**, *264*, 112787. [CrossRef] [PubMed]
157. Aissa, T.; Aissaoui-Zid, D.; Moslah, W.; Khamessi, O.; Ksiksi, R.; Oltermann, M.; Ruck, M.; Zid, M.F.; Srairi-Abid, N. Synthesis, physicochemical and pharmacological characterizations of a tetra-[methylimidazolium] dihydrogen decavanadate, inhibiting the IGR39 human melanoma cells development. *J. Inorg. Biochem.* **2024**, *260*, 112672. [CrossRef] [PubMed]
158. Selvaraj, S.; Krishnan, U.M. Vanadium-Flavonoid Complexes: A Promising Class of Molecules for Therapeutic Applications. *J. Med. Chem.* **2021**, *64*, 12435–12452. [CrossRef]
159. Jia, R.; Huang, X.; Dang, P.; Chen, Q.; Zhong, S.; Fan, F.; Wang, C.; Song, J.; Chorover, J.; Rensing, C. Fe(III) reduction mediates vanadium release and reduction in vanadium contaminated paddy soil under different organic amendments. *Environ. Int.* **2024**, *193*, 109073. [CrossRef]
160. Hu, Y.; Wang, Y.; Han, X.; Shan, Y.; Li, F.; Shi, L. Biofilm Biology and Engineering of Geobacter and Shewanella spp. for Energy Applications. *Front. Bioeng. Biotech.* **2021**, *9*, 786416. [CrossRef]
161. McMillan, D.G.G.; Marritt, S.J.; Butt, J.N.; Jeuken, L.J.C. Menaquinone-7 Is Specific Cofactor in Tetraheme Quinol Dehydrogenase CymA. *J. Biol. Chem.* **2012**, *287*, 14215–14225. [CrossRef] [PubMed]
162. Portela, P.C.; Silva, M.A.; Teixeira, L.R.; Salgueiro, C.A. A unique aromatic residue modulates the redox range of a periplasmic multiheme cytochrome from *Geobacter metallireducens*. *J. Biol. Chem.* **2021**, *296*, 100711. [CrossRef]
163. Tielens, A.G.M.; Van Hellemond, J.J. The electron transport chain in anaerobically functioning eukaryotes. *Biochim. Biophs. Acta* **1998**, *1365*, 71–78. [CrossRef]
164. Enomoto, K.; Arikawa, Y.; Muratsubaki, H. Physiological role of soluble fumarate reductase in redox balancing during anaerobiosis in Saccharomyces cerevisiae. *FEMS Microbiol. Lett.* **2002**, *215*, 103–108. [CrossRef]
165. Jiang, X.; van Wonderen, J.H.; Butt, J.N.; Edwards, M.J.; Clarke, T.A.; Blumberger, J. Which Multi-Heme Protein Complex Transfers Electrons More Efficiently? Comparing MtrCAB from *Shewanella* with OmcS from *Geobacter*. *J. Phys. Chem. Lett.* **2020**, *11*, 9421–9425. [CrossRef]

166. Mitchell, P. Chemiosmotic coupling in oxidative and photosynthetic phosphorylation. *Biochim. Biophs. Acta* **2011**, *1807*, 1507–1538. [CrossRef] [PubMed]
167. Feist, A.M.; Nagarajan, H.; Rotaru, A.-E.; Tremblay, P.-L.; Zhang, T.; Nevin, K.P.; Lovley, D.R.; Zengler, K. Constraint-Based Modeling of Carbon Fixation and the Energetics of Electron Transfer in Geobacter metallireducens. *PLoS Comput. Biol.* **2014**, *10*, e1003575. [CrossRef] [PubMed]
168. Butler, A.; Carter-Franklin, J.N. The role of vanadium bromoperoxidase in the biosynthesis of halogenated marine natural products. *Nat. Prod. Rep.* **2004**, *21*, 180–188. [CrossRef]
169. Cochereau, B.; Le Strat, Y.; Ji, Q.; Pawtowski, A.; Delage, L.; Weill, A.; Mazéas, L.; Hervé, C.; Burgaud, G.; Gunde-Cimerman, N.; et al. Heterologous Expression and Biochemical Characterization of a New Chloroperoxidase Isolated from the Deep-Sea Hydrothermal Vent Black Yeast Hortaea werneckii UBOCC-A-208029. *Mar. Biotechnol.* **2023**, *25*, 519–536. [CrossRef] [PubMed]
170. Cochereau, B.; Meslet-Cladière, L.; Pouchus, Y.F.; Grovel, O.; Roullier, C. Halogenation in Fungi: What Do We Know and What Remains to Be Discovered? *Molecules* **2022**, *27*, 3157. [CrossRef]
171. Wever, R.; Krenn, B.E.; Renirie, R. Marine Vanadium-Dependent Haloperoxidases, Their Isolation, Characterization, and Application. *Methods Enzym.* **2018**, *605*, 141–201.
172. Winter, J.M.; Moore, B.S. Exploring the Chemistry and Biology of Vanadium-dependent Haloperoxidases. *J. Biol. Chem* **2009**, *284*, 18577–18581. [CrossRef]
173. Gérard, E.F.; Mokkawes, T.; Johannissen, L.O.; Warwicker, J.; Spiess, R.R.; Blanford, C.F.; Hay, S.; Heyes, D.J.; de Visser, S.P. How Is Substrate Halogenation Triggered by the Vanadium Haloperoxidase from Curvularia inaequalis? *ACS Catal.* **2023**, *13*, 8247–8261. [CrossRef]
174. Zhao, Q.; Zhang, R.; Döbber, J.; Gulder, T. Chemoenzymatic C,C-Bond Forming Cascades by Cryptic Vanadium Haloperoxidase Catalyzed Bromination. *Org. Lett.* **2025**, *27*, 159–164. [CrossRef]
175. Zhao, G.; Dong, H.; Xue, K.; Lou, S.; Qi, R.; Zhang, X.; Cao, Z.; Qin, Q.; Yi, B.; Lei, H.; et al. Nonheme iron catalyst mimics heme-dependent haloperoxidase for efficient bromination and oxidation. *Sci. Adv.* **2024**, *10*, eadq0028. [CrossRef]
176. Zhang, Y.H.; Zou, Y.T.; Zeng, Y.Y.; Liu, L.; Chen, B.S. Enantioselectivity in Vanadium-Dependent Haloperoxidases of Different Marine Sources for Sulfide Oxidation to Sulfoxides. *Mar. Drugs* **2024**, *22*, 419. [CrossRef] [PubMed]
177. Baumgartner, J.T.; McKinnie, S.M.K. Regioselective Halogenation of Lavanducyanin by a Site-Selective Vanadium-Dependent Chloroperoxidase. *Org. Lett.* **2024**, *26*, 5725–5730. [CrossRef]
178. Sweeney, D.; Chase, A.B.; Bogdanov, A.; Jensen, P.R. MAR4 Streptomyces: A Unique Resource for Natural Product Discovery. *J. Nat. Prod.* **2024**, *87*, 439–452. [CrossRef] [PubMed]
179. Sharma, M.; Patton, Z.E.; Shoemaker, C.R.; Bacsa, J.; Biegasiewicz, K.F. N-Halogenation by Vanadium-Dependent Haloperoxidases Enables 1,2,4-Oxadiazole Synthesis. *Ange. Chem. Int. Ed. Engl.* **2024**, *63*, e202411387. [CrossRef]
180. Chen, P.Y.; Adak, S.; Chekan, J.R.; Liscombe, D.K.; Miyanaga, A.; Bernhardt, P.; Diethelm, S.; Fielding, E.N.; George, J.H.; Miles, Z.D.; et al. Structural Basis of Stereospecific Vanadium-Dependent Haloperoxidase Family Enzymes in Napyradiomycin Biosynthesis. *Biochemistry* **2022**, *61*, 1844–1852. [CrossRef]
181. Lazic, J.; Filipovic, V.; Pantelic, L.; Milovanovic, J.; Vojnovic, S.; Nikodinovic-Runic, J. Late-stage diversification of bacterial natural products through biocatalysis. *Front. Bioeng. Biotechnol.* **2024**, *12*, 1351583. [CrossRef] [PubMed]
182. Fernández-Espejo, E. Is there a halo-enzymopathy in Parkinson's disease? *Neurologia* **2022**, *37*, 661–667. [CrossRef]
183. Radlow, M.; Czjzek, M.; Jeudy, A.; Dabin, J.; Delage, L.; Leblanc, C.; Hartung, J. X-ray Diffraction and Density Functional Theory Provide Insight into Vanadate Binding to Homohexameric Bromoperoxidase II and the Mechanism of Bromide Oxidation. *ACS Chem. Biol.* **2018**, *13*, 1243–1259. [CrossRef]
184. Peters, J.W.; Szilagyi, R.K. Exploring new frontiers of nitrogenase structure and mechanism. *Curr. Opin. Chem. Biol.* **2006**, *10*, 101–108. [CrossRef]
185. Decamps, L.; Rice, D.B.; DeBeer, S. An Fe_6C Core in All Nitrogenase Cofactors. *Angew. Chem. Int. Ed. Engl.* **2022**, *61*, e202209190. [CrossRef]
186. Eady, R.R. Structure−Function Relationships of Alternative Nitrogenases. *Chem. Rev.* **1996**, *96*, 3013–3030. [CrossRef]
187. Garcia, A.K.; McShea, H.; Kolaczkowski, B.; Kaçar, B. Reconstructing the evolutionary history of nitrogenases: Evidence for ancestral molybdenum-cofactor utilization. *Geobiology* **2020**, *18*, 394–411. [CrossRef]
188. Miller, R.W.; Eady, R.R. Molybdenum and vanadium nitrogenases of *Azotobacter chroococcum.* Low temperature favours N_2 reduction by vanadium nitrogenase. *Biochem. J.* **1988**, *256*, 429–432. [CrossRef]
189. Seefeldt, L.C.; Yang, Z.-Y.; Lukoyanov, D.A.; Harris, D.F.; Dean, D.R.; Raugei, S.; Hoffman, B.M. Reduction of Substrates by Nitrogenases. *Chem. Rev.* **2020**, *120*, 5082–5106. [CrossRef]
190. Sippel, D.; Einsle, O. The structure of vanadium nitrogenase reveals an unusual bridging ligand. *Nat. Chem. Biol.* **2017**, *13*, 956–960. [CrossRef]
191. Howard, J.B.; Rees, D.C. Structural Basis of Biological Nitrogen Fixation. *Chem. Rev.* **1996**, *96*, 2965–2982. [CrossRef]
192. Rutledge, H.L.; Tezcan, F.A. Electron Transfer in Nitrogenase. *Chem. Rev.* **2020**, *120*, 5158–5193. [CrossRef]

193. Van Stappen, C.; Decamps, L.; Cutsail, G.E., III; Bjornsson, R.; Henthorn, J.T.; Birrell, J.A.; DeBeer, S. The Spectroscopy of Nitrogenases. *Chem. Rev.* **2020**, *120*, 5005–5081. [CrossRef]
194. Wahl, I.M.; Sengupta, K.; van Gastel, M.; Decamps, L.; DeBeer, S. Understanding the P-Cluster of Vanadium Nitrogenase: An EPR and XAS Study of the Holo vs. Apo Forms of the Enzyme. *ChemBiochem* **2024**, *26*, e202400833. [CrossRef]
195. Franke, P.; Freiberger, S.; Zhang, L.; Einsle, O. Conformational protection of molybdenum nitrogenase by Shethna protein II. *Nature* **2025**, *in press*. [CrossRef]
196. Narehood, S.M.; Cook, B.D.; Srisantitham, S.; Eng, V.H.; Shiau, A.A.; McGuire, K.L.; Britt, R.D.; Herzik, M.A.; Tezcan, F.A. Structural basis for the conformational protection of nitrogenase from O_2. *Nature* **2025**, *in press*. [CrossRef]
197. Bjornsson, R.; Neese, F.; DeBeer, S. Revisiting the Mössbauer Isomer Shifts of the FeMoco Cluster of Nitrogenase and the Cofactor Charge. *Inorg. Chem.* **2017**, *56*, 1470–1477. [CrossRef]
198. Siegbahn, P.E.M.; Wei, W.-J. The energetics of N2 reduction by vanadium containing nitrogenase. *Phys. Chem. Chem. Phys.* **2024**, *26*, 1684–1695. [CrossRef]
199. Yang, Z.-Y.; Jimenez-Vicente, E.; Kallas, H.; Lukoyanov, D.A.; Yang, H.; Martin del Campo, J.S.; Dean, D.R.; Hoffman, B.M.; Seefeldt, L.C. The electronic structure of FeV-cofactor in vanadium-dependent nitrogenase. *Chem. Sci.* **2021**, *12*, 6913–6922. [CrossRef]
200. Burgess, B.K.; Lowe, D.J. Mechanism of Molybdenum Nitrogenase. *Chem. Rev.* **1996**, *96*, 2983–3012. [CrossRef]
201. Lukoyanov, D.; Yang, Z.-Y.; Khadka, N.; Dean, D.R.; Seefeldt, L.C.; Hoffman, B.M. Identification of a Key Catalytic Intermediate Demonstrates That Nitrogenase Is Activated by the Reversible Exchange of N2 for H2. *J. Am. Chem. Soc.* **2015**, *137*, 3610–3615. [CrossRef]
202. Sengupta, K.; Joyce, J.P.; Decamps, L.; Kang, L.; Bjornsson, R.; Rüdiger, O.; DeBeer, S. Investigating the Molybdenum Nitrogenase Mechanistic Cycle Using Spectroelectrochemistry. *J. Am. Chem. Soc.* **2025**, *147*, 2099–2144. [CrossRef]
203. Harwood, C.S. Iron-Only and Vanadium Nitrogenases: Fail-Safe Enzymes or Something More? *Ann. Rev. Microbiol.* **2020**, *74*, 247–266. [CrossRef]
204. Jiang, H.; Ryde, U. H_2 formation from the E(2)-E(4) states of nitrogenase. *Phys. Chem. Chem. Phys.* **2024**, *26*, 1364–1375. [CrossRef]
205. Sippel, D.; Rohde, M.; Netzer, J.; Trncik, C.; Gies, J.; Grunau, K.; Djurdjevic, I.; Decamps, L.; Andrade, S.L.A.; Einsle, O. A bound reaction intermediate sheds light on the mechanism of nitrogenase. *Science* **2018**, *359*, 1484–1489. [CrossRef]
206. Benediktsson, B.; Thorhallsson, A.T.; Bjornsson, R. QM/MM calculations reveal a bridging hydroxo group in a vanadium nitrogenase crystal structure. *Chem. Commun.* **2018**, *54*, 7310–7313. [CrossRef]
207. Cao, L.; Caldararu, O.; Ryde, U. Does the crystal structure of vanadium nitrogenase contain a reaction intermediate? Evidence from quantum refinement. *J. Biol. Inorg. Chem.* **2020**, *25*, 847–861. [CrossRef]
208. Lee, C.C.; Hu, Y.; Ribbe, M.W. Vanadium Nitrogenase Reduces CO. *Science* **2010**, *329*, 642. [CrossRef]
209. Rohde, M.; Laun, K.; Zebger, I.; Stripp, S.T.; Einsle, O. Two ligand-binding sites in CO-reducing V nitrogenase reveal a general mechanistic principle. *Sci. Adv.* **2021**, *7*, eabg4474. [CrossRef]
210. Oehlmann, N.N.; Rebelein, J.G. Cover Feature: The Conversion of Carbon Monoxide and Carbon Dioxide by Nitrogenases. *Chem. Bio. Chem.* **2022**, *23*, e202100674.
211. Natzke, J.; Bruno-Bárcena, J.M. Two-Stage Continuous Conversion of Carbon Monoxide to Ethylene by Whole Cells of Azotobacter vinelandii. *Appl. Environ. Microbiol.* **2020**, *86*, e00446-20. [CrossRef]
212. Sickerman, N.S.; Hu, Y.; Ribbe, M.W. Activation of CO2 by Vanadium Nitrogenase. *Chem. Asian J.* **2017**, *12*, 1985–1996. [CrossRef]
213. Rohde, M.; Grunau, K.; Einsle, O. CO Binding to the FeV Cofactor of CO-Reducing Vanadium Nitrogenase at Atomic Resolution. *Angew Chem. Int. Edn.* **2020**, *59*, 23626–23630. [CrossRef]
214. Yamaguchi, N.; Yoshinaga, M.; Kamino, K.; Ueki, T. Vanadium-Binding Ability of Nucleoside Diphosphate Kinase from the Vanadium-Rich Fan Worm, *Pseudopotamilla occelata*. *Zool. Sci.* **2016**, *33*, 266–271. [CrossRef]
215. Hamada, T.; Asanuma, M.; Ueki, T.; Hayashi, F.; Kobayashi, N.; Yokoyama, S.; Michibata, H.; Hirota, H. Solution Structure of Vanabin2, a Vanadium(IV)-Binding Protein from the Vanadium-Rich Ascidian *Ascidia sydneiensis samea*. *J. Am. Chem. Soc.* **2005**, *127*, 4216–4222. [CrossRef]
216. da Silva, J.A.L.; Frausto da Silva, J.J.R.; Pombeiro, A.J.L. Amavadin, a vanadium natural complex: Its role and applications. *Coord. Chem. Rev.* **2013**, *257*, 2388–2400. [CrossRef]
217. Bertini, L.; Barbieri, V.; Fantucci, P.; Gioia, L.D.; Zampella, G. DFT characterization of key intermediates in thiols oxidation catalyzed by amavadin. *Dalton Trans.* **2011**, *40*, 7704–7712. [CrossRef]
218. Rehder, D. Vanadium. Its Role for Humans. In *Interrelations Between Essential Metal Ions and Human Diseases*; Sigel, A., Sigel, H., Sigel, R.K.O., Eds.; Springer Netherlands: Dordrecht, The Netherlands, 2013; Volume 13, pp. 139–169.
219. Kohlmeier, M. Vanadium. In *Nutrient Metabolism*; Kohlmeier, M., Ed.; Academic Press: London, UK, 2003; pp. 762–766.
220. Costa Pessoa, J.; Tomaz, I. Transport of Therapeutic Vanadium and Ruthenium Complexes by Blood Plasma Components. *Current Med. Chem.* **2010**, *17*, 3701–3738. [CrossRef]

221. Correia, I.; Jakusch, T.; Cobbinna, E.; Mehtab, S.; Tomaz, I.; Nagy, N.V.; Rockenbauer, A.; Costa Pessoa, J.; Kiss, T. Evaluation of the binding of oxovanadium(iv) to human serum albumin. *Dalton Trans.* **2012**, *41*, 6477–6487. [CrossRef]
222. Goutam Mukherjee, A.; Ramesh Wanjari, U.; Renu, K.; Vellingiri, B.; Valsala Gopalakrishnan, A. Heavy metal and metalloid—Induced reproductive toxicity. *Environ. Toxicol. Pharmacol.* **2022**, *92*, 103859. [CrossRef]
223. Ommati, M.M.; Heidari, R. Amino acids ameliorate heavy metals-induced oxidative stress in male/female reproductive tissue. In *Toxicology*; Patel, V.B., Preedy, V.R., Eds.; Academic Press: New York, NY, USA, 2021; pp. 371–386.
224. Aureliano, M.; De Sousa-Coelho, A.L.; Dolan, C.C.; Roess, D.A.; Crans, D.C. Biological Consequences of Vanadium Effects on Formation of Reactive Oxygen Species and Lipid Peroxidation. *Int. J. Mol. Sci.* **2023**, *24*, 5382. [CrossRef]
225. Vasilaki, A.T.; McMillan, D.C. Lipid Peroxidation. In *Encyclopedia of Cancer*; Schwab, M., Ed.; Springer: Berlin/Heidelberg, Germany, 2011; pp. 2054–2055.
226. Kehrer, J.P.; Robertson, J.D.; Smith, C.V. Free Radicals and Reactive Oxygen Species. In *Comprehensive Toxicology*, 2nd ed.; McQueen, C.A., Ed.; Elsevier: Oxford, UK, 2010; pp. 277–307.
227. Hanus-Fajerska, E.; Wiszniewska, A.; Kamińska, I. A Dual Role of Vanadium in Environmental Systems-Beneficial and Detrimental Effects on Terrestrial Plants and Humans. *Plants* **2021**, *10*, 1110. [CrossRef]
228. Domingo, J.L.; Gómez, M. Vanadium compounds for the treatment of human diabetes mellitus: A scientific curiosity? A review of thirty years of research. *Food Chem. Toxicol.* **2016**, *95*, 137–141. [CrossRef]
229. Bailey, N.; Carrington, A.; Lott, K.A.K.; Symons, M.C.R. 55. Structure and reactivity of the oxyanions of transition metals. Part VIII. Acidities and spectra of protonated oxyanions. *J. Chem. Soc.* **1960**, 290–297. [CrossRef]
230. Shechter, Y.; Karlish, S.J.D. Insulin-like stimulation of glucose oxidation in rat adipocytes by vanadyl (IV) ions. *Nature* **1980**, *284*, 556–558. [CrossRef]
231. Ramanadham, S.; Mongold, J.J.; Brownsey, R.W.; Cros, G.H.; McNeill, J.H. Oral vanadyl sulfate in treatment of diabetes mellitus in rats. *Am. J. Physiol. Heart Circ. Physiol.* **1989**, *257*, H904–H911. [CrossRef]
232. Sciortino, G.; Maréchal, J.-D.; Garribba, E. Integrated experimental/computational approaches to characterize the systems formed by vanadium with proteins and enzymes. *Inorg. Chem. Front.* **2021**, *8*, 1951–1974. [CrossRef]
233. Crans, D.C.; Henry, L.; Cardiff, G.; Posner, B.I. Developing vanadium as an antidiabetic or anticancer drug: A clinical and historical perspective. *Met. Ions Life Sci.* **2019**, *19*, 203–230.
234. Chromium—Health Professionals. Available online: https://ods.od.nih.gov/factsheets/Chromium-HealthProfessional/ (accessed on 15 May 2023).
235. Mertz, W. Chromium occurrence and function in biological systems. *Physiol. Rev.* **1969**, *49*, 163–239. [CrossRef]
236. Lukaski, H.C. Chromium as a supplement. *Ann. Rev. Nutr.* **1999**, *19*, 279–302. [CrossRef] [PubMed]
237. Raman, P.; Elmendorf, J.S. Unifying mechanisms of trivalent chromium in health and disease. In *Essential and Toxic Trace Elements and Vitamins in Human Health*; Prasad, A.S., Brewer, G.J., Eds.; Academic Press: New York, NY, USA, 2020; pp. 127–139.
238. Genchi, G.; Lauria, G.; Catalano, A.; Carocci, A.; Sinicropi, M.S. The Double Face of Metals: The Intriguing Case of Chromium. *Appl. Sci.* **2021**, *11*, 638. [CrossRef]
239. Tian, H.; Guo, X.; Wang, X.; He, Z.; Sun, R.; Ge, S.; Zhang, Z. Chromium picolinate supplementation for overweight or obese adults. *Cochrane Database Syst. Rev.* **2013**, *11*, CD010063.
240. Panel, E.; Nda, A. Scientific opinion on dietary reference values for chromium. *EFSA J.* **2014**, *12*, 3845.
241. Vajdi, M.; Khajeh, M.; Safaei, E.; Moeinolsadat, S.; Mousavi, S.; Seyedhosseini-Ghaheh, H.; Abbasalizad-Farhangi, M.; Askari, G. Effects of chromium supplementation on body composition in patients with type 2 diabetes: A dose-response systematic review and meta-analysis of randomized controlled trials. *J. Trace Elem. Med. Biol.* **2024**, *81*, 127338. [CrossRef]
242. Khodavirdipour, A.; Haddadi, F.; Keshavarzi, S. Chromium Supplementation; Negotiation with Diabetes Mellitus, Hyperlipidemia and Depression. *J. Diabetes Metab. Disord.* **2020**, *19*, 585–595. [CrossRef]
243. Trumbo, P.R.; Ellwood, K.C. Chromium Picolinate Intake and Risk of Type 2 Diabetes: An Evidence-Based Review by the United States Food and Drug Administration. *Nutr. Rev.* **2006**, *64*, 357–363. [CrossRef] [PubMed]
244. Afzal, S.; Ocasio Quinones, G.A. *Chromium Deficiency*; StatPearls Publishing: Treasure Island, FL, USA, 2025.
245. Vincent, J.B. Is chromium(III) pharmacologically relevant? An update focused on studies with diabetic rodent models. *J. Trace Elem. Med. Biol.* **2024**, *84*, 127453. [CrossRef]
246. Vincent, J.B. Is chromium(III) supplementation beneficial for dietary rodent models of prediabetes? *J. Trace Elem. Med. Biol.* **2024**, *85*, 127482. [CrossRef]
247. Vincent, J.B.; Love, S. The binding and transport of alternative metals by transferrin. *Biochim. Biophys. Acta* **2012**, *1820*, 362–378. [CrossRef]
248. Petersen, C.M.; Edwards, K.C.; Gilbert, N.C.; Vincent, J.B.; Thompson, M.K. X-ray structure of chromium(III)-containing transferrin: First structure of a physiological Cr(III)-binding protein. *J. Inorg. Biochem.* **2020**, *210*, 111101. [CrossRef]

249. Sun, Y.; Ramirez, J.; Woski, S.A.; Vincent, J.B. The binding of trivalent chromium to low-molecular-weight chromium-binding substance (LMWCr) and the transfer of chromium from transferrin and chromium picolinate to LMWCr. *J. Biol. Inorg. Chem.* **2000**, *5*, 129–136. [CrossRef] [PubMed]
250. Levina, A.; Pham, T.H.N.; Lay, P.A. Binding of Chromium(III) to Transferrin Could Be Involved in Detoxification of Dietary Chromium(III) Rather than Transport of an Essential Trace Element. *Angew. Chem. Int. Ed.* **2016**, *55*, 8104–8107. [CrossRef] [PubMed]
251. Vincent, J.B. Relationship between Glucose Tolerance Factor and Low-Molecular-Weight Chromium-Binding Substance. *J. Nutr.* **1994**, *124*, 117–118. [CrossRef]
252. Lai, M.-H. Antioxidant Effects and Insulin Resistance Improvement of Chromium Combined with Vitamin C and E Supplementation for Type 2 Diabetes Mellitus. *J. Clin. Biochem. Nutr.* **2008**, *43*, 191–198. [CrossRef]
253. Wallach, S. Clinical and biochemical aspects of chromium deficiency. *J. Am. Coll. Nutr.* **1985**, *4*, 107–120. [CrossRef]
254. Anderson, R.A. Chromium in the prevention and control of diabetes. *Diabetes Metab.* **2000**, *26*, 22–27.
255. Wilbur, S.; Abadin, H.; Fay, M.; Yu, D.; Tencza, B.; Ingerman, L.; Klotzbach, J.; James, S. Toxicological Profile for Chromium. Available online: https://www.ncbi.nlm.nih.gov/books/NBK158855/ (accessed on 24 May 2023).
256. Viera, M.; Davis-McGibony, C.M. Isolation and Characterization of Low-Molecular-Weight Chromium-binding Substance (LMWCr) from Chicken Liver. *Protein J.* **2008**, *27*, 371–375. [CrossRef] [PubMed]
257. Toepfer, E.W.; Mertz, W.; Polansky, M.M.; Roginski, E.E.; Wolf, W.R. Preparation of Chromium-Containing Material of Glucose Tolerance Factor Activity from Brewer's Yeast Extracts and by Synthesis. *J. Agric. Food Chem.* **1977**, *25*, 162–166. [CrossRef] [PubMed]
258. Vincent, J.B. Is the Pharmacological Mode of Action of Chromium(III) as a Second Messenger? *Biol. Trace Elem. Res.* **2015**, *166*, 7–12. [CrossRef]
259. Vincent, J.B. The biochemistry of chromium. *J. Nutr.* **2000**, *130*, 715–718. [CrossRef]
260. Vincent, J.B. Recent advances in the nutritional biochemistry of trivalent chromium. *Proc. Nutr. Soc.* **2004**, *63*, 41–47. [CrossRef]
261. Vincent, J.B. Biochemical Mechanisms. In *The Bioinorganic Chemistry of Chromium*; Vincent, J.B., Ed.; John Wiley & Sons: Chichester, UK, 2012; pp. 125–167.
262. Jacquamet, L.; Sun, Y.; Hatfield, J.; Gu, W.; Cramer, S.P.; Crowder, M.W.; Lorigan, G.A.; Vincent, J.B.; Latour, J.-M. Characterization of Chromodulin by X-ray Absorption and Electron Paramagnetic Resonance Spectroscopies and Magnetic Susceptibility Measurements. *J. Am. Chem. Soc.* **2003**, *125*, 774–780. [CrossRef] [PubMed]
263. Vincent, J.B. Elucidating a Biological Role for Chromium at a Molecular. *Acc. Chem. Res.* **2000**, *33*, 503–510. [CrossRef]
264. Clodfelder, B.J.; Emamaullee, J.; Hepburn, D.D.; Chakov, N.E.; Nettles, H.S.; Vincent, J.B. The trail of chromium(III) in vivo from the blood to the urine: The roles of transferrin and chromodulin. *J. Biol. Inorg. Chem.* **2001**, *6*, 608–617. [CrossRef]
265. Hua, Y.; Clark, S.; Ren, J.; Sreejayan, N. Molecular mechanisms of chromium in alleviating insulin resistance. *J. Nutr. Biochem.* **2012**, *23*, 313–319. [CrossRef]
266. Cefalu, W.T.; Hu, F.B. Role of Chromium in Human Health and in Diabetes. *Diabetes Care* **2004**, *27*, 2741–2751. [CrossRef] [PubMed]
267. Wang, H.; Hu, L.; Li, H.; Lai, Y.-T.; Wei, X.; Xu, X.; Cao, Z.; Cao, H.; Wan, Q.; Chang, Y.-Y.; et al. Mitochondrial ATP synthase as a direct molecular target of chromium(III) to ameliorate hyperglycaemia stress. *Nat. Commun.* **2023**, *14*, 1738. [CrossRef]
268. Mattos Pereira, V.; Nair, S. Targeting Mitochondrial ATP-Synthase: Evolving Role of Chromium as a Regulator of Carbohydrate and Fat Metabolism. *Biol. Trace Elem. Res.* **2024**, *202*, 1318–1324. [CrossRef] [PubMed]
269. Gencoglu, H.; Orhan, C.; Sahin, K. Understanding Cr(III) Action on Mitochondrial ATP Synthase and AMPK Efficacy: Insights from Previous Studies—A Review. *Biol. Trace Elem. Res.* **2024**, *202*, 1325–1334. [CrossRef] [PubMed]
270. Herzig, S.; Shaw, R.J. AMPK: Guardian of metabolism and mitochondrial homeostasis. *Nat. Rev. Molec. Cell Biol.* **2018**, *19*, 121–135. [CrossRef]
271. Mihaylova, M.M.; Shaw, R.J. The AMPK signalling pathway coordinates cell growth, autophagy and metabolism. *Nat. Cell Biol.* **2011**, *13*, 1016–1023. [CrossRef]
272. Kaikini, A.A.; Kanchan, D.M.; Nerurkar, U.N.; Sathaye, S. Targeting Mitochondrial Dysfunction for the Treatment of Diabetic Complications: Pharmacological Interventions through Natural Products. *Pharmacogn. Rev.* **2017**, *11*, 128–135.
273. Vincent, J.B. What Are the Implications of Cr(III) Serving as an Inhibitor of the Beta Subunit of Mitochondrial ATP Synthase? *Biol. Trace Elem. Res.* **2024**, *202*, 1335–1344. [CrossRef]
274. Oliveira, H. Chromium as an Environmental Pollutant: Insights on Induced Plant Toxicity. *J. Bot.* **2012**, *2012*, 375843. [CrossRef]
275. DesMarias, T.L.; Costa, M. Mechanisms of chromium-induced toxicity. *Curr. Op. Toxicol.* **2019**, *14*, 1–7. [CrossRef]
276. Chen, B.; Xiong, J.; Ding, J.-H.; Yuan, B.-F.; Feng, Y.-Q. Analysis of the Effects of Cr(VI) Exposure on mRNA Modifications. *Chem. Res. Toxicol.* **2019**, *32*, 2078–2085. [CrossRef] [PubMed]
277. Sharma, P.; Singh, S.P.; Parakh, S.K.; Tong, Y.W. Health hazards of hexavalent chromium (Cr (VI)) and its microbial reduction. *Bioengineered* **2022**, *13*, 4923–4938. [CrossRef] [PubMed]

278. Ali, S.; Mir, R.A.; Tyagi, A.; Manzar, N.; Kashyap, A.S.; Mushtaq, M.; Raina, A.; Park, S.; Sharma, S.; Mir, Z.A.; et al. Chromium Toxicity in Plants: Signaling, Mitigation, and Future Perspectives. *Plants* **2023**, *12*, 1502. [CrossRef]
279. Suljević, D.; Muhamed, F.; Alijagic, A. Assessing chromium toxicity across aquatic and terrestrial environments: A cross-species review. *Drug Chem. Toxicol.* **2024**, *47*, 1312–1324. [CrossRef]
280. Hassan, M.U.; Lihong, W.; Nawaz, M.; Ali, B.; Tang, H.; Rasheed, A.; Zain, M.; Alqahtani, F.M.; Hashem, M.; Qari, S.H.; et al. Silicon a key player to mitigate chromium toxicity in plants: Mechanisms and future prospective. *Plant Physiol. Biochem.* **2024**, *208*, 108529. [CrossRef] [PubMed]
281. Sazakli, E. Human Health Effects of Oral Exposure to Chromium: A Systematic Review of the Epidemiological Evidence. *Int. J. Environ. Res. Public Health* **2024**, *21*, 406. [CrossRef]
282. Meaza, I.; Williams, A.R.; Wise, S.S.; Lu, H.; Wise, J.P. Carcinogenic Mechanisms of Hexavalent Chromium: From DNA Breaks to Chromosome Instability and Neoplastic Transformation. *Curr. Environ. Health Rep.* **2024**, *11*, 484–546. [CrossRef]
283. Levina, A.; Lay, P.A. Chapter 9—Redox chemistry and biological activities of chromium(III) complexes. In *The Nutritional Biochemistry of Chromium (III)*, 2nd ed.; Vincent, J.B., Ed.; Elsevier: Amsterdam, The Netherlands, 2019; pp. 281–321.
284. Paul, M.; Pranjaya, P.P.; Thatoi, H. In silico studies on structural, functional, and evolutionary analysis of bacterial chromate reductase family responsible for high chromate bioremediation efficiency. *SN Appl. Sci.* **2020**, *2*, 1997. [CrossRef]
285. Park, C.H.; Keyhan, M.; Wielinga, B.; Fendorf, S.; Matin, A. Purification to Homogeneity and Characterization of a Novel *Pseudomonas putida* Chromate Reductase. *Appl. Environ. Micro.* **2000**, *66*, 1788–1795. [CrossRef]
286. Jin, H.; Zhang, Y.; Buchko, G.W.; Varnum, S.M.; Robinson, H.; Squier, T.C.; Long, P.E. Structure Determination and Functional Analysis of a Chromate Reductase from Gluconacetobacter hansenii. *PLoS ONE* **2012**, *7*, e42432. [CrossRef]
287. Ackerley, D.F.; Gonzalez, C.F.; Keyhan, M.; Blake II, R.; Matin, A. Mechanism of chromate reduction by the Escherichia coli protein, NfsA, and the role of different chromate reductases in minimizing oxidative stress during chromate reduction. *Environ. Micro.* **2004**, *6*, 851–860. [CrossRef] [PubMed]
288. Viti, C.; Marchi, E.; Decorosi, F.; Giovannetti, L. Molecular mechanisms of Cr(VI) resistance in bacteria and fungi. *FEMS Micro. Rev.* **2014**, *38*, 633–659. [CrossRef] [PubMed]
289. Alur, A.; John, P.; Xu, D. Effects of hexavalent chromium on mitochondria and their implications in carcinogenesis. *J. Env. Sci. Health C* **2024**, *42*, 109–125. [CrossRef]
290. Gerke, T.L.; Little, B.J. Manganese. In *Encyclopedia of Geochemistry: A Comprehensive Reference Source on the Chemistry of the Earth*; White, W.M., Ed.; Springer International Publishing: Cham, Switzerland, 2018; pp. 864–867.
291. Čapek, J.; Večerek, B. Why is manganese so valuable to bacterial pathogens? *Front. Cell Infect. Micro.* **2023**, *13*, 943390. [CrossRef]
292. Roth, J.; Ponzoni, S.; Aschner, M. Manganese Homeostasis and Transport. In *Matallomics and the Cell*; Banci, L., Ed.; Springer Netherlands: Dordrecht, The Netherlands, 2013; pp. 169–201.
293. Soares, M.V.; Quines, C.B.; Ávila, D.S. Manganese. In *Essential and Toxic Trace Elements and Vitamins in Human Health*; Prasad, A.S., Brewer, G.J., Eds.; Academic Press: London, UK, 2020; pp. 141–152.
294. Studer, J.M.; Schweer, W.P.; Gabler, N.K.; Ross, J.W. Functions of manganese in reproduction. *Anim. Reprod. Sci.* **2022**, *238*, 106924. [CrossRef]
295. Marques dos Santos, D.; Aschner, M.; Marreilha dos Santos, A.P. Manganese and Neurodegeneration. In *Biometals in Neurodegenerative Diseases: Mechanisms and Therapeutics*; White, A.R., Aschner, M., Costa, L.G., Bush, A.I., Eds.; Elsevier: London, UK, 2017; pp. 117–151.
296. Socha, A.L.; Guerinot, M.L. Mn-euvering manganese: The role of transporter gene family members in manganese uptake and mobilization in plants. *Front. Plant Sci.* **2014**, *5*, 00106. [CrossRef] [PubMed]
297. Obeng, S.K.; Kulhánek, M.; Balík, J.; Černý, J.; Sedlář, O. Manganese: From Soil to Human Health—A Comprehensive Overview of Its Biological and Environmental Significance. *Nutrients* **2024**, *16*, 3455. [CrossRef]
298. Syiemlieh, I.; Kumar, A.; Kurbah, S.D.; De, A.K.; Lal, R.A. Low-spin manganese(II) and high-spin manganese(III) complexes derived from disalicylaldehyde oxaloyldihydrazone: Synthesis, spectral characterization and electrochemical studies. *J. Mol. Str.* **2018**, *1151*, 343–352. [CrossRef]
299. Saha, A.; Majumdar, P.; Goswami, S. Low-spin manganese(II) and cobalt(III) complexes of N-aryl-2-pyridylazophenylamines: New tridentate N,N,N-donors derived from cobalt mediated aromatic ring amination of 2-(phenylazo)pyridine. Crystal structure of a manganese(II) complex. *J. Chem. Soc. Dalton Trans.* **2000**, 1703–1708. [CrossRef]
300. Basu, P.; Chakravorty, A. Low-spin tris(quinone oximates) of manganese(II,III). Synthesis, isomerism, and equilibria. *Inorg. Chem.* **1992**, *31*, 4980–4986. [CrossRef]
301. Basumatary, D.; Lal, R.A.; Kumar, A. Synthesis, and characterization of low- and high-spin manganese(II) complexes of polyfunctional adipoyldihydrazone: Effect of coordination of N-donor ligands on stereo-redox chemistry. *J. Mol. Str.* **2015**, *1092*, 122–129. [CrossRef]
302. Baj, J.; Flieger, W.; Barbachowska, A.; Kowalska, B.; Flieger, M.; Forma, A.; Teresiński, G.; Portincasa, P.; Buszewicz, G.; Radzikowska-Büchner, E.; et al. Consequences of Disturbing Manganese Homeostasis. *Int. J. Mol. Sci.* **2023**, *24*, 14959. [CrossRef]

303. Reinert, J.P.; Forbes, L.D. Manganese Toxicity Associated With Total Parenteral Nutrition: A Review. *J. Pharm. Technol.* **2021**, *37*, 260–266. [CrossRef]
304. Wu, Q.; Mu, Q.; Xia, Z.; Min, J.; Wang, F. Manganese homeostasis at the host-pathogen interface and in the host immune system. *Semin. Cell Dev. Biol.* **2021**, *115*, 45–53. [CrossRef]
305. Martins, A.C.; Krum, B.N.; Queirós, L.; Tinkov, A.A.; Skalny, A.V.; Bowman, A.B.; Aschner, M. Manganese in the Diet: Bioaccessibility, Adequate Intake, and Neurotoxicological Effects. *J. Agric. Food Chem.* **2020**, *68*, 12893–12903. [CrossRef]
306. Tinkov, A.A.; Paoliello, M.M.B.; Mazilina, A.N.; Skalny, A.V.; Martins, A.C.; Voskresenskaya, O.N.; Aaseth, J.; Santamaria, A.; Notova, S.V.; Tsatsakis, A.; et al. Molecular Targets of Manganese-Induced Neurotoxicity: A Five-Year Update. *Int. J. Mol. Sci.* **2021**, *22*, 4646. [CrossRef]
307. Soares, A.T.G.; Silva, A.C.; Tinkov, A.A.; Khan, H.; Santamaría, A.; Skalnaya, M.G.; Skalny, A.V.; Tsatsakis, A.; Bowman, A.B.; Aschner, M.; et al. The impact of manganese on neurotransmitter systems. *J. Trace Elem. Med. Biol.* **2020**, *61*, 126554. [CrossRef]
308. Sule, K.; Umbsaar, J.; Prenner, E.J. Mechanisms of Co, Ni, and Mn toxicity: From exposure and homeostasis to their interactions with and impact on lipids and biomembranes. *Biochim. Biophys. Acta* **2020**, *1862*, 183250. [CrossRef]
309. Balachandran, R.C.; Mukhopadhyay, S.; McBride, D.; Veevers, J.; Harrison, F.E.; Aschner, M.; Haynes, E.N.; Bowman, A.B. Brain manganese and the balance between essential roles and neurotoxicity. *J. Biol. Chem.* **2020**, *295*, 6312–6329. [CrossRef]
310. McCabe, S.; Limesand, K.; Zhao, N. Recent progress toward understanding the role of ZIP14 in regulating systemic manganese homeostasis. *Comput. Struct. Biotechnol. J.* **2023**, *21*, 2332–2338. [CrossRef]
311. Winslow, J.W.W.; Limesand, K.H.; Zhao, N. The Functions of ZIP8, ZIP14, and ZnT10 in the Regulation of Systemic Manganese Homeostasis. *Int. J. Mol. Sci.* **2020**, *21*, 3304. [CrossRef]
312. Liu, Q.; Barker, S.; Knutson, M.D. Iron and manganese transport in mammalian systems. *Biochim. Biophys. Acta* **2021**, *1868*, 118890. [CrossRef] [PubMed]
313. Mims, M.P.; Prchal, J.T. Divalent metal transporter 1. *Hematology* **2005**, *10*, 339–345. [CrossRef] [PubMed]
314. Fujishiro, H.; Kambe, T. Manganese transport in mammals by zinc transporter family proteins, ZNT and ZIP. *J. Pharmcol. Sci.* **2022**, *148*, 125–133. [CrossRef] [PubMed]
315. Gunter, T.E.; Gerstner, B.; Gunter, K.K.; Malecki, J.; Gelein, R.; Valentine, W.M.; Aschner, M.; Yule, D.I. Manganese transport via the transferrin mechanism. *NeuroToxicology* **2013**, *34*, 118–127. [CrossRef]
316. Liu, M.; Sun, X.; Chen, B.; Dai, R.; Xi, Z.; Xu, H. Insights into Manganese Superoxide Dismutase and Human Diseases. *Int. J. Mol. Sci.* **2022**, *23*, 15893. [CrossRef]
317. Fischer, W.W.; Hemp, J.; Valentine, J.S. How did life survive Earth's great oxygenation? *Curr. Opp. Chem. Biol.* **2016**, *31*, 166–178. [CrossRef]
318. Halliwell, B.; Adhikary, A.; Dingfelder, M.; Dizdaroglu, M. Hydroxyl radical is a significant player in oxidative DNA damage in vivo. *Chem. Soc. Rev.* **2021**, *50*, 8355–8360. [CrossRef]
319. Koppenol, W.H. The Haber-Weiss cycle—70 years later. *Redox Rep.* **2001**, *6*, 229–234. [CrossRef]
320. Koppenol, W.H.; Hider, R.H. Iron and redox cycling. Do's and don'ts. *Free. Radic. Biol. Med.* **2019**, *133*, 3–10. [CrossRef]
321. Holley, A.K.; Bakthavatchalu, V.; Velez-Roman, J.M.; Clair, D.K.S. Manganese Superoxide Dismutase: Guardian of the Powerhouse. *Int. J. Mol. Sci.* **2011**, *12*, 7114–7162. [CrossRef]
322. Steinman, H.M. Bacterial Superoxide Dismutases. In *Oxygen Radicals in Biology and Medicine*; Simic, M.G., Taylor, K.A., Ward, J.F., von Sonntag, C., Eds.; Springer: Boston, MA, USA, 1988; pp. 641–646.
323. McCord, J.M. Superoxide dismutase in aging and disease: An overview. In *Methods Enzymology*; Academic Press: San Diego, CA, USA, 2002; Volume 349, pp. 331–341.
324. Marques, H.M. Electron transfer in biological systems. *J. Biol. Inorg. Chem.* **2024**, *29*, 641–683. [CrossRef] [PubMed]
325. Sheng, Y.; Abreu, I.A.; Cabelli, D.E.; Maroney, M.J.; Miller, A.-F.; Teixeira, M.; Valentine, J.S. Superoxide Dismutases and Superoxide Reductases. *Chem. Rev.* **2014**, *114*, 3854–3918. [CrossRef]
326. Mondola, P.; Damiano, S.; Sasso, A.; Santillo, M. The Cu, Zn Superoxide Dismutase: Not Only a Dismutase Enzyme. *Front. Physiol.* **2016**, *7*, 594. [CrossRef]
327. Ambrosone, C.B.; Freudenheim, J.L.; Thompson, P.A.; Bowman, E.; Vena, J.E.; Marshall, J.R.; Graham, S.; Laughlin, R.; Nemoto, T.; Shields, P.G. Manganese superoxide dismutase (MnSOD) genetic polymorphisms, dietary antioxidants, and risk of breast cancer. *Cancer Res.* **1999**, *59*, 602–606. [PubMed]
328. Valenti, L.; Conte, D.; Piperno, A.; Dongiovanni, P.; Fracanzani, A.L.; Fraquelli, M.; Vergani, A.; Gianni, C.; Carmagnola, L.; Fargion, S. The mitochondrial superoxide dismutase A16V polymorphism in the cardiomyopathy associated with hereditary haemochromatosis. *J. Med. Genet.* **2004**, *41*, 946–950. [CrossRef]
329. Martin, R.C.G.; Ahn, J.; Nowell, S.A.; Hein, D.W.; Doll, M.A.; Martini, B.D.; Ambrosone, C.B. Association between manganese superoxide dismutase promoter gene polymorphism and breast cancer survival. *Breast Cancer Res.* **2006**, *8*, R45. [CrossRef]
330. Hewitt, J.; Morris, J.G. Superoxide dismutase in some obligately anaerobic bacteria. *FEBS Lett.* **1975**, *50*, 315–318. [CrossRef] [PubMed]

331. Schäfer, G.; Kardinahl, S. Iron superoxide dismutases: Structure and function of an archaic enzyme. *Biochem. Soc. Trans.* **2003**, *31*, 1330–1334. [CrossRef]
332. Rahman, I.; Biswas, S.K. Oxidants and Antioxidants | Antioxidants, Enzymatic. In *Encyclopedia of Respiratory Medicine*; Laurent, G.J., Shapiro, S.D., Eds.; Academic Press: Oxford, UK, 2006; pp. 258–266.
333. Ryan, K.C.; Johnson, O.E.; Cabelli, D.E.; Brunold, T.C.; Maroney, M.J. Nickel superoxide dismutase: Structural and functional roles of Cys2 and Cys6. *J. Biol. Inorg. Chem.* **2010**, *15*, 795–807. [CrossRef]
334. Perry, J.J.P.; Shin, D.S.; Getzoff, E.D.; Tainer, J.A. The structural biochemistry of the superoxide dismutases. *Biochim. Biophs. Acta* **2010**, *1804*, 245–262. [CrossRef]
335. Mendoza, E.R.; Stelmastchuk, L.B.F.; Ferreira, J.R.S.; Garratt, R.C. Crystal Structure Analysis of Superoxide Dismutase from Trichoderma reesei (Protein Databank PDB Code 6DQY). Available online: https://www.rcsb.org/structure/6DQY (accessed on 3 April 2024).
336. Lah, M.S.; Dixon, M.M.; Pattridge, K.A.; Stallings, W.C.; Fee, J.A.; Ludwig, M.L. Structure-function in Escherichia coli iron superoxide dismutase: Comparisons with the manganese enzyme from Thermus thermophilus. *Biochemistry* **1995**, *34*, 1646–1660. [CrossRef]
337. Ludwig, M.L.; Metzger, A.L.; Pattridge, K.A.; Stallings, W.C. Manganese superoxide dismutase from *Thermus thermophilus:* A structural model refined at 1.8 Å resolution. *J. Molec. Biol.* **1991**, *219*, 335–358. [CrossRef]
338. Tierney, D.L.; Fee, J.A.; Ludwig, M.L.; Penner-Hahn, J.E. X-ray Absorption Spectroscopy of the Iron Site in Escherichia coli Fe(III) Superoxide Dismutase. *Biochemistry* **1995**, *34*, 1661–1668. [CrossRef]
339. Whittaker, M.M.; Whittaker, J.W. Low-Temperature Thermochromism Marks a Change in Coordination for the Metal Ion in Manganese Superoxide Dismutase. *Biochemistry* **1996**, *35*, 6762–6770. [CrossRef]
340. Whittaker, M.M.; Whittaker, J.W. A "thermophilic shift" in ligand interactions for Thermus thermophilus manganese superoxide dismutase. *J. Biol. Inorg. Chem.* **1997**, *2*, 667–671. [CrossRef]
341. Azadmanesh, J.; Trickel, S.R.; Borgstahl, G.E.O. Substrate-analog binding aand electrostatic surfaces of human manganese superoxide dismutase. *J. Struct. Biol.* **2017**, *199*, 68–75. [CrossRef]
342. Azadmanesh, J.; Borgstahl, G.E.O. A Review of the Catalytic Mechanism of Human Manganese Superoxide Dismutase. *Antioxidants* **2018**, *7*, 25. [CrossRef]
343. Azadmanesh, J.; Lutz, W.E.; Coates, L.; Weiss, K.L.; Borgstahl, G.E.O. Direct detection of coupled proton and electron transfers in human manganese superoxide dismutase. *Nat. Commun.* **2021**, *12*, 2079. [CrossRef]
344. Abreu, I.A.; Cabelli, D.E. Superoxide dismutases—A review of the metal-associated mechanistic variations. *Biochim. Biophs. Acta* **2010**, *1804*, 263–274. [CrossRef]
345. Srnec, M.; Aquilante, F.; Ryde, U.; Rulísek, L. Reaction mechanism of manganese superoxide dismutase studied by combined quantum and molecular mechanical calculations and multiconfigurational methods. *J. Phys. Chem. B* **2009**, *113*, 6074–6086. [CrossRef]
346. Palma, F.R.; He, C.; Danes, J.M.; Paviani, V.; Coelho, D.R.; Gantner, B.N.; Bonini, M.G. Mitochondrial Superoxide Dismutase: What the Established, the Intriguing, and the Novel Reveal About a Key Cellular Redox Switch. *Antioxid. Redox Signal.* **2020**, *32*, 701–714. [CrossRef]
347. Pravda, J. Hydrogen peroxide and disease: Towards a unified system of pathogenesis and therapeutics. *Molec. Med.* **2020**, *26*, 41. [CrossRef]
348. Azadmanesh, J.; Slobodnik, K.; Struble, L.R.; Lutz, W.E.; Coates, L.; Weiss, K.L.; Myles, D.A.A.; Kroll, T.; Borgstahl, G.E.O. Revealing the atomic and electronic mechanism of human manganese superoxide dismutase product inhibition. *Nat. Commun.* **2024**, *15*, 5973. [CrossRef]
349. Lennicke, C.; Rahn, J.; Lichtenfels, R.; Wessjohann, L.A.; Seliger, B. Hydrogen peroxide—Production, fate and role in redox signaling of tumor cells. *Cell Commun. Signal.* **2015**, *13*, 39. [CrossRef]
350. Brudvig, G.W. Structure and Function of Manganese in Photosystem II. In *Mechanistic Bioinorganic Chemistry*; Thorp, H.H., Pecoraro, V.L., Eds.; Advances in Chemistry; American Chemical Society: Washington, DC, USA, 1996; Volume 246, pp. 249–263.
351. Schmidt, S.B.; Jensen, P.E.; Husted, S. Manganese Deficiency in Plants: The Impact on Photosystem II. *Trends Plant Sci.* **2016**, *21*, 622–632. [CrossRef]
352. Narzi, D.; Bovi, D.; De Gaetano, P.; Guidoni, L. Dynamics of the Special Pair of Chlorophylls of Photosystem II. *J. Am. Chem. Soc.* **2016**, *138*, 257–264. [CrossRef]
353. Lokstein, H.; Renger, G.; Götze, J.P. Photosynthetic Light-Harvesting (Antenna) Complexes—Structures and Functions. *Molecules* **2021**, *26*, 3378. [CrossRef]
354. Oliver, N.; Avramov, A.P.; Nürnberg, D.J.; Dau, H.; Burnap, R.L. From manganese oxidation to water oxidation: Assembly and evolution of the water-splitting complex in photosystem II. *Photosynth. Res.* **2022**, *152*, 107–133. [CrossRef]
355. John, C.; Pedraza-González, L.; Betti, E.; Cupellini, L.; Mennucci, B. A Computational Approach to Modeling Excitation Energy Transfer and Quenching in Light-Harvesting Complexes. *J. Phys. Chem. B* **2024**, *in press*. [CrossRef]

356. Zhang, M.; Ming, Y.; Wang, H.-B.; Jin, H.-L. Strategies for adaptation to high light in plants. *aBIOTECH* **2024**, *5*, 381–393. [CrossRef]
357. Didaran, F.; Kordrostami, M.; Ghasemi-Soloklui, A.A.; Pashkovskiy, P.; Kreslavski, V.; Kuznetsov, V.; Allakhverdiev, S.I. The mechanisms of photoinhibition and repair in plants under high light conditions and interplay with abiotic stressors. *J. Photochem. Photobiol. B* **2024**, *259*, 113004. [CrossRef]
358. Marulanda Valencia, W.; Pandit, A. Photosystem II Subunit S (PsbS): A Nano Regulator of Plant Photosynthesis. *J. Molec. Biol.* **2024**, *436*, 168407. [CrossRef]
359. Semin, B.; Loktyushkin, A.; Lovyagina, E. Current analysis of cations substitution in the oxygen-evolving complex of photosystem II. *Biophys. Rev.* **2024**, *16*, 237–247. [CrossRef]
360. Umena, Y.; Kawakami, K.; Shen, J.-R.; Kamiya, N. Crystal structure of oxygen-evolving photosystem II at a resolution of 1.9 Å. *Nature* **2011**, *473*, 55–60. [CrossRef]
361. Hamilton, T.L.; Bryant, D.A.; Macalady, J.L. The role of biology in planetary evolution: Cyanobacterial primary production in low-oxygen Proterozoic oceans. *Environ. Microbiol.* **2016**, *18*, 325–340. [CrossRef]
362. Rexroth, S.; Nowaczyk, M.M.; Rögner, M. Cyanobacterial Photosynthesis: The Light Reactions. In *Modern Topics in the Phototrophic Prokaryotes: Metabolism, Bioenergetics, and Omics*; Hallenbeck, P.C., Ed.; Springer International Publishing: Cham, Switzerland, 2017; pp. 163–191.
363. Mittler, R.; Vanderauwera, S.; Suzuki, N.; Miller, G.; Tognetti, V.B.; Vandepoele, K.; Gollery, M.; Shulaev, V.; Van Breusegem, F. ROS signaling: The new wave? *Trends Plant Sci.* **2011**, *16*, 300–309. [CrossRef]
364. Mandal, M.; Saito, K.; Ishikita, H. Requirement of Chloride for the Downhill Electron Transfer Pathway from the Water-Splitting Center in Natural Photosynthesis. *J. Phys. Chem. B* **2022**, *126*, 123–131. [CrossRef]
365. Rivalta, I.; Amin, M.; Luber, S.; Vassiliev, S.; Pokhrel, R.; Umena, Y.; Kawakami, K.; Shen, J.-R.; Kamiya, N.; Bruce, D.; et al. Structural–Functional Role of Chloride in Photosystem II. *Biochemistry* **2011**, *50*, 6312–6315. [CrossRef]
366. Allgöwer, F.; Pöverlein, M.C.; Rutherford, A.W.; Kaila, V.R.I. Mechanism of proton release during water oxidation in Photosystem II. *Proc. Natl. Acad. Sci. USA* **2024**, *121*, e2413396121. [CrossRef]
367. Hofbauer, W.; Zouni, A.; Bittl, R.; Kern, J.; Orth, P.; Lendzian, F.; Fromme, P.; Witt, H.T.; Lubitz, W. Photosystem II single crystals studied by EPR spectroscopy at 94 GHz: The tyrosine radical Y(D). *Proc. Natl. Acad. Sci. USA* **2001**, *98*, 6623–6628. [CrossRef]
368. Ferreira, K.N.; Iverson, T.M.; Maghlaoui, K.; Barber, J.; Iwata, S. Architecture of the Photosynthetic Oxygen-Evolving Center. *Science* **2004**, *303*, 1831–1838. [CrossRef]
369. Loll, B.; Kern, J.; Saenger, W.; Zouni, A.; Biesiadka, J. Towards complete cofactor arrangement in the 3.0 Å resolution structure of photosystem II. *Nature* **2005**, *438*, 1040–1044. [CrossRef] [PubMed]
370. Suga, M.; Akita, F.; Hirata, K.; Ueno, G.; Murakami, H.; Nakajima, Y.; Shimizu, T.; Yamashita, K.; Yamamoto, M.; Ago, H.; et al. Native structure of photosystem II at 1.95 Å resolution viewed by femtosecond X-ray pulses. *Nature* **2015**, *517*, 99–103. [CrossRef]
371. Fatima, S.; Olshansky, L. Conformational control over proton-coupled electron transfer in metalloenzymes. *Nat. Rev. Chem.* **2024**, *8*, 762–775. [CrossRef] [PubMed]
372. Flesher, D.A.; Liu, J.; Wang, J.; Gisriel, C.J.; Yang, K.R.; Batista, V.S.; Debus, R.J.; Brudvig, G.W. Mutation-induced shift of the photosystem II active site reveals insight into conserved water channels. *J. Biol. Chem.* **2024**, *300*, 107475. [CrossRef]
373. Kok, B.; Forbush, B.; McGloin, M. Cooperation of charges in photosynthetic O_2 evolution—I. A linear four step mechanism. *Photochem. Photobiol.* **1970**, *11*, 457–475. [CrossRef] [PubMed]
374. Bury, G.; Pushkar, Y. Insights from $Ca^{2+} \rightarrow Sr^{2+}$ substitution on the mechanism of O-O bond formation in photosystem II. *Photosynth. Res.* **2024**, *162*, 331–351. [CrossRef]
375. Yamaguchi, K.; Miyagawa, K.; Shoji, M.; Kawakami, T.; Isobe, H.; Yamanaka, S.; Nakajima, T. Theoretical elucidation of the structure, bonding, and reactivity of the $CaMn_4O_x$ clusters in the whole Kok cycle for water oxidation embedded in the oxygen evolving center of photosystem II. New molecular and quantum insights into the mechanism of the O–O bond formation. *Photosynth. Res.* **2024**, *162*, 291–330.
376. Mattila, H.; Mishra, S.; Tyystjärvi, T.; Tyystjärvi, E. Singlet oxygen production by photosystem II is caused by misses of the oxygen evolving complex. *New Phytol.* **2023**, *237*, 113–125. [CrossRef]
377. Vinyard, D.J.; Khan, S.; Brudvig, G.W. Photosynthetic water oxidation: Binding and activation of substrate waters for O–O bond formation. *Faraday Discuss.* **2015**, *185*, 37–50. [CrossRef]
378. Zhang, B.; Sun, L. Why nature chose the Mn4CaO5 cluster as water-splitting catalyst in photosystem II: A new hypothesis for the mechanism of O–O bond formation. *Dalton Trans.* **2018**, *47*, 14381–14387. [CrossRef] [PubMed]
379. Yehia, S.; Wang, J.; Brudvig, G.W.; Gunner, M.R.; Brooks, B.R.; Amin, M. An analysis of the structural changes of the oxygen evolving complex of Photosystem II in the S1 and S3 states revealed by serial femtosecond crystallography. *Biochim. Biophys. Acta* **2025**, *1866*, 149531. [CrossRef]
380. Vinyard, D.J.; Ananyev, G.M.; Charles Dismukes, G. Photosystem II: The Reaction Center of Oxygenic Photosynthesis*. *Ann. Rev. Biochem.* **2013**, *82*, 577–606. [CrossRef]

381. Pace, R.J.; Jin, L.; Stranger, R. What spectroscopy reveals concerning the Mn oxidation levels in the oxygen evolving complex of photosystem II: X-ray to near infra-red. *Dalton Trans.* **2012**, *41*, 11145–11160. [CrossRef]
382. Wang, J. Cryo-EM meets crystallography: A model-independent view of the heteronuclear Mn_4Ca cluster structure of photosystem II. *Proc. Natl. Acad. Sci. USA* **2025**, *122*, e2423012122. [CrossRef] [PubMed]
383. Cheah, M.H.; Zhang, M.; Shevela, D.; Mamedov, F.; Zouni, A.; Messinger, J. Assessment of the manganese cluster's oxidation state via photoactivation of photosystem II microcrystals. *Proc. Natl. Acad. Sci. USA* **2020**, *117*, 141–145. [CrossRef] [PubMed]
384. Krewald, V.; Retegan, M.; Cox, N.; Messinger, J.; Lubitz, W.; DeBeer, S.; Neese, F.; Pantazis, D.A. Metal oxidation states in biological water splitting. *Chem. Sci.* **2015**, *6*, 1676–1695. [CrossRef]
385. Mermigki, M.A.; Drosou, M.; Pantazis, D.A. On the nature of high-spin forms in the S(2) state of the oxygen-evolving complex. *Chem. Sci.* **2025**, *16*, 4023–4047. [CrossRef]
386. Li, H.; Nakajima, Y.; Nango, E.; Owada, S.; Yamada, D.; Hashimoto, K.; Luo, F.; Tanaka, R.; Akita, F.; Kato, K.; et al. Oxygen-evolving photosystem II structures during S1–S2–S3 transitions. *Nature* **2024**, *626*, 670–677. [CrossRef]
387. Guo, Y.; Kloo, L.; Sun, L. Quantum Chemical Understanding of the O_2 Release Process from Nature's Water Splitting Cofactor. *Angew. Chem. Int. Ed.* **2025**, *64*, e202421383. [CrossRef]
388. Armstrong, F.A. Why did Nature choose manganese to make oxygen? *Phil. Trans. Roy. Soc. B. Biol. Sci.* **2008**, *363*, 1263–1270. [CrossRef] [PubMed]
389. Ruskoski, T.B.; Boal, A.K. The periodic table of ribonucleotide reductases. *J. Biol. Chem.* **2021**, *297*, 101137. [CrossRef]
390. Sjöberg, B.M. Ribonucleotide Reductase. In *Encyclopedia of Metalloproteins*; Kretsinger, R.H., Uversky, V.N., Permyakov, E.A., Eds.; Springer: New York, NY, USA, 2013.
391. Hofer, A.; Crona, M.; Logan, D.T.; Sjöberg, B.-M. DNA building blocks: Keeping control of manufacture. *Crit. Rev. Biochem. Molec. Biol.* **2012**, *47*, 50–63. [CrossRef] [PubMed]
392. Torrents, E. Ribonucleotide reductases: Essential enzymes for bacterial life. *Front. Cell Infect. Micro* **2014**, *4*, 52. [CrossRef]
393. Grāve, K.; Griese, J.J.; Berggren, G.; Bennett, M.D.; Högbom, M. The Bacillus anthracis class Ib ribonucleotide reductase subunit NrdF intrinsically selects manganese over iron. *J. Biol. Inorg. Chem.* **2020**, *25*, 571–582. [CrossRef]
394. Marques, H.M. The inorganic chemistry of the cobalt corrinoids—An update. *J. Inorg. Biochem.* **2023**, *242*, 112154.
395. Cotruvo, J.A., Jr.; Stich, T.A.; Britt, R.D.; Stubbe, J. Mechanism of Assembly of the Dimanganese-Tyrosyl Radical Cofactor of Class Ib Ribonucleotide Reductase: Enzymatic Generation of Superoxide Is Required for Tyrosine Oxidation via a Mn(III)Mn(IV) Intermediate. *J. Am. Chem. Soc.* **2013**, *135*, 4027–4039. [CrossRef]
396. Yadav, L.R.; Sharma, V.; Shanmugam, M.; Mande, S.C. Structural insights into the initiation of free radical formation in the Class Ib ribonucleotide reductases in Mycobacteria. *Curr. Res. Struct. Biol.* **2024**, *8*, 100157. [CrossRef]
397. John, J.; Aurelius, O.; Srinivas, V.; Saura, P.; Kim, I.-S.; Bhowmick, A.; Simon, P.S.; Dasgupta, M.; Pham, C.; Gul, S.; et al. Redox-controlled reorganization and flavin strain within the ribonucleotide reductase R2b–NrdI complex monitored by serial femtosecond crystallography. *eLife* **2022**, *11*, e79226. [CrossRef]
398. Doyle, L.M.; Bienenmann, R.L.M.; Gericke, R.; Xu, S.; Farquhar, E.R.; Que, L.; McDonald, A.R. Preparation and characterization of MnIIMnIII complexes with relevance to class Ib ribonucleotide reductases. *J. Inorg. Biochem.* **2024**, *257*, 112583. [CrossRef]
399. Doyle, L.; Magherusan, A.; Xu, S.; Murphy, K.; Farquhar, E.R.; Molton, F.; Duboc, C.; Que, L., Jr.; McDonald, A.R. Class Ib Ribonucleotide Reductases: Activation of a Peroxido-$Mn^{II}Mn^{III}$ to Generate a Reactive Oxo-$Mn^{III}Mn^{IV}$ Oxidant. *Inorg. Chem.* **2024**, *63*, 2194–2203. [CrossRef] [PubMed]
400. Högbom, M.; Stenmark, P.; Voevodskaya, N.; McClarty, G.; Gräslund, A.; Nordlund, P. The Radical Site in Chlamydial Ribonucleotide Reductase Defines a New R_2 Subclass. *Science* **2004**, *305*, 245–248. [CrossRef] [PubMed]
401. Jiang, W.; Yun, D.; Saleh, L.; Barr, E.W.; Xing, G.; Hoffart, L.M.; Maslak, M.-A.; Krebs, C.; Bollinger, J.M. A Manganese(IV)/Iron(III) Cofactor in *Chlamydia trachomatis* Ribonucleotide Reductase. *Science* **2007**, *316*, 1188–1191. [CrossRef] [PubMed]
402. Kisgeropoulos, E.C.; Gan, Y.J.; Greer, S.M.; Hazel, J.M.; Shafaat, H.S. Pulsed Multifrequency Electron Paramagnetic Resonance Spectroscopy Reveals Key Branch Points for One- vs Two-Electron Reactivity in Mn/Fe Proteins. *J. Am. Chem. Soc.* **2022**, *144*, 11991–12006. [CrossRef]
403. Rozman Grinberg, I.; Berglund, S.; Hasan, M.; Lundin, D.; Ho, F.M.; Magnuson, A.; Logan, D.T.; Sjöberg, B.-M.; Berggren, G. Class Id ribonucleotide reductase utilizes a Mn_2(IV,III) cofactor and undergoes large conformational changes on metal loading. *J. Biol. Inorg. Chem.* **2019**, *24*, 863–877. [CrossRef]
404. Sánchez-Ruiz, M.I.; Santillana, E.; Linde, D.; Romero, A.; Martínez, A.T.; Ruiz-Dueñas, F.J. Structure-function characterization of two enzymes from novel subfamilies of manganese peroxidases secreted by the lignocellulose-degrading Agaricales fungi *Agrocybe pediades* and *Cyathus striatus*. *Biotech. Biofuels Bioprod.* **2024**, *17*, 74. [CrossRef]
405. Bilal, M.; Zdarta, J.; Jesionowski, T.; Iqbal, H.M.N. Manganese peroxidases as robust biocatalytic tool—An overview of sources, immobilization, and biotechnological applications. *Int. J. Biol. Macromolec.* **2023**, *234*, 123531. [CrossRef]
406. Jofré-Fernández, I.; Matus-Baeza, F.; Merino-Guzmán, C. White-rot fungi scavenge reactive oxygen species, which drives pH-dependent exo-enzymatic mechanisms and promotes CO_2 efflux. *Front. Microbiol.* **2023**, *14*, 1148750. [CrossRef]

407. Sellami, K.; Couvert, A.; Nasrallah, N.; Maachi, R.; Abouseoud, M.; Amrane, A. Peroxidase enzymes as green catalysts for bioremediation and biotechnological applications: A review. *Sci. Total Environ.* **2022**, *806*, 150500. [CrossRef]
408. Kumar, V.; Pallavi, P.; Sen, S.K.; Raut, S. Harnessing the potential of white rot fungi and ligninolytic enzymes for efficient textile dye degradation: A comprehensive review. *Water Environ. Res.* **2024**, *96*, e10959. [CrossRef]
409. Liu, X.; Ding, S.; Gao, F.; Wang, Y.; Taherzadeh, M.J.; Wang, Y.; Qin, X.; Wang, X.; Luo, H.; Yao, B.; et al. Exploring the cellulolytic and hemicellulolytic activities of manganese peroxidase for lignocellulose deconstruction. *Biotech. Biofuels Bioprod.* **2023**, *16*, 139. [CrossRef] [PubMed]
410. Guo, C.; Fan, L.; Yang, Q.; Ning, M.; Zhang, B.; Ren, X. Characterization and mechanism of simultaneous degradation of aflatoxin B1 and zearalenone by an edible fungus of Agrocybe cylindracea GC-Ac2. *Front. Microbiol.* **2024**, *15*, 1292824. [CrossRef] [PubMed]
411. Sundaramoorthy, M.; Gold, M.H.; Poulos, T.L. Ultrahigh (0.93Å) resolution structure of manganese peroxidase from Phanerochaete chrysosporium: Implications for the catalytic mechanism. *J. Inorg. Biochem.* **2010**, *104*, 683–690. [CrossRef]
412. Ding, Y.; Cui, K.; Guo, Z.; Cui, M.; Chen, Y. Manganese peroxidase mediated oxidation of sulfamethoxazole: Integrating the computational analysis to reveal the reaction kinetics, mechanistic insights, and oxidation pathway. *J. Hazard. Mater.* **2021**, *415*, 125719. [CrossRef]
413. Hoang, H.G.; Tran, H.T.; Nguyen, M.K.; Nguyen, N.S.H.; Thuy, B.T.P. Investigating the polyethylene degradation mechanism using docking and molecular dynamics simulations. *Environ. Sci. Pollut. Res. Int.* **2024**, *31*, 64857–64869. [CrossRef]
414. Wu, F.; Guo, Z.; Cui, K.; Dong, D.; Yang, X.; Li, J.; Wu, Z.; Li, L.; Dai, Y.; Pan, T. Insights into characteristics of white rot fungus during environmental plastics adhesion and degradation mechanism of plastics. *J. Hazard Mater.* **2023**, *448*, 130878. [CrossRef]
415. Wang, F.; Zhang, D.; Zhang, L.; Wu, X.; Deng, S.; Yuan, X. Biodegradation of anionic polyacrylamide by manganese peroxidase: Docking, virtual mutation based on affinity, QM/MM calculation and molecular dynamics simulation. *Bioprocess Biosyst. Eng.* **2022**, *45*, 1349–1358. [CrossRef] [PubMed]
416. Wang, J.; Yang, J.; Huang, W.; Huang, W.; Jia, R. A mutant R70V/E166A of short manganese peroxidase showing Mn^{2+}-independent dye decolorization. *Appl. Microbiol. Biotechnol.* **2023**, *107*, 2303–2319. [CrossRef]
417. Christie, W.W.; Harwood, J.L. Oxidation of polyunsaturated fatty acids to produce lipid mediators. *Essays Biochem.* **2020**, *64*, 401–421.
418. Oliw, E.H. Diversity of the manganese lipoxygenase gene family—A mini-review. *Fungal Genet. Biol.* **2022**, *163*, 103746. [CrossRef]
419. Oliw, E.H. Iron and manganese lipoxygenases of plant pathogenic fungi and their role in biosynthesis of jasmonates. *Arch. Biochem. Biophys.* **2022**, *722*, 109169. [CrossRef] [PubMed]
420. Prigge, S.T.; Boyington, J.C.; Faig, M.; Doctor, K.S.; Gaffney, B.J.; Amzel, L.M. Structure and mechanism of lipoxygenases. *Biochimie* **1997**, *79*, 629–636. [CrossRef]
421. Opalade, A.A.; Grotemeyer, E.N.; Jackson, T.A. Mimicking Elementary Reactions of Manganese Lipoxygenase Using Mn-hydroxo and Mn-alkylperoxo Complexes. *Molecules* **2021**, *26*, 7151. [CrossRef] [PubMed]
422. Wennman, A.; Oliw, E.H.; Karkehabadi, S.; Chen, Y. Crystal Structure of Manganese Lipoxygenase of the Rice Blast Fungus *Magnaporthe oryzae*. *J. Biol. Chem.* **2016**, *291*, 8130–8139. [CrossRef] [PubMed]
423. Rini, J.M.; Moremen, K.W.; Davis, B.G.; Esko, J.D. Glycosyltransferases and Glycan-Processing Enzymes. In *Essentials of Glycobiology*, 4th ed.; Varki, A., Cummings, R.D., Esko, J.D., Stanley, P., Hart, G.W., Aebi, M., Mohnen, D., Kinoshita, T., Packer, N.H., Prestegard, J.H., et al., Eds.; Cold Spring Harbor Laboratory Press: Cold Spring Habor, NY, USA, 2022.
424. Breton, C.; Šnajdrová, L.; Jeanneau, C.; Koča, J.; Imberty, A. Structures and mechanisms of glycosyltransferases. *Glycobiology* **2005**, *16*, 29R–37R. [CrossRef]
425. Ramakrishnan, B.; Boeggeman, E.; Ramasamy, V.; Qasba, P.K. Structure and catalytic cycle of β-1,4-galactosyltransferase. *Curr. Opin. Struct. Biol.* **2004**, *14*, 593–600. [CrossRef]
426. Ramakrishnan, B.; Ramasamy, V.; Qasba, P.K. Structural snapshots of beta-1,4-galactosyltransferase-I along the kinetic pathway. *J. Mol. Biol.* **2006**, *357*, 1619–1633. [CrossRef]
427. Kóňa, J. How inverting β-1,4-galactosyltransferase-1 can quench a high charge of the by-product UDP3− in catalysis: A QM/MM study of enzymatic reaction with native and UDP-5′ thio galactose substrates. *Org. Biomol. Chem.* **2020**, *18*, 7585–7596. [CrossRef]
428. Christianson, D.W. Arginase: Structure, Mechanism, and Physiological Role in Male and Female Sexual Arousal. *Acc. Chem. Res.* **2005**, *38*, 191–201. [CrossRef]
429. Ash, D.E.; Cox, J.D.; Christianson, D.W. Arginase: A binuclear manganese metalloenzyme. *Met. Ions Biol. Syst.* **2000**, *37*, 407–428.
430. Li, Z.; Wang, L.; Ren, Y.; Huang, Y.; Liu, W.; Lv, Z.; Qian, L.; Yu, Y.; Xiong, Y. Arginase: Shedding light on the mechanisms and opportunities in cardiovascular diseases. *Cell Death Discov.* **2022**, *8*, 413. [CrossRef]
431. K, D.; Kuramitsu, S.; Yokoyama, S.; Thirumananseri, K.; Ponnuraj, K. Crystal structure analysis and molecular dynamics simulations of arginase from *Thermus thermophilus*. *J. Biomolec. Struct. Dynam.* **2023**, *41*, 6811–6821. [CrossRef] [PubMed]

432. Cox, J.D.; Cama, E.; Colleluori, D.M.; Pethe, S.; Boucher, J.-L.; Mansuy, D.; Ash, D.E.; Christianson, D.W. Mechanistic and Metabolic Inferences from the Binding of Substrate Analogues and Products to Arginase. *Biochemistry* **2001**, *40*, 2689–2701. [CrossRef] [PubMed]
433. Kanyo, Z.F.; Scolnick, L.R.; Ash, D.E.; Christianson, D.W. Structure of a unique binuclear manganese cluster in arginase. *Nature* **1996**, *383*, 554–557. [CrossRef] [PubMed]
434. Lindley, P.F. Iron in biology: A structural viewpoint. *Rep. Prog. Phys.* **1996**, *59*, 867–933. [CrossRef]
435. Kadish, K.M.; Smith, K.M.; Guilard, R. (Eds.) *The Porphyrin Handbook*; Academic Press: San Diego, CA, USA, 2003.
436. Walker, F.A.; Simonis, U. Iron Porphyrin Chemistry. In *Encyclopedia of Inorganic Chemistry*; King, R.B., Crabtree, R.H., Lukehart, C.M., Atwood, D.A., Scott, R.A., Eds.; John Wiley & Sons: Hoboken, NJ, USA, 2005.
437. Liu, J.; Chakraborty, S.; Hosseinzadeh, P.; Yu, Y.; Tian, S.; Petrik, I.; Bhagi, A.; Lu, Y. Metalloproteins Containing Cytochrome, Iron–Sulfur, or Copper Redox Centers. *Chem. Rev.* **2014**, *114*, 4366–4469.
438. Crichton, R. *Iron Metabolism—From Molecular Mechanisms to Clinical Consequences, 4th, ed.*; John Wiley & Sons: Chichester, UK, 2016.
439. Turilli-Ghisolfi, E.S.; Lualdi, M.; Fasano, M. Ligand-Based Regulation of Dynamics and Reactivity of Hemoproteins. *Biomolecules* **2023**, *13*, 683. [CrossRef]
440. Antonini, E.; Brunori, M. *Hemoglobin and Myoglobin in Their Reactions with Ligands*; North-Holland: Amsterdam, The Netherlands, 1971.
441. Perutz, M.F.; Fermi, G.; Luisi, B.; Shaanan, B.; Liddington, R.C. Stereochemistry of cooperative mechanisms in hemoglobin. *Acc. Chem. Res.* **1987**, *20*, 309–321. [CrossRef]
442. Collman, J.P.; Fu, L. Synthetic Models for Hemoglobin and Myoglobin. *Acc. Chem. Res.* **1999**, *32*, 455–463. [CrossRef]
443. Olson, J.S. Kinetic mechanisms for O_2 binding to myoglobins and hemoglobins. *Mol. Asp. Med.* **2022**, *84*, 101024. [CrossRef]
444. Sil, R.; Chakraborti, A.S. Major heme proteins hemoglobin and myoglobin with respect to their roles in oxidative stress—A brief review. *Front. Chem.* **2025**, *13*, 1543455. [CrossRef] [PubMed]
445. Chong, G.W.; Karbelkar, A.A.; El-Naggar, M.Y. Nature's conductors: What can microbial multi-heme cytochromes teach us about electron transport and biological energy conversion? *Curr. Opin. Chem. Biol.* **2018**, *47*, 7–17. [CrossRef]
446. Santucci, R.; Sinibaldi, F.; Cozza, P.; Polticelli, F.; Fiorucci, L. Cytochrome c: An extreme multifunctional protein with a key role in cell fate. *Int. J. Biol. Macromol.* **2019**, *136*, 1237–1246. [CrossRef]
447. Davidson, V.L. What Controls the Rates of Interprotein Electron-Transfer Reactions? *Acc. Chem. Res.* **2000**, *33*, 87–93. [CrossRef] [PubMed]
448. Crowley, P.B.; Ubbink, M. Close Encounters of the Transient Kind: Protein Interactions in the Photosynthetic Redox Chain Investigated by NMR Spectroscopy. *Acc. Chem. Res.* **2003**, *36*, 723–730. [CrossRef]
449. Dell'Acqua, S.; Pauleta, S.R.; Monzani, E.; Pereira, A.S.; Casella, L.; Moura, J.J.G.; Moura, I. Electron Transfer Complex between Nitrous Oxide Reductase and Cytochrome c_{552} from *Pseudomonas nautica:* Kinetic, Nuclear Magnetic Resonance, and Docking Studies. *Biochemistry* **2008**, *47*, 10852–10862. [CrossRef] [PubMed]
450. Hille, R. The Mononuclear Molybdenum Enzymes. *Chem. Rev.* **1996**, *96*, 2757–2816. [CrossRef] [PubMed]
451. Chen, K.; Bonagura, C.A.; Tilley, G.J.; McEvoy, J.P.; Jung, Y.-S.; Armstrong, F.A.; Stout, C.D.; Burgess, B.K. Crystal structures of ferredoxin variants exhibiting large changes in [Fe–S] reduction potential. *Nat. Struct. Biol.* **2002**, *9*, 188–192. [CrossRef]
452. Azzi, A.; Müller, M. Cytochrome c oxidases: Polypeptide composition, role of subunits, and location of active metal centers. *Arch. Biochem. Biophys.* **1990**, *280*, 242–251. [CrossRef]
453. Dawson, J.H. Probing structure-function relations in heme-containing oxygenases and peroxidases. *Science* **1988**, *240*, 433–439. [CrossRef]
454. Esposti, M.D. On the evolution of cytochrome oxidases consuming oxygen. *Biochim. Biophys. Acta Bioenerg.* **2020**, *1861*, 148304. [CrossRef] [PubMed]
455. Song, Y.S.; Annalora, A.J.; Marcus, C.B.; Jefcoate, C.R.; Sorenson, C.M.; Sheibani, N. Cytochrome P_{450} 1B1: A Key Regulator of Ocular Iron Homeostasis and Oxidative Stress. *Cells* **2022**, *11*, 2930. [CrossRef] [PubMed]
456. Smulevich, G. The functional role of the key residues in the active site of peroxidases. *Biochem. Soc. Trans.* **1995**, *23*, 240–244. [CrossRef]
457. Isaac, I.S.; Dawson, J.H. Haem iron-containing peroxidases. *Essays Biochem.* **1999**, *34*, 51–69.
458. Battistuzzi, G.; Bellei, M.; Bortolotti, C.A.; Sola, M. Redox properties of heme peroxidases. *Arch. Biochem. Biophys.* **2010**, *500*, 21–36. [CrossRef]
459. Singh, P.K.; Iqbal, N.; Sirohi, H.V.; Bairagya, H.R.; Kaur, P.; Sharma, S.; Singh, T.P. Structural basis of activation of mammalian heme peroxidases. *Prog. Biophys. Mol. Biol.* **2018**, *133*, 49–55. [CrossRef] [PubMed]
460. Deisseroth, A.; Dounce, A.L. Catalase: Physical and chemical properties, mechanism of catalysis, and physiological role. *Physiol. Rev.* **1970**, *50*, 319–375. [CrossRef]
461. Bravo, J.; Fita, I.; Gouet, P.; Jouve, H.M.; Melik-Adamyan, W.-L.; Murshudov, G.N. Structure of catalases. *Cold Spring Harbor Mongr. Ser.* **1997**, *34*, 407–445.

462. Goyal, M.M.; Basak, A. Human catalase: Looking for complete identity. *Protein Cell* **2010**, *1*, 888–897. [CrossRef]
463. James, M.O.; Boyle, S.M. Cytochromes P450 in crustacea. *Comp. Biochem. Physiol. C Pharmacol. Toxicol. Endocrinol.* **1998**, *121*, 157–172. [CrossRef]
464. Vanden Bossche, H.; Koymans, L. Cytochromes P450 in fungi. *Mycoses* **1998**, *41* (Suppl. 1), 32–38. [PubMed]
465. Pikuleva, I.A.; Waterman, M.R. Cytochromes p450: Roles in diseases. *J. Biol. Chem.* **2013**, *288*, 17091–17098. [CrossRef]
466. Distéfano, A.M.; Setzes, N.; Cascallares, M.; Fiol, D.F.; Zabaleta, E.; Pagnussat, G.C. Roles of cytochromes P450 in plant reproductive development. *Int. J. Dev. Biol.* **2021**, *65*, 187–194. [CrossRef]
467. Mauzerall, D. Porphyrins, Chlorophyll, and Photosynthesis. In *Photosynthesis I: Photosynthetic Electron Transport and Photophosphorylation*; Trebst, A., Avron, M., Eds.; Springer: Berlin/Heidelberg, Germany, 1977; pp. 117–124.
468. Boxer, S.G. Model reactions in photosynthesis. *Biochim. Biophys. Acta* **1983**, *726*, 265–292. [CrossRef]
469. Chen, M. Chlorophyll modifications and their spectral extension in oxygenic photosynthesis. *Annu. Rev. Biochem.* **2014**, *83*, 317–340. [CrossRef]
470. Yamazaki, T.; Oyanagi, H.; Fujiwara, T.; Fukumori, Y. Nitrite reductase from the magnetotactic bacterium Magnetospirillum magnetotacticum; A novel cytochrome cd1 with Fe(II):nitrite oxidoreductase activity. *Eur. J. Biochem.* **1995**, *233*, 665–671. [CrossRef] [PubMed]
471. Zheng, Y.; Deng, W.; Liu, D.; Li, Y.; Peng, K.; Lorimer, G.H.; Wang, J. Redox and spectroscopic properties of mammalian nitrite reductase-like hemoproteins. *J. Inorg. Biochem.* **2022**, *237*, 111982. [CrossRef]
472. Murphy, M.J.; Siegel, L.M.; Tove, S.R.; Kamin, H. Siroheme: A New Prosthetic Group Participating in Six-Electron Reduction Reactions Catalyzed by Both Sulfite and Nitrite Reductases. *Proc. Natl. Acad. Sci. USA* **1974**, *71*, 612–616. [CrossRef]
473. Crane, B.R.; Siegel, L.M.; Getzoff, E.D. Structures of the Siroheme- and Fe_4S_4-Containing Active Center of Sulfite Reductase in Different States of Oxidation: Heme Activation via Reduction-Gated Exogenous Ligand Exchange. *Biochemistry* **1997**, *36*, 12101–12119. [CrossRef]
474. Kappler, U.; Enemark, J.H. Sulfite-oxidizing enzymes. *J. Biol. Inorg. Chem.* **2015**, *20*, 253–264. [CrossRef]
475. Ems, T.; St Lucia, K.; Huecker, M.R. Biochemistry, Iron Absorption. In *StatPearls*; StatPearls Publishing: Treasure Island, FL, USA, 2025.
476. Wang, H.; Shi, H.; Rajan, M.; Canarie, E.R.; Hong, S.; Simoneschi, D.; Pagano, M.; Bush, M.F.; Stoll, S.; Leibold, E.A.; et al. FBXL5 Regulates IRP2 Stability in Iron Homeostasis via an Oxygen-Responsive [2Fe2S] Cluster. *Molec. Cell* **2020**, *78*, 31–41.e35. [CrossRef] [PubMed]
477. Del Vecchio, L.; Girelli, D.; Vinchi, F.; Cozzolino, M.; Elliott, S.; Mark, P.B.; Valenti, L.; Qian, C.; Guo, Q.; Qian, Z.M.; et al. Iron biology. *Nephrol. Dial. Transplant.* **2024**, *39*, 1404–1415. [CrossRef]
478. Lincoln, S.F. Mechanistic Studies of Metal Aqua Ions: A Semi-Historical Perspective. *Helv. Chim. Acta* **2005**, *88*, 523–545. [CrossRef]
479. Senge, M. Highly Substituted Porphyrins. In *The Porphyrin Handbook*; Kadish, K.M., Smith, K.M., Guilard, R., Eds.; Academic Press: New York, NY, USA, 2000; Volume 1, pp. 239–347.
480. Frey, P.A.; Reed, G.H. The Ubiquity of Iron. *ACS Chem. Biol.* **2012**, *7*, 1477–1481. [CrossRef] [PubMed]
481. Wedepohl, K.H. The composition of the continental crust. *Geochim. Cosmochim. Acta* **1995**, *59*, 1217–1232. [CrossRef]
482. Sánchez-Baracaldo, P.; Cardona, T. On the origin of oxygenic photosynthesis and Cyanobacteria. *New Phytol.* **2020**, *225*, 1440–1446. [CrossRef] [PubMed]
483. Warke, M.R.; Di Rocco, T.; Zerkle, A.L.; Lepland, A.; Prave, A.R.; Martin, A.P.; Ueno, Y.; Condon, D.J.; Claire, M.W. The Great Oxidation Event preceded a Paleoproterozoic "snowball Earth". *Proc. Natl. Acad. Sci. USA* **2020**, *117*, 13314–13320. [CrossRef]
484. Kraus, A.; Spät, P.; Timm, S.; Wilson, A.; Schumann, R.; Hagemann, M.; Maček, B.; Hess, W.R. Protein NirP1 regulates nitrite reductase and nitrite excretion in cyanobacteria. *Nat. Commun.* **2024**, *15*, 1911. [CrossRef]
485. Schirrmeister, B.E.; Gugger, M.; Donoghue, P.C.J. Cyanobacteria and the Great Oxidation Event: Evidence from genes and fossils. *Palaeontology* **2015**, *58*, 769–785. [CrossRef]
486. Sweetman, A.K.; Smith, A.J.; de Jonge, D.S.W.; Hahn, T.; Schroedl, P.; Silverstein, M.; Andrade, C.; Edwards, R.L.; Lough, A.J.M.; Woulds, C.; et al. Evidence of dark oxygen production at the abyssal seafloor. *Nat. Geosci.* **2024**, *17*, 737–739. [CrossRef]
487. Schwertmann, U. Solubility and dissolution of iron oxides. *Plant Soil* **1991**, *130*, 1–25. [CrossRef]
488. Hannauer, M.; Barda, Y.; Mislin, G.L.A.; Shanzer, A.; Schalk, I.J. The Ferrichrome Uptake Pathway in *Pseudomonas aeruginosa* Involves an Iron Release Mechanism with Acylation of the Siderophore and Recycling of the Modified Desferrichrome. *J. Bacteriol.* **2010**, *192*, 1212–1220. [CrossRef]
489. Llamas, M.A.; Sparrius, M.; Kloet, R.; Jiménez, C.R.; Vandenbroucke-Grauls, C.; Bitter, W. The Heterologous Siderophores Ferrioxamine B and Ferrichrome Activate Signaling Pathways in *Pseudomonas aeruginosa*. *J. Bacteriol.* **2006**, *188*, 1882–1891. [CrossRef] [PubMed]
490. Hider, R.C.; Kong, X. Chemistry and biology of siderophores. *Nat. Prod. Rep.* **2010**, *27*, 637–657. [CrossRef]
491. Saito, H. Metabolism of Iron Stores. *Nagoya J. Med. Sci.* **2014**, *76*, 235–254. [PubMed]
492. Wallace, D.F. The Regulation of Iron Absorption and Homeostasis. *Clin. Biochem. Rev.* **2016**, *37*, 51–62.

493. Vogt, A.-C.S.; Arsiwala, T.; Mohsen, M.; Vogel, M.; Manolova, V.; Bachmann, M.F. On Iron Metabolism and Its Regulation. *Int. J. Mol. Sci.* **2021**, *22*, 4591. [CrossRef]
494. Ben Zichri-David, S.; Shkuri, L.; Ast, T. Pulling back the mitochondria's iron curtain. *NPJ Metab. Health Dis.* **2025**, *3*, 6. [CrossRef]
495. Berndt, C.; Alborzinia, H.; Amen, V.S.; Ayton, S.; Barayeu, U.; Bartelt, A.; Bayir, H.; Bebber, C.M.; Birsoy, K.; Böttcher, J.P.; et al. Ferroptosis in health and disease. *Redox Biol.* **2024**, *75*, 103211. [CrossRef]
496. Glover, H.L.; Schreiner, A.; Dewson, G.; Tait, S.W.G. Mitochondria and cell death. *Nat. Cell Biol.* **2024**, *26*, 1434–1446. [CrossRef]
497. Kraiter, D.C.; Zak, O.; Aisen, P.; Crumbliss, A.L. A Determination of the Reduction Potentials for Diferric and C- and N-Lobe Monoferric Transferrins at Endosomal pH (5.8). *Inorg. Chem.* **1998**, *37*, 964–968. [CrossRef]
498. Dhungana, S.; Taboy, C.H.; Zak, O.; Larvie, M.; Crumbliss, A.L.; Aisen, P. Redox Properties of Human Transferrin Bound to Its Receptor. *Biochemistry* **2004**, *43*, 205–209. [CrossRef] [PubMed]
499. Terpstra, T.; McNally, J.; Han, T.-H.-L.; Ha-Duong, N.-T.; El-Hage-Chahine, J.-M.; Bou-Abdallah, F. Direct thermodynamic and kinetic measurements of Fe2+ and Zn2+ binding to human serum transferrin. *J. Inorg. Biochem.* **2014**, *136*, 24–32. [CrossRef] [PubMed]
500. Reedy, C.J.; Gibney, B.R. Heme protein assemblies. *Chem. Rev.* **2004**, *104*, 617–649. [CrossRef] [PubMed]
501. Zhuang, J.; Reddi, A.R.; Wang, Z.; Khodaverdian, B.; Hegg, E.L.; Gibney, B.R. Evaluating the Roles of the Heme a Side Chains in Cytochrome c Oxidase Using Designed Heme Proteins. *Biochemistry* **2006**, *45*, 12530–12538. [CrossRef]
502. Perutz, M.F. Regulation of oxygen affinity of hemoglobin: Influence of structure of the globin on the heme iron. *Ann. Rev. Biochem.* **1979**, *48*, 327–386. [CrossRef]
503. Ahmed, M.H.; Ghatge, M.S.; Safo, M.K. Hemoglobin: Structure, Function and Allostery. In *Vertebrate and Invertebrate Respiratory Proteins, Lipoproteins and other Body Fluid Proteins*; Hoeger, U., Harris, J.R., Eds.; Springer International Publishing: Cham, Switzerland, 2020; pp. 345–382.
504. Poole, D.C.; Musch, T.I.; Colburn, T.D. Oxygen flux from capillary to mitochondria: Integration of contemporary discoveries. *Eur. J. Appl. Physiol.* **2022**, *122*, 7–28. [CrossRef]
505. D'Alessandro, A.; Anastasiadi, A.T.; Tzounakas, V.L.; Nemkov, T.; Reisz, J.A.; Kriebardis, A.G.; Zimring, J.C.; Spitalnik, S.L.; Busch, M.P. Red Blood Cell Metabolism In Vivo and In Vitro. *Metabolites* **2023**, *13*, 793. [CrossRef]
506. Kosmachevskaya, O.V.; Topunov, A.F. Alternate and Additional Functions of Erythrocyte Hemoglobin. *Biochemistry* **2018**, *83*, 1575–1593. [CrossRef]
507. Feher, J. Oxygen and Carbon Dioxide Transport. In *Quantitative Human Physiology*, 2nd ed.; Feher, J., Ed.; Academic Press: Boston, MA, USA, 2017; pp. 656–664.
508. Pauling, L.; Coryell, C.D. The Magnetic Properties and Structure of Hemoglobin, Oxyhemoglobin and Carbonmonoxyhemoglobin. *Proc. Natl. Acad. Sci. USA* **1936**, *22*, 210–216. [CrossRef]
509. Harrington, D.J.; Adachi, K.; Royer, W.E. The high resolution crystal structure of deoxyhemoglobin S11Edited by K. Nagai. *J. Molec. Biol.* **1997**, *272*, 398–407. [CrossRef] [PubMed]
510. Etti, S.; Shanmugam, G.; Karthe, P.; Gunasekaran, K. PDB 3A0G: Crystal Structure Analysis of Guinea Pig Oxyhemoglobin at 2.5 Angstroms Resolution. Available online: https://www.rcsb.org/structure/3A0G (accessed on 18 May 2024).
511. Munro, O.Q.; Bradley, J.C.; Hancock, R.D.; Marques, H.M.; Marsicano, F.; Wade, P.W. Molecular Mechanics Study of the Ruffling of Metalloporphyrins. *J. Am. Chem. Soc.* **1992**, *114*, 7218–7230. [CrossRef]
512. Olson, J.S. Lessons Learned from 50 Years of Hemoglobin Research: Unstirred and Cell-Free Layers, Electrostatics, Baseball Gloves, and Molten Globules. *Antioxid. Redox Signal.* **2020**, *32*, 228–246. [CrossRef] [PubMed]
513. Weiss, J.J. Nature of the Iron–Oxygen Bond in Oxyhæmoglobin. *Nature* **1964**, *202*, 83–84. [CrossRef]
514. Pauling, L. Nature of the Iron–Oxygen Bond in Oxyhæmoglobin. *Nature* **1964**, *203*, 182–183. [CrossRef]
515. Weiss, J.J. Nature of the Iron–Oxygen Bond in Oxyhæmoglobin. *Nature* **1964**, *203*, 183. [CrossRef]
516. McClure, D.S. Electronic Structure of Transition-Metal Complex Ions. *Rad. Res. Suppl.* **1960**, *2*, 218–242. [CrossRef]
517. Goddard, W.A.; Olafson, B.D. Ozone Model for Bonding of an O_2 to Heme in Oxyhemoglobin. *Proc. Natl. Acad. Sci. USA* **1975**, *72*, 2335–2339. [CrossRef]
518. Barlow, C.H.; Maxwell, J.C.; Wallace, W.J.; Caughey, W.S. Elucidation of the mode of binding of oxygen to iron in oxyhemoglobin by infrared spectroscopy. *Biochem. Biophys. Res. Commun.* **1973**, *55*, 91–95. [CrossRef]
519. Maxwell, J.C.; Caughey, W.S. Infrared evidence for similar metal-dioxygen bonding in iron and cobalt oxyhemoglobins. *Biochem. Biophys. Res. Commun.* **1974**, *60*, 1309–1314. [CrossRef]
520. Wittenberg, J.B.; Wittenberg, B.A.; Peisach, J.; Blumberg, W.E. On the State of the Iron and the Nature of the Ligand in Oxyhemoglobin. *Proc. Natl. Acad. Sci. USA* **1970**, *67*, 1846–1853. [CrossRef] [PubMed]
521. Gupta, R.K.; Mildvan, A.S.; Yonetani, T.; Srivastava, T.S. EPR study of ^{17}O nuclear hyperfine interaction in cobalt-oxyhemoglobin: Conformation of bound oxygen. *Biochem. Biophys. Res. Commun.* **1975**, *67*, 1005–1012. [CrossRef]
522. Lang, G.; Marshali, W. Mössbauer effect in some haemoglobin compounds. *Proc. Phys. Soc.* **1966**, *87*, 3–34. [CrossRef]

523. Van Doorslaer, S.; Schweiger, A.; Kräutler, B. A Continuous Wave and Pulse EPR and ENDOR Investigation of Oxygenated Co(II) Corrin Complexes. *J. Phys. Chem. B* **2001**, *105*, 7554–7563. [CrossRef]
524. Schuth, N.; Mebs, S.; Huwald, D.; Wrzolek, P.; Schwalbe, M.; Hemschemeier, A.; Haumann, M. Effective intermediate-spin iron in O_2-transporting heme proteins. *Proc. Natl. Acad. Sci. USA* **2017**, *114*, 8556–8561. [CrossRef]
525. Sugawara, Y.; Shikama, K. Autoxidation of Native Oxymyoglobin. *Eur. J. Biochem.* **1980**, *110*, 241–246. [CrossRef]
526. Eaton, W.A.; Henry, E.R.; Hofrichter, J.; Mozzarelli, A. Is cooperative oxygen binding by hemoglobin really understood? *Nat. Struct. Biol.* **1999**, *6*, 351–358. [CrossRef] [PubMed]
527. Fermi, G.; Perutz, M.F.; Shaanan, B.; Fourme, R. The crystal structure of human deoxyhaemoglobin at 1.74 Å resolution. *J. Mol. Biol.* **1984**, *175*, 159–174. [CrossRef]
528. Yi, J.; Thomas, L.M.; Musayev, F.N.; Safo, M.K.; Richter-Addo, G.B. Crystallographic Trapping of Heme Loss Intermediates during the Nitrite-Induced Degradation of Human Hemoglobin. *Biochemistry* **2011**, *50*, 8323–8332. [CrossRef]
529. Perutz, M.F. Stereochemistry of Cooperative Effects in Haemoglobin: Haem–Haem Interaction and the Problem of Allostery. *Nature* **1970**, *228*, 726–734. [CrossRef]
530. Perutz, M.F.; Wilkinson, A.J.; Paoli, M.; Dodson, G.G. The stereochemical mechanism of the cooperative effects in hemoglobin revisited. *Annu. Rev. Biophys. Biomol. Struct.* **1998**, *27*, 1–34. [CrossRef] [PubMed]
531. Szabo, A.; Karplus, M. A mathematical model for structure-function relations in hemoglobin. *J. Molec. Biol.* **1972**, *72*, 163–197. [CrossRef] [PubMed]
532. Rivetti, C.; Mozzarelli, A.; Rossi, G.L.; Henry, E.R.; Eaton, W.A. Oxygen binding by single crystals of hemoglobin. *Biochemistry* **1993**, *32*, 2888–2906. [CrossRef]
533. Shibayama, N.; Saigo, S. Fixation of the Quaternary Structures of Human Adult Haemoglobin by Encapsulation in Transparent Porous Silica Gels. *J. Molec. Biol.* **1995**, *251*, 203–209. [CrossRef]
534. Yin, Z.; Li, D.; Guo, Q.; Wang, R.; Li, W. Effect of Hb conformational changes on oxygen transport physiology. *Zhong Nan Da Xue Xue Bao Yi Xue Ban* **2024**, *49*, 467–475.
535. D'Alessandro, A.; Xia, Y. Erythrocyte adaptive metabolic reprogramming under physiological and pathological hypoxia. *Curr. Opin. Hematol.* **2020**, *27*, 155–162. [CrossRef] [PubMed]
536. Liao, M.-S.; Scheiner, S. Electronic structure and bonding in unligated and ligated porphyrins. *J. Chem. Phys.* **2002**, *116*, 3635–3645. [CrossRef]
537. Jensen, K.P.; Ryde, U. How O_2 Binds to Heme: Reasons for rapid binding an spin inversion. *J. Biol. Chem.* **2004**, *279*, 14561–14569. [CrossRef]
538. Nakashima, H.; Hasegawa, J.-Y.; Nakatsuji, H. On the reversible O2 binding of the Fe–porphyrin complex. *J. Comput. Chem.* **2006**, *27*, 426–433. [CrossRef]
539. Vacek, J.; Zatloukalova, M.; Kabelac, M. Redox biology and electrochemistry. Towards evaluation of bioactive electron donors and acceptors. *Curr. Opin. Electrochem.* **2022**, *36*, 101142. [CrossRef]
540. Fukuzumi, S. (Ed.) *Electron Transfer: Mechanisms and Applications*; Wiley-VCH Verlag GmbH & Co.: Weinheim, Germany, 2020; pp. i–vii.
541. Vercellino, I.; Sazanov, L.A. The assembly, regulation and function of the mitochondrial respiratory chain. *Nat. Rev. Mol. Cell Biol.* **2022**, *23*, 141–161. [CrossRef]
542. Glass, J.B.; Elbon, C.E.; Williams, L.D. Something old, something new, something borrowed, something blue: The anaerobic microbial ancestry of aerobic respiration. *Trends Microbiol.* **2023**, *31*, 135–141. [CrossRef] [PubMed]
543. Sharma, K.L.; Lu, J.; Bai, Y. Mitochondrial Respiratory Complex I: Structure, Function and Implication in Human Diseases. *Curr. Med. Chem.* **2009**, *16*, 1266–1277. [CrossRef] [PubMed]
544. Mitchell, P. Coupling of Phosphorylation to Electron and Hydrogen Transfer by a Chemi-Osmotic type of Mechanism. *Nature* **1961**, *191*, 144–148. [CrossRef]
545. Berry, B.J.; Trewin, A.J.; Amitrano, A.M.; Kim, M.; Wojtovich, A.P. Use the Protonmotive Force: Mitochondrial Uncoupling and Reactive Oxygen Species. *J. Mol. Biol.* **2018**, *430*, 3873–3891. [CrossRef] [PubMed]
546. Mitchell, P. The protonmotive Q cycle: A general formulation. *FEBS Lett.* **1975**, *59*, 137–139. [CrossRef]
547. Baldwin, D.A.; Campbell, V.M.; Carleo, L.A.; Marques, H.M.; Pratt, J.M. Reduction of bis(histidine)hemin; model for the proton-coupled reduction of hemoproteins. *J. Am. Chem. Soc.* **1981**, *103*, 186–188. [CrossRef]
548. Baldwin, D.A.; Campbell, V.M.; Marques, H.M.; Pratt, J.M. Protein-free models for the proton-coupled reduction of haemoproteins. *FEBS Lett.* **1984**, *167*, 339–342. [CrossRef]
549. Desbois, A.; Lutz, M. Redox control of proton transfers in membrane b-type cytochromes: An absorption and resonance Raman study on bis(imidazole) and bis(imidazolate) model complexes of iron-protoporphyrin. *Eur. Biophys. J.* **1992**, *20*, 321–335. [CrossRef]
550. Warren, J.J.; Mayer, J.M. Proton-Coupled Electron Transfer Reactions at a Heme-Propionate in an Iron-Protoporphyrin-IX Model Compound. *J. Am. Chem. Soc.* **2011**, *133*, 8544–8551. [CrossRef]

551. Weinberg, D.R.; Gagliardi, C.J.; Hull, J.F.; Murphy, C.F.; Kent, C.A.; Westlake, B.C.; Paul, A.; Ess, D.H.; McCafferty, D.G.; Meyer, T.J. Proton-Coupled Electron Transfer. *Chem. Rev.* **2012**, *112*, 4016–4093. [CrossRef] [PubMed]
552. Tyburski, R.; Liu, T.; Glover, S.D.; Hammarström, L. Proton-Coupled Electron Transfer Guidelines, Fair and Square. *J. Am. Chem. Soc.* **2021**, *143*, 560–576. [CrossRef]
553. Hammes-Schiffer, S. Exploring proton-coupled electron transfer at multiple scales. *Nat. Comput. Sci.* **2023**, *3*, 291–300. [CrossRef]
554. Sazanov, L.A. A giant molecular proton pump: Structure and mechanism of respiratory complex I. *Nat. Rev. Mol. Cell Biol.* **2015**, *16*, 375–388. [CrossRef]
555. Hosseinzadeh, P.; Lu, Y. Design and fine-tuning redox potentials of metalloproteins involved in electron transfer in bioenergetics. *Biochim. Biophs. Acta* **2016**, *1857*, 557–581. [CrossRef]
556. Wenke, B.B.; Spatzal, T.; Rees, D.C. Site-Specific Oxidation State Assignments of the Iron Atoms in the [4Fe:4S]2+/1+/0 States of the Nitrogenase Fe-Protein. *Angew. Chem. Int. Ed.* **2019**, *58*, 3894–3897. [CrossRef] [PubMed]
557. Harris, T.V.; Szilagyi, R.K. Iron–sulfur bond covalency from electronic structure calculations for classical iron–sulfur clusters. *J. Comp. Chem.* **2014**, *35*, 540–552. [CrossRef]
558. Sun, J.; Trumpower, B.L. Superoxide anion generation by the cytochrome bc1 complex. *Arch. Biochem. Biophys.* **2003**, *419*, 198–206. [CrossRef] [PubMed]
559. Yun, C.H.; Crofts, A.R.; Gennis, R.B. Assignment of the histidine axial ligands to the cytochrome bH and cytochrome bL components of the bc1 complex from Rhodobacter sphaeroides by site-directed mutagenesis. *Biochemistry* **1991**, *30*, 6747–6754. [CrossRef]
560. Fischer, W.W.; Hemp, J.; Johnson, J.E. Evolution of Oxygenic Photosynthesis. *Ann. Rev. Earth Planet. Sci.* **2016**, *44*, 647–683. [CrossRef]
561. Garcia, P.S.; D'Angelo, F.; Ollagnier de Choudens, S.; Dussouchaud, M.; Bouveret, E.; Gribaldo, S.; Barras, F. An early origin of iron–sulfur cluster biosynthesis machineries before Earth oxygenation. *Nat. Ecol. Evol.* **2022**, *6*, 1564–1572. [CrossRef] [PubMed]
562. Moore, G.R.; Pettigrew, G.W. *Cytochromes c. Evolutionary, Structural and Physicochemical Aspects*; Springer-Verlag: Berlin, Germany, 1990.
563. Johnson, D.C.; Dean, D.R.; Smith, A.D.; Johnson, M.K. Structure, Function, and Formation of Biological Iron Iron-Sulfor Clusters. *Ann. Rev. Biochem.* **2005**, *74*, 247–281. [CrossRef] [PubMed]
564. Meyer, J. Iron–sulfur protein folds, iron–sulfur chemistry, and evolution. *J. Biol. Inorg. Chem.* **2008**, *13*, 157–170. [CrossRef] [PubMed]
565. Lill, R. Function and biogenesis of iron–sulphur proteins. *Nature* **2009**, *460*, 831–838. [CrossRef]
566. Garcia, P.S.; Gribaldo, S.; Barras, F. When iron and sulfur met on an anoxic planet and eventually made clusters essential for life. *Biochim. Biophys. Acta Mol. Cell Res.* **2024**, *1871*, 119730. [CrossRef]
567. Flint, D.H.; Allen, R.M. Iron−Sulfur Proteins with Nonredox Functions. *Chem. Rev.* **1996**, *96*, 2315–2334. [CrossRef]
568. Guo, Z.; Xu, S.; Chen, X.; Wang, C.; Yang, P.; Qin, S.; Zhao, C.; Fei, F.; Zhao, X.; Tan, P.-H.; et al. Modulation of MagR magnetic properties via iron–sulfur cluster binding. *Sci. Rep.* **2021**, *11*, 23941. [CrossRef]
569. Schmidt, C.L.; Shaw, L. A Comprehensive Phylogenetic Analysis of Rieske and Rieske-Type Iron-Sulfur Proteins. *J. Bioenerg. Biomembr.* **2001**, *33*, 9–26. [CrossRef]
570. Era, I.; Kitagawa, Y.; Yasuda, N.; Kamimura, T.; Amamizu, N.; Sato, H.; Cho, K.; Okumura, M.; Nakano, M. Theoretical Study on Redox Potential Control of Iron-Sulfur Cluster by Hydrogen Bonds: A Possibility of Redox Potential Programming. *Molecules* **2021**, *26*, 6129. [CrossRef]
571. Zu, Y.; Couture, M.M.J.; Kolling, D.R.J.; Crofts, A.R.; Eltis, L.D.; Fee, J.A.; Hirst, J. Reduction Potentials of Rieske Clusters: Importance of the Coupling between Oxidation State and Histidine Protonation State. *Biochemistry* **2003**, *42*, 12400–12408. [CrossRef]
572. Kuznetsov, A.M.; Zueva, E.M.; Masliy, A.N.; Krishtalik, L.I. Redox potential of the Rieske iron–sulfur protein: Quantum-chemical and electrostatic study. *Biochim. Biophys. Acta* **2010**, *1797*, 347–359. [CrossRef] [PubMed]
573. Zu, Y.; Fee, J.A.; Hirst, J. Complete Thermodynamic Characterization of Reduction and Protonation of the bc1-type Rieske [2Fe–2S] Center of Thermus thermophilus. *J. Am. Chem. Soc.* **2001**, *123*, 9906–9907. [CrossRef]
574. Danyal, K.; Dean, D.R.; Hoffman, B.M.; Seefeldt, L.C. Electron Transfer within Nitrogenase: Evidence for a Deficit-Spending Mechanism. *Biochemistry* **2011**, *50*, 9255–9263. [CrossRef]
575. Lanzilotta, W.N.; Seefeldt, L.C. Electron Transfer from the Nitrogenase Iron Protein to the [8Fe-(7/8)S] Clusters of the Molybdenum−Iron Protein. *Biochemistry* **1996**, *35*, 16770–16776. [CrossRef]
576. Jeoung, J.-H.; Martins, B.M.; Dobbek, H. Double-Cubane [8Fe9S] Clusters: A Novel Nitrogenase-Related Cofactor in Biology. *Chem. Bio. Chem.* **2020**, *21*, 1710–1716. [CrossRef] [PubMed]
577. Elghobashi-Meinhardt, N.; Tombolelli, D.; Mroginski, M.A. Electronic and Structural Properties of the Double Cubane Iron-Sulfur Cluster. *Catalysts* **2021**, *11*, 245. [CrossRef]

578. Ullmann, M.G.; Noodleman, L.; Case, D.A. Density functional calculation of pKa values and redox potentials in the bovine Rieske iron-sulfur protein. *J. Biol. Inorg. Chem.* **2002**, *7*, 632–639. [CrossRef]
579. Marcus, R.A. Electron Transfer Reactions in Chemistry: Theory and Experiment. Available online: https://www.nobelprize.org/prizes/chemistry/1992/marcus/lecture/ (accessed on 9 December 2023).
580. Gray, H.B.; Winkler, J.R. Electron transfer in proteins. *Ann. Rev. Biochem.* **1996**, *65*, 537–561. [CrossRef]
581. Sánchez, M.; Sabio, L.; Gálvez, N.; Capdevila, M.; Dominguez-Vera, J.M. Iron chemistry at the service of life. *IUBMB Life* **2017**, *69*, 382–388. [CrossRef]
582. Andreini, C.; Rosato, A. Structural Bioinformatics and Deep Learning of Metalloproteins: Recent Advances and Applications. *Int. J. Mol. Sci.* **2022**, *23*, 7684. [CrossRef]
583. Jeong, W.J.; Lee, J.; Eom, H.; Song, W.J. A Specific Guide for Metalloenzyme Designers: Introduction and Evolution of Metal-Coordination Spheres Embedded in Protein Environments. *Acc. Chem. Res.* **2023**, *56*, 2416–2425. [CrossRef]
584. Moore, G.R.; Pettigrew, G.W.; Rogers, N.K. Factors influencing redox potentials of electron transfer proteins. *Proc. Natl. Acad. Sci. USA* **1986**, *83*, 4998–4999. [CrossRef] [PubMed]
585. Perrin, B.S.; Ichiye, T. Characterizing the effects of the protein environment on the reduction potentials of metalloproteins. *J. Biol. Inorg. Chem.* **2013**, *18*, 103–110. [CrossRef] [PubMed]
586. Matsuo, T.; Kono, T.; Shobu, I.; Ishida, M.; Gonda, K.; Hirota, S. Global Structural Flexibility of Metalloproteins Regulates Reactivity of Transition Metal Ion in the Protein Core: An Experimental Study Using Thiol-subtilisin as a Model Protein. *Chem. Eur. J.* **2018**, *24*, 2767–2775. [CrossRef]
587. Lee, Y.-m.; Lim, C. Physical Basis of Structural and Catalytic Zn-Binding Sites in Proteins. *J. Mol. Biol.* **2008**, *379*, 545–553. [CrossRef]
588. Valasatava, Y.; Rosato, A.; Furnham, N.; Thornton, J.M.; Andreini, C. To what extent do structural changes in catalytic metal sites affect enzyme function? *J. Inorg. Biochem.* **2018**, *179*, 40–53. [CrossRef] [PubMed]
589. Zaballa, M.-E.; Abriata, L.A.; Donaire, A.; Vila, A.J. Flexibility of the metal-binding region in apo-cupredoxins. *Proc. Natl. Acad. Sci. USA* **2012**, *109*, 9254–9259. [CrossRef]
590. Ohnishi, T. Iron–sulfur clusters/semiquinones in Complex I. *Biochim. Biophys. Acta* **1998**, *1364*, 186–206. [CrossRef]
591. Carroll, J.; Fearnley, I.M.; Skehel, J.M.; Shannon, R.J.; Hirst, J.; Walker, J.E. Bovine Complex I Is a Complex of 45 Different Subunits. *J. Biol. Chem.* **2006**, *281*, 32724–32727. [CrossRef]
592. Hirst, J.; Carroll, J.; Fearnley, I.M.; Shannon, R.J.; Walker, J.E. The nuclear encoded subunits of complex I from bovine heart mitochondria. *Biochim. Biophys. Acta* **2003**, *1604*, 135–150. [CrossRef]
593. Rees, D.C.; Howard, J.B. The Interface Between the Biological and Inorganic Worlds: Iron-Sulfur Metalloclusters. *Science* **2003**, *300*, 929–931. [CrossRef] [PubMed]
594. Camprubi, E.; Jordan, S.F.; Vasiliadou, R.; Lane, N. Iron catalysis at the origin of life. *IUBMB Life* **2017**, *69*, 373–381. [CrossRef] [PubMed]
595. Yu, H.; Haja, D.K.; Schut, G.J.; Wu, C.H.; Meng, X.; Zhao, G.; Li, H.; Adams, M.W.W. Structure of the respiratory MBS complex reveals iron-sulfur cluster catalyzed sulfane sulfur reduction in ancient life. *Nat. Commun.* **2020**, *11*, 5953, Erratum in *Nat. Commun.* **2021**, *12*, 5831. [CrossRef] [PubMed]
596. Mukherjee, A.; Ghosh, K.K.; Chakrabortty, S.; Gulyás, B.; Padmanabhan, P.; Ball, W.B. Mitochondrial Reactive Oxygen Species in Infection and Immunity. *Biomolecules* **2024**, *14*, 670. [CrossRef] [PubMed]
597. Selivanov, V.A.; Votyakova, T.V.; Zeak, J.A.; Trucco, M.; Roca, J.; Cascante, M. Bistability of Mitochondrial Respiration Underlies Paradoxical Reactive Oxygen Species Generation Induced by Anoxia. *PLoS Comput. Biol.* **2009**, *5*, e1000619. [CrossRef]
598. Mailloux, R.J. Teaching the fundamentals of electron transfer reactions in mitochondria and the production and detection of reactive oxygen species. *Redox Biol.* **2015**, *4*, 381–398. [CrossRef]
599. Okoye, C.N.; Koren, S.A.; Wojtovich, A.P. Mitochondrial complex I ROS production and redox signaling in hypoxia. *Redox Biol.* **2023**, *67*, 102926. [CrossRef]
600. Mulkidjanian, A.Y. Ubiquinol oxidation in the cytochrome bc1 complex: Reaction mechanism and prevention of short-circuiting. *Biochim. Biophs. Acta* **2005**, *1709*, 5–34. [CrossRef]
601. Guzy, R.D.; Schumacker, P.T. Oxygen sensing by mitochondria at complex III: The paradox of increased reactive oxygen species during hypoxia. *Exp. Physiol.* **2006**, *91*, 807–819. [CrossRef]
602. Brzezinski, P.; Moe, A.; Ädelroth, P. Structure and Mechanism of Respiratory III–IV Supercomplexes in Bioenergetic Membranes. *Chem. Rev.* **2021**, *121*, 9644–9673. [CrossRef]
603. Bolisetty, S.; Jaimes, E.A. Mitochondria and Reactive Oxygen Species: Physiology and Pathophysiology. *Int. J. Mol. Sci.* **2013**, *14*, 6306–6344. [CrossRef] [PubMed]
604. Povea-Cabello, S.; Brischigliaro, M.; Fernández-Vizarra, E. Emerging mechanisms in the redox regulation of mitochondrial cytochrome c oxidase assembly and function. *Biochem. Soc. Trans.* **2024**, *52*, 873–885. [CrossRef]

605. Sato, W.; Ishimori, K. Regulation of electron transfer in the terminal step of the respiratory chain. *Biochem. Soc. Trans.* **2023**, *51*, 1611–1619. [CrossRef]
606. Luo, F.; Shinzawa-Itoh, K.; Hagimoto, K.; Shimada, A.; Shimada, S.; Yamashita, E.; Yoshikawa, S.; Tsukihara, T. Structure of bovine cytochrome c oxidase crystallized at a neutral pH using a fluorinated detergent. *Acta Cryst. F* **2017**, *73*, 416–422. [CrossRef]
607. Wikström, M.; Krab, K.; Sharma, V. Oxygen Activation and Energy Conservation by Cytochrome c Oxidase. *Chem. Rev.* **2018**, *118*, 2469–2490. [CrossRef]
608. Rich, P.R. Mitochondrial cytochrome c oxidase: Catalysis, coupling and controversies. *Biochem. Soc. Trans.* **2017**, *45*, 813–829. [CrossRef] [PubMed]
609. Meunier, B.; de Visser, S.P.; Shaik, S. Mechanism of Oxidation Reactions Catalyzed by Cytochrome P450 Enzymes. *Chem. Rev.* **2004**, *104*, 3947–3980. [CrossRef] [PubMed]
610. Ortiz de Montellano, P.R. Hydrocarbon Hydroxylation by Cytochrome P450 Enzymes. *Chem. Rev.* **2010**, *110*, 932–948. [CrossRef]
611. Denisov, I.G.; Sligar, S.G. Activation of Molecular Oxygen in Cytochromes P450. In *Cytochrome P450: Structure, Mechanism, and Biochemistry*; Ortiz de Montellano, P.R., Ed.; Springer International Publishing: Cham, Switzerland, 2015; pp. 69–109.
612. Guengerich, F.P. Mechanisms of Cytochrome P450-Catalyzed Oxidations. *ACS Catal.* **2018**, *8*, 10964–10976. [CrossRef]
613. Cook, D.J.; Finnigan, J.D.; Cook, K.; Black, G.W.; Charnock, S.J. Cytochromes P450: History, Classes, Catalytic Mechanism, and Industrial Application. In *Advances in Protein Chemistry and Structural Biology*; Christov, C.Z., Ed.; Academic Press: New Yrok, NY, USA, 2016; Volume 105, pp. 105–126.
614. Koroleva, P.I.; Bulko, T.V.; Agafonova, L.E.; Shumyantseva, V.V. Catalytic and Electrocatalytic Mechanisms of Cytochromes P450 in the Development of Biosensors and Bioreactors. *Biochemistry* **2023**, *88*, 1645–1657.
615. Zhou, T.P.; Fan, Y.; Zhang, J.; Wang, B. Mechanistic Perspective on C-N and C-S Bond Construction Catalyzed by Cytochrome P450 Enzymes. *ACS Bio. Med. Chem. Au.* **2025**, *5*, 16–30. [CrossRef] [PubMed]
616. Cunningham, K.M.; Shin, W.; Yang, Z.J. Computational Studies of Enzymes for C-F Bond Degradation and Functionalization. *Chem. Phys. Chem.* **2025**, e202401130. [CrossRef]
617. Leite Dias, S.; D'Auria, J.C. The bitter truth: How insects cope with toxic plant alkaloids. *J. Exp. Bot.* **2025**, *76*, 5–15. [CrossRef]
618. Efimov, I.; Basran, J.; Thackray, S.J.; Handa, S.; Mowat, C.G.; Raven, E.L. Structure and Reaction Mechanism in the Heme Dioxygenases. *Biochemistry* **2011**, *50*, 2717–2724. [CrossRef] [PubMed]
619. Alfonso-Prieto, M.; Biarnés, X.; Vidossich, P.; Rovira, C. The Molecular Mechanism of the Catalase Reaction. *J. Am. Chem. Soc.* **2009**, *131*, 11751–11761. [CrossRef] [PubMed]
620. Veitch, N.C. Horseradish peroxidase: A modern view of a classic enzyme. *Phytochemistry* **2004**, *65*, 249–259. [CrossRef]
621. Aboelnga, M.M. Mechanistic insights into the chemistry of compound I formation in heme peroxidases: Quantum chemical investigations of cytochrome c peroxidase. *RSC Adv.* **2022**, *12*, 15543–15554. [CrossRef]
622. Auclair, K.; Moeenne-Laccoz, P.; Ortiz de Montellano, P.R. Roles of the Proximal Heme Thiolate Ligand in Cytochrome P400cam. *J. Am. Chem Soc.* **2001**, *123*, 4877–4885. [CrossRef]
623. Shaik, S.; Dubey, K.D. The catalytic cycle of cytochrome P450: A fascinating choreography. *Trends Chem.* **2021**, *3*, 1027–1044. [CrossRef]
624. He, J.; Liu, X.; Li, C. Engineering Electron Transfer Pathway of Cytochrome P450s. *Molecules* **2024**, *29*, 2480. [CrossRef]
625. Schlichting, I.; Berendzen, J.; Chu, K.; Stock, A.M.; Maves, S.A.; Benson, D.E.; Sweet, R.M.; Ringe, D.; Petsko, G.A.; Sligar, S.G. The catalytic pathway of cytochrome p450cam at atomic resolution. *Science* **2000**, *287*, 1615–1622. [CrossRef] [PubMed]
626. Bach, R.D.; Dmitrenko, O. The "Somersault" Mechanism for the P-450 Hydroxylation of Hydrocarbons. The Intervention of Transient Inverted Metastable Hydroperoxides. *J. Am. Chem. Soc.* **2006**, *128*, 1474–1488. [CrossRef]
627. Tateishi, Y.; McCarty, K.D.; Martin, M.V.; Yoshimoto, F.K.; Guengerich, F.P. Roles of Ferric Peroxide Anion Intermediates (Fe(3+)O(2) (-), Compound 0) in Cytochrome P450 19A1 Steroid Aromatization and a Cytochrome P450 2B4 Secosteroid Oxidation Model. *Angew. Chem. Int. Ed. Engl.* **2024**, *63*, e202406542. [CrossRef]
628. Tateishi, Y.; McCarty, K.D.; Martin, M.V.; Guengerich, F.P. Oxygen-18 Labeling Defines a Ferric Peroxide (Compound 0) Mechanism in the Oxidative Deformylation of Aldehydes by Cytochrome P450 2B4. *ACS Catal.* **2024**, *14*, 2388–2394. [CrossRef] [PubMed]
629. McCarty, K.D.; Tateishi, Y.; Hargrove, T.Y.; Lepesheva, G.I.; Guengerich, F.P. Oxygen-18 Labeling Reveals a Mixed Fe-O Mechanism in the Last Step of Cytochrome P450 51 Sterol 14α-Demethylation. *Angew. Chem. Int. Ed. Engl.* **2024**, *63*, e202317711. [CrossRef] [PubMed]
630. Rittle, J.; Green, M.T. Cytochrome P450 Compound I: Capture, Characterization, and C-H Bond Activation Kinetics. *Science* **2010**, *330*, 933–937. [CrossRef]
631. Han, A.-R.; Jin Jeong, Y.; Kang, Y.; Yoon Lee, J.; Sook Seo, M.; Nam, W. Direct evidence for an iron(iv)-oxo porphyrin π-cation radical as an active oxidant in catalytic oxygenation reactions. *Chem. Commun.* **2008**, *7*, 1076–1078. [CrossRef]
632. Seefeldt, L.C.; Hoffman, B.M.; Dean, D.R. Mechanism of Mo-dependent nitrogenase. *Annu. Rev. Biochem.* **2009**, *78*, 701–722. [CrossRef]

633. Pourret, O.; Faucon, M.-P. Cobalt. In *Encyclopedia of Geochemistry: A Comprehensive Reference Source on the Chemistry of the Earth*; White, W.M., Ed.; Springer International Publishing: Cham, Switzerland, 2017; pp. 1–4.
634. Rollinson, C.L.; Bailar, J.C.; Emeléus, H.J.; Nyholm, R. *The Chemistry of Chromium, Molybdenum and Tungsten: Pergamon International Library of Science, Technology, Engineering and Social Studies*; Elsevier Science: Oxford, UK, 2015.
635. Basolo, F.; Pearson, R.G. *Mechanisms of Inorganic Reactions: A Study of Metal Complexes in Solution*; Wiley: New York, NY, USA, 1958.
636. Rutenberg, A.C.; Taube, H.J. The Exchange of Water between $Co(NH_3)_5H_2O^{+++}$ and Solvent. *Chem. Phys.* **1952**, *20*, 825–826.
637. Hunt, J.; Plane, R.A. The Kinetics of the Exchange of Water between $Cr(H_2O)_6{}^{+3}$ and Solvent. *J. Am. Chem. Soc.* **1954**, *76*, 5960–5962. [CrossRef]
638. Fiat, D.; Connick, R.E. Oxygen-17 magnetic resonance studies of ion solvation. The hydration of aluminum (III) and gallium (III) ions. *J. Am. Chem. Soc.* **1968**, *90*, 608–615. [CrossRef]
639. Swift, T.J.; Connick, R.E. NMR-Relaxation Mechanisms of O^{17} in Aqueous Solutions of Paramagnetic Cations and the Lifetime of Water Molecules in the First Coordination Sphere. *J. Chem. Phys.* **1962**, *37*, 307–320. [CrossRef]
640. Genchi, G.; Lauria, G.; Catalano, A.; Carocci, A.; Sinicropi, M.S. Prevalence of Cobalt in the Environment and Its Role in Biological Processes. *Biology* **2023**, *12*, 1335. [CrossRef]
641. Kräutler, B.; Jaun, B.M. Vitamin B_{12} and Cofactor F430. In *Fundamentals of Porphyrin Chemistry: A 21st Century Approach*; Brothers, P.J., Senge, M.O., Eds.; John Wiley & Sons Ltd.: Hoboken, NJ, USA, 2022; Volume 1, pp. 777–814.
642. Kräutler, B. Organometallic B_{12}-derivatives in life processes. In *Bioorganometallic Chemistry*; Wolfgang, W., Ulf-Peter, A., Eds.; De Gruyter: Berlin, Germany, 2020; pp. 243–284.
643. Osman, D.; Cooke, A.; Young, T.R.; Deery, E.; Robinson, N.J.; Warren, M.J. The requirement for cobalt in vitamin B_{12}: A paradigm for protein metalation. *Biochim. Biophs. Acta* **2021**, *1868*, 118896. [CrossRef]
644. Mendoza, J.; Purchal, M.; Yamada, K.; Koutmos, M. Structure of full-length cobalamin-dependent methionine synthase and cofactor loading captured in crystallo. *Nat. Commun.* **2023**, *14*, 6365. [CrossRef] [PubMed]
645. Yabuta, Y.; Kamei, Y.; Bito, T.; Arima, J.; Yoneda, K.; Sakuraba, H.; Ohshima, T.; Nakano, Y.; Watanabe, F. Functional and structural characteristics of methylmalonyl-CoA mutase from *Pyrococcus horikoshii*. *Biosci. Biotechnol. Biochem.* **2015**, *79*, 710–717. [CrossRef]
646. Benjdia, A.; Berteau, O. B_{12}-dependent radical SAM enzymes: Ever expanding structural and mechanistic diversity. *Curr. Opin. Structur. Biol.* **2023**, *83*, 102725. [CrossRef]
647. Fincker, M.; Spormann, A.M. Biochemistry of Catabolic Reductive Dehalogenation. *Annu. Rev. Biochem.* **2017**, *86*, 357–386. [CrossRef]
648. Conrad, K.S.; Jordan, C.D.; Brown, K.L.; Brunold, T.C. Spectroscopic and computational studies of cobalamin species with variable lower axial ligation: Implications for the mechanism of Co-C bond activation by class I cobalamin-dependent isomerases. *Inorg. Chem.* **2015**, *54*, 3736–3747. [CrossRef]
649. Schrapers, P.; Mebs, S.; Goetzl, S.; Hennig, S.E.; Dau, H.; Dobbek, H.; Haumann, M. Axial Ligation and Redox Changes at the Cobalt Ion in Cobalamin Bound to Corrinoid Iron-Sulfur Protein (CoFeSP) or in Solution Characterized by XAS and DFT. *PLoS ONE* **2016**, *11*, e0158681. [CrossRef]
650. Park, K.; Mera, P.E.; Escalante-Semerena, J.C.; Brunold, T.C. Resonance Raman spectroscopic study of the interaction between Co(II)rrinoids and the ATP:corrinoid adenosyltransferase PduO from Lactobacillus reuteri. *J. Biol. Inorg. Chem.* **2016**, *21*, 669–681. [CrossRef] [PubMed]
651. Stracey, N.G.; Costa, F.G.; Escalante-Semerena, J.C.; Brunold, T.C. Spectroscopic Study of the EutT Adenosyltransferase from Listeria monocytogenes: Evidence for the Formation of a Four-Coordinate Cob(II)alamin Intermediate. *Biochemistry* **2018**, *57*, 5088–5095. [CrossRef] [PubMed]
652. Lukinović, V.; Woodward, J.R.; Marrafa, T.C.; Shanmugam, M.; Heyes, D.J.; Hardman, S.J.O.; Scrutton, N.S.; Hay, S.; Fielding, A.J.; Jones, A.R. Photochemical Spin Dynamics of the Vitamin B_{12} Derivative, Methylcobalamin. *J. Phys. Chem. B* **2019**, *123*, 4663–4672. [CrossRef]
653. Qu, Z.W.; Hansen, A.; Grimme, S. Co-C Bond Dissociation Energies in Cobalamin Derivatives and Dispersion Effects: Anomaly or Just Challenging? *J. Chem. Theory. Comput.* **2015**, *11*, 1037–1045. [CrossRef]
654. Salerno, E.V.; Miller, N.A.; Konar, A.; Li, Y.; Kieninger, C.; Kräutler, B.; Sension, R.J. Ultrafast Excited State Dynamics and Fluorescence from Vitamin B_{12} and Organometallic [Co]-C≡C-R Cobalamins. *J. Phys. Chem. B* **2020**, *124*, 6651–6656. [CrossRef] [PubMed]
655. Miller, N.A.; Michocki, L.B.; Konar, A.; Alonso-Mori, R.; Deb, A.; Glownia, J.M.; Sofferman, D.L.; Song, S.; Kozlowski, P.M.; Kubarych, K.J.; et al. Ultrafast XANES Monitors Femtosecond Sequential Structural Evolution in Photoexcited Coenzyme B_{12}. *J. Phys. Chem. B* **2020**, *124*, 199–209. [CrossRef]
656. Reckziegel, A.; Kour, M.; Battistella, B.; Mebs, S.; Beuthert, K.; Berger, R.; Werncke, C.G. High-Spin Imido Cobalt Complexes with Imidyl Radical Character. *Angew. Chem. Int. Ed.* **2021**, *60*, 15376–15380. [CrossRef]
657. Toda, M.J.; Lodowski, P.; Mamun, A.A.; Kozlowski, P.M. Electronic and photolytic properties of hydridocobalamin. *J. Photochem. Photobiol. B* **2021**, *224*, 112295. [CrossRef]

658. Lehene, M.; Plesa, D.; Ionescu-Zinca, S.; Iancu, S.D.; Leopold, N.; Makarov, S.V.; Brânzanic, A.M.V.; Silaghi-Dumitrescu, R. Adduct of Aquacobalamin with Hydrogen Peroxide. *Inorg. Chem.* **2021**, *60*, 12681–12684. [CrossRef]
659. Elmendorf, L.D.; Brunold, T.C. Electronic structure studies of free and enzyme-bound B_{12} species by magnetic circular dichroism and complementary spectroscopic techniques. In *Methods in Enzymology*; Marsh, E.N.G., Ed.; Academic Press: New York, NY, USA, 2022; Volume 669, pp. 333–365.
660. Mumcu, T.; Oncuoglu, S.; Hizliates, C.G.; Ertekin, K. Emission-based sensing of cobalt (II) and vitamin B12 via a bis-indole derivative. *Luminescence* **2024**, *39*, e4863. [CrossRef]
661. Elmendorf, L.D.; Brunold, T.C. Vibronic Coupling in Vitamin B_{12}: A Combined Spectroscopic and Computational Study. *Inorg. Chem.* **2023**, *62*, 12762–12772. [CrossRef]
662. Spataru, T. The Miracle of Vitamin B_{12} Biochemistry. *Reactions* **2024**, *5*, 20–76. [CrossRef]
663. Spataru, T. The complete electronic structure and mechanism of the methionine synthase process as determined by the MCSCF method. *J. Organometal. Chem.* **2021**, *942*, 121811. [CrossRef]
664. Fang, H.; Kang, J.; Zhang, D. Microbial production of vitamin B_{12}: A review and future perspectives. *Microb. Cell Fact.* **2017**, mboxemph16, 15. [CrossRef]
665. Roth, J.R.; Lawrence, J.G.; Bobik, T.A. Cobalamin (coenzymne B12): Synthesis and biological significance. *Annu. Rev. Microbiol.* **1996**, *50*, 137–181. [CrossRef]
666. Martens, J.H.; Barg, H.; Warren, M.; Jahn, D. Microbial production of vitamin B_{12}. *Appl. Microbiol. Biotechnol.* **2002**, *58*, 275–285. [CrossRef]
667. Scott, A.I.; Roessner, C.A. Biosynthesis of cobalamin (vitamin B_{12}). *Biochem. Soc. Trans.* **2002**, *30*, 613–620. [CrossRef]
668. Mrnjavac, N.; Degli Esposti, M.; Mizrahi, I.; Martin, W.F.; Allen, J.F. Three enzymes governed the rise of O_2 on Earth. *Biochim. Biophys. Acta* **2024**, *1865*, 149495. [CrossRef]
669. Mrnjavac, N.; Schwander, L.; Brabender, M.; Martin, W.F. Chemical Antiquity in Metabolism. *Acc. Chem. Res.* **2024**, *57*, 2267–2278. [CrossRef]
670. Dorrell, R.G.; Nef, C.; Altan-Ochir, S.; Bowler, C.; Smith, A.G. Presence of vitamin B_{12} metabolism in the last common ancestor of land plants. *Phil. Trans. Roy. Soc. B* **2024**, *379*, 20230354. [CrossRef]
671. Modjewski, L.D.; Karavaeva, V.; Mrnjavac, N.; Knopp, M.; Martin, W.F.; Sousa, F.L. Evidence for corrin biosynthesis in the last universal common ancestor. *FEBS J.* **2025**, *292*, 827–850. [CrossRef]
672. Croft, M.T.; Lawrence, A.D.; Raux-Deery, E.; Warren, M.J.; Smith, A.G. Algae acquire vitamin B_{12} through a symbiotic relationship with bacteria. *Nature* **2005**, *438*, 90–93. [CrossRef] [PubMed]
673. Banerjee, R. B_{12} Trafficking in Mammals: A Case for Coenzyme Escort Service. *ACS Chem. Biol.* **2006**, *1*, 149–159. [CrossRef] [PubMed]
674. Banerjee, R.; Gherasim, C.; Padovani, D. The tinker, tailor, soldier in intracellular B_{12} trafficking. *Curr. Opin. Chem. Biol.* **2009**, *13*, 484–491. [CrossRef]
675. Li, Z.; Gouda, H.; Pillay, S.; Yaw, M.; Ruetz, M.; Banerjee, R. The human B_{12} trafficking chaperones: CblA, ATR, CblC and CblD. *Methods Enzym.* **2022**, *668*, 137–156.
676. Nijland, M.; Martínez Felices, J.M.; Slotboom, D.J.; Thangaratnarajah, C. Membrane transport of cobalamin. *Vitam. Horm.* **2022**, *119*, 121–148. [PubMed]
677. Calvillo, Á.; Pellicer, T.; Carnicer, M.; Planas, A. Bioprocess Strategies for Vitamin B_{12} Production by Microbial Fermentation and Its Market Applications. *Bioengineering* **2022**, *9*, 365. [CrossRef]
678. Kumar, R.; Singh, U.; Tiwari, A.; Tiwari, P.; Sahu, J.K.; Sharma, S. Vitamin B_{12}: Strategies for enhanced production, fortified functional food products and health benefits. *Process. Biochem.* **2023**, *127*, 44–55. [CrossRef]
679. Banerjee, R. (Ed.) *Chemistry and Biochemistry of B_{12}*; Wiley: New York, NY, USA, 1999.
680. Kräutler, B. Biochemistry of B12-cofactors in human metabolism. *Sub-Cell Biochem.* **2012**, *56*, 323–346.
681. Okamoto, S.; Eltis, L.D. The biological occurrence and trafficking of cobalt. *Metallomics* **2011**, *3*, 963–970. [CrossRef]
682. Kobayashi, M.; Shimizu, S. Cobalt proteins. *Eur. J. Biochem.* **1999**, *261*, 1–9. [CrossRef]
683. Harrop, T.C.; Mascharak, P.K. Cobalt-containing Enzymes. In *Encyclopedia of Metalloproteins*; Kretsinger, R.H., Uversky, V.N., Permyakov, E.A., Eds.; Springer: New York, NY, USA, 2013; pp. 684–690.
684. Odaka, M.; Kobayashi, M. Cobalt Proteins, Overview. In *Encyclopedia of Metalloproteins*; Kretsinger, R.H., Uversky, V.N., Permyakov, E.A., Eds.; Springer: New York, NY, USA, 2013; pp. 670–678.
685. Walker, K.W.; Bradshaw, R.A. Methionyl Aminopeptidase Type 1. In *Handbook of Proteolytic Enzymes*, 3rd ed.; Rawlings, N.D., Salvesen, G., Eds.; Academic Press: New York, NY, USA, 2013; pp. 1495–1500.
686. Lee, Y.; Kim, H.; Lee, E.; Hahn, H.; Heo, Y.; Jang, D.M.; Kwak, K.; Kim, H.J.; Kim, H.S. Structural insights into N-terminal methionine cleavage by the human mitochondrial methionine aminopeptidase, MetAP1D. *Sci. Rep.* **2023**, *13*, 22326. [CrossRef] [PubMed]

687. Glueck, D.S. Intramolecular attack on coordinated nitriles: Metallacycle intermediates in catalytic hydration and beyond. *Dalton Trans.* **2021**, *50*, 15953–15960. [CrossRef]
688. Katayama, Y.; Hashimoto, K.; Nakayama, H.; Mino, H.; Nojiri, M.; Ono, T.-a.; Nyunoya, H.; Yohda, M.; Takio, K.; Odaka, M. Thiocyanate Hydrolase Is a Cobalt-Containing Metalloenzyme with a Cysteine-Sulfinic Acid Ligand. *J. Am. Chem. Soc.* **2006**, *128*, 728–729. [CrossRef] [PubMed]
689. Fatima, B.; Javed, M.M. Production, purification and physicochemical characterization of D-xylose/glucose isomerase from Escherichia coli strain BL21. *3 Biotech* **2020**, *10*, 39. [CrossRef]
690. Hoffman, A.; Hilpert, W.; Dimroth, P. The carboxyltransferase activity of the sodium-ion-translocating methylmalonyl-CoA decarboxylase of Veillonella alcalescens. *Eur. J. Biochem.* **1989**, *179*, 645–650. [CrossRef] [PubMed]
691. Marsh, E.N.G.; Waugh, M.W. Aldehyde Decarbonylases: Enigmatic Enzymes of Hydrocarbon Biosynthesis. *ACS Catal.* **2013**, *3*, 2515–2521. [CrossRef]
692. Broderick, J.B. Iron–Sulfur Clusters in Enzyme Catalysis. In *Comprehensive Coordination Chemistry II*; McCleverty, J.A., Meyer, T.J., Eds.; Pergamon: Oxford, UK, 2003; pp. 739–757.
693. Maity, A.N.; Chen, J.R.; Ke, S.C. Exploring the mechanism of action of lysine 5,6-aminomutase using EPR and ENDOR spectroscopies. *Methods Enzym.* **2022**, *669*, 197–228.
694. Miura, J.; Itoh, N. Determination of Vanadium, Cobalt, Nickel, And Iron In Bromoperoxidases from *Pseudomonas Putida* and *Corallina Pilulifera* by High Performance Liquid Chromatography with Spectrophotometric Detection. *J. Liq. Chromatogr. Relat. Technol.* **1997**, *20*, 2367–2376. [CrossRef]
695. Ortiz-Guerrero, J.M.; Polanco, M.C.; Murillo, F.J.; Padmanabhan, S.; Elías-Arnanz, M. Light-dependent gene regulation by a coenzyme B12-based photoreceptor. *Proc. Natl. Acad. Sci. USA* **2011**, *108*, 7565–7570. [CrossRef]
696. Kennedy, K.J.; Widner, F.J.; Sokolovskaya, O.M.; Innocent, L.V.; Procknow, R.R.; Mok, K.C.; Taga, M.E. Cobalamin Riboswitches Are Broadly Sensitive to Corrinoid Cofactors to Enable an Efficient Gene Regulatory Strategy. *mBio* **2022**, *13*, e0112122. [CrossRef] [PubMed]
697. Toda, M.J.; Mamun, A.A.; Lodowski, P.; Kozlowski, P.M. Why is CarH photolytically active in comparison to other B_{12}-dependent enzymes? *J. Photochem. Photobiol. B* **2020**, *209*, 111919. [CrossRef] [PubMed]
698. Padmanabhan, S.; Pérez-Castaño, R.; Osete-Alcaraz, L.; Polanco, M.C.; Elías-Arnanz, M. Vitamin B_{12} photoreceptors. *Vitam. Horm.* **2022**, *119*, 149–184.
699. Ghosh, A.P.; Toda, M.J.; Kozlowski, P.M. Photolytic properties of B_{12}-dependent enzymes: A theoretical perspective. *Vitam. Horm.* **2022**, *119*, 185–220.
700. Ghosh, A.P.; Lodowski, P.; Kozlowski, P.M. Aerobic photolysis of methylcobalamin: Unraveling the photoreaction mechanism. *Phys. Chem. Chem. Phys.* **2022**, *24*, 6093–6106. [CrossRef] [PubMed]
701. Miller, N.A.; Kaneshiro, A.K.; Konar, A.; Alonso-Mori, R.; Britz, A.; Deb, A.; Glownia, J.M.; Koralek, J.D.; Mallik, L.; Meadows, J.H.; et al. The Photoactive Excited State of the B(12)-Based Photoreceptor CarH. *J. Phys. Chem. B* **2020**, *124*, 10732–10738. [CrossRef]
702. Kipkorir, T.; Polgar, P.; Barker, D.; D'Halluin, A.; Patel, Z.; Arnvig, K.B. A novel regulatory interplay between atypical B12 riboswitches and uORF translation in *Mycobacterium tuberculosis*. *Nucleic Acids Res.* **2024**, *52*, 7876–7892. [CrossRef]
703. Degnan, P.H.; Taga, M.E.; Goodman, A.L. Vitamin B12 as a modulator of gut microbial ecology. *Cell Metab.* **2014**, *20*, 769–778. [CrossRef]
704. Mok, K.C.; Sokolovskaya, O.M.; Nicolas, A.M.; Hallberg, Z.F.; Deutschbauer, A.; Carlson, H.K.; Taga, M.E. Identification of a Novel Cobamide Remodeling Enzyme in the Beneficial Human Gut Bacterium *Akkermansia muciniphila*. *mBio* **2020**, *11*, e02507. [CrossRef]
705. Li, H.; Ye, F.; Li, Z.; Peng, X.; Wu, L.; Liu, Q. The response of gut microbiota to arsenic metabolism is involved in arsenic-induced liver injury, which is influenced by the interaction between arsenic and methionine synthase. *Environ. Int.* **2024**, *190*, 108824. [CrossRef]
706. Bannon, C.C.; Mudge, E.M.; Bertrand, E.M. Shedding light on cobalamin photodegradation in the ocean. *Limnol. Oceanogr. Lett.* **2024**, *9*, 135–144. [CrossRef]
707. Lison, D. Cobalt. In *Handbook of the Toxicology of Metals*, 3rd ed.; Nordberg, G.F., Fowler, B.A., Nordberg, M., Friberg, L.T., Eds.; Elsevier: Amsterdam, The Netherlands, 2007; pp. 511–528.
708. Czarnek, K.; Terpiłowska, S.; Siwicki, A.K. Selected aspects of the action of cobalt ions in the human body. *Central Eur. J. Immunol.* **2015**, *40*, 236–242. [CrossRef]
709. Danzeisen, R.; Weight, D.; Blakeney, M.; Boyle, D. A tiered approach to investigate the inhalation toxicity of cobalt substances. Introduction: Cobalt's essential role in nature and technology. *Reg. Toxicol. Pharmacol.* **2022**, *130*, 105125. [CrossRef]
710. Azzini, E.; Raguzzini, A.; Polito, A. A Brief Review on Vitamin B12 Deficiency Looking at Some Case Study Reports in Adults. *Int. J. Mol. Sci.* **2021**, *22*, 9694. [CrossRef] [PubMed]
711. Shipton, M.J.; Thachil, J. Vitamin B12 deficiency—A 21st century perspective. *Clin. Med.* **2015**, *15*, 145–150. [CrossRef]

712. Sobczyńska-Malefora, A.; Delvin, E.; McCaddon, A.; Ahmadi, K.R.; Harrington, D.J. Vitamin B_{12} status in health and disease: A critical review. Diagnosis of deficiency and insufficiency—Clinical and laboratory pitfalls. *Crit. Rev. Clinic. Lab. Sci.* **2021**, *58*, 399–429. [CrossRef]
713. Simonenko, S.Y.; Bogdanova, D.A.; Kuldyushev, N.A. Emerging Roles of Vitamin B_{12} in Aging and Inflammation. *Int. J. Mol. Sci.* **2024**, *25*, 5044. [CrossRef] [PubMed]
714. Hassan, Z.; Coelho, D.; Bossenmeyer-Pourié, C.; Matmat, K.; Arnold, C.; Savladori, A.; Alberto, J.M.; Umoret, R.; Guéant, J.L.; Pourié, G. Cognitive Impairment Is Associated with AMPAR Glutamatergic Dysfunction in a Mouse Model of Neuronal Methionine Synthase Deficiency. *Cells* **2023**, *12*, 1267. [CrossRef]
715. Watson, W.P.; Munter, T.; Golding, B.T. The effect of vitamin B_{12} on DNA adduction by styrene oxide, a genotoxic xenobiotic. *Chem. Biol. Interact.* **2023**, *382*, 110591. [CrossRef]
716. Kräutler, B. Antivitamins B_{12}—Some Inaugural Milestones. *Chem. Eur. J.* **2020**, *26*, 15438–15445. [CrossRef]
717. Wiedemair, M.; Kieninger, C.; Wurst, K.; Podewitz, M.; Deery, E.; Paxhia, M.D.; Warren, M.J.; Kräutler, B. Solution, Crystal and in Silico Structures of the Organometallic Vitamin B_{12}-Derivative Acetylcobalamin and of its Novel Rhodium-Analogue Acetylrhodibalamin. *Helv. Chim. Acta* **2023**, *106*, e202200158. [CrossRef]
718. Gromova, O.A.; Torshin, I.Y.; Maiorova, L.A.; Koifman, O.I.; Salnikov, D.S. Bioinformatic and chemoneurocytological analysis of the pharmacological properties of vitamin B_{12} and some of its derivatives. *J. Porph. Phthalocyan.* **2021**, *25*, 835–842. [CrossRef]
719. Salerno, E.V.; Miller, N.A.; Konar, A.; Salchner, R.; Kieninger, C.; Wurst, K.; Spears, K.G.; Kräutler, B.; Sension, R.J. Exceptional Photochemical Stability of the Co–C Bond of Alkynyl Cobalamins, Potential Antivitamins B_{12} and Core Elements of B_{12}-Based Biological Vectors. *Inorg. Chem.* **2020**, *59*, 6422–6431. [CrossRef] [PubMed]
720. Ruetz, M.; Mascarenhas, R.; Widner, F.; Kieninger, C.; Koutmos, M.; Kräutler, B.; Banerjee, R. A Noble Metal Substitution Leads to B_{12} Cofactor Mimicry by a Rhodibalamin. *Biochemistry* **2024**, *63*, 1955–1962. [CrossRef] [PubMed]
721. Williams, R.; Billig, E.; Waters, J.H.; Gray, H.B. The Toluenedithiolate and Maleonitriledithiolate Square-Matrix Systems. *J. Am. Chem. Soc.* **1966**, *88*, 43–50. [CrossRef]
722. Röhrscheid, F.; Balch, A.L.; Holm, R.H. Potential Electron Transfer Complexes of the [M-O_4] Type: Synthesis and Properties of Complexes Derived from Pyrocatechol and Tetrachloropyrocatechol. *Inorg. Chem.* **1966**, *5*, 1542–1551. [CrossRef]
723. Fleischer, E.B.; Jacobs, S.; Mestichelli, L. The Kinetics of the Reaction of Cobalt (III) and Iron (III) Hematoporphyrin with Cyanide and Thiocyanate. Evidence for a Dissociative Mechanism. *J. Am. Chem. Soc.* **1968**, *90*, 2527–2531. [CrossRef]
724. Kräutler, B.; Arigoni, D.; Golding, B. (Eds.) *Vitamin B_{12} and B_{12}-Proteins*; Wiley-VCH: Weinheim, Germany, 1998.
725. Toraya, T. Radical catalysis of B_{12} enzymes: Structure, mechanism, inactivation, and reactivation of diol and glycerol dehydratases. *Cell Mol. Life Sci.* **2000**, *57*, 106–127. [CrossRef]
726. Marsh, E.N.G.; Holloway, D.E. Adenosylcobalamin-dependent enzymes. *Subcell Biochem* **2000**, *35*, 351–403.
727. Marsh, E.N.G. Coenzyme-B12-Dependent Glutamate Mutase. *Bioorg. Chem.* **2000**, *28*, 176–189. [CrossRef]
728. Marsh, E.N.G.; Drennan, C.L. Adenosyl-cobalamin dependent isomerases: New insights into structure and mechanism. *Curr. Op. Chem. Biol.* **2001**, *5*, 499–505. [CrossRef] [PubMed]
729. Frey, P.A. Radical mechanisms of enzymatic catalysis. *Ann. Rev. Biochem.* **2001**, *70*, 121–148. [CrossRef] [PubMed]
730. Banerjee, R. Radical peregrinations catalyzed by coenzyme B12-dependent enzymes. *Biochemistry* **2001**, *40*, 6191–6198. [CrossRef] [PubMed]
731. Gruber, K.; Kratky, C. Coenzyme B_{12} dependent glutamate mutase. *Curr. Op. Chem. Biol.* **2002**, *6*, 598–603. [CrossRef]
732. Brown, K.L. Chemistry and enzymology of vitamin B-12. *Chem. Rev.* **2005**, *105*, 2075–2149. [CrossRef]
733. Heldt, D.; Lawrence, A.D.; Lindenmeyer, M.; Deery, E.; Heathcote, P.; Rigby, S.E.; Warren, M.J. Aerobic synthesis of vitamin B_{12}: Ring contraction and cobalt chelation. *Biochem. Soc. Trans.* **2005**, *33*, 815–819. [CrossRef]
734. Gruber, K.; Puffer, B.; Kräutler, B. Vitamin B_{12}-derivatives—Enzyme cofactors and ligands of proteins and nucleic acids. *Chem. Soc. Rev.* **2011**, *40*, 4346–4363. [CrossRef]
735. Moore, S.J.; Warren, M.J. The anaerobic biosynthesis of vitamin B_{12}. *Biochem. Soc. Trans.* **2012**, *40*, 581–586. [CrossRef]
736. Moore, S.J.; Lawrence, A.D.; Biedendieck, R.; Deery, E.; Frank, S.; Howard, M.J.; Rigby, S.E.J.; Warren, M.J. Elucidation of the anaerobic pathway for the corrin component of cobalamin (vitamin B_{12}). *Proc. Natl. Acad. Sci. USA* **2013**, *110*, 14906–14911. [CrossRef]
737. Bridwell-Rabb, J.; Drennan, C.L. Vitamin B_{12} in the spotlight again. *Curr. Opin. Chem. Biol.* **2017**, *37*, 63–70. [CrossRef]
738. Mattes, T.A.; Deery, E.; Warren, M.J.; Escalante-Semerena, J.C. Cobalamin Biosynthesis and Insertion. In *Encyclopedia of Inorganic and Bioinorganic Chemistry*; Scott, R.A., Ed.; John Wiley & Sons: Hoboken, NJ, USA, 2017; pp. 1–24.
739. Monteverde, D.R.; Gómez-Consarnau, L.; Suffridge, C.; Sañudo-Wilhelmy, S.A. Life's utilization of B vitamins on early Earth. *Geobiology* **2017**, *15*, 3–18. [CrossRef] [PubMed]
740. Pratt, J.M. *The Inorganic Chemistry of Vitamin B_{12}*; Academic Press: London, UK, 1972.
741. Giedyk, M.; Gryko, D. Vitamin B_{12}: An efficient cobalt catalyst for sustainable generation of radical species. *Chem. Catal.* **2022**, *2*, 1534–1548. [CrossRef]

742. Shimakoshi, H. Application of bioorganometallic B_{12} in green organic synthesis. In *Vitamins and Hormones*; Litwack, G., Ed.; Academic Press: New York, NY, USA, 2022; Volume 119, pp. 23–42.
743. Pleșa, D.; Lehene, M.; Silaghi-Dumitrescu, R. On the reaction of Co(II) cobalamin with hydrogen peroxide. *Reac. Kinet. Mech. Catal.* **2023**, *136*, 1791–1799. [CrossRef]
744. Salnikov, D.S.; Makarov, S.V.; Koifman, O.I. The radical versus ionic mechanisms of reduced cobalamin inactivation by tert-butyl hydroperoxide and hydrogen peroxide in aqueous solution. *New J. Chem.* **2021**, *45*, 535–543. [CrossRef]
745. Lexa, D.; Savéant, J.M. Electrochemistry of vitamin B_{12}. 3. One-electron intermediates in the reduction of methylcobalamin and methylcobinamide. *J. Am. Chem. Soc.* **1978**, *100*, 3220–3222. [CrossRef]
746. Lexa, D.; Savéant, J.M. The electrochemistry of vitamin B_{12}. *Acc. Chem. Res.* **1983**, *16*, 235–243. [CrossRef]
747. Birke, R.L.; Huang, Q.; Spataru, T.; Gosser, D.K. Electroreduction of a Series of Alkylcobalamins: Mechanism of Stepwise Reductive Cleavage of the Co−C Bond. *J. Am. Chem. Soc.* **2006**, *128*, 1922–1936. [CrossRef]
748. Rubinson, K.A.; Parekh, H.V.; Itabashi, E.; Mark, H.B. The Chemistry of [CoICobalamins: Equilibrium Constants and Energies of Formation of Species in Aqueous Solution. *Inorg. Chem.* **1983**, *22*, 458–463. [CrossRef]
749. Martin, B.D.; Finke, R.G. Methylcobalamin's full- vs half-strenghth cobalt-cobalt bonds and bond dissociation enthalpies: A > 10^{15} Co-CH_3 homolysis rate enhancement following one-antibonding-electron reduction of methylcobalamin. *J. Am. Chem. Soc.* **1992**, *114*, 585–592. [CrossRef]
750. Finke, R.G.; Hay, B.P. Thermolysis of adenosylcobalamin: A product, kinetic, and cobalt-carbon (C5') bond dissociation energy study. *Inorg. Chem.* **1984**, *23*, 3041–3043. [CrossRef]
751. Finke, R.G. Coenzyme B_{12}-based chemical precedent for Co-C bond homolysis and other key elementary steps. In *Vitamin B_{12} and B_{12}-Proteins*; Krautler, B., Arigoni, D., Golding, B.J., Eds.; Wiley-VCH: Weinheim, Germany, 1998; pp. 383–402.
752. Schrauzer, G.N.; Deutsch, E. Reactions of Cobalt(I) Supernucleophiles: The Alkylations of Vitamin B_{12s}, Cobaloximes(I), and Related Compounds. *J. Am. Chem. Soc.* **1969**, *91*, 3341–3350. [CrossRef] [PubMed]
753. Mascarenhas, R.; Guha, A.; Li, Z.; Ruetz, M.; An, S.; Seravalli, J.; Banerjee, R. Cobalt–Sulfur Coordination Chemistry Drives B12 Loading onto Methionine Synthase. *J. Am. Chem. Soc.* **2023**, *145*, 24678–24689. [CrossRef]
754. Esser, A.J.; Sastre, S.; Dinh, T.J.; Tanner, V.; Wingert, V.; Klotz, K.; Jacobsen, D.W.; Spiekerkoetter, U.; Schilling, O.; Zeida, A.; et al. A Noncatalytic Cysteine Residue Modulates Cobalamin Reactivity in the Human B(12) Processing Enzyme CblC. *Biochemistry* **2025**, *64*, 692–709. [CrossRef] [PubMed]
755. Banerjee, R.; Ragsdale, S.W. The many faces of vitamin B_{12}: Catalysis by cobalamin-dependent enzymes. *Ann. Rev. Biochem.* **2003**, *72*, 209–247. [CrossRef]
756. Ludwig, M.L.; Matthews, R.G. Structure-based perspectives on B_{12}-dependent enzymes. *Annu. Rev. Biochem.* **1997**, *66*, 269–313. [CrossRef]
757. Kumar, M.; Hirao, H.; Kozlowski, P.M. Co^{+}–H interaction inspired alternate coordination geometries of biologically important cob(I)alamin: Possible structural and mechanistic consequences for methyltransferases. *J. Biol. Inorg. Chem.* **2012**, *17*, 1107–1121. [CrossRef] [PubMed]
758. Fyfe, C.D.; Bernardo-García, N.; Fradale, L.; Grimaldi, S.; Guillot, A.; Brewee, C.; Chavas, L.M.G.; Legrand, P.; Benjdia, A.; Berteau, O. Crystallographic snapshots of a B_{12}-dependent radical SAM methyltransferase. *Nature* **2022**, *602*, 336–342. [CrossRef]
759. Matthews, R.G. Cobalamin-dependent methyltransferases. *Acc. Chem. Res.* **2001**, *34*, 681–689. [CrossRef]
760. Guéant, J.L.; Guéant-Rodriguez, R.M.; Kosgei, V.J.; Coelho, D. Causes and consequences of impaired methionine synthase activity in acquired and inherited disorders of vitamin B_{12} metabolism. *Crit. Rev. Biochem. Mol. Biol.* **2022**, *57*, 133–155. [CrossRef]
761. Mascarenhas, R.; Gouda, H.; Ruetz, M.; Banerjee, R. Chapter Twelve—Human B_{12}-dependent enzymes: Methionine synthase and Methylmalonyl-CoA mutase. In *Methods in Enzymology*; Marsh, E.N.G., Ed.; Academic Press: Cambridge, MA, USA, 2022; Volume 668, pp. 309–326.
762. Bennett, M.R.; Shepherd, S.A.; Cronin, V.A.; Micklefield, J. Recent advances in methyltransferase biocatalysis. *Curr. Opin. Chem. Biol.* **2017**, *37*, 97–106. [CrossRef]
763. Kong, L.; Zhang, J.; Wang, H.; Wei, Z.; Wang, W.; Hu, J.; Dong, M. B_{12}-Dependent Radical SAM Enzymes Catalyze C-Fluoromethylation via a CH_2F-Cobalamin Intermediate. *Angew. Chem. Int. Ed.* **2025**, *64*, e202419815. [CrossRef] [PubMed]
764. Struck, A.-W.; Thompson, M.L.; Wong, L.S.; Micklefield, J. S-Adenosyl-Methionine-Dependent Methyltransferases: Highly Versatile Enzymes in Biocatalysis, Biosynthesis and Other Biotechnological Applications. *Chem. Bio. Chem.* **2012**, *13*, 2642–2655. [CrossRef]
765. Tengg, M.; Stecher, H.; Offner, L.; Plasch, K.; Anderl, F.; Weber, H.; Schwab, H.; Gruber-Khadjawi, M. Methyltransferases: Green Catalysts for Friedel–Crafts Alkylations. *Chem. Cat Chem.* **2016**, *8*, 1354–1360. [CrossRef]
766. Wolthers, K.R.; Scrutton, N.S. Protein interactions in the human methionine synthase-methionine synthase reductase complex and implications for the mechanism of enzyme reactivation. *Biochemistry* **2007**, *46*, 6696–6709. [CrossRef] [PubMed]

767. Haque, M.M.; Bayachou, M.; Tejero, J.; Kenney, C.T.; Pearl, N.M.; Im, S.C.; Waskell, L.; Stuehr, D.J. Distinct conformational behaviors of four mammalian dual-flavin reductases (cytochrome P450 reductase, methionine synthase reductase, neuronal nitric oxide synthase, endothelial nitric oxide synthase) determine their unique catalytic profiles. *FEBS J.* **2014**, *281*, 5325–5340. [CrossRef] [PubMed]
768. Brimberry, M.A.; Mathew, L.; Lanzilotta, W. Making and breaking carbon-carbon bonds in class C radical SAM methyltransferases. *J. Inorg. Biochem.* **2022**, *226*, 111636. [CrossRef]
769. Marsh, E.N.G.; Román Meléndez, G.D. Adenosylcobalamin enzymes: Theory and experiment begin to converge. *Biochim. Biophs. Acta* **2012**, *1824*, 1154–1164. [CrossRef]
770. Mascarenhas, R.; Ruetz, M.; McDevitt, L.; Koutmos, M.; Banerjee, R. Mobile loop dynamics in adenosyltransferase control binding and reactivity of coenzyme B_{12}. *Proc. Natl. Acad. Sci. USA* **2020**, *117*, 30412–30422. [CrossRef]
771. Toraya, T.; Tobimatsu, T.; Mori, K.; Yamanishi, M.; Shibata, N. Coenzyme B(12)-dependent eliminases: Diol and glycerol dehydratases and ethanolamine ammonia-lyase. *Methods Enzym.* **2022**, *668*, 181–242.
772. Sintchak, M.D.; Arjara, G.; Kellogg, B.A.; Stubbe, J.; Drennan, C.L. The crystal structure of class II ribonucleotide reductase reveals how an allosterically regulated monomer mimics a dimer. *Nat. Struct. Biol.* **2002**, *9*, 293–300. [CrossRef]
773. Drennan, C.L.; Huang, S.; Drummond, J.T.; Matthews, R.G.; Ludwig, M.L. How a protein binds B_{12}: A 3.0 A X-ray structure of B_{12}-binding domains of methionine synthase. *Science* **1994**, *266*, 1669–1674. [CrossRef] [PubMed]
774. Perry, C.B.; Marques, H.M. Fifty years of X-ray crystallography of vitamin B-12 and its derivatives. *S. Afr. J. Sci.* **2004**, *100*, 368–380.
775. Jensen, K.P.; Ryde, U. The axial N-base has minor influence on Co–C bond cleavage in cobalamins. *J. Mol. Struct. (THEOCHEM)* **2002**, *585*, 239–255. [CrossRef]
776. Andruniow, T.; Zgierski, M.Z.; Kozlowski, P.M. Theoretical Determination of the Co-C Bond Energy Dissociation in Cobalamins. *J. Am. Chem. Soc.* **2001**, *123*, 2679–2680. [CrossRef]
777. Dölker, N.; Maseras, F.; Lledós, A. Density functional study on the effect of the trans axial ligand of B_{12} cofactors on the heterolytic cleavage of the Co-C bond. *J. Phys. Chem. B* **2003**, *107*, 306–315. [CrossRef]
778. Darbyshire, A.L.; Wolthers, K.R. Characterization of a Structurally Distinct ATP-Dependent Reactivating Factor of Adenosylcobalamin-Dependent Lysine 5,6-Aminomutase. *Biochemistry* **2024**, *63*, 913–925. [CrossRef] [PubMed]
779. Chowdhury, S.; Banerjee, R. Thermodynamic and Kinetic Characterization of Co−C Bond Homolysis Catalyzed by Coenzyme B12-Dependent Methylmalonyl-CoA Mutase. *Biochemistry* **2000**, *39*, 7998–8006. [CrossRef] [PubMed]
780. Reed, G.H. Radical mechanisms in adenosylcobalamin-dependent enzymes. *Curr. Op. Chem. Biol.* **2004**, *8*, 477–483. [CrossRef] [PubMed]
781. Padmakumar, R.; Banerjee, R. Evidence that cobalt-carbon bond homolysis is coupled to hydrogen atom abstraction from substrate in methylmalonyl-CoA mutase. *Biochemistry* **1997**, *36*, 3713–3718. [CrossRef]
782. Hay, B.P.; Finke, R.G. Thermolysis of the cobalt-carbon bond of adenosylcobalamin. 2. Products, kinetics, and cobalt-carbon bond dissociation energy in aqueous solution. *J. Am. Chem. Soc.* **1986**, *108*, 4820–4829. [CrossRef]
783. Hay, B.P.; Finke, R.G. Thermolysis of the cobalt-carbon bond in adenosylcorrins. 3. Quantification of the axial base effect in adenosylcobalamin by the synthesis and thermolysis of axial base-free adenosylcobinamide. Insights into the energetics of enzyme-assisted cobalt-carbon bond homolysis. *J. Am. Chem. Soc.* **1987**, *109*, 8012–8018.
784. Marzilli, L.G.; Toscano, P.J.; Randaccio, L.; Bresciani-Pahor, N.; Calligaris, M. An unusually long Co-C bond. Molecular structure of trans-Bis(dimethylglyoximato)(isopropyl)(pyridine)cobalt(III). Implications with regard to the conformational trigger mechanism of cobalt-carbon bond cleavage in coenzyme B_{12}. *J. Am. Chem. Soc.* **1979**, *101*, 6754–6756. [CrossRef]
785. Ng, F.T.T.; Rempel, G.L. Ligand effects on transition metal-alkyl bond dissociation energies. *J. Am. Chem. Soc.* **1982**, *104*, 621–623. [CrossRef]
786. Geno, M.K.; Halpern, J. Why does nature not use the porphyrin ligand in vitamin B12? *J. Am. Chem. Soc.* **1987**, *109*, 1238–1240. [CrossRef]
787. Brown, K.L.; Brooks, H.B. Effects of Axial Ligation on the Thermolysis of Benzylcobamides and Neopentylcobamides—Analysis of the Base-on Effect. *Inorg. Chem.* **1991**, *30*, 3420–3430. [CrossRef]
788. Kräutler, B.; Konrat, R.; Stupperich, E.; Färber, G.; Gruber, K.; Kratky, C. Direct Evidence for the Conformational Deformation of the Corrin Ring by the Nucleotide Base in Vitamin B12: Synthesis and Solution Spectroscopic and Crystal Structure Analysis of Co.beta.-Cyanoimidazolylcobamide. *Inorg. Chem.* **1994**, *33*, 4128–4139.
789. Banerjee, R.; Chowdhury, S. Methylmalonyl-CoA mutase. In *Chemistry and Biochemistry of B_{12}*; Banerjee, R., Ed.; Wiley Interscience: New York, NY, USA, 1999; pp. 707–729.
790. Sharma, P.K.; Chu, Z.T.; Olsson, M.H.M.; Warshel, A. A New Paradigm for Electrostatic Catalysis of Radical Reactions in Vitamin B_{12} Enzymes. *Proc. Natl. Acad. Sci. USA* **2007**, *104*, 9661–9666. [CrossRef]
791. Gruber, K.; Csitkovits, V.; Łyskowski, A.; Kratky, C.; Kräutler, B. Structure-Based Demystification of Radical Catalysis by a Coenzyme B12 Dependent Enzyme—Crystallographic Study of Glutamate Mutase with Cofactor Homologues. *Angew Chem. Int. Edn.* **2022**, *61*, e202208295. [CrossRef]

792. Wang, M.; Warncke, K. Entropic Origin of Cobalt−Carbon Bond Cleavage Catalysis in Adenosylcobalamin-Dependent Ethanolamine Ammonia-Lyase. *J. Am. Chem. Soc.* **2013**, *135*, 15077–15084. [CrossRef]
793. Elmendorf, L.D.; Hall, R.L.; Costa, F.G.; Escalante-Semerena, J.C.; Brunold, T.C. Spectroscopic and Computational Insights into the Mechanism of Cofactor Cobalt–Carbon Bond Homolysis by the Adenosylcobalamin-Dependent Enzyme Ethanolamine Ammonia-Lyase. *J. Am. Chem. Soc.* **2025**, *147*, 2380–2392. [CrossRef]
794. Licht, S.S.; Lawrence, C.C.; Stubbe, J. Thermodynamic and Kinetic Studies on Carbon- Cobalt Bond Homolysis by Ribonucleoside Triphosphate Reductase: The Importance of Entropy in Catalysis. *Biochemistry* **1999**, *38*, 1234–1242. [CrossRef] [PubMed]
795. Shibata, N.; Toraya, T. Structural Basis for the Activation of the Cobalt-Carbon Bond and Control of the Adenosyl Radical in Coenzyme B_{12} Catalysis. *Chem. Bio. Chem.* **2023**, *24*, e202300021. [CrossRef] [PubMed]
796. Buckel, W.; Friedrich, P.; Golding, B.T. Hydrogen Bonds Guide the Short-Lived 5′-Deoxyadenosyl Radical to the Place of Action. *Angew. Chem. Int. Ed.* **2012**, *51*, 9974–9976. [CrossRef]
797. Marsh, E.N.G.; Holloway, D.E. Cloning and sequencing of glutamate mutase component S from *Clostridium tetanomorphum* Homologies with other cobalamin-dependent enzymes. *FEBS Lett.* **1992**, *310*, 167–170. [CrossRef] [PubMed]
798. Ratnatilleke, A.; Vrijbloed, J.W.; Robinson, J.A. Cloning and Sequencing of the Coenzyme B_{12}-binding Domain of Isobutyryl-CoA Mutase from *Streptomyces cinnamonensis*, Reconstitution of Mutase Activity, and Characterization of the Recombinant Enzyme Produced in *Escherichia coli*. *J. Biol. Chem.* **1999**, *274*, 31679–31685. [CrossRef]
799. Beatrix, B.; Zelder, O.; Linder, D.; Buckel, W. Cloning, sequencing and expression of the gene encoding the coenzyme B12-dependent 2-methyleneglutarate mutase from *Clostridium barkeri* in *Escherichia coli*. *Eur. J. Biochem.* **1994**, *221*, 101–109. [CrossRef]
800. Jensen, K.P.; Ryde, U. How the Co−C bond is Cleaved in Coenzyme B_{12} Enzymes: A Theoretical Study. *J. Am. Chem. Soc.* **2005**, *127*, 9117–9128. [CrossRef]
801. Payne, K.A.P.; Quezada, C.P.; Fisher, K.; Dunstan, M.S.; Collins, F.A.; Sjuts, H.; Levy, C.; Hay, S.; Rigby, S.E.J.; Leys, D. Reductive dehalogenase structure suggests a mechanism for B12-dependent dehalogenation. *Nature* **2015**, *517*, 513–516. [CrossRef]
802. Miller, E.; Wohlfarth, G.; Diekert, G. Studies on tetrachloroethene respiration in Dehalospirillum multivorans. *Arch. Microbiol.* **1996**, *166*, 379–387. [CrossRef]
803. Holliger, C.; Hahn, D.; Harmsen, H.; Ludwig, W.; Schumacher, W.; Tindall, B.; Vazquez, F.; Weiss, N.; Zehnder, A.J.B. *Dehalobacter restrictus* gen. nov. and sp. nov., a strictly anaerobic bacterium that reductively dechlorinates tetra-and trichloroethene in an anaerobic respiration. *Arch. Microbiol.* **1998**, *169*, 313–321. [CrossRef]
804. Liao, R.-Z.; Chen, S.-L.; Siegbahn, P.E.M. Which Oxidation State Initiates Dehalogenation in the B12-Dependent Enzyme NpRdhA: CoII, CoI, or Co0? *ACS Catal.* **2015**, *5*, 7350–7358. [CrossRef]
805. Gantzer, C.J.; Wackett, L.P. Reductive dechlorination catalyzed by bacterial transition-metal coenzymes. *Environ. Sci. Technol.* **1991**, *25*, 715–722. [CrossRef]
806. Marques, H.M. Corrins and porphyrins: Two of nature's pigments of life. *J. Coord. Chem.* **2024**, *77*, 1161–1210. [CrossRef]
807. Scott, A.I. Discovering Nature's Diverse Pathways to Vitamin B12: A 35-Year Odyssey. *J. Org. Chem.* **2003**, *68*, 2529–2539. [CrossRef]
808. Schubert, T. The organohalide-respiring bacterium Sulfurospirillum multivorans: A natural source for unusual cobamides. *World J. Microbiol. Biotechnol.* **2017**, *33*, 93. [CrossRef]
809. Battersby, A.R. Tetrapyrroles: The pigments of life. *Nat. Prod. Rep.* **2000**, *17*, 507–526. [CrossRef]
810. Eschenmoser, A. Robert Robinson Lecture. Post-B12 problems in corrin synthesis. *Chem. Soc. Rev.* **1976**, *5*, 377–410. [CrossRef]
811. Eschenmoser, A. Vitamin B12: Experiments Concerning the Origin of Its Molecular Structure. *Angew. Chem. Int. Ed. Engl.* **1988**, *27*, 5–39. [CrossRef]
812. Jensen, K.P.; Ryde, U. Comparison of the chemical properties of iron and cobalt porphyrins and corrins. *Chem. Bio. Chem.* **2003**, *4*, 413–424. [CrossRef]
813. Jensen, K.P.; Ryde, U. Comparison of chemical properties of iron, cobalt, and nickel porphyrins, corrins, and hydrocorphins. *J. Porph. Phthal.* **2005**, *9*, 581–606. [CrossRef]
814. Li Manni, G.; Alavi, A. Understanding the Mechanism Stabilizing Intermediate Spin States in Fe(II)-Porphyrin. *J. Phys. Chem. A* **2018**, *122*, 4935–4947. [CrossRef] [PubMed]
815. Rovira, C.; Kunc, K.; Hutter, J.; Parrinello, M. Structural and Electronic Properties of Co-corrole, Co-corrin, and Co-porphyrin. *Inorg. Chem.* **2001**, *40*, 11–17. [CrossRef] [PubMed]
816. Bieganowski, R.; Friedrich, W. Preparation and some properties of ferribalamin, the Fe(III)-analogue of vitamin B12. *FEBS Lett.* **1979**, *97*, 325–326.
817. Dozza, B.; Rodrigues, B.M.; Tisoco, I.; de Souza, V.B.; Angnes, L.; Iglesias, B.A. Spectroelectrochemistry as a powerful technique for porphyrins/corroles derivatives electro-characterization: Fundamentals and some examples. *Microchem. J.* **2022**, *183*, 108041. [CrossRef]
818. Lexa, D.; Mispelter, J.; Saveant, J.M. Electroreductive alkylation of iron in porphyrin complexes. Electrochemical and spectral characteristics of σ-alkylironporphyrins. *J. Am. Chem. Soc.* **1981**, *103*, 6806–6812. [CrossRef]

819. Battioni, J.-P.; Dupré, D.; Mansuy, D. Synthèse de complexes σ-vinyliques de ferriporphyrines et leur oxydation en *N*-vinyl-porphyrines: Rétention de la stéréochimie de la double liaison. *J. Organomet. Chem.* **1987**, *328*, 173–184. [CrossRef]
820. Riordan, C.G.; Halpern, J. Kinetics, mechanism and thermodynamics of iron carbon bond dissociation in organoiron porphyrin complexes. *Inorg. Chim. Acta* **1996**, *243*, 19–24. [CrossRef]
821. Arafa, I.M.; Shin, K.; Goff, H.M. Carbon monoxide and carbon dioxide carbon-metal bond insertion chemistry of alkyliron(III) porphyrin complexes. *J. Am. Chem. Soc.* **1988**, *110*, 5228–5229. [CrossRef]
822. Pratt, J.M. Nature's design and use of catalysts based on Co and the macrocyclic corrin ligand: 4 x 10^9 years of coordination chemistry. *Pure Appl. Chem.* **1993**, *65*, 1513–1520. [CrossRef]
823. Cao, L.; Caldararu, O.; Ryde, U. Protonation and Reduction of the FeMo Cluster in Nitrogenase Studied by Quantum Mechanics/Molecular Mechanics (QM/MM) Calculations. *J. Chem. Theory Comp.* **2018**, *14*, 6653–6678. [CrossRef]
824. Hu, Y.; Ribbe, M.W. Nitrogenases—A Tale of Carbon Atom(s). *Angew. Chem. Int. Ed.* **2016**, *55*, 8216–8226. [CrossRef] [PubMed]
825. Raugei, S.; Seefeldt, L.C.; Hoffman, B.M. Critical computational analysis illuminates the reductive-elimination mechanism that activates nitrogenase for N_2 reduction. *Proc. Natl. Acad. Sci. USA* **2018**, *115*, E10521–E10530. [CrossRef]
826. Thauer, R.K.; Kaster, A.-K.; Goenrich, M.; Schick, M.; Hiromoto, T.; Shima, S. Hydrogenases from Methanogenic Archaea, Nickel, a Novel Cofactor, and H_2 Storage. *Ann. Rev. Biochem.* **2010**, *79*, 507–536. [CrossRef] [PubMed]
827. Shima, S.; Pilak, O.; Vogt, S.; Schick, M.; Stagni, M.S.; Meyer-Klaucke, W.; Warkentin, E.; Thauer, R.K.; Ermler, U. The Crystal Structure of [Fe]-Hydrogenase Reveals the Geometry of the Active Site. *Science* **2008**, *321*, 572–575. [CrossRef]
828. Byer, A.S.; Yang, H.; McDaniel, E.C.; Kathiresan, V.; Impano, S.; Pagnier, A.; Watts, H.; Denler, C.; Vagstad, A.L.; Piel, J.; et al. Paradigm Shift for Radical *S*-Adenosyl-L-methionine Reactions: The Organometallic Intermediate Ω Is Central to Catalysis. *J. Am. Chem. Soc.* **2018**, *140*, 8634–8638. [CrossRef] [PubMed]
829. Broderick, W.E.; Hoffman, B.M.; Broderick, J.B. Mechanism of Radical Initiation in the Radical S-Adenosyl-l-methionine Superfamily. *Acc. Chem. Res.* **2018**, *51*, 2611–2619. [CrossRef]
830. Dobbek, H.; Svetlitchnyi, V.; Gremer, L.; Huber, R.; Meyer, O. Crystal Structure of a Carbon Monoxide Dehydrogenase Reveals a [Ni–4Fe–5S] Cluster. *Science* **2001**, *293*, 1281–1285. [CrossRef]
831. Jeoung, J.-H.; Dobbek, H. Carbon Dioxide Activation at the Ni,Fe–Cluster of Anaerobic Carbon Monoxide Dehydrogenase. *Science* **2007**, *318*, 1461–1464. [CrossRef]
832. Can, M.; Armstrong, F.A.; Ragsdale, S.W. Structure, Function, and Mechanism of the Nickel Metalloenzymes, CO Dehydrogenase, and Acetyl-CoA Synthase. *Chem. Rev.* **2014**, *114*, 4149–4174. [CrossRef]
833. Duin, E.C. Methyl Coenzyme M Reductase. In *Encyclopedia of Metalloproteins*; Kretsinger, R.H., Uversky, V.N., Permyakov, E.A., Eds.; Springer: New York, NY, USA, 2013; pp. 1410–1418.
834. Wongnate, T.; Ragsdale, S.W. The Reaction Mechanism of Methyl-Coenzyme M Reductase. *J. Biol. Chem.* **2015**, *290*, 9322–9334. [CrossRef]
835. Chen, H.; Gan, Q.; Fan, C. Methyl-Coenzyme M Reductase and Its Post-translational Modifications. *Front. Microbiol.* **2020**, *11*, 578356. [CrossRef] [PubMed]
836. Wongnate, T.; Sliwa, D.; Ginovska, B.; Smith, D.; Wolf, M.W.; Lehnert, N.; Raugei, S.; Ragsdale, S.W. The radical mechanism of biological methane synthesis by methyl-coenzyme M reductase. *Science* **2016**, *352*, 953–958. [CrossRef] [PubMed]
837. Boer, J.L.; Mulrooney, S.B.; Hausinger, R.P. Nickel-dependent metalloenzymes. *Arch. Biochem. Biophys.* **2014**, *544*, 142–152. [CrossRef] [PubMed]
838. Blackburn, R.; Cox, D.L.; Phillips, G.O. Effects of gamma radiation on vitamin B12 systems. *J. Chem. Soc. Faraday Trans. 1* **1972**, *68*, 1687–1696. [CrossRef]
839. Abel, E.W.; Pratt, J.M.; Whelan, E.; Wilkinson, P.J. The mechanism of oxidation of vitamin B_{12r} by oxygen. *S. Afr. J. Chem.* **1977**, *30*, 1–12.
840. Hoffman, B.M.; Petering, D.H. Coboglobins: Oxygen-Carrying Cobalt-Reconstituted Hemoglobin and Myoglobin. *Proc. Natl. Acad. Sci. USA* **1970**, *67*, 637–643. [CrossRef] [PubMed]
841. Dickinson, L.C.; Chien, J.C.W. Comparative Biological Chemistry of Cobalt Hemoglobin. *J. Biol. Chem.* **1973**, *248*, 5005–5011. [CrossRef]
842. Stynes, H.C.; Ibers, J.A. Thermodynamics of the reversible oxygenation of amine complexes of cobalt(II) protoporphyrin IX dimethyl ester in a nonaqueous medium. *J. Am. Chem. Soc.* **1972**, *94*, 1559–1562. [CrossRef]
843. Hsu, G.C.; Spilburg, C.A.; Bull, C.; Hoffman, B.M. Coboglobins: Heterotropic Linkage and the Existence of a Quaternary Structure Change Upon Oxygenation of Cobaltohemoglobin. *Proc. Natl. Acad. Sci. USA* **1972**, *69*, 2122–2124. [CrossRef] [PubMed]
844. Walker, F.A. Reactions of monomeric cobalt-oxygen complexes. I. Thermodynamics of reaction of molecular oxygen with five- and six-coordinate amine complexes of a cobalt porphyrin. *J. Am. Chem. Soc.* **1973**, *95*, 1154–1159. [CrossRef]
845. Wang, M.Y.; Hoffman, B.M.; Hollenberg, P.F. Cobalt-substituted horseradish peroxidase. *J. Biol. Chem.* **1977**, *252*, 6268–6275. [CrossRef] [PubMed]

846. Drago, R.S.; Beugelsdijk, T.; Breese, J.A.; Cannady, J.P. The relationship of thermodynamic data for base adduct formation with cobalt protoporphyrin IX dimethyl ester to the corresponding enthalpies of forming dioxygen adducts with implications to oxygen binding cooperativity. *J. Am. Chem. Soc.* **1978**, *100*, 5374–5382. [CrossRef]
847. Wagner, G.C.; Gunsalus, I.C.; Wang, M.Y.; Hoffman, B.M. Cobalt-substituted cytochrome P-450$_{cam}$. *J. Biol. Chem.* **1981**, *256*, 6266–6273. [CrossRef]
848. Marden, M.C.; Kiger, L.; Poyart, C.; Rashid, A.K.; Kister, J.; Stetzkowski-Marden, F.; Caron, G.; Haque, M.; Moens, L. Modulation of the oxygen affinity of cobalt-porphyrin by globin. *FEBS Lett.* **2000**, *472*, 221–224. [CrossRef]
849. Brucker, E.A.; Olson, J.S.; Phillips, G.N.; Dou, Y.; Ikeda-Saito, M. High Resolution Crystal Structures of the Deoxy, Oxy, and Aquomet Forms of Cobalt Myoglobin*. *J. Biol. Chem.* **1996**, *271*, 25419–25422. [CrossRef] [PubMed]
850. Halpern, J. Mechanisms of coenzyme B_{12} dependent rearrangements. *Science* **1985**, *227*, 869–875. [CrossRef]
851. Broderick, J.B.; Broderick, W.E.; Hoffman, B.M. Radical SAM enzymes: Nature's choice for radical reactions. *FEBS Lett.* **2023**, *597*, 92–101. [CrossRef] [PubMed]
852. Mobley, H.L.; Hausinger, R.P. Microbial ureases: Significance, regulation, and molecular characterization. *Microbiol. Rev.* **1989**, *53*, 85–108. [CrossRef]
853. Song, X.; Fiati Kenston, S.S.; Kong, L.; Zhao, J. Molecular mechanisms of nickel induced neurotoxicity and chemoprevention. *Toxicology* **2017**, *392*, 47–54. [CrossRef]
854. Alfano, M.; Cavazza, C. Structure, function, and biosynthesis of nickel-dependent enzymes. *Protein Sci.* **2020**, *29*, 1071–1089. [CrossRef]
855. Macomber, L.; Hausinger, R.P. Mechanisms of nickel toxicity in microorganisms. *Metallomics* **2011**, *3*, 1153–1162. [CrossRef] [PubMed]
856. Kim, N.; Filipovic, D.; Bhattacharya, S.; Cuddapah, S. Epigenetic toxicity of heavy metals—Implications for embryonic stem cells. *Environ. Int.* **2024**, *193*, 109084. [CrossRef] [PubMed]
857. Rizwan, M.; Usman, K.; Alsafran, M. Ecological impacts and potential hazards of nickel on soil microbes, plants, and human health. *Chemosphere* **2024**, *357*, 142028. [CrossRef]
858. Kumar, M.; Singh, S.; Jain, A.; Yadav, S.; Dubey, A.; Trivedi, S.P. A review on heavy metal-induced toxicity in fishes: Bioaccumulation, antioxidant defense system, histopathological manifestations, and transcriptional profiling of genes. *J. Trace Elem. Med. Biol.* **2024**, *83*, 127377. [CrossRef]
859. Yu, H.; Li, W.; Liu, X.; Song, Q.; Li, J.; Xu, J. Physiological and molecular bases of the nickel toxicity responses in tomato. *Stress Biol.* **2024**, *4*, 25. [CrossRef]
860. Mao, X.; Ahmad, B.; Hussain, S.; Azeem, F.; Waseem, M.; Alhaj Hamoud, Y.; Shaghaleh, H.; Abeed, A.H.A.; Rizwan, M.; Yong, J.W.H. Microbial assisted alleviation of nickel toxicity in plants: A review. *Ecotoxicol. Environ. Saf.* **2025**, *289*, 117669. [CrossRef] [PubMed]
861. Ragsdale, S.W. Nickel-based Enzyme Systems. *J. Biol. Chem.* **2009**, *284*, 18571–18575. [CrossRef]
862. Campeciño, J.O.; Maroney, M.J. Reinventing the Wheel: The NiSOD Story. In *The Biological Chemistry of Nickel*; Zamble, D., Rowińska-Żyrek, M., Kozlowski, H., Eds.; The Royal Society of Chemistry: London, UK, 2017.
863. Yao, M.; Tu, W.; Chen, X.; Zhan, C.-G. Reaction pathways and free energy profiles for spontaneous hydrolysis of urea and tetramethylurea: Unexpected substituent effects. *Org. Biomol. Chem.* **2013**, *11*, 7595–7605. [CrossRef]
864. Maier, R.J.; Benoit, S.L. Role of Nickel in Microbial Pathogenesis. *Inorganics* **2019**, *7*, 80. [CrossRef]
865. Rutherford, J.C. The Emerging Role of Urease as a General Microbial Virulence Factor. *PLoS Pathog.* **2014**, *10*, e1004062. [CrossRef]
866. de Brito, B.B.; da Silva, F.A.F.; Soares, A.S.; Pereira, V.A.; Santos, M.L.C.; Sampaio, M.M.; Neves, P.H.M.; de Melo, F.F. Pathogenesis and clinical management of *Helicobacter pylori* gastric infection. *World J. Gastroenterol.* **2019**, *25*, 5578–5589. [CrossRef] [PubMed]
867. Hernandez, J.A.; Micus, P.S.; Sunga, S.A.L.; Mazzei, L.; Ciurli, S.; Meloni, G. Metal selectivity and translocation mechanism characterization in proteoliposomes of the transmembrane NiCoT transporter NixA from Helicobacter pylori. *Chem. Sci.* **2024**, *15*, 651–665. [CrossRef]
868. Zhou, C.; Bhinderwala, F.; Lehman, M.K.; Thomas, V.C.; Chaudhari, S.S.; Yamada, K.J.; Foster, K.W.; Powers, R.; Kielian, T.; Fey, P.D. Urease is an essential component of the acid response network of Staphylococcus aureus and is required for a persistent murine kidney infection. *PLoS Pathog.* **2019**, *15*, e1007538. [CrossRef] [PubMed]
869. Clemens, D.L.; Lee, B.Y.; Horwitz, M.A. Purification, characterization, and genetic analysis of Mycobacterium tuberculosis urease, a potentially critical determinant of host-pathogen interaction. *J. Bacteriol.* **1995**, *177*, 5644–5652. [CrossRef]
870. Nim, Y.S.; Fong, I.Y.H.; Deme, J.; Tsang, K.L.; Caesar, J.; Johnson, S.; Pang, L.T.H.; Yuen, N.M.H.; Ng, T.L.C.; Choi, T.; et al. Delivering a toxic metal to the active site of urease. *Sci. Adv.* **2023**, *9*, eadf7790. [CrossRef]
871. Tsang, K.L.; Wong, K.B. Moving nickel along the hydrogenase-urease maturation pathway. *Metallomics* **2022**, *14*, mfac003. [CrossRef]
872. Kumar, S.; Vinella, D.; De Reuse, H. Nickel, an essential virulence determinant of Helicobacter pylori: Transport and trafficking pathways and their targeting by bismuth. *Adv. Microb. Physiol.* **2022**, *80*, 1–33.

873. Masetti, M.; Bertazzo, M.; Recanatini, M.; Ciurli, S.; Musiani, F. Probing the transport of Ni(II) ions through the internal tunnels of the Helicobacter pylori UreDFG multimeric protein complex. *J. Inorg. Biochem.* **2021**, *223*, 111554. [CrossRef] [PubMed]
874. Dixon, N.E.; Gazzola, C.; Blakeley, R.L.; Zerner, B. Jack bean urease (EC 3.5.1.5). Metalloenzyme. Simple biological role for nickel. *J. Am. Chem. Soc.* **1975**, *97*, 4131–4133. [CrossRef]
875. Mazzei, L.; Musiani, F.; Ciurli, S. The structure-based reaction mechanism of urease, a nickel dependent enzyme: Tale of a long debate. *J. Biol. Inorg. Chem.* **2020**, *25*, 829–845, Erratum in *Commun. Math. Phys.* **1976**, *46*, 206. [CrossRef]
876. Pearson, M.A.; Michel, L.O.; Hausinger, R.P.; Karplus, P.A. Structures of Cys319 Variants and Acetohydroxamate-Inhibited Klebsiella aerogenes Urease. *Biochemistry* **1997**, *36*, 8164–8172. [CrossRef] [PubMed]
877. Dixon, N.E.; Riddles, P.W.; Gazzola, C.; Blakeley, R.L.; Zerner, B. Jack bean urease (EC 3.5.1.5). V. On the mechanism of action of urease on urea, formamide, acetamide, N-methylurea, and related compounds. *Can. J. Biochem.* **1980**, *58*, 1335–1344. [CrossRef] [PubMed]
878. Karplus, P.A.; Pearson, M.A.; Hausinger, R.P. 70 Years of Crystalline Urease: What Have We Learned? *Acc. Chem. Res.* **1997**, *30*, 330–337. [CrossRef]
879. Zambelli, B.; Musiani, F.; Benini, S.; Ciurli, S. Chemistry of Ni^{2+} in Urease: Sensing, Trafficking, and Catalysis. *Acc. Chem. Res.* **2011**, *44*, 520–530. [CrossRef]
880. Martins, C.O.; Sebastiany, L.K.; Lopez-Castillo, A.; Freitas, R.S.; Andrade, L.H.; Toma, H.E.; Netto, C.G.C.M. Urea Decomposition Mechanism by Dinuclear Nickel Complexes. *Molecules* **2023**, *28*, 1659. [CrossRef]
881. Saito, T.; Takano, Y. QM/MM Molecular Dynamics Simulations Revealed Catalytic Mechanism of Urease. *J. Phys. Chem. B* **2022**, *126*, 2087–2097. [CrossRef]
882. Mazzei, L.; Tria, G.; Ciurli, S.; Cianci, M. Exploring the conformational space of the mobile flap in Sporosarcina pasteurii urease by cryo-electron microscopy. *Int. J. Biol. Macromol.* **2024**, *283*, 137904. [CrossRef]
883. Mazzei, L.; Paul, A.; Cianci, M.; Devodier, M.; Mandelli, D.; Carloni, P.; Ciurli, S. Kinetic and structural details of urease inactivation by thiuram disulphides. *J. Inorg. Biochem.* **2024**, *250*, 112398. [CrossRef]
884. Mazzei, L.; Cianci, M.; Ciurli, S. Inhibition of Urease by Hydroquinones: A Structural and Kinetic Study. *Chemistry* **2022**, *28*, e202201770. [CrossRef]
885. Evans, P.N.; Boyd, J.A.; Leu, A.O.; Woodcroft, B.J.; Parks, D.H.; Hugenholtz, P.; Tyson, G.W. An evolving view of methane metabolism in the Archaea. *Nat. Rev. Microbiol.* **2019**, *17*, 219–232. [CrossRef]
886. Timmers, P.H.A.; Welte, C.U.; Koehorst, J.J.; Plugge, C.M.; Jetten, M.S.M.; Stams, A.J.M. Reverse Methanogenesis and Respiration in Methanotrophic Archaea. *Archaea* **2017**, *2017*, 1654237. [CrossRef] [PubMed]
887. Becker, D.F.; Ragsdale, S.W. Activation of Methyl-SCoM Reductase to High Specific Activity after Treatment of Whole Cells with Sodium Sulfide. *Biochemistry* **1998**, *37*, 2639–2647. [CrossRef] [PubMed]
888. Thauer, R.K. Methyl (Alkyl)-Coenzyme M Reductases: Nickel F-430-Containing Enzymes Involved in Anaerobic Methane Formation and in Anaerobic Oxidation of Methane or of Short Chain Alkanes. *Biochemistry* **2019**, *58*, 5198–5220. [CrossRef] [PubMed]
889. Holliger, C.; Pierik, A.J.; Reijerse, E.J.; Hagen, W.R. A spectroelectrochemical study of factor F430 nickel(II/I) from methanogenic bacteria in aqueous solution. *J. Am. Chem. Soc.* **1993**, *115*, 5651–5656. [CrossRef]
890. Grabarse, W.; Mahlert, F.; Shima, S.; Thauer, R.K.; Ermler, U. Comparison of three methyl-coenzyme M reductases from phylogenetically distant organisms: Unusual amino acid modification, conservation and adaptation. *J. Molec. Biol.* **2000**, *303*, 329–344. [CrossRef]
891. Zhou, Y.; Sliwa, D.A.; Ragsdale, S.W. Biochemistry of Methyl-CoM Reductase and Coenzyme F_{430}. In *Handbook of Porphyrin Science*; Kadish, K.M., Smith, K.M., Guilard, R., Eds.; World Scientific: Singapore, 2012; Volume 19, pp. 1–44.
892. Ohmer, C.J.; Dasgupta, M.; Patwardhan, A.; Bogacz, I.; Kaminsky, C.; Doyle, M.D.; Chen, P.Y.-T.; Keable, S.M.; Makita, H.; Simon, P.S.; et al. XFEL serial crystallography reveals the room temperature structure of methyl-coenzyme M reductase. *J. Inorg. Biochem.* **2022**, *230*, 111768. [CrossRef]
893. Miyazaki, Y.; Oohora, K.; Hayashi, T. Focusing on a nickel hydrocorphinoid in a protein matrix: Methane generation by methyl-coenzyme M reductase with F_{430} cofactor and its models. *Chem. Soc. Rev.* **2022**, *51*, 1629–1639. [CrossRef] [PubMed]
894. Patwardhan, A.; Sarangi, R.; Ginovska, B.; Raugei, S.; Ragsdale, S.W. Nickel-Sulfonate Mode of Substrate Binding for Forward and Reverse Reactions of Methyl-SCoM Reductase Suggest a Radical Mechanism Involving Long-Range Electron Transfer. *J. Am. Chem. Soc.* **2021**, *143*, 5481–5496. [CrossRef]
895. Wagner, T.; Kahnt, J.; Ermler, U.; Shima, S. Didehydroaspartate Modification in Methyl-Coenzyme M Reductase Catalyzing Methane Formation. *Angew. Chem. Int. Ed.* **2016**, *55*, 10630–10633. [CrossRef]
896. Duin, E.C.; Wagner, T.; Shima, S.; Prakash, D.; Cronin, B.; Yáñez-Ruiz, D.R.; Duval, S.; Rümbeli, R.; Stemmler, R.T.; Thauer, R.K.; et al. Mode of action uncovered for the specific reduction of methane emissions from ruminants by the small molecule 3-nitrooxypropanol. *Proc. Natl. Acad. Sci. USA* **2016**, *113*, 6172–6177. [CrossRef]

897. Prakash, D.; Wu, Y.; Suh, S.-J.; Duin, E.C. Elucidating the Process of Activation of Methyl-Coenzyme M Reductase. *J. Bacteriol.* **2014**, *196*, 2491–2498. [CrossRef] [PubMed]
898. Polêto, M.D.; Allen, K.D.; Lemkul, J.A. Structural Dynamics of the Methyl-Coenzyme M Reductase Active Site Are Influenced by Coenzyme F_{430} Modifications. *Biochemistry* **2024**, *63*, 1783–1794. [CrossRef] [PubMed]
899. Lubitz, W.; Ogata, H.; Rüdiger, O.; Reijerse, E. Hydrogenases. *Chem. Rev.* **2014**, *114*, 4081–4148. [CrossRef] [PubMed]
900. Greene, B.L.; Vansuch, G.E.; Chica, B.C.; Adams, M.W.W.; Dyer, R.B. Applications of Photogating and Time Resolved Spectroscopy to Mechanistic Studies of Hydrogenases. *Acc. Chem. Res.* **2017**, *50*, 2718–2726. [CrossRef]
901. Tai, H.; Higuchi, Y.; Hirota, S. Comprehensive reaction mechanisms at and near the Ni–Fe active sites of [NiFe] hydrogenases. *Dalton Trans.* **2018**, *47*, 4408–4423. [CrossRef] [PubMed]
902. Tai, H.; Hirota, S. Mechanism and Application of the Catalytic Reaction of [NiFe] Hydrogenase: Recent Developments. *ChemBioChem* **2020**, *21*, 1573–1581. [CrossRef]
903. Schoelmerich, M.C.; Müller, V. Energy-converting hydrogenases: The link between H(2) metabolism and energy conservation. *Cell Mol. Life Sci.* **2020**, *77*, 1461–1481. [CrossRef]
904. Chenevier, P.; Mugherli, L.; Darbe, S.; Darchy, L.; DiManno, S.; Tran, P.D.; Valentino, F.; Iannello, M.; Volbeda, A.; Cavazza, C.; et al. Hydrogenase enzymes: Application in biofuel cells and inspiration for the design of noble-metal free catalysts for H2 oxidation. *Compt. Rend. Chim.* **2013**, *16*, 491–505. [CrossRef]
905. Ogata, H.; Lubitz, W.; Higuchi, Y. Structure and function of [NiFe] hydrogenases. *J. Biochem.* **2016**, *160*, 251–258. [CrossRef]
906. Kwiatkowski, A.; Caserta, G.; Schulz, A.-C.; Frielingsdorf, S.; Pelmenschikov, V.; Weisser, K.; Belsom, A.; Rappsilber, J.; Sergueev, I.; Limberg, C.; et al. ATP-Triggered Fe(CN)2CO Synthon Transfer from the Maturase HypCD to the Active Site of Apo-[NiFe]-Hydrogenase. *J. Am. Chem. Soc.* **2024**, *146*, 30976–30989. [CrossRef]
907. Schmidt, A.; Kalms, J.; Lorent, C.; Katz, S.; Frielingsdorf, S.; Evans, R.M.; Fritsch, J.; Siebert, E.; Teutloff, C.; Armstrong, F.A.; et al. Stepwise conversion of the Cys_6[4Fe–3S] to a Cys_4[4Fe–4S] cluster and its impact on the oxygen tolerance of [NiFe]-hydrogenase. *Chem. Sci.* **2023**, *14*, 11105–11120. [CrossRef] [PubMed]
908. Tai, H.; Nishikawa, K.; Higuchi, Y.; Mao, Z.-w.; Hirota, S. Cysteine SH and Glutamate COOH Contributions to [NiFe] Hydrogenase Proton Transfer Revealed by Highly Sensitive FTIR Spectroscopy. *Angew. Chem. Int. Ed.* **2019**, *58*, 13285–13290. [CrossRef] [PubMed]
909. Ogata, H.; Lubitz, W.; Higuchi, Y. [NiFe] hydrogenases: Structural and spectroscopic studies of the reaction mechanism. *Dalton Trans.* **2009**, *37*, 7577–7587. [CrossRef] [PubMed]
910. Dong, G.; Phung, Q.M.; Hallaert, S.D.; Pierloot, K.; Ryde, U. H_2 binding to the active site of [NiFe] hydrogenase studied by multiconfigurational and coupled-cluster methods. *Phys. Chem. Chem. Phys.* **2017**, *19*, 10590–10601. [CrossRef]
911. Evans, R.M.; Krahn, N.; Weiss, J.; Vincent, K.A.; Söll, D.; Armstrong, F.A. Replacing a Cysteine Ligand by Selenocysteine in a [NiFe]-Hydrogenase Unlocks Hydrogen Production Activity and Addresses the Role of Concerted Proton-Coupled Electron Transfer in Electrocatalytic Reversibility. *J. Am. Chem. Soc.* **2024**, *146*, 16971–16976. [CrossRef]
912. Tai, H.; Hirota, S.; Stripp, S.T. Proton Transfer Mechanisms in Bimetallic Hydrogenases. *Acc. Chem. Res.* **2021**, *54*, 232–241. [CrossRef]
913. Desguin, B.; Urdiain-Arraiza, J.; Da Costa, M.; Fellner, M.; Hu, J.; Hausinger, R.P.; Desmet, T.; Hols, P.; Soumillion, P. Uncovering a superfamily of nickel-dependent hydroxyacid racemases and epimerases. *Sci. Rep.* **2020**, *10*, 18123. [CrossRef]
914. Chatterjee, S.; Gatreddi, S.; Gupta, S.; Nevarez, J.L.; Rankin, J.A.; Turmo, A.; Hu, J.; Hausinger, R.P. Unveiling the mechanisms and biosynthesis of a novel nickel-pincer enzyme. *Biochem. Soc. Trans.* **2022**, *50*, 1187–1196. [CrossRef]
915. Hausinger, R.P.; Hu, J.; Desguin, B. The nickel-pincer coenzyme of lactate racemase: A case study of uncovering cofactor structure and biosynthesis. *Methods Enzym.* **2023**, *685*, 341–371.
916. Wang, B.; Shaik, S. The Nickel-Pincer Complex in Lactate Racemase Is an Electron Relay and Sink that acts through Proton-Coupled Electron Transfer. *Angew. Chem.* **2017**, *129*, 10232–10236. [CrossRef]
917. Zhang, X.; Chung, L.W. Alternative Mechanistic Strategy for Enzyme Catalysis in a Ni-Dependent Lactate Racemase (LarA): Intermediate Destabilization by the Cofactor. *Chem. Eur. J.* **2017**, *23*, 3623–3630. [CrossRef] [PubMed]
918. Yu, M.-J.; Chen, S.-L. From NAD+ to Nickel Pincer Complex: A Significant Cofactor Evolution Presented by Lactate Racemase. *Chem. Eur. J.* **2017**, *23*, 7545–7557. [CrossRef] [PubMed]
919. Qiu, B.; Yang, X. A bio-inspired design and computational prediction of scorpion-like SCS nickel pincer complexes for lactate racemization. *Chem. Commun.* **2017**, *53*, 11410–11413. [CrossRef]
920. Rankin, J.A.; Mauban, R.C.; Fellner, M.; Desguin, B.; McCracken, J.; Hu, J.; Varganov, S.A.; Hausinger, R.P. Lactate Racemase Nickel-Pincer Cofactor Operates by a Proton-Coupled Hydride Transfer Mechanism. *Biochemistry* **2018**, *57*, 3244–3251. [CrossRef]
921. Gatreddi, S.; Sui, D.; Hausinger, R.P.; Hu, J. Irreversible inactivation of lactate racemase by sodium borohydride reveals reactivity of the nickel-pincer nucleotide cofactor. *ACS Catal.* **2023**, *13*, 1441–1448. [CrossRef]
922. Liu, X.; Xiong, X. Copper. In *Encyclopedia of Geochemistry: A Comprehensive Reference Source on the Chemistry of the Earth*; White, W.M., Ed.; Springer: Cham, Switzerland, 2018; pp. 303–305.

923. Tsang, T.; Davis, C.I.; Brady, D.C. Copper biology. *Curr. Biol.* **2021**, *31*, R421–R427. [CrossRef]
924. Ruiz, L.M.; Libedinsky, A.; Elorza, A.A. Role of Copper on Mitochondrial Function and Metabolism. *Front. Mol. Biosci.* **2021**, *8*, 711227. [CrossRef] [PubMed]
925. Cobine, P.A.; Moore, S.A.; Leary, S.C. Getting out what you put in: Copper in mitochondria and its impacts on human disease. *Biochim. Biophs. Acta* **2021**, *1868*, 118867. [CrossRef]
926. Mydy, L.S.; Chigumba, D.N.; Kersten, R.D. Plant Copper Metalloenzymes As Prospects for New Metabolism Involving Aromatic Compounds. *Front. Plant Sci.* **2021**, *12*, 692108. [CrossRef]
927. Patnaik, P. *Handbook of Inorganic Chemicals*; McGraw-Hill: New York, NY, USA, 2003.
928. Johnson, J.E.; Present, T.M.; Valentine, J.S. Iron: Life's primeval transition metal. *Proc. Natl. Acad. Sci. USA* **2024**, *121*, e2318692121. [CrossRef]
929. Rode, B.M.; Schwendinger, M.G. Copper-catalyzed amino acid condensation in wate—A simple possible way of prebiotic peptide formation. *Orig. Life Evol. Biosph.* **1990**, *20*, 401–410. [CrossRef]
930. Liu, Z.; Mariani, A.; Wu, L.; Ritson, D.; Folli, A.; Murphy, D.; Sutherland, J. Tuning the reactivity of nitriles using Cu(II) catalysis—Potentially prebiotic activation of nucleotides. *Chem. Sci.* **2018**, *9*, 7053–7057. [CrossRef]
931. Fu, X.; Liao, Y.; Aspin, A.; Yang, Z. Effect of Copper Salts on Amide Hydrothermal Formation and Reactivity. *ACS Earth Space Chem.* **2020**, *4*, 1596–1603. [CrossRef]
932. Gaylor, M.O.; Miro, P.; Vlaisavljevich, B.; Kondage, A.A.S.; Barge, L.M.; Omran, A.; Videau, P.; Swenson, V.A.; Leinen, L.J.; Fitch, N.W.; et al. Plausible Emergence and Self Assembly of a Primitive Phospholipid from Reduced Phosphorus on the Primordial Earth. *Orig. Life Evol. Biosph.* **2021**, *51*, 185–213. [CrossRef]
933. Aithal, A.; Dagar, S.; Rajamani, S. Metals in Prebiotic Catalysis: A Possible Evolutionary Pathway for the Emergence of Metalloproteins. *ACS Omega* **2023**, *8*, 5197–5208. [CrossRef] [PubMed]
934. Bhattacharya, A.; Tanwar, L.; Fracassi, A.; Brea, R.J.; Salvador-Castell, M.; Khanal, S.; Sinha, S.K.; Devaraj, N.K. Chemoselective Esterification of Natural and Prebiotic 1,2-Amino Alcohol Amphiphiles in Water. *J. Am. Chem. Soc.* **2023**, *145*, 27149–27159. [CrossRef] [PubMed]
935. Solomon, E.I.; Heppner, D.E.; Johnston, E.M.; Ginsbach, J.W.; Cirera, J.; Qayyum, M.; Kieber-Emmons, M.T.; Kjaergaard, C.H.; Hadt, R.G.; Tian, L. Copper Active Sites in Biology. *Chem. Rev.* **2014**, *114*, 3659–3853.
936. Llases, M.E.; Morgada, M.N.; Vila, A.J. Biochemistry of Copper Site Assembly in Heme-Copper Oxidases: A Theme with Variations. *Int. J. Mol. Sci.* **2019**, *20*, 3830. [CrossRef]
937. Bhadra, M.; Karlin, K.D. Copper Enzymes Involved in Multi-Electron Processes. In *Comprehensive Coordination Chemistry III*; Constable, E.C., Parkin, G., Que, L., Jr., Eds.; Elsevier: Oxford, UK, 2021; pp. 524–540.
938. Gao, L.; Zhang, A. Copper-instigated modulatory cell mortality mechanisms and progress in oncological treatment investigations. *Front. Immunol.* **2023**, *14*, 1236063. [CrossRef]
939. Lutsenko, S.; Roy, S.; Tsvetkov, P. Mammalian copper homeostasis: Physiological roles and molecular mechanisms. *Physiol. Rev.* **2025**, *105*, 441–491. [CrossRef]
940. Yang, Y.; Wu, J.; Wang, L.; Ji, G.; Dang, Y. Copper homeostasis and cuproptosis in health and disease. *Med. Comm.* **2024**, *5*, e724. [CrossRef] [PubMed]
941. Xu, E.; Liu, Y.; Gu, D.; Zhan, X.; Li, J.; Zhou, K.; Zhang, P.; Zou, Y. Molecular Mechanisms of Plant Responses to Copper: From Deficiency to Excess. *Int. J. Mol. Sci.* **2024**, *25*, 6993. [CrossRef] [PubMed]
942. Kosman, D.J. Multicopper oxidases: A workshop on copper coordination chemistry, electron transfer, and metallophysiology. *J. Biol. Inorg. Chem.* **2010**, *15*, 15–28. [CrossRef]
943. Itoh, S. The Role of Copper in Biocatalysis. In *Redox-Based Catalytic Chemistry of Transition Metal Complexes*; Kojima, T., Ed.; Royal Society of Chemistry: London, UK, 2024; Volume 2, pp. 41–60.
944. Shim, D.; Han, J. Coordination chemistry of mitochondrial copper metalloenzymes: Exploring implications for copper dyshomeostasis in cell death. *BMB Rep.* **2023**, *56*, 575–583. [CrossRef]
945. Guo, J.; Fisher, O.S. Orchestrating copper binding: Structure and variations on the cupredoxin fold. *J. Biol. Inorg. Chem.* **2022**, *27*, 529–540. [CrossRef]
946. Pérez-Henarejos, S.A.; Alcaraz, L.A.; Donaire, A. Blue Copper Proteins: A rigid machine for efficient electron transfer, a flexible device for metal uptake. *Arch. Biochem. Biophys.* **2015**, *584*, 134–148. [CrossRef]
947. Bím, D.; Alexandrova, A.N. Electrostatic regulation of blue copper sites. *Chem. Sci.* **2021**, *12*, 11406–11413. [CrossRef]
948. Arcos-López, T.; Schuth, N.; Quintanar, L. The Type 1 Blue Copper Site: From Electron Transfer to Biological Function. In *Transition Metals and Sulfur—A Strong Relationship for Life*; Martha Sosa, T., Peter, K., Eds.; De Gruyter: Berlin, Germany, 2020; pp. 51–90.
949. Karlin, S.; Zhu, Z.-Y.; Karlin, K.D. The extended environment of mononuclear metal centers in protein structures. *Proc. Natl. Acad. Sci. USA* **1997**, *94*, 14225–14230. [CrossRef] [PubMed]

950. Broadley, M.; Brown, P.; Cakmak, I.; Rengel, Z.; Zhao, F. Function of Nutrients: Micronutrients. In *Marschner's Mineral Nutrition of Higher Plants*, 3rd ed.; Marschner, P., Ed.; Academic Press: San Diego, CA, USA, 2012; pp. 191–248.
951. Solomon, E.I.; Gorelsky, S.I.; Dey, A. Metal–thiolate bonds in bioinorganic chemistry. *J. Comp. Chem.* **2006**, *27*, 1415–1428. [CrossRef]
952. Solomon, E.I.; Szilagyi, R.K.; DeBeer George, S.; Basumallick, L. Electronic Structures of Metal Sites in Proteins and Models: Contributions to Function in Blue Copper Proteins. *Chem. Rev.* **2004**, *104*, 419–458. [CrossRef]
953. Solomon, E.I.; Jose, A. Spiers Memorial Lecture: Activating metal sites for biological electron transfer. *Faraday Discuss.* **2022**, *234*, 9–30. [CrossRef]
954. Vallee, B.L.; Williams, R.J. Metalloenzymes: The entatic nature of their active sites. *Proc. Natl. Acad. Sci. USA* **1968**, *59*, 498–505. [CrossRef]
955. Williams, R.J.P. Energised (entatic) states of groups and of secondary structures in proteins and metalloproteins. *Eur. J. Biochem.* **1995**, *234*, 363–381. [CrossRef] [PubMed]
956. Gray, H.B.; Malmstroem, B.G. Long-range electron transfer in multisite metalloproteins. *Biochemistry* **1989**, *28*, 7499–7505. [CrossRef] [PubMed]
957. Comba, P. Coordination compounds in the entatic state. *Coord. Chem. Rev.* **2000**, *200–202*, 217–245. [CrossRef]
958. Comba, P.; Schiek, W. Fit and misfit between ligands and metal ions. *Coord. Chem. Rev.* **2003**, *238–239*, 21–29. [CrossRef]
959. Matyushov, D.V. Reorganization energy of electron transfer. *Phys. Chem. Chem. Phys.* **2023**, *25*, 7589–7610. [CrossRef]
960. Hansen, D.F.; Led, J.J. Determination of the geometric structure of the metal site in a blue copper protein by paramagnetic NMR. *Proc. Natl. Acad. Sci. USA* **2006**, *103*, 1738–1743. [CrossRef]
961. Gray, H.B.; Malmstrom, B.G.; Williams, R.J.P. Copper coordination in blue proteins. *J. Biol. Inorg. Chem.* **2000**, *5*, 551–559. [CrossRef]
962. Kontkanen, O.V.; Biriukov, D.; Futera, Z. Reorganization free energy of copper proteins in solution, in vacuum, and on metal surfaces. *J. Chem. Phys.* **2022**, *156*, 175101. [CrossRef]
963. Bard, A.J. *Standard Potentials in Aqueous Solution*, 1st ed.; Routeledge: New York, NY, USA, 1985.
964. Choi, M.; Davidson, V.L. Cupredoxins—A study of how proteins may evolve to use metals for bioenergetic processes. *Metallomics* **2011**, *3*, 140–151. [CrossRef] [PubMed]
965. Warren, J.J.; Lancaster, K.M.; Richards, J.H.; Gray, H.B. Inner- and outer-sphere metal coordination in blue copper proteins. *J. Inorg. Biochem.* **2012**, *115*, 119–126. [CrossRef]
966. Machczynski, M.C.; Gray, H.B.; Richards, J.H. An outer-sphere hydrogen-bond network constrains copper coordination in blue proteins. *J. Inorg. Biochem.* **2002**, *88*, 375–380. [CrossRef] [PubMed]
967. Mammoser, C.C.; LeMasters, B.E.; Edwards, S.G.; McRae, E.M.; Mullins, M.H.; Wang, Y.; Garcia, N.M.; Edmonds, K.A.; Giedroc, D.P.; Thielges, M.C. The structure of plastocyanin tunes the midpoint potential by restricting axial ligation of the reduced copper ion. *Commun. Chem.* **2023**, *6*, 175. [CrossRef]
968. Lam, Q.; Van Stappen, C.; Lu, Y.; Dikanov, S.A. HYSCORE and QM/MM Studies of Second Sphere Variants of the Type 1 Copper Site in Azurin: Influence of Mutations on the Hyperfine Couplings of Remote Nitrogens. *J. Phys. Chem. B* **2024**, *128*, 3350–3359. [CrossRef]
969. Wang, J.X.; Vilbert, A.C.; Cui, C.; Mirts, E.N.; Williams, L.H.; Kim, W.; Jessie Zhang, Y.; Lu, Y. Increasing Reduction Potentials of Type 1 Copper Center and Catalytic Efficiency of Small Laccase from Streptomyces coelicolor through Secondary Coordination Sphere Mutations. *Angew. Chem. Int. Ed.* **2023**, *62*, e202314019. [CrossRef]
970. Merello Oyarzún, G.; Olivares-Costa, M.; Basile, L.; Pástor, T.P.; Mendoza-Soto, P.; Padilla-Santiago, L.; Mardones, G.A.; Binda, C.; Opazo, J.C. Evolutionary and Functional Analysis of Monoamine Oxidase F: A Novel Member of the Monoamine Oxidase Gene Family. *Genome Biol. Evol.* **2025**, *17*, evae280. [CrossRef] [PubMed]
971. Zaffryar-Eilot, S.; Hasson, P. Lysyl Oxidases: Orchestrators of Cellular Behavior and ECM Remodeling and Homeostasis. *Int. J. Mol. Sci.* **2022**, *23*, 11378. [CrossRef]
972. McGuirl, M.A.; Dooley, D.M. Copper Proteins with Type 2 Sites. In *Encyclopedia of Inorganic and Bioinorganic Chemistry*; Scott, R.A., Ed.; Wiley: Hoboken, NJ, USA, 2011.
973. Ji, R.; Guan, L.; Hu, Z.; Cheng, Y.; Cai, M.; Zhao, G.; Zang, J. A comprehensive review on hemocyanin from marine products: Structure, functions, its implications for the food industry and beyond. *Int. J. Biol. Macromol.* **2024**, *269*, 132041. [CrossRef]
974. Di Costanzo, L.F. Structural characterization of tyrosinases and an update on human enzymes. In *The Enzymes*; Supuran, C.T., Ed.; Academic Press: New York, NY, USA, 2024; Volume 56, pp. 55–83.
975. Pauleta, S.R.; Carepo, M.S.P.; Moura, I. The Tetranuclear Copper-Sulfide Center of Nitrous Oxide Reductase. In *Transition Metals and Sulfur—A Strong Relationship for Life*; Martha Sosa, T., Peter, K., Eds.; De Gruyter: Berlin, Germany; Boston, MA, USA, 2020; pp. 139–164.
976. Pomowski, A.; Dell'Acqua, S.; Wüst, A.; Pauleta, S.R.; Moura, I.; Einsle, O. Revisiting the metal sites of nitrous oxide reductase in a low-dose structure from Marinobacter nauticus. *J. Biol. Inorg. Chem.* **2024**, *29*, 279–290. [CrossRef]

977. Mellidou, I.; Kanellis, A.K. Revisiting the role of ascorbate oxidase in plant systems. *J. Exp. Bot.* **2024**, *75*, 2740–2753. [CrossRef] [PubMed]
978. Tikhonova, T.V.; Sorokin, D.Y.; Hagen, W.R.; Khrenova, M.G.; Muyzer, G.; Rakitina, T.V.; Shabalin, I.G.; Trofimov, A.A.; Tsallagov, S.I.; Popov, V.O. Trinuclear copper biocatalytic center forms an active site of thiocyanate dehydrogenase. *Proc. Natl. Acad. Sci. USA* **2020**, *117*, 5280–5290. [CrossRef] [PubMed]
979. Gudmundsson, M.; Kim, S.; Wu, M.; Ishida, T.; Momeni, M.H.; Vaaje-Kolstad, G.; Lundberg, D.; Royant, A.; Ståhlberg, J.; Eijsink, V.G.H.; et al. Structural and Electronic Snapshots during the Transition from a Cu(II) to Cu(I) Metal Center of a Lytic Polysaccharide Monooxygenase by X-ray Photoreduction. *J. Biol. Chem.* **2014**, *289*, 18782–18792. [CrossRef]
980. Solomon, E.I.; Augustine, A.J.; Yoon, J. O_2 Reduction to H_2O by the multicopper oxidases. *Dalton Trans.* **2008**, *30*, 3921–3932. [CrossRef]
981. Gräff, M.; Buchholz, P.C.F.; Le Roes-Hill, M.; Pleiss, J. Multicopper oxidases: Modular structure, sequence space, and evolutionary relationships. *Proteins* **2020**, *88*, 1329–1339. [CrossRef]
982. Sakurai, T.; Kataoka, K. Structure and function of type I copper in multicopper oxidases. *Cell Mol. Life Sci.* **2007**, *64*, 2642. [CrossRef] [PubMed]
983. Nakamura, K.; Go, N. Function and molecular evolution of multicopper blue proteins. *Cell Mol. Life Sci.* **2005**, *62*, 2050–2066. [CrossRef] [PubMed]
984. Ellis, M.J.; Grossmann, J.G.; Eady, R.R.; Hasnain, S.S. Genomic analysis reveals widespread occurrence of new classes of copper nitrite reductases. *J. Biol. Inorg. Chem.* **2007**, *12*, 1119–1127. [CrossRef]
985. Roberts, S.A.; Weichsel, A.; Grass, G.; Thakali, K.; Hazzard, J.T.; Tollin, G.; Rensing, C.; Montfort, W.R. Crystal structure and electron transfer kinetics of CueO, a multicopper oxidase required for copper homeostasis in *Escherichia coli*. *Proc. Natl. Acad. Sci. USA* **2002**, *99*, 2766–2771. [CrossRef]
986. Djoko, K.Y.; Chong, L.X.; Wedd, A.G.; Xiao, Z. Reaction mechanisms of the multicopper oxidase CueO from Escherichia coli support its functional role as a cuprous oxidase. *J. Am. Chem. Soc.* **2010**, *132*, 2005–2015. [CrossRef]
987. Li, J.; Farrokhnia, M.; Rulíšek, L.; Ryde, U. Catalytic Cycle of Multicopper Oxidases Studied by Combined Quantum- and Molecular-Mechanical Free-Energy Perturbation Methods. *J. Phys. Chem. B* **2015**, *119*, 8268–8284. [CrossRef] [PubMed]
988. Siegbahn, P.E.M. Theoretical Study of O2 Reduction and Water Oxidation in Multicopper Oxidases. *J. Phys. Chem. A* **2020**, *124*, 5849–5855. [CrossRef]
989. Shin, W.; Sundaram, U.M.; Cole, J.L.; Zhang, H.H.; Hedman, B.; Hodgson, K.O.; Solomon, E.I. Chemical and Spectroscopic Definition of the Peroxide-Level Intermediate in the Multicopper Oxidases: Relevance to the Catalytic Mechanism of Dioxygen Reduction to Water. *J. Am. Chem. Soc.* **1996**, *118*, 3202–3215. [CrossRef]
990. Augustine, A.J.; Quintanar, L.; Stoj, C.S.; Kosman, D.J.; Solomon, E.I. Spectroscopic and Kinetic Studies of Perturbed Trinuclear Copper Clusters: The Role of Protons in Reductive Cleavage of the O−O Bond in the Multicopper Oxidase Fet3p. *J. Am. Chem. Soc.* **2007**, *129*, 13118–13126. [CrossRef]
991. Srnec, M.; Ryde, U.; Rulíšek, L. Reductive cleavage of the O–O bond in multicopper oxidases: A QM/MM and QM study. *Faraday Discuss.* **2011**, *148*, 41–53. [CrossRef]
992. Robinett, N.G.; Peterson, R.L.; Culotta, V.C. Eukaryotic copper-only superoxide dismutases (SODs): A new class of SOD enzymes and SOD-like protein domains. *J. Biol. Chem.* **2018**, *293*, 4636–4643. [CrossRef] [PubMed]
993. Switzer, C.H.; Kasamatsu, S.; Ihara, H.; Eaton, P. SOD1 is an essential H(2)S detoxifying enzyme. *Proc. Natl. Acad. Sci. USA* **2023**, *120*, e2205044120. [CrossRef]
994. Franco Cairo, J.P.L.; Mandelli, F.; Tramontina, R.; Cannella, D.; Paradisi, A.; Ciano, L.; Ferreira, M.R.; Liberato, M.V.; Brenelli, L.B.; Gonçalves, T.A.; et al. Oxidative cleavage of polysaccharides by a termite-derived superoxide dismutase boosts the degradation of biomass by glycoside hydrolases. *Green Chem.* **2022**, *24*, 4845–4858. [CrossRef] [PubMed]
995. Montllor-Albalate, C.; Kim, H.; Thompson, A.E.; Jonke, A.P.; Torres, M.P.; Reddi, A.R. Sod1 integrates oxygen availability to redox regulate NADPH production and the thiol redoxome. *Proc. Natl. Acad. Sci. USA* **2022**, *119*, e2023328119. [CrossRef]
996. Fielden, E.M.; Roberts, P.B.; Bray, R.C.; Lowe, D.J.; Mautner, G.N.; Rotilio, G.; Calabrese, L. Mechanism of action of superoxide dismutase from pulse radiolysis and electron paramagnetic resonance. Evidence that only half the active sites function in catalysis. *Biochem. J.* **1974**, *139*, 49–60. [CrossRef]
997. Hough, M.A.; Hasnain, S.S. Crystallographic structures of bovine copper-zinc superoxide dismutase reveal asymmetry in two subunits: Functionally important three and five coordinate copper sites captured in the same crystal. *J. Mol. Biol.* **1999**, *287*, 579–592. [CrossRef]
998. Pantoliano, M.W.; Valentine, J.S.; Burger, A.R.; Lippard, S.J. A pH-dependent superoxide dismutase activity for zinc-free bovine erythrocuprein. Reexamination of the role of zinc in the holoprotein. *J. Inorg. Biochem.* **1982**, *17*, 325–341. [CrossRef] [PubMed]
999. Sannigrahi, A.; Chowdhury, S.; Das, B.; Banerjee, A.; Halder, A.; Kumar, A.; Saleem, M.; Naganathan, A.N.; Karmakar, S.; Chattopadhyay, K. The metal cofactor zinc and interacting membranes modulate SOD1 conformation-aggregation landscape in an in vitro ALS model. *Elife* **2021**, *10*, e61453. [CrossRef]

1000. Bakavayev, S.; Chetrit, N.; Zvagelsky, T.; Mansour, R.; Vyazmensky, M.; Barak, Z.; Israelson, A.; Engel, S. Cu/Zn-superoxide dismutase and wild-type like fALS SOD1 mutants produce cytotoxic quantities of H_2O_2 via cysteine-dependent redox short-circuit. *Sci. Rep.* **2019**, *9*, 10826. [CrossRef]
1001. Tainer, J.A.; Getzoff, E.D.; Richardson, J.S.; Richardson, D.C. Structure and mechanism of copper, zinc superoxide dismutase. *Nature* **1983**, *306*, 284–287. [CrossRef] [PubMed]
1002. Pelmenschikov, V.; Siegbahn, P.E.M. Copper−Zinc Superoxide Dismutase: Theoretical Insights into the Catalytic Mechanism. *Inorg. Chem.* **2005**, *44*, 3311–3320. [CrossRef] [PubMed]
1003. Wuebbles, D.J. Nitrous Oxide: No Laughing Matter. *Science* **2009**, *326*, 56–57. [CrossRef]
1004. Arat, S.; Bullerjahn, G.S.; Laubenbacher, R. A Network Biology Approach to Denitrification in Pseudomonas aeruginosa. *PLoS ONE* **2015**, *10*, e0118235. [CrossRef]
1005. Zumft, W.G.; Matsubara, T. A novel kind of multi-copper protein as terminal oxidoreductase of nitrous oxide respiration in *Pseudomonas perfectomarinus*. *FEBS Lett.* **1982**, *148*, 107–112. [CrossRef]
1006. Brown, K.; Tegoni, M.; Prudêncio, M.; Pereira, A.S.; Besson, S.; Moura, J.J.; Moura, I.; Cambillau, C. A novel type of catalytic copper cluster in nitrous oxide reductase. *Nat. Struct. Biol.* **2000**, *7*, 191–195. [CrossRef]
1007. Farrar, J.A.; Thomson, A.J.; Cheesman, M.R.; Dooley, D.M.; Zumft, W.G. A model of the copper centres of nitrous oxide reductase (*Pseudomonas stutzeri*). *FEBS Lett.* **1991**, *294*, 11–15. [CrossRef]
1008. Rathnayaka, S.C.; Mankad, N.P. Coordination chemistry of the Cu_Z site in nitrous oxide reductase and its synthetic mimics. *Coord. Chem. Rev.* **2021**, *429*, 213718. [CrossRef] [PubMed]
1009. Kroneck, P.M.H.; Antholine, W.A.; Riester, J.; Zumft, W.G. The nature of the cupric site in nitrous oxide reductase and of CuA in cytochrome c oxidase. *FEBS Lett.* **1989**, *248*, 212–213. [CrossRef] [PubMed]
1010. Morgada, M.N.; Murgida, D.H.; Vila, A.J. Purple Mixed-Valent Copper A. In *Transition Metals and Sulfur—A Strong Relationship for Life*; De Gruyter: Berlin, Germany, 2020; pp. 91–138.
1011. Zhang, L.; Bill, E.; Kroneck, P.M.H.; Einsle, O. Histidine-Gated Proton-Coupled Electron Transfer to the Cu_A Site of Nitrous Oxide Reductase. *J. Am. Chem. Soc.* **2021**, *143*, 830–838. [CrossRef]
1012. Carreira, C.; Dos Santos, M.M.C.; Pauleta, S.R.; Moura, I. Proton-coupled electron transfer mechanisms of the copper centres of nitrous oxide reductase from Marinobacter hydrocarbonoclasticus—An electrochemical study. *Bioelectrochemistry* **2020**, *133*, 107483. [CrossRef]
1013. Johnston, E.M.; Dell'Acqua, S.; Pauleta, S.R.; Moura, I.; Solomon, E.I. Protonation state of the Cu_4S_2 Cu_Z site in nitrous oxide reductase: Redox dependence and insight into reactivity. *Chem. Sci.* **2015**, *6*, 5670–5679. [CrossRef]
1014. Johnston, E.M.; Dell'Acqua, S.; Ramos, S.; Pauleta, S.R.; Moura, I.; Solomon, E.I. Determination of the Active Form of the Tetranuclear Copper Sulfur Cluster in Nitrous Oxide Reductase. *J. Am. Chem. Soc.* **2014**, *136*, 614–617. [CrossRef] [PubMed]
1015. Carreira, C.; Pauleta, S.R.; Moura, I. The catalytic cycle of nitrous oxide reductase—The enzyme that catalyzes the last step of denitrification. *J. Inorg. Biochem.* **2017**, *177*, 423–434. [CrossRef]
1016. Sánchez-Ferrer, A.; Rodríguez-López, J.N.; García-Cánovas, F.; García-Carmona, F. Tyrosinase: A comprehensive review of its mechanism. *Biochim. Biophys. Acta* **1995**, *1247*, 1–11. [CrossRef]
1017. Pretzler, M.; Rompel, A. Beyond Phenolics: Alternative Substrates for Type III Copper Enzymes. *Chem. Bio. Chem.* **2025**, *26*, e202400982. [CrossRef]
1018. Ivković, Đ.; Andrić, F.; Senćanski, M.; Stević, T.; Krstić Ristivojević, M.; Ristivojević, P. Innovative analytical methodology for skin anti-aging compounds discovery from plant extracts: Integration of High-Performance Thin-Layer Chromatography-in vitro spectrophotometry bioassays with multivariate modeling and molecular docking. *J. Chromatogr. A* **2024**, *1742*, 465640. [CrossRef] [PubMed]
1019. Alruhaimi, R.S.; Mahmoud, A.M.; Alnasser, S.M.; Alotaibi, M.F.; Elbagory, I.; El-Bassuony, A.A.; Lamsabhi, A.M.; Kamel, E.M. Integrating Computational Modeling and Experimental Validation to Unveil Tyrosinase Inhibition Mechanisms of Flavonoids from Alhagi graecorum. *ACS Omega* **2024**, *9*, 47167–47179. [CrossRef] [PubMed]
1020. Garcia-Jimenez, A.; Teruel-Puche, J.A.; Ortiz-Ruiz, C.V.; Berna, J.; Tudela, J.; Garcia-Canovas, F. 4-n-butylresorcinol, a depigmenting agent used in cosmetics, reacts with tyrosinase. *IUBMB Life* **2016**, *68*, 663–672. [CrossRef]
1021. Lee, S.Y.; Baek, N.; Nam, T.-g. Natural, semisynthetic and synthetic tyrosinase inhibitors. *J. Enzym. Inhib. Med. Chem.* **2016**, *31*, 1–13. [CrossRef] [PubMed]
1022. Peng, Z.; Wang, G.; Zeng, Q.-H.; Li, Y.; Liu, H.; Wang, J.J.; Zhao, Y. A systematic review of synthetic tyrosinase inhibitors and their structure-activity relationship. *Crit. Rev. Food Sci. Nutr.* **2022**, *62*, 4053–4094. [CrossRef]
1023. Min, X.; Su, Z.; Zhou, H.; Kou, X.; Li, D.; Xu, X. Insights into inhibitory action and interaction of bisdemethoxycurcumin on tyrosinase: Spectroscopic and docking analysis. *Int. J. Biol. Macromol.* **2024**, *281*, 136655. [CrossRef]
1024. Beaumet, M.; Lazinski, L.M.; Maresca, M.; Haudecoeur, R. Tyrosinase Inhibition and Antimelanogenic Effects of Resorcinol-Containing Compounds. *ChemMedChem* **2024**, *19*, e202400314. [CrossRef]

1025. Meena, P.; Das, P.; Rathore, V.; Panda, S.; Popa, C. Snow White's tale in nephrology: The emerging threat of skin-whitening creams on kidney health. *Clin. Kidney J.* **2025**, *18*, sfae358. [CrossRef]
1026. Jujjavarapu, S.E.; Mishra, A. Unravelling the Role of Tyrosine and Tyrosine Hydroxylase in Parkinson's Disease: Exploring Nanoparticle-based Gene Therapies. *CNS Neurol. Disord. Drug Targets* **2025**, *24*, 325–339. [CrossRef]
1027. Panda, S.; Phan, H.; Dunietz, E.M.; Brueggemeyer, M.T.; Hota, P.K.; Siegler, M.A.; Jose, A.; Bhadra, M.; Solomon, E.I.; Karlin, K.D. Intramolecular Phenolic H-Atom Abstraction by a N(3)ArOH Ligand-Supported (μ-η(2):η(2)-Peroxo)dicopper(II) Species Relevant to the Active Site Function of oxy-Tyrosinase. *J. Am. Chem. Soc.* **2024**, *146*, 14942–14947. [CrossRef]
1028. Matoba, Y.; Kihara, S.; Bando, N.; Yoshitsu, H.; Sakaguchi, M.; Kayama, K.e.; Yanagisawa, S.; Ogura, T.; Sugiyama, M. Catalytic mechanism of the tyrosinase reaction toward the Tyr98 residue in the caddie protein. *PLoS Biol.* **2019**, *16*, e3000077. [CrossRef] [PubMed]
1029. Fujieda, N.; Umakoshi, K.; Ochi, Y.; Nishikawa, Y.; Yanagisawa, S.; Kubo, M.; Kurisu, G.; Itoh, S. Copper–Oxygen Dynamics in the Tyrosinase Mechanism. *Angew. Chem. Int. Ed.* **2020**, *59*, 13385–13390. [CrossRef] [PubMed]
1030. Stefanidou, M.; Maravelias, C.; Dona, A.; Spiliopoulou, C. Zinc: A multipurpose trace element. *Arch. Toxicol.* **2006**, *80*, 1–9. [CrossRef]
1031. Costa, M.I.; Sarmento-Ribeiro, A.B.; Gonçalves, A.C. Zinc: From Biological Functions to Therapeutic Potential. *Int. J. Mol. Sci.* **2023**, *24*, 4822. [CrossRef]
1032. Kambe, T.; Tsuji, T.; Hashimoto, A.; Itsumura, N. The Physiological, Biochemical, and Molecular Roles of Zinc Transporters in Zinc Homeostasis and Metabolism. *Physiol. Rev.* **2015**, *95*, 749–784. [CrossRef] [PubMed]
1033. Wong, C.P.; Magnusson, K.R.; Sharpton, T.J.; Ho, E. Effects of zinc status on age-related T cell dysfunction and chronic inflammation. *BioMetals* **2021**, *34*, 291–301. [CrossRef]
1034. Azargoonjahromi, A. A systematic review of the association between zinc and anxiety. *Nutrit. Rev.* **2023**, *82*, 612–621. [CrossRef]
1035. Roohani, N.; Hurrell, R.; Kelishadi, R.; Schulin, R. Zinc and its importance for human health: An integrative review. *J. Res. Med. Sci.* **2013**, *18*, 144–157.
1036. Thompson, M.W. Regulation of zinc-dependent enzymes by metal carrier proteins. *BioMetals* **2022**, *35*, 187–213. [CrossRef]
1037. Stanton, C.; Sanders, D.; Krämer, U.; Podar, D. Zinc in plants: Integrating homeostasis and biofortification. *Mol. Plant* **2022**, *15*, 65–85. [CrossRef]
1038. Inada, Y.; Mohammed, A.M.; Loeffler, H.H.; Funahashi, S. Water-Exchange Mechanism for Zinc(II), Cadmium(II), and Mercury(II) Ions in Water as Studied by Umbrella-Sampling Molecular-Dynamics Simulations. *Helv. Chim. Acta* **2005**, *88*, 461–469. [CrossRef]
1039. Pearson, R.G. Hard and Soft Acids and Bases. *J. Am. Chem. Soc.* **1963**, *85*, 3533–3539. [CrossRef]
1040. McCall, K.A.; Huang, C.-c.; Fierke, C.A. Function and Mechanism of Zinc Metalloenzymes. *J. Nutr.* **2000**, *130*, 1437S–1446S. [CrossRef] [PubMed]
1041. Li, X.; Han, M.; Zhang, H.; Liu, F.; Pan, Y.; Zhu, J.; Liao, Z.; Chen, X.; Zhang, B. Structures and biological functions of zinc finger proteins and their roles in hepatocellular carcinoma. *Biomark. Res.* **2022**, *10*, 2. [CrossRef] [PubMed]
1042. Rakhra, G.; Rakhra, G. Zinc finger proteins: Insights into the transcriptional and post transcriptional regulation of immune response. *Mol. Biol. Rep.* **2021**, *48*, 5735–5743. [CrossRef]
1043. Andreini, C.; Banci, L.; Bertini, I.; Rosato, A. Counting the Zinc-Proteins Encoded in the Human Genome. *J. Proteome Res.* **2006**, *5*, 196–201. [CrossRef]
1044. Krężel, A.; Maret, W. The biological inorganic chemistry of zinc ions. *Arch. Biochem. Biophys.* **2016**, *611*, 3–19. [CrossRef]
1045. Krężel, A.; Maret, W. Zinc-buffering capacity of a eukaryotic cell at physiological pZn. *J. Biol. Inorg. Chem.* **2006**, *11*, 1049–1062. [CrossRef]
1046. Colvin, R.A.; Holmes, W.R.; Fontaine, C.P.; Maret, W. Cytosolic zinc buffering and muffling: Their role in intracellularzinc homeostasis. *Metallomics* **2010**, *2*, 306–317. [CrossRef]
1047. Maret, W. Zinc and Human Disease. In *Interrelations Between Essential Metal Ions and Human Disease*; Sigel, A., Sigel, H., Sigel, R.K.O., Eds.; Springer Science+Business Media: Dordrecht, The Netherlands, 2013; pp. 389–414.
1048. Maret, W. Zinc Biochemistry: From a Single Zinc Enzyme to a Key Element of Life. *Adv. Nutr.* **2013**, *4*, 82–91. [CrossRef]
1049. Djoko, K.Y.; Ong, C.-l.Y.; Walker, M.J.; McEwan, A.G. The Role of Copper and Zinc Toxicity in Innate Immune Defense against Bacterial Pathogens*. *J. Biol. Chem.* **2015**, *290*, 18954–18961. [CrossRef] [PubMed]
1050. Crichton, R.R. 12—Zinc: Lewis Acid and Gene Regulator. In *Biological Inorganic Chemistry*; Crichton, R.R., Ed.; Elsevier: Amsterdam, The Netherlands, 2008; pp. 197–210.
1051. Hu, Y.; Liu, B. Roles of zinc-binding domain of bacterial RNA polymerase in transcription. *Trends Biochem. Sci.* **2022**, *47*, 710–724. [CrossRef] [PubMed]
1052. Chanfreau, G.F. Zinc'ing down RNA polymerase I. *Transcription* **2013**, *4*, 217–220. [CrossRef]
1053. Markov, D.; Naryshkina, T.; Mustaev, A.; Severinov, K. A zinc-binding site in the largest subunit of DNA-dependent RNA polymerase is involved in enzyme assembly. *Genes Dev.* **1999**, *13*, 2439–2448. [CrossRef] [PubMed]

1054. Bassiouni, W.; Ali, M.A.M.; Schulz, R. Multifunctional intracellular matrix metalloproteinases: Implications in disease. *FEBS J.* **2021**, *288*, 7162–7182. [CrossRef]
1055. Tu, C.; Foster, L.; Alvarado, A.; McKenna, R.; Silverman, D.N.; Frost, S.C. Role of zinc in catalytic activity of carbonic anhydrase IX. *Arch. Biochem. Biophys.* **2012**, *521*, 90–94. [CrossRef]
1056. Covarrubias, A.S.; Bergfors, T.; Jones, T.A.; Högbom, M. Structural mechanics of the pH-dependent activity of beta-carbonic anhydrase from Mycobacterium tuberculosis. *J. Biol. Chem.* **2006**, *281*, 4993–4999. [CrossRef]
1057. Kim, J.K.; Lee, C.; Lim, S.W.; Adhikari, A.; Andring, J.T.; McKenna, R.; Ghim, C.-M.; Kim, C.U. Elucidating the role of metal ions in carbonic anhydrase catalysis. *Nat. Commun.* **2020**, *11*, 4557. [CrossRef]
1058. Cho, Y.E.; Lomeda, R.A.; Ryu, S.H.; Sohn, H.Y.; Shin, H.I.; Beattie, J.H.; Kwun, I.S. Zinc deficiency negatively affects alkaline phosphatase and the concentration of Ca, Mg and P in rats. *Nutr. Res. Pract.* **2007**, *1*, 113–119. [CrossRef]
1059. Peretz, A.; Papadopoulos, T.; Willems, D.; Hotimsky, A.; Michiels, N.; Siderova, V.; Bergmann, P.; Neve, J. Zinc supplementation increases bone alkaline phosphatase in healthy men. *J. Trace Elem. Med. Biol.* **2001**, *15*, 175–178. [CrossRef]
1060. Holtz, K.M.; Kantrowitz, E.R. The mechanism of the alkaline phosphatase reaction: Insights from NMR, crystallography and site-specific mutagenesis. *FEBS Lett.* **1999**, *462*, 7–11. [CrossRef]
1061. Miller, J.; McLachlan, A.D.; Klug, A. Repetitive zinc-binding domains in the protein transcription factor IIIA from Xenopus oocytes. *EMBO J.* **1985**, *4*, 1609–1614. [CrossRef]
1062. Cassandri, M.; Smirnov, A.; Novelli, F.; Pitolli, C.; Agostini, M.; Malewicz, M.; Melino, G.; Raschellà, G. Zinc-finger proteins in health and disease. *Cell Death Discov.* **2017**, *3*, 17071. [CrossRef] [PubMed]
1063. Wang, X.; Jiao, A.; Sun, L.; Li, W.; Yang, B.; Su, Y.; Ding, R.; Zhang, C.; Liu, H.; Yang, X.; et al. Zinc finger protein Zfp335 controls early T-cell development and survival through β-selection-dependent and -independent mechanisms. *eLife* **2022**, *11*, e75508. [CrossRef] [PubMed]
1064. Sedaghat, Y.; Miranda, W.F.; Sonnenfeld, M.J. The jing Zn-finger transcription factor is a mediator of cellular differentiation in the Drosophila CNS midline and trachea. *Development* **2002**, *129*, 2591–2606. [CrossRef] [PubMed]
1065. Omichinski, J.G.; Clore, G.M.; Appella, E.; Sakaguchi, K.; Gronenborn, A.M. High-resolution three-dimensional structure of a single zinc finger from a human enhancer binding protein in solution. *Biochemistry* **1990**, *29*, 9324–9334. [CrossRef]
1066. Rink, L.; Gabriel, P. Zinc and the immune system. *Proc. Nutr. Soc.* **2000**, *59*, 541–552. [CrossRef]
1067. Wessels, I.; Rolles, B.; Slusarenko, A.J.; Rink, L. Zinc deficiency as a possible risk factor for increased susceptibility and severe progression of Corona Virus Disease 19. *Br. J. Nutr.* **2022**, *127*, 214–232. [CrossRef]
1068. Krall, R.F.; Tzounopoulos, T.; Aizenman, E. The Function and Regulation of Zinc in the Brain. *Neuroscience* **2021**, *457*, 235–258. [CrossRef]
1069. Lin, P.H.; Sermersheim, M.; Li, H.; Lee, P.H.U.; Steinberg, S.M.; Ma, J. Zinc in Wound Healing Modulation. *Nutrients* **2017**, *10*, 16. [CrossRef]
1070. Prasad, A.S. Zinc and Hormones. In *Biochemistry of Zinc*; Prasad, A.S., Ed.; Springer: Boston, MA, USA, 1993; pp. 93–117.
1071. Baltaci, A.K.; Mogulkoc, R.; Baltaci, S.B. Review: The role of zinc in the endocrine system. *Pak. J. Pharm. Sci.* **2019**, *32*, 231–239.
1072. Nasiadek, M.; Stragierowicz, J.; Klimczak, M.; Kilanowicz, A. The Role of Zinc in Selected Female Reproductive System Disorders. *Nutrients* **2020**, *12*, 2464. [CrossRef] [PubMed]
1073. Vickram, S.; Rohini, K.; Srinivasan, S.; Nancy Veenakumari, D.; Archana, K.; Anbarasu, K.; Jeyanthi, P.; Thanigaivel, S.; Gulothungan, G.; Rajendiran, N.; et al. Role of Zinc (Zn) in Human Reproduction: A Journey from Initial Spermatogenesis to Childbirth. *Int. J. Mol. Sci.* **2021**, *22*, 2188. [CrossRef]
1074. Knez, M.; Stangoulis, J.C.R. Dietary Zn deficiency, the current situation and potential solutions. *Nutr. Res. Rev.* **2023**, *36*, 199–215. [CrossRef] [PubMed]
1075. Lindskog, S. Structure and mechanism of carbonic anhydrase. *Pharmacol. Ther.* **1997**, *74*, 1–20. [CrossRef] [PubMed]
1076. Lipscomb, W.N. Carboxypeptidase A mechanisms. *Proc. Natl. Acad. Sci. USA* **1980**, *77*, 3875–3878. [CrossRef]
1077. Supuran, C.T. Carbonic anhydrases--an overview. *Curr. Pharm. Des.* **2008**, *14*, 603–614. [CrossRef]
1078. Jonsson, B.H.; Liljas, A. Perspectives on the Classical Enzyme Carbonic Anhydrase and the Search for Inhibitors. *Biophys. J.* **2020**, *119*, 1275–1280. [CrossRef]
1079. Jensen, E.L.; Maberly, S.C.; Gontero, B. Insights on the Functions and Ecophysiological Relevance of the Diverse Carbonic Anhydrases in Microalgae. *Int. J. Mol. Sci.* **2020**, *21*, 2922. [CrossRef]
1080. Christianson, D.W.; Cox, J.D. Catalysis by metal-activated hydroxide in zinc and manganese metalloenzymes. *Annu. Rev. Biochem.* **1999**, *68*, 33–57. [CrossRef]
1081. Mazumdar, P.A.; Kumaran, D.; Swaminathan, S.; Das, A.K. A novel acetate-bound complex of human carbonic anhydrase II. *Acta Crystallogr. F* **2008**, *64*, 163–166. [CrossRef] [PubMed]
1082. Lesniewicz, K.; Karlowski, W.M.; Pienkowska, J.R.; Krzywkowski, P.; Poreba, E. The Plant S1-Like Nuclease Family Has Evolved a Highly Diverse Range of Catalytic Capabilities. *Plant Cell Physiol.* **2013**, *54*, 1064–1078. [CrossRef]

1083. Byrne, E.M.; Visomirski-Robic, L.; Cheng, Y.W.; Rhee, A.C.; Gott, J.M. RNA Editing in Physarum Mitochondria: Assays and Biochemical Approaches. In *Methods in Enzymology*; Gott, J.M., Ed.; Academic Press: New York, NY, USA, 2007; Volume 424, pp. 143–172.
1084. Yang, W. Nucleases: Diversity of structure, function and mechanism. *Quart. Rev. Biophys.* **2011**, *44*, 1–93. [CrossRef] [PubMed]
1085. Koval, T.; Dohnálek, J. Characteristics and application of S1–P1 nucleases in biotechnology and medicine. *Biotech. Adv.* **2018**, *36*, 603–612. [CrossRef]
1086. Koval', T.; Østergaard, L.H.; Lehmbeck, J.; Nørgaard, A.; Lipovová, P.; Dušková, J.; Skálová, T.; Trundová, M.; Kolenko, P.; Fejfarová, K.; et al. Structural and Catalytic Properties of S1 Nuclease from Aspergillus oryzae Responsible for Substrate Recognition, Cleavage, Non–Specificity, and Inhibition. *PLoS ONE* **2016**, *11*, e0168832. [CrossRef]
1087. Liao, R.-Z.; Yu, J.-G.; Himo, F. Phosphate Mono- and Diesterase Activities of the Trinuclear Zinc Enzyme Nuclease P1—Insights from Quantum Chemical Calculations. *Inorg. Chem.* **2010**, *49*, 6883–6888. [CrossRef]
1088. Stransky, J.; Koval', T.; Podzimek, T.; Tycova, A.; Lipovova, P.; Matousek, J.; Kolenko, P.; Fejfarova, K.; Duskova, J.; Skalova, T.; et al. Phosphate binding in the active centre of tomato multifunctional nuclease TBN1 and analysis of superhelix formation by the enzyme. *Acta Crystallog. F* **2015**, *71*, 1408–1415. [CrossRef] [PubMed]
1089. Page-McCaw, A.; Ewald, A.J.; Werb, Z. Matrix metalloproteinases and the regulation of tissue remodelling. *Nat. Rev. Molec. Cell Biol.* **2007**, *8*, 221–233. [CrossRef]
1090. Quiocho, F.A.; Lipscomb, W.N. Carboxypeptidase A: A protein and an enzyme. *Adv. Protein Chem.* **1971**, *25*, 1–78.
1091. Lipscomb, W.N. Relationship of the three dimensional structure of carboxypeptidase A to catalysis: Possible intermediates and pH effects. *Tetrahedron* **1974**, *30*, 1725–1732. [CrossRef]
1092. Breslow, R.; Wernick, D.L. Unified picture of mechanisms of catalysis by carboxypeptidase A. *Proc. Natl. Acad. Sci. USA* **1977**, *74*, 1303–1307. [CrossRef] [PubMed]
1093. Christianson, D.W.; Lipscomb, W.N. Carboxypeptidase A. *Acc. Chem. Res.* **1989**, *22*, 62–69. [CrossRef]
1094. Mock, W.L.; Zhang, J.Z. Mechanistically significant diastereoselection in the sulfoximine inhibition of carboxypeptidase A. *J. Biol. Chem.* **1991**, *266*, 6393–6400. [CrossRef]
1095. Lipscomb, W.N.; Sträter, N. Recent Advances in Zinc Enzymology. *Chem. Rev.* **1996**, *96*, 2375–2434. [CrossRef] [PubMed]
1096. Wu, S.; Zhang, C.; Xu, D.; Guo, H. Catalysis of Carboxypeptidase A: Promoted-Water versus Nucleophilic Pathways. *J. Phys. Chem. B* **2010**, *114*, 9259–9267. [CrossRef]
1097. Simpson, M.C.; Harding, C.J.; Czekster, R.M.; Remmel, L.; Bode, B.E.; Czekster, C.M. Unveiling the Catalytic Mechanism of a Processive Metalloaminopeptidase. *Biochemistry* **2023**, *62*, 3188–3205. [CrossRef] [PubMed]
1098. Dembek, G.; Lingens, F. Isolation and characterization of a meta-cleavage product in the degradation of quinaldic acid by Azotobacter sp. *FEMS Microbiol. Lett.* **1988**, *56*, 261–264. [CrossRef]
1099. Bobyr, E.; Lassila, J.K.; Wiersma-Koch, H.I.; Fenn, T.D.; Lee, J.J.; Nikolic-Hughes, I.; Hodgson, K.O.; Rees, D.C.; Hedman, B.; Herschlag, D. High-Resolution Analysis of Zn^{2+} Coordination in the Alkaline Phosphatase Superfamily by EXAFS and X-ray Crystallography. *J. Molec. Biol.* **2012**, *415*, 102–117. [CrossRef]
1100. Fernley, H.N. Mammalian alkaline phosphatase. In *The Enzymes*, 3rd ed.; Boeyer, P.D., Ed.; Acadamic Press: New York, NY, USA, 1971; pp. 417–447.
1101. Coleman, J.E. Structure and Mechanism of Alkaline Phosphatase. *Annu. Rev. Biophys.* **1992**, *21*, 441–483. [CrossRef]
1102. Borosky, G.L. Quantum-Mechanical Study on the Catalytic Mechanism of Alkaline Phosphatases. *J. Chem. Inf. Model.* **2017**, *57*, 540–549. [CrossRef]
1103. Anderson, R.A.; Bosron, W.F.; Kennedy, F.S.; Vallee, B.L. Role of magnesium in Escherichia coli alkaline phosphatase. *Proc. Natl. Acad. Sci. USA* **1975**, *72*, 2989–2993. [CrossRef]
1104. Tibbitts, T.T.; Murphy, J.E.; Kantrowitz, E.R. Kinetic and structural consequences of replacing the aspartate bridge by asparagine in the catalytic metal triad of Escherichia coli alkaline phosphatase. *J. Mol. Biol.* **1996**, *257*, 700–715. [CrossRef]
1105. Storozhuk, M.; Cherninskyi, A.; Maximyuk, O.; Isaev, D.; Krishtal, O. Acid-Sensing Ion Channels: Focus on Physiological and Some Pathological Roles in the Brain. *Curr. Neuropharmacol.* **2021**, *19*, 1570–1589. [CrossRef] [PubMed]
1106. Ojiakor, O.A.; Rylett, R.J. Modulation of sodium-coupled choline transporter CHT function in health and disease. *Neurochem. Int.* **2020**, *140*, 104810. [CrossRef] [PubMed]
1107. McKenna, M.J.; Renaud, J.M.; Ørtenblad, N.; Overgaard, K. A century of exercise physiology: Effects of muscle contraction and exercise on skeletal muscle Na(+),K(+)-ATPase, Na(+) and K(+) ions, and on plasma K(+) concentration-historical developments. *Eur. J. Appl. Physiol.* **2024**, *124*, 681–751. [CrossRef]
1108. Sommer, B.; Flores-Soto, E.; Gonzalez-Avila, G. Cellular Na+ handling mechanisms involved in airway smooth muscle contraction (Review). *Int. J. Mol. Med.* **2017**, *40*, 3–9. [CrossRef]
1109. Bortner, C.D.; Cidlowski, J.A. Ions, the Movement of Water and the Apoptotic Volume Decrease. *Front. Cell Dev. Biol.* **2020**, *8*, 611211. [CrossRef] [PubMed]

1110. Orlov, S.N.; Koltsova, S.V.; Kapilevich, L.V.; Dulin, N.O.; Gusakova, S.V. Cation-chloride cotransporters: Regulation, physiological significance, and role in pathogenesis of arterial hypertension. *Biochemistry* **2014**, *79*, 1546–1561. [CrossRef]
1111. Pressley, T.A. Structure and function of the Na,K pump: Ten years of molecular biology. *Miner. Electrolyte Metab.* **1996**, *22*, 264–271.
1112. Bueno-Orovio, A.; Sánchez, C.; Pueyo, E.; Rodriguez, B. Na/K pump regulation of cardiac repolarization: Insights from a systems biology approach. *Pflugers Arch.* **2014**, *466*, 183–193. [CrossRef]
1113. Perrone, M.; Patergnani, S.; Di Mambro, T.; Palumbo, L.; Wieckowski, M.R.; Giorgi, C.; Pinton, P. Calcium Homeostasis in the Control of Mitophagy. *Antioxid. Redox Signal.* **2023**, *38*, 581–598. [CrossRef] [PubMed]
1114. Jackson, W.F. Ion channels and the regulation of myogenic tone in peripheral arterioles. *Curr. Top. Membr.* **2020**, *85*, 19–58.
1115. Hepler, P.K. The role of calcium in cell division. *Cell Calcium* **1994**, *16*, 322–330. [CrossRef]
1116. Bachs, O.; Agell, N. *Calcium and Calmodulin Fuction in the Cell Nucleus*; Springer: Berlin/Heidelberg, Germany, 1995; pp. 1–9.
1117. Schulman, H. Calcium Regulation of Cytosolic Enzymes. In *Integrative Aspects of Calcium Signalling*; Verkhratsky, A., Toescu, E.C., Eds.; Springer: Boston, MA, USA, 1998; pp. 35–57.
1118. Tokumitsu, H.; Sakagami, H. Molecular Mechanisms Underlying Ca^{2+}/Calmodulin-Dependent Protein Kinase Kinase Signal Transduction. *Int. J. Mol. Sci.* **2022**, *23*, 11025. [CrossRef] [PubMed]
1119. Fiorentini, D.; Cappadone, C.; Farruggia, G.; Prata, C. Magnesium: Biochemistry, Nutrition, Detection, and Social Impact of Diseases Linked to Its Deficiency. *Nutrients* **2021**, *13*, 1136. [CrossRef] [PubMed]
1120. Ecco, G.; Imbeault, M.; Trono, D. KRAB zinc finger proteins. *Development* **2017**, *144*, 2719–2729. [CrossRef]
1121. Jen, J.; Wang, Y.C. Zinc finger proteins in cancer progression. *J. Biomed. Sci.* **2016**, *23*, 53. [CrossRef]
1122. Laity, J.H.; Lee, B.M.; Wright, P.E. Zinc finger proteins: New insights into structural and functional diversity. *Curr. Opin. Struct. Biol.* **2001**, *11*, 39–46. [CrossRef]
1123. Iyer, A.S.; Shaik, M.R.; Raufman, J.P.; Xie, G. The Roles of Zinc Finger Proteins in Colorectal Cancer. *Int. J. Mol. Sci.* **2023**, *24*, 10249. [CrossRef]

Disclaimer/Publisher's Note: The statements, opinions and data contained in all publications are solely those of the individual author(s) and contributor(s) and not of MDPI and/or the editor(s). MDPI and/or the editor(s) disclaim responsibility for any injury to people or property resulting from any ideas, methods, instructions or products referred to in the content.